Analysis of the Spin Dynamics of a Single-Engine Low-Wing Aeroplane

STEFFEN HAAKON SCHRADER

A thesis submitted in partial fulfilment of the requirements of the University of the West of England, Bristol for the degree of Doctor of Philosophy

Faculty of Environment and Technology, Department of Engineering Design and Mathematics, University of the West of England, Bristol

March 2019

Table of contents

Glossary

A

A (also I_x)	Moment of inertia about the longitudinal (x) axis
Absolute pressure	Pressure referenced to complete vacuum
Aerobatic category aeroplane	See Appendix A5
Aeroplane configuration	here: Aeroplane design features
Aileron	Lateral control of an aeroplane
Air–Data-Boom	Pylon or mast at an aeroplane with air–data sensors installed (e.g. wind vanes, pitot-static-system)
Aerofoil (or Airfoil) section	Part of a shape of a wing moving through a fluid
Airline Transport Pilot	Highest category of Pilot License, holder can act as a Pilot-In-Command of a transport category aeroplane
Angle of Attack	Angle between the chord line of an aerofoil and the vector of the relative wind
Antialiasing cutoff frequency	
Aspect ratio	$AR = b^2/S = b/MAC$, with b = wingspan, S = wing surface area, MAC = Mean Aerodynamic Chordline
ATO	Approved Training Organization

B

B (also I_y)	Moment of inertia about the lateral (y) axis
Bank angle or Angle of Bank	Roll Angle
Basic Empty Mass (BEM)	Aeroplanes empty mass including basic equipment according to the 'Airplane Flight Manual' (see Fuji Heavy Industries (2011), page 17 – 28) and unusable fuel and oil
Basic Trainer	Aeroplanes with the design role of training students in the first phase of flight training
Baud	Communication speed, symbols per second

C

C (also I_z)	Moment of inertia about the directional or normal (z) axis
CAD	Computer Aided Design
CALT	Calibrated Altitude
Certifying Authority	EASA for Europe, FAA for the USA, in addition to that the corresponding National Aviation Authorities
CG	Centre of Gravity
COM	Communication
Commercial Pilot	Second highest category of Pilot Licence, holder can act as a Pilot-In-Command of aeroplanes which are not transport category aeroplanes
Commuter Category Aeroplane	See Appendix A5

CS 23	Certification Specification for Normal, Utility, Aerobatic and Commuter Category Aeroplanes
CS 25	Certification Specification for Large Aeroplane
CS 27	Certification Specification for Light Rotorcraft
CS 29	Certification Specification for Large Rotorcraft
CSV	Comma-separated values

D

d	Damping coefficient
Datum line	Reference line for weighing an aeroplane and calculating the CG position and corresponding moments
DC	Direct current
Departure characteristics	Aeroplane´s stall and subsequent post stall gyration behaviour
Design Diving Speed V_D	Speed up to which the aeroplane Design Organisation needs to demonstrate that the aeroplane´s structure is free from flutter effects
Difference pressure	Pressure difference between total pressure and atmospheric pressure, normally the dynamic pressure of the airflow
Dihedral	Upward tilt angle (see in y-direction) from horizontal of the

	wings or tailplane of a fixed-wing aeroplane
Dynamic model	Models use in wind tunnels with geometric and mass distribution similarities to an original
E	
e^a	Amplitude
EASA	European Aviation Safety Agency
Empennage	Tail section of an aeroplane
Engine gyroscopic effects	Torque effect of a rotating propeller and / or precession effect of a rotating propeller during pitching
Elevator	Vertical control of an aeroplane, acting about the y-axis of an aeroplane
e (θ)	Quadratic error
F	
FAA	Federal Aviation Administration
Fatalities	Accident after which an injured person dies within the following 30 days
FCL	Flight Crew Licensing
Flat spin	General opinion: Spin of which the Pitch Angle Θ is smaller than 45°
Flight Envelope	Loosely applied term to different parameter combinations, operating rang. Here: parameter field of the aeroplane's mass and CG position

Flight Test Engineers	According to EASA definition: A Flight Test Engineer (FTE) is an engineer involved in the flight testing of prototype aircraft or aircraft systems
Flying Qualities	Characteristics, or dynamics, of the aeroplane involving the structure, the aerodynamics and the flight control system
Fuselage heavy	If the result of the expression for IYP is negative (e.g. heaviest parts of an aeroplane - like engines and fuel - are located in the fuselage)

G

g	Acceleration into a specified direction, 1 g = 9,81 m/s^2
Gross mass	Actual mass of an aeroplane during a specific phase of a flight
g	Acceleration of gravity

H

Handling Qualities	Characteristics, or dynamics, of the aeroplane involving the structure, the aerodynamics, the flight control system and additionally the pilot as a human being
Helix angle	Angle between aeroplane's trajectory and vertical / spin axis

I

I_x (also A)	Moment of inertia in roll
I_y (also B)	Moment of inertia in pitch

I_z (also C)	Moment of inertia in yaw
IMU	Inertial Measurement Unit
Incidence (angle) at root, at tip	Angle between the aeroplane´s longitudinal axis and the chord line of the wing (at the wing root or the wing tip)
Inertia yawing – moment parameter (IYP)	$IYP = \frac{Ix - Iy}{mb^2}$
Ix	Momentum about the X-axes
Iy	Momentum about the y-axes

J

j (as an Index, e.g. θ_{mj})	Running index

K

KCAS	Knots Calibrated Airspeed
Knot	Nautical Miles per hour

L

L	Rolling moment (positive to the right)
LAN	Local Area Network
Lemo-plug	Self-arresting push-pull plug, named after the inventor Léon Mouttet

Linearized, coupled, six degree of freedom, small perturbation airplane motion

Linearity	Linearity error
Low-wing aeroplane	Aeroplane with the wings mounted near or below the bottom of the fuselage
LRC	Langley Research Center

M

M	Pitching moment (positive: nose-up)

m	Mass
Mach or Mach number	Ratio of True Airspeed to Local Speed of Sound
Mean aerodynamic chord (MAC)	$l\mu = MAC = 2 \cdot \int_{-S}^{+S} c^2 dy / S$ With: y = coordinate along the wing span, c = chord at the coordinate y, S = wing surface area,
Monoplane	Fixed-wing aeroplane with one main wing plane attached, in contrast to a biplane with two main wing planes attached

N

N	yawing moment (positive to the right)
NACA	National Advisory Committee for Aeronautics, predecessor of the NASA
NASA	National Aeronautics and Space Administration
Normal category aeroplane	See Appendix A5

O

P

p	Roll rate or rate of roll (positive to the right)
Part-21	Airworthiness and Environmental Certification, regulation issued by the EASA. Regulation according to which a European Design

	Organization for aeroplanes is certified by the EASA
Pitch Angle	Rotation or angular change about the aeroplanes y-axis, referenced to the local horizon
Pitch Rate	Pitch angle change per second
Pitot-Static-System	System which measures the dynamic and static pressure within an airflow to determine its (and by that the aeroplane´s) speed
PPS	Pulse per second
Precession effect	Gyroscopic effect caused by the rotating mass of the propeller during the aeroplane is rotating about its y and z-axis
Propeller wash effect	Aerodynamic effect on the aeroplane caused by the aeroplane´s propeller stream and its corresponding turning direction
Q	
q	Pitch Rate (positive: nose-up)
R	
R	Spin radius
r	Yaw Rate (positive to the right)
Rate of roll or roll rate	Roll angle change per second
Relative density, μ	Relation between the (mass) density of the aeroplane and the (mass) density of the air $\mu = \frac{m}{\rho \cdot S \cdot b}$

Relative wind	Airflow encountering the aeroplane from a certain direction
Recovery parachute	Device in form of a parachute mounted at the tail of an aeroplane which can recover an aeroplane from a spin which cannot be recovered by control inputs alone
Roll Angle	Rotation or angular change about the aeroplanes x-axis
RS 232	Recommended Standard for serial communication transmission of data
Rudder	Directional control of an aeroplane

S

S	Wing surface area
SAE	Society of Automotive Engineers
Scale Error	Errors within the results of wind tunnel measurements compared to the original full scale test object due to different masses, mass distributions, different (critical) Reynolds numbers, including also other influences like wall effects within a wind tunnel
Space attitude angles	Orientation (attitude) of a rigid body in space about its x,y,z-axis
Spin matrix	Table with (all) spin relevant parameter and parameter combinations

Spiral dive	A lateral instability of an aeroplane which is in a steep descending, unstalled turn with the aircraft in an excessively nose-down attitude and with the airspeed increasing rapidly
SMA	Sub Miniature version A, coaxial cable
SSD	Solid-State-Drive
Stall	Airflow separation from wing
Static pressure	Actual atmospheric pressure
Station	Longitudinal position (along the x-axis) within an aeroplane
Suction System	Vacuum system to drive gyroscopic instruments in a cockpit of an aeroplane

T

t	Time
Tab or Trim Tab	Auxiliary flight control surface
Tail configuration	Design features of an aeroplane tail
Taper Ratio	$\lambda = c_{wingtip} / c_{wingroot}$, with: c = corresponding chordline length
True Airspeed (TAS)	Speed of an aeroplane relative to air mass in which it is flying
Technical Aviation	Field within the Aviation sector which covers Maintenance Flights, Certification Test Flights, Research Test Flights
THA	Threat and Hazard Assessment
Time compression	Psychological phenomenon that or when a human being is

	not capable to perceive a period of time correctly under mental pressure. Time seems to be much longer than it really is
Tip chord	Chordline of an aerofoil at the wing tip
Torque effect	Torque which acts on the aeroplane due to the propeller rotation
Total angular velocity	$\Omega = (p^2 + q^2 + r^2)^{1/2}$
Total pressure	Sum of dynamic pressure and static pressure
Total temperature (TAT)	Static Air Temperature SAT
	(= Outside Air Temperature) plus dynamic heating (= kinetic heating, ram rise)
	$TAT = SAT + (TAS/100)^2$
T-Tail	Tail configuration of an aeroplane with the elevator on top of the vertical tail (example: see NASA research aeroplane mentioned in Stough (1985) and Chapter 7)
U	
Unaugmented equation of motion	
USB	Universal Serial Bus
Utility category aeroplane	See Appendix A5
V	
V_A	Design maneuvering speed
VDC	Volts of direct current
Vestibulo – ocular	Ear – eye
VGA	Video Graphic Array

VMC	Visual Meteorological Conditions
W	
W	Weight
Wing heavy	If the result of the expression for IYP is positive (heaviest parts of an aeroplane - like engines and fuel - are located in the wings)
Wing root chord	Chordline of an aerofoil at the wing root
Wing tilt angle	Angle between aeroplane's y-axis and perpendicular line to the spin axis
X	
X-axis	Longitudinal Axis of an aeroplane, pointing forwards of an aeroplane
Y	
Yaw Angle	Rotation or angular change about the aeroplanes z-axis
Yaw Rate	Yaw angle change per second
Y-axis	Lateral Axis of an aeroplane, pointing to the right side of an aeroplane
Z	
Z-axis	Vertical Axis of an aeroplane, pointing downwards
Zero Loading	If the result of the expression for IYP is between $-50 \cdot 10^{-4}$ and $+ 50 \cdot 10^{-4}$ (masses within the aeroplane are distributed equally)

Greek Symbols

α	Alpha	Angle of Attack
β	Beta	Angle of Sideslip
δ	Delta	Phase shift
ζ	Zeta	Rudder defection angle
η	Eta	Elevator deflection angle
ξ	Xi	Aileron deflection angle
ρ	Rho	Density of the air
ϕ	Phi	Roll angle
Θ	Theta	Pitch Angle
Θ_g		guessed value for Θ
Θ_m		Θ at minimum or maximum of Θ- function
Θ_l		
Θ_{limit}		
Ψ	Psi	Heading

Parameter acronym list (Measurement System)

acronym	unit	description
alpha_le_c	°	calibrated angle of attack left wing
alpha_le_m	°	angle of attack relative to boom
alpha_le_r	V	angle of attack raw data
alpha_ri_c	°	calibrated angle of attack right wing
alpha_ri_m	°	angle of attack relative to boom
alpha_ri_r	V	angle of attack raw data
BAS	m/s	basic airspeed, compressibility for MSL included
beta_le_c	°	calibrated angle of side slip left wing
beta_le_m	°	angle of side slip relative to boom
beta_le_r	V	angle of side slip raw data
beta_ri_c	°	calibrated angle of side slip right wing
beta_ri_m	°	angle of side slip relative to boom
beta_ri_r	V	angle of side slip raw data
cycle_cnt	system	
cycle_dur	system	
cycle_err	system	
density	kg/m³	air density
eta_ca	°	elevator control surface deflection, positive when surface down
eta_horn	mm	position of elevator control, positive when pull
eta_rd	V	elevator wire sensor raw data
Event	-	Event Marker
GPSAlt_uB	m	geometric altitude (WGS84)
GPSGDOP_uB		satellite constellation
GPSHDOP_uB		satellite constellation
GPSLat_uB	°	Latitude
GPSLon_uB	°	Longitude
GPSPDOP_uB		satellite constellation
GPSStdAlt_uB	m	standard deviation
GPSStdLat_uB	m	standard deviation
GPSStdLon_uB	m	standard deviation
GPSTime_uB	s	GPS time
GPSVDir_uB	°	track
GPSVDOP_uB	m/s	vertical speed, postive down
GPSVDown_uB	m/s	vertical speed, postive down
GPSVEast_uB	m/s	horizontal speed, east component
GPSVHor_uB	m/s	horizontal ground speed
GPSViSat_uB		visibel satellite
GPSVNorth_uB	m/s	horizontal speed, north component
GPSVVer_uB	m/s	verical speed, postive up
Hbaro	m	barometric altitude over 1013.25 hPa
Hdens	m	density altitude
Hpunkt	m/s	vertical speed based on Hbaro, postive up
In_AccX	g	longitudinal acceleration
In_AccY	g	lateral acceleration
In_AccZ	g	vertical acceleration
In_p	°/s	roll rate
In_Phi	°	roll angle

Table 1: Parameter acronym list part 1 (Einbaubeschreibung_revision D)

Parameter acronym list

acronym	unit	description
In_Psi	°	heading
In_q	°/s	ptich rate
In_r	°/s	yaw rate
In_Theta	°	pitch angle
In_Time	s	time of INS
Ma_r	-	Mach number
pps_cnt	system	
pps_dur	system	
pps_pha_res	system	
pps_time_uB	system	
Pstat_r	hPa	static pressure
Pstau_r	hPa	dynamic pressure
sync_stat2	system	
sys_time	s	system time in seconds since midnight
T_ISA	°C	temperature of ISA at Hbaro
TAS_r	m/s	true airspeed, based on uncorrected pitot pressure
Tstat	°C	static air temperature
Ttotal_r	°C	total air temperatur
UBXData_uB	binary	GPS raw data
USV_Cap_A	%	UPS cell A capacity
USV_Cap_B	%	UPS cell B capacity
USV_Power	-	external power available
VRU_pps	system	
VRU_status	system	
VRUData	binary	INS raw data
xi_horn	°	position of aileron control, positive when left
xi_le_ca	°	left aileron control surface deflection, positive when surface down
xi_rd	V	aileron wire sensor raw data
xi_ri_ca	°	right aileron control surface deflection, positive when surface down
zeta_ca	°	rudder control surface deflection, positive when left
zeta_rd	V	rudder wire sensor raw data

Table 2: Parameter acronym list part 2 (Einbaubeschreibung_revision D)

I. Declaration

The work described in this thesis is the result of my own investigations. All sections of the text and the results that have been obtained from the work of others are fully referenced. I understand that cheating and plagiarism constitute a breach of University Regulations and will be dealt with accordingly.

Signed: Steffen H. Schrader Date: 31.03.2019

II. Abstract

Title: Analysis of the Spin Dynamics of a Single-Engine Low-Wing Aeroplane

As spinning is still involved in around 60% of all aircraft accidents (BFU, 1985 and Belcastro, 2009), this aerodynamic phenomenon is still not fully understood. As U.S. and European Certification Specifications do not require recoveries from fully developed spins of Normal Category aeroplanes, certification test flights will not discover aeroplane mass and centre of gravity combinations which may result in unrecoverable spins.

This thesis aims to contribute to a better understanding of the spin phenomenon through investigating the spin regime for normal, utility and aerobatic aircraft, and to explain what happens to the aircraft in terms of the aerodynamics, flight mechanics and the aircraft stability. The approach used is to vary the main geometric parameters such as the centre of gravity position and the aeroplane's mass across the flight envelope, and to investigate the subsequent effect on the main spin characteristic parameters such as the angle of attack, pitch angle, sideslip angle, rotational rates, and recovery time.

First of all, a literature review sums up the range of technical aspects that affect the problem of spinning. It reviews the experimental measurement techniques used, theoretical methods developed and flight test results obtained by previous researchers. The published results have been studied to extract the effect on spinning of aircraft geometry, control surface effectiveness, flight operational parameters and atmospheric effects. Consideration is also made of the influence on human performance of spinning, the current spin regulations and the available training material for pilots.

A conventional-geometry, single-engine low-wing aeroplane, the basic trainer Fuji FA-200-160, has been instrumented with a proven digital flight measurement system and 27 spins have been systematically conducted inside and outside the certified flight envelope. The accuracy of the flight measurements is ensured through effective calibration, and the choice of sensors has varied through the study, with earlier sensors suffering from more drift than the current sensors (Belcastro, 2009 and Schrader, 2013).

In-flight parameter data collected includes left and right wing α and β-angles, roll-pitch-yaw angles and corresponding rates, all control surface deflections, vertical speeds, altitude losses and the aeroplane's accelerations in all three directions.

Such data have been statistically analysed. The pitch behaviour has been mathematically modelled on the basis of the gathered flight test data.

Nine observations have been proposed. These mainly cover the effects of centre of gravity and aircraft mass variations on spin characteristic behaviour. They have all been proven as true through the results of this thesis. The final observation concerns the generalisation of the Fuji results, to the spin behaviour of other aircraft in the same category.

These observations can be used to improve flight test programmes, aircraft design processes, flight training materials and hence contribute strongly to better flight safety.

III. Acknowledgements

This research project has been conducted against the background of a long-standing collaboration between the University of the West of England (UWE) and the Osnabrueck University of Applied Science (Osnabrueck UAS).

Both Institutions are contributing to the Course of Studies ‘Aircraft and Flight Engineering’ (AFE) which has been founded by me in 1998.

During my training and later work as a qualified Experimental Test Pilot and work as a Senior Lecturer at the Osnabrueck UAS I gathered much theoretical and practical experience in the field of flight mechanics, aeroplane dynamic behaviour and spinning.

During the course of the almost 21 years (between 1998 and today) a lot of people supported me and contributed to this work at hand.

It is absolutely essential and my paramount wish to thank all these fantastic persons who gave me so much knowledge, support and by that parts of their lifetime.

Nobody can ever expect to get so much from other people than I got in my lifetime!

I would like to thank especially Dr. Chris Toomer. She is much much more than a colleague and my Supervisor on this research project. She became a dear friend and endless helping person. She brought so much value into the project with her amazing bright and creative ideas! How much intellectual power can be in a single human? Always so friendly, laughing and a problems solving woman. What a contribution to the work. Words cannot express!

I would like to thank Prof. Dr. Jürgen Biermann. What a helping, kind and calm character. Also a real friend to me who supported me with his deep and professional mathematical and programming skills and experiences. In countless meetings and even more working hours he gave me so much of his knowledge. Always accompanied by ‘feinstem Tee’!

I would like to thank Prof. Dr.-Ing. Jörg Hoffmann, again a dear friend and colleague from Osnabrueck. As the head of the ‘Labor für Messtechnik und Messsignalverarbeitung’ - of which I am a part of - he supported my PhD in all phases. From the very beginning and with a lot of ‘turbulences’ during the project he was always at my side as a kind, calm and experienced expert and a down-to-earth human.

I would like to thank especially Werner Trentmann, my dear personal friend and colleague from our Laboratory in Osnabrueck. He gave me so much support during the entire time of the project. He contributed in a brilliant way with his amazing technical knowledge and his

kind and calm character. Always friendly and inspiring to my. He is a person how makes things work. With his knowledge he earns a Professorship!

I would like to thank Matthias Cremer, owner and CEO of the company Messwerk GmbH (Braunschweig), who gave me his entire measurement system – the only system his company owns – to let me conduct the flight tests. He supported me by installing and calibrating the system at our aeroplane. His experience in the field of flight data collection was really a strong contribution to my research. Just brilliant!

I would like to thank especially Bernd Hamacher. How many hours did we discuss our topics on aviation, our AFE development, flight training. He convinced me to buy an aeroplane with which I could do scientific test flying. He bought is for us, and he gave it to me for the flight training with our students and for my spin tests. Words cannot express my gratitude.

I would like to conclude with Gertrud who I know since 1988 and who desperately convinced me to carry on with school to achieve the Abitur (A-Level) and to join the Uni later. She was successful at the very ending, after a long ‘battle’.

And I would like to thank her again, because in the meantime she became my wife and she supported me with her love, brightness, open-minded and inspiring intellect together with her amazing patients. What on Earth could promote and motivate me more than you!

I will never forget what you all did for me!!!

Chapter 1 Introduction

1.1 The problem with spinning

Spinning of an aeroplane is for an average pilot a totally unknown flight mode. According to the European Certification Specifications (EASA, 2012) the definition of spinning is:

…'a sustained auto rotation at angles of attack above stall. …The fully developed spin is attained when the flight path has become vertical.'

Kimberlin (2003) defines spinning as an:

…'out-of-control maneuver at angles of attack beyond the stall during which the airplane rotates about its Center of Gravity (C.G.) and an axis perpendicular to the Earth while descending vertically at high rates of descent.'

High turning rates about all three axes, unusual aeroplane attitudes and a sudden loss of control; spinning is confusing, disorientating and dangerous for the pilot, passengers and the public. The associated stress on the pilot and the required manual control inputs reduces the pilot's mental capacity to approximately 30 %, leading to the psychological phenomenon of 'time compression' (Anderson et al., 1983), in other words the pilot's reactions can become very slow and / or wrong. Spin recoveries also put high demands on the aeroplane, e.g. it may over-stress the structure of an aeroplane and thus it contributes to the danger of this kind of flight mode.

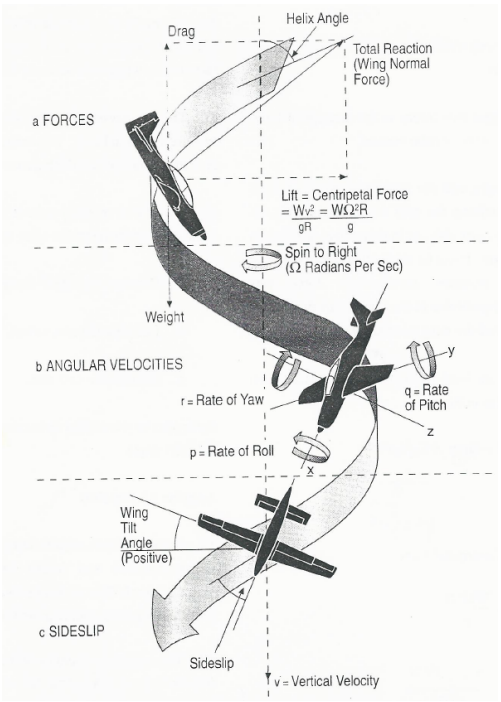

Figure 1.1: Example of a spin motion, including the flight mechanical nomenclature of the corresponding axes, angles, rates and velocities (Air Ministry, 1995)

AXIS (Symbol)	LONGITUDINAL(x)	LATERAL (y)	NORMAL (z)
Positive Direction	Forwards	To right	Downwards
ANGULAR VELOCITY			
Designation	Roll	Pitch	Yaw
Symbol	p	q	r
Positive Direction	to right	nose-up	to right
MOMENTS OF INERTIA	A	B	C
MOMENTS			
Designation	rolling moment	pitching moment	yawing moment
Symbol	L	M	N
Positive Direction	to right	nose-up	to right

Table 1.1: Typical sign conventions which are also used in the thesis, (Air Ministry, 1995)

A detailed description of spinning can be found in Appendices 1a and 1b.

A pilot can inadvertently and easily cause a spin when, due to a high workload situation in an approach or departure phase of a flight, he or she may enter the aircraft into a high angle of attack attitude combined with a high amount of sideslip or yaw angle. Unfortunately many cases of spinning have occurred in aviation, leading in most cases to accidents and even fatalities. These incidents have been collected in data banks, e.g. the US. National Transportation Safety Board (NTSB), providing a valuable resource for research. One survey using this data gives the impact positions of 38 spin related aircraft accidents within a normal traffic circuit along with some selected spin accidents (Pätzold et al., 2013).

Every year there are flight accidents which are caused by low visibility weather situations (BFU, 1986). Pilots without an instrument rating, without a proper equipped aeroplane or without sufficient proficiency, are entering clouds or foggy areas. As a result these pilots are likely to lose control of their aircraft by stalling it – exceeding the maximum angle of attack of the wing's aerofoil and subsequently experiencing an (asymmetric) airflow separation from the aeroplane's wings – which may lead to a spin. Especially in clouds or even in (low altitude) fog the recovery from a spin is not possible for these pilots. Such a situation may occur over populated areas and thus be a danger to the public.

According to flight accident investigations in Europe and the USA over the last decades, spinning results in more aeroplane losses and fatal accidents than all other flight manoeuvres together caused by its complexity and it being poorly understood by most pilots. A report published by the German Flight Accident Investigation Authority (BFU, 1985) states that between 1973 and 1985, 235 spin related flight accidents occurred with 67 fatalities. Within the last two years of that time interval 46% of all flight accidents were related to spins. If glider spin accidents are also taken into account that number rises to

60%. Similarly, in the period 1997 to 2006, a NASA study found that ‘59% of fatal aircraft accidents were associated with Loss–of–Control’ (Belcastro et al., 2009).

During the aircraft certification process, spinning trials are an extensive part of the entire process because spinning is influenced by a large number of factors. Among these factors are: total mass; mass distribution in the aeroplane (wing or fuselage heavy, zero loading); power settings; atmospheric conditions (mainly the air density); aerodynamic wing profile; centre of gravity position; and aeroplane configuration of flap settings, gear position (extended/retracted), control surface deflections, and tail design.

Due to this complexity the certifying authority (e.g. CAA, FAA, and EASA) needs to define the most safety critical areas of the flight envelope to test. A spin matrix is created which consists of several hundred parameter combinations to be flown. The critical areas in the matrix vary with aircraft design and their identification is currently dependent on experienced professionals such as test pilots and flight test engineers as no theories exist to aid (new) test crews or predict spin trial results. In addition the aircraft behaviour can vary substantially during a spin because of the non-linear nature of the dynamics, increasing the danger in these critical areas of the test matrix and the difficulty in terms of modelling the phenomena. Background information and explanations on certification spin test planning are provided in Appendices 2 and 3. Information on spin tests documented in-flight by pilots, are written on flight test cards: their relevance depends on the perception and experience of the pilot (Table 1.2).

Spin Matrix, Chipmunk N 735 DH

Spin No.	Airspeed	Entry Alt Altitude loss Per turn Recovery Alt	ROD	Needle -=left +=right	Ball L = LH R= RH	Attitude [flat, steep, extremely steep]	Time Per turn	Rate [slow, fast extremely fast]	Oscillation [smooth Mild Oscillatory High violent]	Control Force [Light Medium Heavy]	Turns to recover	
1	50-60	8.1/6.2	25'/turn			Med 30-45		slow	Smooth	med light	2¼ turn	R
2		8.3/6.7		rt	rt	Med 30-45		slow-med	Mild osc burst	med light	1¼	R
3	40	8.3/6.7	4K+	left	left	same 30-45	~2 sec	Rapid to fast	light	light	¾	L
4		8.2/6.9	4K+	"	"	same 30-45		fast+	med	"	¼	LL
5	50-60	8.2/6.5	~4K+	rt	rt	shallow		slow	Smth	Smth	1¾	RL
6											1.5	RL
7		9.0/6.5									2¼	RRL

Table 1.2: Typical Flight Test Card for spin trials (by the Author, 2011)

Even in a professional flight test environment, spinning may lead to accidents. In Table 1.3 all flights listed involved qualified test pilots who were prepared for the trials and were used to spin aeroplanes in the specific aeroplane category.

Type of aeroplane	Year	Aeroplane	Crew	Recovery parachute / Remarks
Siat 222	1961	crashed	killed	No spin recovery parachute installed
Windecker Eagle	1970	crashed	Escaped by parachute	Spin recovery parachute jettisoned instead of deployed
Pützer Sportsman	1970	crashed	killed	No spin recovery parachute installed
Grob G-110	1982	crashed	Escaped by parachute	Spin recovery parachute deployed, but not effective
Fournier RF-10	1983	crashed	Escaped by parachute	No spin recovery parachute installed
Glasair II-S-RG	1997	Safe landing	Not hurt	Spin recovery parachute fired after 10 turns, one turn was planned, recovery successful
Cirrus SR 22	2002	Safe landing	Not hurt	Spin recovery parachute fired after 10 turns, one turn was planned, recovery successful
Eta	2002	crashed	Escaped by parachute	Structural damage due to spiral dive
Lanceair Columbia 400	2003	crashed	Escaped by parachute	Spin recovery parachute deployed, but could not be jettisoned

Table 1.3: Known spin accidents during certification test programmes between the years 1961 and 2003. Note that this list is not exhaustive (Neumann, 2002).

Analysing the complex flight dynamics and flight physics of a spin – even in a small defined range of different parameters - leads to a better understanding of this potentially dangerous flight manoeuvre and better flight safety. This better understanding can be used to improve the accuracy of certification flight test processes: for example, critical parameter combinations in spin matrices can be added in. Also it can improve the design

of aircraft e.g. spin prevention systems and / or spin prevention designs and influence future flight training.

1.2 Scope of the research

Aircraft spin characteristics vary greatly due to aeroplane geometry, mass distribution and human factors, resulting in significant cross-coupling effects and complex flow phenomena. This makes spinning difficult to model, complex to measure and difficult to exactly replicate.

This thesis research concentrates on general aviation aircraft. Spin flight tests are conducted by the author using the Fuji FA 200-160, a single-engine low-wing basic training aeroplane (see Appendix 4 for specifications). The Fuji aircraft used in this study retains the original shape, i.e. no leading edge modifications and spin resistant additions have been made. Thus reference to other studies on modified aircraft is limited.

1.3 Reasoning for the research and its relevance

If spinning results in more aeroplane losses and fatal accidents than all other flight manoeuvres together, what makes spinning so different or special? The following items are central topics when dealing with the spin problem:

For the aeroplane:

1. High descent rates
2. Vertical trajectories
3. It may move to a “flat spin” situation which may be a non-recoverable spin

For the pilot:

4. Since the aircraft is rapidly changing its attitude in three-dimensional motion and these attitudes that are not normally adopted in an aircraft, this manoeuvre can be confusing and disorientating to the normal pilot.
5. Identification of spin parameter combinations which confuse pilots the most.
6. Fear and panic leading to wrong or chaotic control inputs of the pilot in response to sudden and unusual harsh movements of the aeroplane
7. Pilot’s inexperience: All Pilots (from Private Pilots to Test Pilots) should conduct more spins so as to gain (recovery) experience for the case of an unintended spin
8. Little knowledge: Flying instructors should be better trained in spinning and have more experience of flying spins (by conducting spinning in spin certified aeroplanes). Student pilots should be more thoroughly trained to be able to recover the aircraft from a spin.

9. Erroneous theories: Pilot training textbooks explain spinning in very general terms and often based on military fighter type aeroplane spin research which is not appropriate for civil aeroplanes. Thus the common ‘Theories’ are not entirely valid for civil pilots and some older or not ‘measured’ theories and ‘assumptions’ need to be revised.

Today’s state of the art Computational Fluid Dynamics (CFD) software tools, whether commercially available or developed in-house by companies, are not capable of accurately simulating the flow field around the aeroplane at high angles of attack, and should not be used to analyse flight conditions with airflows which have angles of attack above, e.g. +25°. This became very clear when the author contacted a leading national aerospace research centre in preparation of this research project where he met their leading CFD specialist. Due to this information, actual flight tests need to be conducted to support the understanding of the complex flight physical effect of spinning.

The selection of the utilised aeroplane (Fuji FA-200) is based on the fact that modern General Aviation fixed wing aeroplanes below 2000 kg maximum take-off mass are mainly low-wing aircraft. Other aircraft examples are Piper, Aquila, Ruschmeyer, Cessna 400 (Columbia), Cirrus, Grob, Socata, Pipistrel (Panthera), and Evektor (Cobra). Due to this trend it is of major relevance for this research project that the utilised aeroplane resembles the aerodynamical and flight mechanical characteristics of the majority of modern aeroplanes.

1.4 Aim of the study

The aim of this research is to improve the current understanding of aeroplane spin behaviour. This is achieved by using actual flight test data to understand the effects on the aircraft and pilot of the major spin parameters, to develop, where possible, new relations to describe this complex motion mathematically and from the research outcomes, to derive practical assistance for flight test engineers, aeroplane designers, test pilots, flying instructors in their working areas.

Spin research has currently been conducted at only a few institutions, some using single-engine, low-wing aeroplanes as used in civil aviation. In this study, the Fuji FA 200-160 aircraft is used to gather the flight test data. This is a rugged basic training aeroplane capable of conducting aerobatic manoeuvres. A data acquisition system is installed in the aircraft which is then flown for 27 recorded spins. The type of spin manoeuvre undertaken has a well-known recovery procedure, already known to the author who has practiced this recovery whilst on test pilot courses and on actual certification test programmes.

The spin test programme is designed to systematically change relevant spin parameters such as the centre of gravity position and the aeroplane mass (Chapter 4). With the

obtained flight data a mathematical model of the subsequent variation in the pitch angle of the aeroplane is generated, backed up by physical justification, using forces and moments, of the aircraft's change in attitude with time (Chapter 5 (Spin description). The corresponding data analysis (including the mathematical model of the pitch angle behaviour) and results are presented in Chapters 6 (Spin test data analysis & Appendix 7), 7 (Flight test data comparison), 8 (Conclusion).

1.5 Research questions and subsequent observations

The following questions and observations are core topics of this research work and they are also pivotal questions for the understanding of generalised spinning.

Research Questions:

1.) How will changes of the aeroplane's mass and the position of the Centre of Gravity affect the spin behaviour (i.e. phases of a spin) and the output flight parameters (i.e. motion and attitude) of an aeroplane?

2.) What are the parameters which characterize a spin in motion? What are the relationships between these characteristic parameters?

3.) Where are the differences between real measured spin test data and the traditional spin theories in a spin situation? Are the traditional spin explanations correct?

4.) Which mass and centre of gravity value combinations makes a spin faster and thus confuses the pilot more so that a recovery is more likely to fail?

5.) Is the spin behaviour of a given conventional low-wing, single-engine aeroplane design reproducible or random?

Out of these basic research questions the following observations have been developed which will be answered in this thesis:

1. The second minimum value of the pitch down (ln_Theta) angle always has the highest negative value.

2. Independent of the aeroplane's mass and CG position, the pitch angle (ln_Theta) tends to a characteristic value.
3. Maximum yaw rate (ln_r) changes with CG position and mass
4. The yaw rate (ln_r) oscillation changes with CG position and / or mass.
5. The maximum difference in angle of attack (AoA) values between left and right wings leads to a maximum in roll rate values (alpha_le_c – alpha_ri_c; ln_p).
6. Roll rate (ln_p) changes with CG Position and the aeroplane's mass.
7. Total angular velocity, Ω, changes with CG position and mass.
8. Recovery time becomes shorter with CG moving in the direction of the tail.
9. The spin behaviour of the Fuji FA 200 – 160 can be generalised for single-engine low-wing aeroplanes.

1.6 Preparation for the Flight Testing

The Author became involved with spin testing when conducting an actual certification spin test programme during the Aquila A-210 basic trainer flight test phase as test pilot. Further spin test experience has been gathered while running an EASA (European Aviation Safety Agency) Approved Training Organisation (ATO) for flight training with an aeroplane which is certified for spinning, and conducting spin training in the role of a Flying Instructor and Senior Lecturer with University students in Northern Germany. On starting these doctoral studies, the author attended an additional spin course at the 'National Test Pilot School', Mojave Desert, USA in order to build up further spin experience and as a safety measure. The Author has also been an Aircraft Accident Investigator at the German Authority 'Bundesstelle für Flugunfalluntersuchung' where he was responsible for investigating some spin related aircraft accidents. The author is also a member of the Metrology, Measurement and Instrumentation Laboratory at the University of Applied Sciences in Osnabrueck. This specialises in the acquisition, processing and analysis of measured experimental data.
A flight-test proven measurement system was provided by the company 'Messwerk GmbH'. Company staff have conducted several research projects in recent years, thus not only the measuring system but also the expertise for installing and calibrating the system was at hand.

1.7 Structure of the Thesis

After the introduction of Chapter 1, a review of the state of the art of spin research is provided in Chapter 2 concentrating on low wing, single engine aircraft. Spin theories are discussed and sources of spin data (flight test, numerical and experimental) identified.

Most spin research is stored in the archives of institutions such as NASA, ONERA, DLR, AIAA, and the RAeS.

The chosen measurement system, its sensors, the data acquisition, and the installation of all measurement components in the research aeroplane are detailed in Chapter 3. Information on the calibration of the different sensor systems and fuel gauges is provided in Appendix 6.

In Chapter 4 are described the choice of the investigated parameter(s), the mass and balance envelope of the aeroplane and the flight trial procedure and conditions including the legal basis for such kinds of flight testing. Also the modifications and special inspections to the aircraft to install the flight measurement system are provided.

Spin motion involves a number of influential parameters. The resulting integrations and test data analysis procedures are presented in Chapters 5. A step by step spin description is provided of the time-dependent forces and moments which explains the influence of the investigated parameters on each other. This is an important contribution to the understanding of spinning because such a detailed explanation has not been published before.

In the context of this research project the fully developed spin will be the main interest. In addition to that some investigations concerning the spin entry and the recovery phase will be conducted. In Chapter 6, the post-processing of the flight data is detailed. This includes a mathematical model for the description, evaluation and processing of the pitch behaviour of the aeroplane (see also Appendix 7). The pitch angle is the most significant parameter in the spin trajectory. This is followed by a description of the statistical methods used to post-process the rest of the flight data.

The work presented in Chapter 7 concerns examining the results in the light of the traditional spin theories and additionally comparing them to spin test data of other single-engine, low-wing aeroplanes. This section answers how generalisable the research findings from this thesis are.

Chapter 8 gives a detailed summary and conclusions as well as the impacts of the present work for flight testers, designers and the flight training community with practical recommendations and safety advice.

Recommendations for further work can be found in Chapter 9 which is followed by the References and Bibliography in Chapter 10. The work finishes with Appendices which include explanatory material linked to the Chapters.

A flow chart of the structure of the thesis is presented in Figure 1.2.

Spin dynamics of single-engine low-wing aeroplanes

What:
Derivation of the research questions

Flight accident investigation: ~ 60% of all flight accidents involve spinning
- Based on scientific paper
- Own experience as flight accident investigator

Certification specifications do not require deep understanding of spinning
- CS / FAR 23

Who:
Did when, where and why, what

Specific **literature review** / State of the Art
- Based on NASA scientific paper, Test Pilot school material, other sources

How:
Conduction by instrumentation / measurement

Flight test instrumentation of a conventional aeroplane
- Fuji FA 200
- Proven high quality measurement system

How:
Conduction by Flight Tests

Systematic **flight testing** and data gathering
- Inside and outside the certified flight envelope
- Relevant flight mechanic parameter

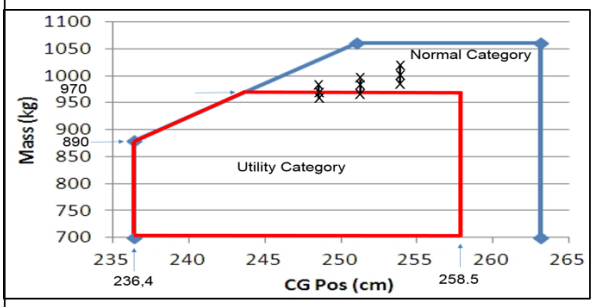

Certified flight envelope

Altitude related	Hbaro	Hpunkt		
Airspeed related	TAS_r			
Relative wind related	Alpha_le_c	Alpha_ri_c	Beta_le_c	Beta_ri_c
Acceleration related	X direction	Y direction	Z direction	
Angular related	In_Phi	In_Theta	In_Psi	
Angular rate related	In_p	In_q	In_r	
Control surface related	Eta_ca	Xi_le_ca	Xi_ri_ca	Zeta_ca

Used flight mechanical parameter

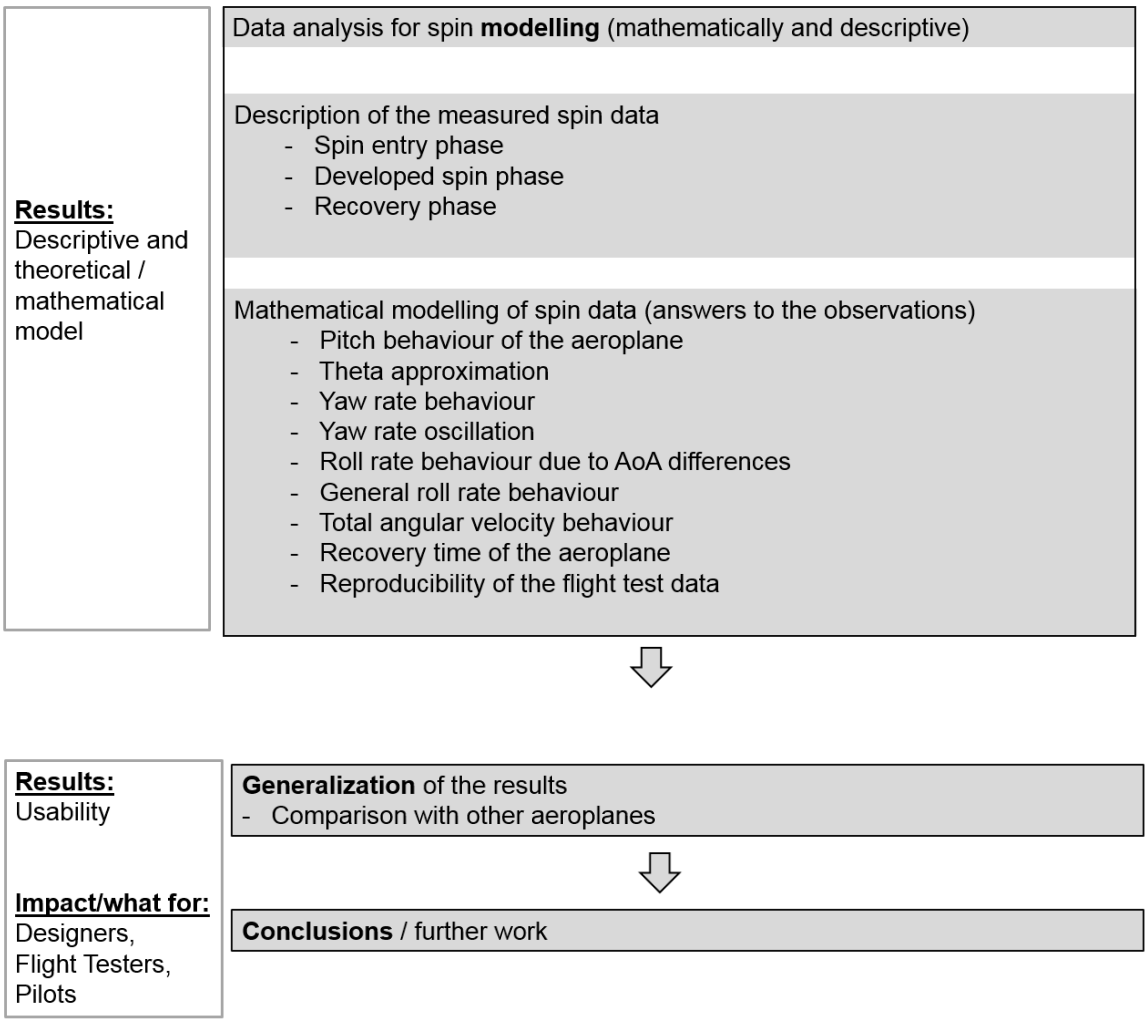

Figure 1.2: Flow pattern of the structure of the work

1.8 Contributions to state of the art / research

The first contribution concerns the interpretation of the centre of gravity's effect on the spin behaviour of the aircraft. This prediction is the opposite of some current thinking from literature.

The second contribution is the development of a set of relevant flight parameters which govern the spin behaviour of an aircraft. This set is more comprehensive than previous studies. The parameters and their subsequent in-flight values and behaviour can be used to predict the spin behaviour of an aircraft. This parameter design space can be used by aerospace engineers to assist the design process of a new aircraft or the modification of an existing aircraft. A particular achievement of this investigation is the prediction of the value for the final pitching angle.

The third contribution is the development of an effective methodology for processing the time dependent, noisy, real data generated by an aircraft's in-flight sensor recording system into mathematical relations. Such relations not only assist understanding of the

flight behaviour of an aircraft but can be used for predicting behaviour in aircraft of a similar type.

The fourth contribution relates to understanding how during a flight, the chances of going into a spin vary, as does the behaviour of the aeroplane, its stability and the perceptions of the pilot. Such information can be incorporated in future into aircraft spin prevention systems.

The fifth contribution concerns the proof that spin predictions can be generalised within the general aviation set of aircraft for low wing aircraft, even when the tail configuration is different. Different tail configurations do have different stability characteristics and rudder effectiveness proportional to their unshielded surface area.

To start the investigation, an analysis of the state of the art of spin studies is presented in Chapter 2.

Chapter 2 Literature review

2.1 Introduction into the literature review

Research into spin flight dynamics has been conducted since around 1912 (Martin et al, 1988) when the first report of a spin was recorded as “Parke’s dive” and only two spin accidents were recorded prior to the First World War. The first aviator who was able to demonstrate a method to recovery from such a Parke´s dive was Harry G. Hawker. He, together with Sopwith and Sigrist founded the Sopwith Aviation Company at Brookland (UK) in 1912.

The largest contribution of research on aircraft spinning was conducted between 1960-1990 by NASA’s Langley Research Center (e.g. Ranaudo, 1977 and Stough et al, 1985). However, since then, research activity has been low due to legal restrictions on pilots to fly in such regimes (i.e. avoiding stall and spin situations). Although this action has succeeded in reducing the number of spin related accidents, it has also reduced the interest in finding out more about this phenomenon as well as reducing the requirement for an aeroplane to show the capability to be recovered from a spin (USAF, 2000). Recent papers on spinning have focussed on unmanned drones (e.g. Gill et al, 2015)

Over 9000 papers, related to aircraft spinning, from different Institutions and sources have been examined for this review. These sources are categorised into the following topics:

- The physics of spin manoeuvres
- Spin flight-testing and flight test data acquisition for single-engine low-wing aeroplanes
- Human factors related to spinning
- Wind tunnel tests
- Manuals for flight test pilots
- Free spinning model aeroplane testing
- Free spinning fighter aeroplane testing
- Generic large transport aeroplane spin modelling
- Anti-spin parachutes
- Anti-spin rockets
- Spin resistant aeroplane
- Wing leading edge modifications
- Spin history

The first three categories are of direct interest to the research questions covered in this thesis. The following sections concentrate on spin cases for which the pilot has influence on the aeroplane’s behaviour, i.e. loss of control situations are not studied here. Also Unmanned Aerial Vehicles or drones are not considered in this study. The intention is to

understand the situation leading up to this dangerous situation so that loss of control can be avoided. Spin recovery devices are also not part of this research project as the test aircraft used for this project does not have such a device. The predominant approach to the investigation of spin has been conducted using spin tunnels and by constructing mathematical models of spin. These approaches have given great insight into the problem but do not model the whole phenomenon. In this thesis, the flight tests provide the primary data source with mathematical and numerical models supplementing this work and used to interpolate and extrapolate the flight test findings.

2.2 Civil and military spin training material

Flight training sources contain the main source of information on spinning provided to pilots (e.g. Air Ministry (1995), Kredel (1998), FAA (2004 & 2008)). Global civil flight training does not cover the subject to the same depth as military sources. However, as many military pilots transfer into the civil aviation sector to become commercial flight instructors or pilots, their military training influences how they perceive and react to any potential spin conditions even when flying commercial aircraft. Most military flight training manuals are not in open literature; but the UK military flight training system is one of the most developed in the world and the basic flight training material (Air Ministry, 1995) is available. This source defines a spin, and describes the different spin phases and the sign conventions of the velocities, forces and moments during a spin (see Table A1.1 & Figures A1.1 & A1.2). It also provides a general understanding of the effects on spin of damping, angular momentum and moment of inertia as well as control surface movement. Finally the source reflects on the spin recovery. Neihouse et al. (1957) commented on their spin flight test results that spin recovery measures should be implemented immediately and not allow the aircraft to settle into a developed spin. Flight training manuals do not refer to flight test results, specific aircraft geometries, control surface shielding, human factors or flight parameter behaviour. Some flight manuals limit their explanations of spin to advice on preventing the aircraft from entering this condition (FAA, 2004). For example the FAA (2008) advises that ‘since spin recoveries are usually effected with the nose much lower than is common in stall recoveries, high airspeeds and consequently higher load factors are to be expected’. Thus spin training is not offered to pilots in a precise fashion and this leads to some pilot´s actions being wrong or not useful in a spin situation.

The Aeroplane Flight Manual of the Fuji FA – 200 – 160 (Fuji Heavy Industries, 1971) is the official handbook of the aircraft used in tests for this research. The handbook is based on flight test data which have been determined during the aircraft’s certification programme. This source is vital for this research as it provides the limits of the aircraft so that flight tests can be developed within these limits. The aeroplane is approved for

spinning for up to six turns within only the aerobatic and utility category envelope. In the Aerobatic category with flaps up the aeroplane is allowed to reach a maximum acceleration of +6.0 g in the z-direction of the aeroplane. The spin manoeuvre steps and the recommended recovery procedure are given in section 4.8. The given acceleration ranges are [-4g, 6g] keeping the aircraft below the "design manoeuvring speed", V_a, and the engine RPM below the maximum permitted value. For manoeuvres outside of this g-force range, the aircraft structure is over-stressed.

2.3 The phases of a spin

A spin is defined as consisting of three phases: incipient spin, developed spin and recovery (Air Ministry, 1995). The incipient phase ends after 2 turns (FAA, 2004), then the developed phase starts when the angular rotation rate, airspeed, and vertical speed are stabilized (i.e. constant) while the flightpath is nearly vertical (and affected only by the wind). This is when the aeroplane's aerodynamic forces and inertial forces are in balance, where the attitude, angles, and self-sustaining motions about the vertical axis are constant or repetitive.

The recovery phase (FAA, 2008) is a multi-step procedure for the pilot consisting of reducing the power (throttle) to idle; positioning the rudder against the turn direction and the ailerons to neutral, elevator a little forward and ending with applying back-elevator pressure to raise the nose to level flight.

2.4 Measurement techniques for spinning

There are a variety of measurement techniques which have been used to gather spin data and increased understanding of the phenomena (Figure 2.1).

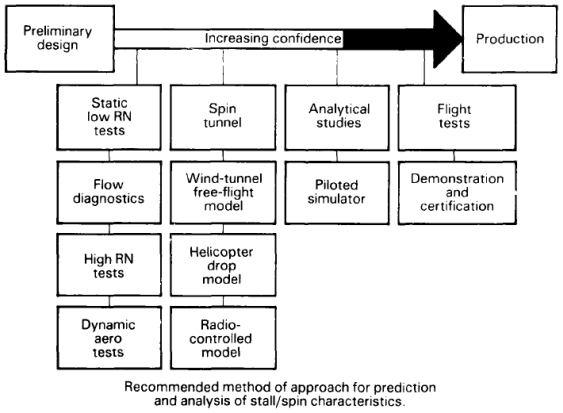

Figure 2.1: Recommended methods to predict stall/spin characteristics (Martin, 1988)

2.4.1 Experimental measurements

Within the available measurement techniques, there is a subset of experimental techniques used to model spin (Figure 2.2). The dynamic model and rotating model

techniques are most commonly used for aircraft development programmes. Dynamic spin model testing facilities include NASA Langley Research Center (e.g. Neihouse et al, 1957) and IMF Lille in France (Gobeltz, 1959). The technique involves launching a dynamically scaled model (i.e. a model with geometric and mass distribution similarities to the real aircraft) into a vertical airstream so that it freely spins, and then recording on video the steady spin behaviour and spin recovery following actuation of controls. Analysis of the recording gives the rate of spin, angle-of-attack, sideslip angle and spin recovery times for the given combination of pro-spin and spin-recovery control settings. One disadvantage of spin tunnels is that the model is tossed into the spin tunnel "much as a Frisbee is launched" (Woodcock & Weissman, 1976) and this action does not determine entry characteristics or is able to mimic real entry conditions. As entry conditions determine the spin characteristics of the subsequent flight path, this makes comparison with real data difficult. Another disadvantage is that windtunnel corrections (e.g. wall effects) are not always fully known as a function of changing Reynolds number (i.e. changes in speed and model length changes).

Spin prediction techniques

Technique	Spin entry	Incipient spin	Steady spin	Spin recovery
Empirical design criteria				
Dynamic model in spin tunnel			NASA Langley	IMFL Lille
Rotary balance technique	NASA Langley/Ames, Aeromacchi B. Aerospace RAE., IMFL Lille			
WIND TUNNEL (FREE FLIGHT)	NASA Langley			
Catapult model technique	NASA Langley, IMFL Lille			
Helicopter drop model	NASA, RAE, ARL			
Powered radio controlled model	NASA, Aeromacchi			

Figure 2.2: Summary of spin prediction techniques (Martin, 1988)

Neihouse et al (1957) used spin tunnel tests to investigate the effectiveness of control during spins and recoveries, the influence of long noses, strakes, and canards on spin and recovery characteristics, and the correlation of (mostly military jet type) aeroplane and model spin and recovery characteristics. Two trainer type aircraft were used but no numerical data is presented. Results indicate that spins and spin recoveries can be conducted in spin tunnels such that the obtained data is of reliable accuracy. Descriptions of the conclusions of spin models in flat, normal, inverted spin and uncontrolled dives, extrapolated to full – scale aircraft are given in Gobeltz (1959) but no data was released from this study.

In a comparison of results of the Langley spin-tunnel investigations against flight test results from 60 different (unspecified) aeroplane designs (Berman, 1950), reliability checks on developed spins and recovery characteristics were conducted. The corresponding data analysis shows that model tests do predict full – scale recovery characteristics up to 90 % of the analysed cases 'satisfactorily'. The remaining 10% are valuable contributions to predict some of the details of the full – scale spins.

When a model is spun at angles of attack less than 45°, the corresponding aeroplanes spun at larger angles of attack; and when the same models were spun at angles of attack greater than 45°, the corresponding airplanes spun at smaller angles of attack.

Also when the tail – damping ratio is greater than 0.02, Berman's models spun with higher rates of rotation than the airplanes; and when it was less than 0.02, the models spun with lower rates of rotation. The tail damping ratio is:

$$TDR = \frac{FL^2}{S\left(\frac{b}{2}\right)^2}$$

Where F is the total fixed area below the horizontal tail, L is the distance from the centroid of area F to the centre of gravity of the aeroplane, S is the wing planform area and b is the wingspan (tip to tip). (Seidman & Donlan, 1939)

The corresponding spin tunnel models also show less altitude losses per spin revolution than the full – scale aeroplane. It was observed that the full – scale aeroplane spins with the inner wing more down than the corresponding spin-tunnel model. Another contribution to spin research comes from Bowman (1971) who used 100 different dynamically scaled general aviation designs (all unspecified) in a spin-tunnel and showed partial correlation with full – scale spin tests. Bowman speculates that important factors for spin recovery include rudder and elevator sizes, tail damping power factor, centre of gravity position, and asymmetric power. However only test results for wing loading and tails are presented. Stough et al. (1987) showed that there were noticeable differences in behaviour between spin tunnel models and the actual aeroplane in flight at low angles of attack, e.g. one configuration indicating that a flat spin would occur, whereas in the actual flight test, this condition was not found.

Rotary balances have been installed in vertical spin tunnels (e.g. Denham & Owens, 2016) and conventional horizontal wind tunnels (e.g. Sohi, 2004). These balances have been used mainly for studying the high angle-of-attack departure problems of combat aircraft and spin behaviour. Rotary balance testing for spin prediction has the following advantages, that:

- Aerodynamic force and moment coefficients are determined.

- The model can be tested with components removed enabling their direct and interference effects to be investigated.
- Changes to the forces and moments can be measured as the model shape is changed.
- When this aerodynamic data is available, the steady spin conditions can be calculated (using the steady spin equations of motion) for a wide range of centre of gravity, inertia, and altitude changes.
- Although the rotary balance technique does not provide all the information required to predict spin recovery, an indication of recovery control effectiveness can be determined and this, coupled with the insight afforded by the method, enables estimates of the recovery capability to be made.

The remaining four techniques listed in Figure 2.2 involve free-flight testing of scale-models. The drop-model technique using approximately 1/4 scale-models has been employed in the U.K. and U.S.A. for investigating the high angle-of-attack behaviour of combat aircraft (Martin, 1988), and has the potential to cover all 3 phases of the spin (see Section 2.3). However drop tests are only used for major projects due to the high cost of manufacturing, staff and operation. While spin design requirements are extremely important for many aircraft, spin testing facilities and spin research activities are confined to a small number of aeronautical establishments.

Although the data from the experimental techniques mentioned above is useful for qualitative understanding of spinning, quantitative comparison is not possible unless the scaled model has the same mass distribution as the real aircraft, and such models are in the minority for windtunnel tests, as well as knowledge of critical Reynolds numbers, and tunnel correction factors (Neihouse at al., 1957).

2.4.2 Theoretical models

2.4.2.1 Force and moment models

Theoretical models of spin have been developed to investigate design effects on spin recoveries, spin stability modes, influences of tail configurations and mathematical attempts to predict spin behaviour. The models are based on the six-degree-of-freedom equations of motion from Newtonian physics, i.e. three equations for predicting the forces (x, y and z) and three equations for moments (x, y and z). These models have then been adapted for a steady state circular spin motion starting with Lindemann et al., (1918). Some models are linearised through small perturbation theory (Brown (2002), Adams (1972)) which is the standard procedure for conventionally behaved passenger aircraft

movements; other theoretical models retain the nonlinear terms (Martin, 1988) for describing more demanding movements such as high angle of attack, aerobatic and military manoeuvres, and for all rotorcraft manoeuvres. With the linearised approach the longitudinal motion (such as pitching) is separated from the lateral and directional equations (for roll, yaw and sideslip). However for spin cases this decoupling is not appropriate so the more complicated nonlinear equations are solved (computationally). The mathematical notation is given in Table A1.1 and the spin equations are given in Appendix 1.4 for the forces and Appendix 1.8 for the moments. Gates and Bryant (1926) published a comprehensive survey on spinning in which the equation required for calculating equilibrium spins were presented. Pamadi (2004) includes the effects of fuselages and tails in his model.

Mainly fighter–type aeroplane configurations have been investigated within this field (e.g. Brown (2002), and Adams (1972)). Brown (2002) includes the modelling of the engine gyroscopic effects and high angle of attack effects. The report also contains a discussion on the prediction of stall behaviour; remarks on the selection of stall test points and stall test manoeuvres; the discussion of stall model validations and its corrections.

Adams (1972) concentrates on identifying stability characteristics, so the values of the angle of attack, sideslip and angular rates for which a spin is stable in its helical motion, concluding that there 'is a need for higher Reynolds number data taken under conditions which more accurately simulate a spin'. By solving differential equations for the stability motion using a minimisation technique, the parameter values for the stable cases are found. Investigation is then made in the vicinity of these stable parameter configurations. The execution of tests to determine the critical angle of attack and the stalling speed as well as the way in which test data can be analysed is shown. The paper uses flight, drop-test, windtunnel, spin tunnel and computational data but the flight data given only provides an estimate of the aeroplane's rotation rate. The data analysis given in this thesis takes fewer spin types but compares more parameters than in the papers referenced above.

Use of these mathematical models requires specific input values at the start of the sortie and throughout the spin trajectory. These include values of the lift and drag coefficients for the specified aircraft at its particular attitude at each point in time. These coefficient values cannot be calculated theoretically due to the stalled nature of the flow. Thus theoretical models can only be used accurately if flight data is supplied.

2.4.2.2 Area models for spin safety

Seidman & Donian (1939) derived a quantitative criterion for aeroplane designers to predict spin behaviour of new aeroplanes in a generalized form. The method involved the use of projected side areas of the proposed aircraft and its three-dimensional mass distribution. From this method the aeroplane designer can derive a rough spin

characteristic for the new aeroplane. The method was tested on results generated in a free spinning tunnel. With this work a simple approach – which is based only on the specific aeroplane's dimensions of the tail section - has been derived to estimate whether the aeroplane under question will meet the minimum requirement for spin safety. The results were verified by actual spin flight tests. Note that for real aircraft the mass distribution in terms of the longitudinal direction is usually not known.

2.4.2.3 Computational programmes for modelling high angle of attack cases

Computational fluid dynamic (CFD) models have had great success in the last decades with flow accuracy equivalent to (if not better in certain cases), that obtained from appropriately corrected windtunnel results. However this success is for pre-stall angles of attack and standard (i.e. affordable) turbulence models. For some industry and commercial CFD packages, predicting the correct stall angle is difficult (Moens et al., 2007) whereas others have predicted the stall angle well but the accompanying drag values have been in error by at least 10% (Jansson et al., 2018). The development of the Zonal Detached Eddy Simulation turbulence model with mesh adaptation is producing correct stall prediction and lift, drag and pressure values within 1% of that measured experimentally at stall but only for 2D cases (Ray & Ballmann, 2018). For angles of attack above the stall prediction some success has been attained in 3D by Rahman et al. (2013) at 44 degrees and Forsythe et al. (2002) up to 65 degrees where CFD results are within 10% of measured data. The state of the art in CFD models is such that it is not mature enough to produce accurate flow results at very high angles of attack such as encountered in a spin.

2.4.3 Flight Tests

The first scientific measurements on spinning were conducted by Lindemann, Glauert and Harris in March 1918. Lindemann stated later that the stresses are not dangerous in a proper spin and that experimental results indicate that this is a stable form of motion. Spin flight test procedures have since then been more rigorously developed (Lawless at al. (1999), Brown et al. (2002), Ambros & Seidler (2013)).

Brown et al. (2002) considers a framework for stall and spin tests where test points for spin analysis are chosen, and an approach for characterization and evaluation of departures and spins, as well as validation methods for departure and spin models, are explained. The paper deals only with fighter type aeroplanes which behave differently to the category to which the Fuji FA-200-160 aircraft belongs, due to its aeroplane mass, CG positions, aerodynamic shape, and multiple pylon configurations.

The position of the wing on the fuselage affects the spin characteristics of the aircraft, as discussed in the next two sections.

2.4.3.1 Low wing aircraft

Uncovering the incipient spinning characteristics of an aeroplane are an important aspect for understanding the relation between design and behaviour. Ranaudo (1977) undertook flight tests using a Beech aeroplane where the centre of gravity was held constant. Control position transducers and a rate measuring system were installed, as were angle of attack and angle of sideslip measuring vanes; and a wing mounted camera. The developed spin and recovery characteristics were not investigated. Some airflow observations at the aft fuselage, the vertical stabilizer and the rudder were added.

An important general aviation set of spin flight tests were conducted by Sliwa (1979) in a low wing research spin aircraft. Time history plots of the pitch angle and angle-of-attack data are presented (see Figures 2.3 and 2.4) for spin trials using 6 complete turns (note the 6 oscillations in the mid-section of the two diagrams below).

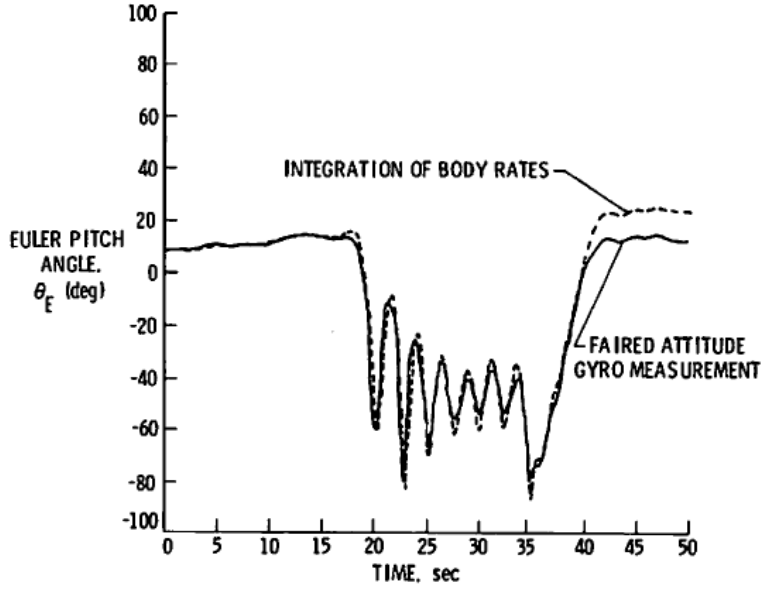

Figure 2.3: Aeroplane pitch attitude during a spin of 6 turns to the right obtained from gyro attitude measurement and integration of body rate gyro measurements (Sliwa, 1979)

Sliwa compared his measured data (“faired attitude”) for the angular rate of change with a set of equations for the same angular rate of change in terms of flight data. By substituting the flight values into the equations, he produced a consistent behaviour until spin recovery (Figure 2.3). However there is no discussion on the influence of certain flight parameters on the spin behaviour of the aircraft.

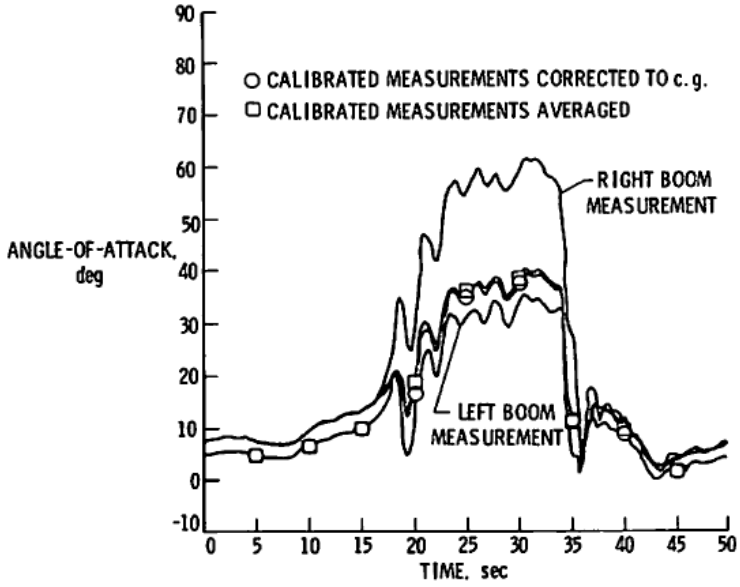

Figure 2.4: Angle-of-attack measurements during a spin to the right illustrating the effect of calibration and corrections (Sliwa, 1979)

As shown in Figure 2.4, the aircraft spinning to the right produces differential flow behaviour over the left and right wings with higher angle of attack values for the wing into the spin. (See chapter 5 for further explanations.)

As will be seen in later chapters, the Fuji FA-200-160 and a NASA research aircraft show corresponding spin behaviour. This, and the data comparison of Chapter 7, makes it likely that the spin behaviour of the Fuji, and thus the corresponding data behaviour and mathematical modelling results, can be generalised.

Sliwa's research concentrates on the measurement and correction methods used during 150 spin flight tests. The required correction terms for the measurement of body accelerations, body velocities, and aircraft orientation are presented. The equations of motion are utilized to derive total aerodynamic coefficients for comparison with model test and for analysis. Engine speed, manifold pressure and spin chute load were not measured during the Fuji flight tests as the engine speed was always idle (700 RPM). Note that the manifold pressure and a spin chute are not available or installed at the Fuji FA–200-160. Control force cannot be measured without interfering with the aeroplane's control system. This is not allowed by EASA.

In contrast to other studies, spin flight tests were conducted (Stough et al., 1985) only at aft centre–of–gravity positions in combination with different flap deflections, landing gear positions and engine power settings. The aircraft used was a single–engine, low-wing, T-Tail configuration. Most of the normal stall situations resulted in a 'roll off' (wing drop). It was noted that by selecting pro-spin control inputs, the aeroplane entered a spin with an average angle of attack of 43° while large oscillations in roll rate and pitch rate were

measured. Changing the aileron deflection into the spin direction caused the amplitudes of both oscillations (roll and pitch) to increase whereas applying an aileron control input against the spin rotation resulted in the amplitudes of both oscillations decreasing.

D. R. Riley (1985) compared results from flight tests and a six degree–of–freedom nonlinear simulation for a two–seat, single–engine, low–wing general aviation aeroplane for the stall and initial spin phase. Two configurations, one with and one without an outboard wing–leading–edge modification (a droop nose), were modelled. Comparisons of the trim characteristics and dynamic response results for straight, turning, and side slipping flight show that at high angles of attack for the configuration with the wing–leading–edge modification, the aircraft was able to fly at lower speeds with greater controllability compared to the original configuration. Time history traces following elevator–ramp inputs showed slower, smoother and thus easier to control, departure characteristics for the modified configuration. Power effects were significant for both configurations. The results show that wing–leading–edge modification does have a positive influence on spin control.

A Slingsby Firefly aerobatic light aircraft was subjected to a two–turn spin (Hoff et al., 2012). A visual tracking system was used to capture the motion and airflow. Wool tufts were used on the wing, fuselage and empennage. The tufts indicate that a large vortex forms over the outer wing. It was observed that there was a correlation in the spanwise motion of the vortex compared to the aircraft's spin motion. Furthermore, tufts on the horizontal tail indicate the presence of a leading edge vortex with the flow mainly in a spanwise outwards direction. The effects observed are three dimensional and time dependent. Finally, it is discussed how this new knowledge does not correspond with the spin theories of the past.

Spin tests on two light aircraft were conducted by Cichocka (2017) and comparison of the flight test results with the MIG 15, MIG 17, and MIG 21 was made for the roll rate. Unfortunately the approach to the actual spin tests was not provided and a limited set of parameters were recorded.

2.4.3.2 High wing aircraft

Results of instrumented flight tests of the stall and spin characteristics of a modified, single–engine, high–wing light airplane were conducted by Stewart et al, (1982). As the propeller turns to the right, entering a spin to the left is easy. However spinning to the right is difficult due to the propeller's moment and the low centre of gravity position in relation to the wing. Where spins were obtained, the aeroplane had a relatively steep spin mode (low angle of attack) with a high load factor and high velocity. The aeroplane recovered almost immediately after any deviation from the pro-spin control position, except for one manoeuvre with deliberately reduced deflection angle of the elevator control system.

Normal control deflection angles, especially in the elevator system, were found to influence the spin characteristics, possibly causing the aeroplane to make a spontaneous transition to a spiral dive.

2.5 Effect of Aeroplane shape on spin behaviour

The effect of aeroplane shape on spin behaviour has been studied by some researchers. For example, the flow behaviour around an aircraft tail when spinning has been looked at, e.g. Sliwa (1970). Spin studies on fighter and transport category aeroplanes have been undertaken. However such aircraft categories have considerably different masses, mass distributions and geometries compared to the utilised test aeroplane (of the Fuji FA-200-160).

2.5.1 Wing leading edge changes

Altering the wing leading edge has been used by a number of research teams to investigate the effect on spin behaviour. Stough et al. (1987) used a low wing single engine T-tail light aircraft with amended outboard wing leading edges. Stalls and attempted spins were performed for various weights, centre–of–gravity positions, power settings, flap deflections, and landing–gear positions. According to the authors 'both stall behaviour and spin resistance were improved (smoother behaviour and ability to enter a spin is reduced) compared with the baseline airplane. The baseline airplane would readily spin for all combinations of power settings, flap deflections, and aileron inputs, but the modified airplane did not spin at idle power or with flaps extended. With maximum power and flaps retracted, the modified aeroplane entered spins with loadings exceeding the maximum recommended values. The modified aeroplane tended to spin at a higher angle of attack than the baseline aeroplane. Amended leading edge shape studies have also been used in conjunction with formulating certification regulations (Riley (1985), FAA (2001 and 2017)).

2.5.2 Control surface effectiveness

Control surface behaviour is also seen as influential to spin recovery, e.g. "only the rudder deflection against the turn direction in conjunction with a forward CG can help to stop the spin" (Berlin Flight Training, 2005), which also states that 'ailerons do not have any influence on the spin'. The general aviation aircraft studied had a relatively equal loading over their surface, whereas Bowman (1971) studied cases (in the same aircraft category) with heavy loadings on the fuselage, and in those cases ailerons were the primary method of recovery control.

Stough et al. (1985) conducted a series of test flights for different engine power settings, flap deflection angles and landing gear positions. They concluded that such geometric changes did not influence the spin characteristics significantly. Furthermore it was seen that anti-spin rudder deflection followed by an elevator control input in the forward direction is the fastest and most effective recovery procedure. In addition the initial application of these recovery control inputs did not always stop the spin motion but over time the spin was stopped. The spin recovery method of Stough et al. has been applied to the spin tests discussed later in this thesis.

2.5.3 Tail effects

Shielding has also been considered an important aspect of spin recovery due to its impact on the control surface effectiveness (Bowman (1971), Brinkworth (2015), Goraj et al. (2002)).The Fuji aircraft used in this thesis does not suffer much of a shielding problem due to the attitude developed in the spin tests.

Stough et al. (Feb. 1987) used four interchangeable tails on a single-engine aeroplane to study the effects of different tail geometries on spinning. So as not to influence the spins by mass and mass distribution effects, the same Centre of Gravity position and the aeroplane's mass have been maintained during the start of each spin. Typical parameters like airflow angles, airspeeds, accelerations, angular rates, control forces, engine power and altitude were recorded. The team noted that although different spin behaviours were observed with different tail configurations, no conclusions could be drawn concerning the vertical position of the horizontal tail or the size of the rudder. The conclusion of the paper was that tail designs cannot be used as sole criteria to define spin recovery characteristics.

2.6 Spin parameters

Early spin tests were conducted with analogue measuring systems which resulted in graphs and tables of mostly limited results for each parameter and few parameters measured. A well run early spin test investigation was undertaken by Soule and Sudder (1931), who collected spin data from several spins of two two-seater training aeroplanes. They used turn meters, accelerometers and a sensitive altimeter to record the aircraft acceleration, angles of turn, pitch and yaw; and the deflection angles of the elevator, rudder and aileron control surfaces.

The recent arrival of in-flight sensors linked to computerised storage systems have enabled greater accuracy (i.e. more digits recorded for each parameter value taken), the capacity to take many measurements per second and an increase in the number of parameters (and consequently a larger number of parameter permutations) that can be

measured. It is evident that such numerical tools bring a broader capability to spin research.

Many geometric and flight operational parameters affect the behaviour of an aircraft when it is in a spin condition. Such parameters include e.g. wing span; fuselage length; tail size and position; control surface sizes and positions; aircraft total mass; mass distribution in longitudinal and lateral directions; CG; entry speed; and air density. The large number of parameters has meant that a full set of experiments for every possibility of parameter change is too high to be practical and therefore most researchers have chosen certain parameters to investigate their effect on spin manoeuvres. Other parameters are the consequence of a spin, including e.g. the spin radius, sideslip, roll, yaw and pitch rates, moments of inertia, angular momentum, and vertical speed. Due to the circular nature of the aeroplane's spin path, the yaw, roll, sideslip angle and total angular speed are considered to be important characteristic parameters. Also since motion is governed by a set of forces and moments which rely on the angular relation of the aeroplane to its direction of flight, i.e. its attitude, the pitch angle and the angle of attack should be considered as important characteristic spin parameters.

Due to the different investigations, researchers have given opinions concerning the importance of certain of these flight parameters. For example, Brinkworth (2014) stated that the effect of yaw is a major influence on spin. Bowman (1971) stated that there are three factors of major importance during a spin. These factors are the density of the aeroplane relative to the density of the air, the mass distribution between the fuselage of the aeroplane and the wings and the design of the tail (configuration). He also showed that it was the mass distribution and the relative density of the aeroplane that really determines the tail design requirements and the control inputs necessary for the spin recovery. He created an empirically determined 'design factor' to interpret what would be a satisfactory spin recovery characteristic. Bowman's main conclusion was that the rudder is the primary control surface for spin recovery. Furthermore the elevator is highly effective in a wing heavy mass distribution and during the incipient spin phase. Whereas it is mostly ineffective during a fully developed spin, flat spins or in situations in which the mass distribution has been changed to a fuselage heavy or zero loading condition or the centre of gravity position has been shifted.

The FAA (2008) handbook states that 'Airspeed in a spin is very low, usually within 2 knots of the unaccelerated stalling speeds', and: 'the aircraft pivots, rather than turns, while it is in a spin'.

Kredel (1998)'s flight training manual, which was written for normal pilot training in all types of commercial aircraft within the designated flight envelopes, states that 'during a spin the aeroplane's pitch angle is 60° - 70°' and 'if the CG is too far aft the effect of the tail section

is not sufficient to get the aeroplane into a steep downwards pointing position. In this case the aeroplane will get into a flat spin'. (Note that the pitch angle for a flat spin is around zero degrees). Also that 'the recovery from a stall in any aircraft becomes progressively more difficult as its CG moves aft.' It will be seen later in this thesis (Chapter 6) that spin flight results do not agree with the first and third of these statements. In the case of the second statement ("too far aft") this is likely to apply to the centre of gravity moving closer to the aircraft tail than the neutral point, making the aircraft statically unstable (and illegal and unsafe to fly).

Similarly from FAA (2017) concerning two seater aircraft: 'an aircraft which cleanly recovers from a prolonged spin with the CG at one position may fail completely to respond to normal recovery attempts when the CG is moved aft by one or two inches'. Hence it is implied (Kredel (1998), FAA (2008)) that there is a limit to how far the CG position can be taken and the aircraft recovered from a spin. Neumann (2003) implies that even if you undertake flight testing no conclusion can be drawn as to the effect of CG on spinning. However, none of these sources provide any evidence to support these observations.

2.7 Spin Accident statistics / Safety

Spinning is often considered within the aviation industry as a cause of flight accidents (BFU (1985), Neumann (2002) and Pätzold et al. (2013)). For example, in the decade before 1985, 235 spin related accidents took place in Germany with 67 fatalities, including in 1983 when 13 severe accidents took place due to spinning. When considering severe flight accidents in Germany in this same period, 46% were due to spin accidents. If one takes glider flight accidents into account the number rises to 60% of all severe flight accidents. The pilots involved in such accidents were mainly pilots with more than 20 years of experience in piloting aeroplanes. The author to these statistics (BFU, 1985) asked how such trained pilots could be surprised into allowing their aircraft to fall into a spin scenario: "Did he know the slow flight, wing drop and spin characteristics of his aeroplane? Was he familiar with the correct countermeasures?"

A similar pattern was found with spin incidents (selected) of German test pilots between 1980 and 2010 (Neumann, 2002). The listed accidents happened during flight test programmes. All involved experienced test pilots, trained for spin tests and mentally and technically prepared for spinning. Nevertheless nine accidents took place.

From my perspective this shows that spinning is not just a special kind of stalling which can be counteracted with easy and straight forward recovery procedures. Spinning is a very complex and highly dynamic situation influenced by many factors. Unfortunately the state of understanding of spinning does not currently extend to predicting which factors influence any particular case.

A spin resistant aeroplane does not need to show that it is recoverable from a spin. Aeroplanes which are certified as ‘spin resistant’ do ‘produce’ more spin related fatal spin accidents than ‘normal’ aeroplanes. The reasons for this are that aeroplanes which are reluctant to enter a spin are also reluctant to recover from a spin (Pätzold et al., 2013) and that U.S. certification procedures are not consistent and do not cover all expectable operational stall and / or spin situations. This leads to actual stall / spin incidents which are not recoverable for (average) pilots.

2.8 Spin related regulations

Certification Specifications – whether in the U.S. or in Europe – are not only regulations developed by an Authority. These documents are also summaries of professional experiences normally made by test pilots, flight test engineers and scientists. These ‘living documents’ are under constant development supported by specific conferences, actual flight test experiences with new technologies - e.g. glass cockpits, envelope protection systems (even for smaller aeroplanes), etc. – and industry demands.

Compliance with the Federal Aviation Regulation, Part 23 (FAA, 2017) and the Flight Test Guide for Certification of Part 23 aeroplanes FAA (2011), EASA (2012), and appendices 2.7 and 3) show that an aircraft is legal to be flown. Section 8 of FAA (2017) deals with spinning in detail and explanations of spins (within different categories of aeroplanes - see Appendix 5), guidelines and procedures are presented. Constraints on the values of the aeroplane’s mass and CG position, moments of inertia and control deflections are given in terms of the aeroplane’s stability envelope.

Section 8 of the FAA regulations also provides information on the required instrumentation for the data acquisition, optional equipment and the possible influence of ‘complex instrumentation’ like wing tip booms or heavy telemetry systems on critical spin tests. This information was used in the development of the test programme for the Fuji FA-200-160.

Spinning outside a certified flight envelope belongs to a category 1 flight test which is – according to the current EU regulation (EASA, 2011b) - the most demanding kind of flight test. In order to conduct such a test, a pilot needs to possess either a category 1 or 2 flight test rating.

An example of applying the spin test regulations for a certification spin test is presented in this thesis in Appendix 2. The document was written by the author in 2003 to assist the development of a reasonable spin test matrix. The document advises build-up approaches (i.e. flying towards the extreme corners of the flight envelope and thus building up risk) regarding recovery characteristics of the aeroplane, the spin entries and recoveries, altitude effects, influence of: engine power; flap settings; abnormal control usage; and spiral characteristics.

2.9 Sources of human factors during spinning

Two aims of the research in this thesis are to improve flight safety and to reduce the number of necessary spin runs during an aircraft certification campaign. In this context the pilot is one of the most critical 'systems' which produce mistakes. A number of studies of pilot error in stall/spin conditions have been undertaken, e.g. Anderson et al. (1983) on supersonic fighter aircraft. The human factor problems investigated included:

(1) the pilot's inability to quickly determine if the aircraft is spinning out of control, or to recognize the type of spin (see thesis conclusions);
(2) unsatisfactory haptic and audio warning cues;
(3) the pilot's inability to decide on and implement the appropriate spin-recovery technique;
(4) the tendency of pilots to wait too long in deciding to abandon an unrecoverable aircraft;
(5) the pilot's inability to move, caused by high angular rotation.

It is point 1 that some of the research in this thesis contributes to.

It is considered that psycho-physiological phenomena influence pilot behaviour in stall / spin situations including:

(1) limitations in precisely controlling certain muscular inputs,
(2) inaccurate judgment of elapsed time,
(3) the focussing of sensory inputs, and
(4) disorientation of vestibular–ocular inputs, i.e. eye and head movements, especially in low visibility conditions.

One proposed solution to reduce the accident rate is the incorporation of flight envelope protection systems. However in so doing there is some reduction in manoeuvrability.

Chelette et al. (1990) investigated pilot induced accidents linked to spatial disorientation, especially studying the aircraft attitude as one of the main parameters, which indicates when an aeroplane can enter a stall, is the angle of attack. The study considered the possible illusions produced by the Vestibular Systems of the human body.

In this thesis, no data has been taken concerning the pilot's situation awareness but the spin results produced are used to assist the conditions that the pilot would have been subjected to.

2.10 Conclusions of the literature review

In this review, the most relevant scientific papers for topics which affect spinning have been considered. Despite spinning being a major cause of fatal aeroplane accidents, research has not yet established a full understanding of the phenomena. Published training material contains some generic advice to pilots who might find themselves in this situation. However some errors are apparent in this material. There have been some detailed experimental studies using windtunnels and spin-tunnels. However the studies have concentrated on certain aspects of the problem and results of these studies have not benefitted from modern accurate measurement systems. Thus there are many parameters which have not been fully explored in their impact on spin behaviour. Theoretical models have been developed which follow the idealised cyclical motion of an aircraft in a spin, but in order for these models to be accurate, they depend on flight measurements due to the stalled nature of the motion. Computational modelling is not yet capable of accurately predicting the flow at high angles of attack.

Flight tests have revealed that the aeroplane geometry, such as the position of the wing on the fuselage, leading edge shape, mass distribution, CG and potentially the shape and position of the tail, all affect the spin path and the ability of the aircraft to recover from a spin. However not only are there a large number of parameters, there have not been systematic approaches to investigating the available parameters and hence there are isolated results, e.g. one source reports the angle of attack tending to 43 degrees by the end of the spin.

The current flight test regulations provide constraints on the values of the aeroplane's mass and CG position, moments of inertia and control deflections in terms of the aeroplane's stability envelope. Thus these parameters are a suitable starting point for a rigorous, systematic set of flight tests.

In terms of the parameters that critically describe the characteristics of the motion: the pitch angle, angle of attack and angular rates are, from the mathematical models and flight/experimental tests, the most useful.

Chapter 3 Measurement system for spin test data acquisition

In the following sections the utilised measurement system will be explained in detail.

3.1 Introduction

For the required flight tests, a set of variables need to be recorded. In order to ensure that the correct measurement facilities were obtained with the correct precision, ranges and resolution; a set of requirements were identified (see below). The company messWERK was identified as having measurement facilities which were able to meet these requirements. Their system has been used during several certification flight test campaigns including spin testing. Therefore such a system has been acquired and fitted to the utilised aeroplane in November 2014. The entire installation and in-flight calibration of the measurement system into the aeroplane has been conducted by the author – supported by the help of a technician of the Osnabrueck University of Applied Sciences.

3.2 System Requirements

In the following the needed features of a reasonable measurement system are described.

3.2.1 What needs to be measured?

To measure the motion during a spin the aeroplane´s attitude and the flow direction of the surrounding air mass are the main parameters of interest. For that pitch-, roll- and yaw angles and the corresponding angular velocity need to be determined to specify a spin. In addition to that the angle of attack and the angle of sideslip have to be measured. Altitude losses and thus the vertical speed in relation to the aeroplane´s attitude need to be determined as well.

A spin is strongly influenced by the control surface deflection of the aeroplane. During the conducted spins the geometry – including the control surface positions- did not change. For documentation reasons the position of the corresponding control surfaces need to be measured.

To understand the accelerations and thus the forces on the aeroplane and the pilot a 3-D measurement of the accelerations need to be determined.

Parameters which are of minor interest are the aeroplane´s airspeed in the x–direction and - in the present case - the density of the air (including its temperature) because during a spin run those parameters will not change significantly.

In addition to the above parameters the system´s power supply should be documented to make sure the gathered data are consistent and not influenced by e.g. power fluctuations.

3.2.2 What precision is needed for the parameters of interest?

Because spinning is a highly dynamic motion a high precision of the determined data is needed. The following accuracies are standard in professional flight test environments (Cremer (2016a) – Cremer (2016f)) (all sensors are made for professional flight test tasks).

Parameter	Accuracies
Airflow sensors (angle of attack and angle of sideslip)	+/- 2°
Attitude angles	+/- 1°
Angular velocities of the aeroplane's attitude	+/- 1°/s
Altitudes and altitude changes	+/- 2 m
Control surface deflections	+/- 2°
Accelerations (in x, y, z-directions)	+/- 0.01 g
Temperature	+/- 1° C

Table 3.1: Required parameter accuracies of measured data

3.2.3 What ranges are needed for the parameters of interest?

Since spinning is a highly dynamic motion, high ranges of the utilised sensors are necessary. Table 3.2 lists the ranges that are standard in professional flight test environments.

Parameter	Ranges
Airflow sensors (angle of attack and angle of sideslip)	+/- 90°
Attitude angles	+/- 180°
Angular velocities of the aeroplane's attitude	+/- 500°/s
Static or absolute pressures for Altitude measurement	0 – 1100 hPa
Pressure difference	Depending on expected airspeed
Control surface deflections	+/- 45°
Accelerations	+/- 15 g
Temperature	+/- 50° C

Table 3.2: Standard parameter ranges in flight test environments

3.2.4 What resolution is needed for the parameters of interest?

For nearly consistent data a minimum of 10 Hz resolutions is needed. In the present case a sample rate of 100 Hz has been available, i.e. all parameters have been measured 100 times per second.

The developer of the measurement system (the company Messwerk GmbH) decided to use a data sample rate of 100 Hz to be able to detect signals below 50 Hz without aliasing errors. To make sure that the utilized input filter and the corresponding edge steepness of the filter lets only pass signals which are below this 50 Hz value an (analogue) input filter with a cutoff frequency of 33 Hz is implemented. The above mentioned values are standard values within the flight test sector because aeroplane responses (motions) and control inputs by a pilot are well below 33 Hz. This is not true for flutter tests. In these cases higher sample rates and filtering frequencies are used.

3.3 The Measurement System

An overview of the utilised measurement system is shown below

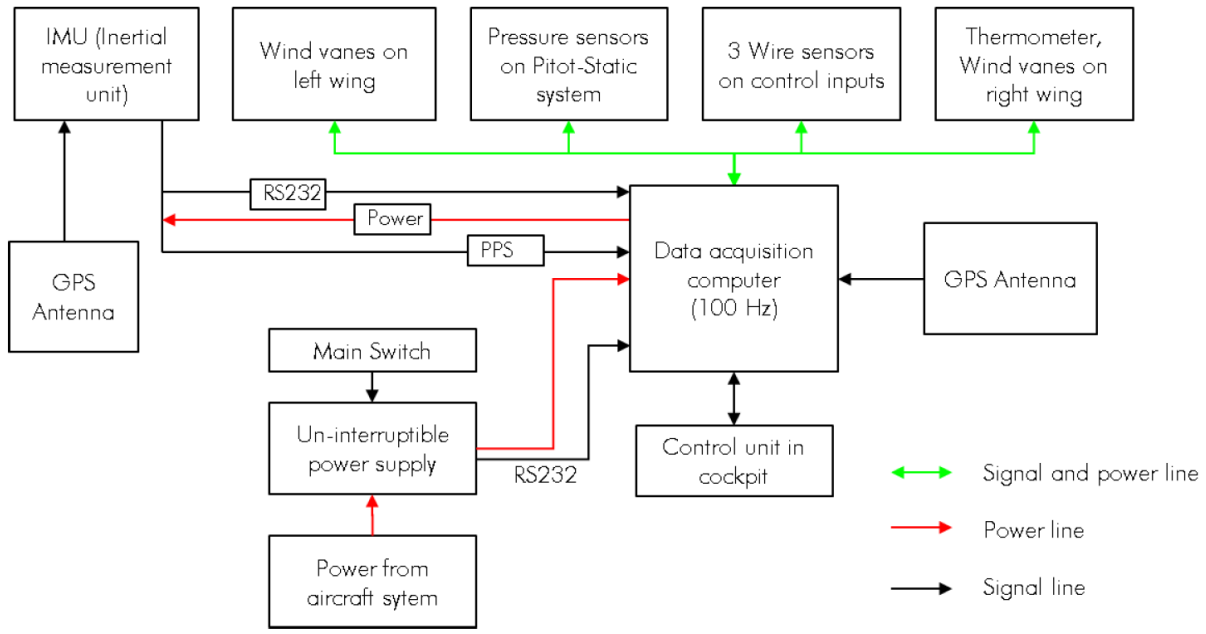

Figure 3.1: Block diagram of the measurement system (Cremer, 2016g)

The system architecture diagram above shows that the data acquisition computer is working at a sample frequency of 100 Hz. A system main switch is installed to make sure a potential cable fire can be stopped immediately by switching off the system power supply. In addition to that, a control unit in the cockpit makes it possible to check whether the system is working properly any time. By pressing an event button on the control unit spin runs or events of interest can be marked within the recorded data.

The utilised measurement system (see Table 3.1) consists of the following sensor systems:

Sensor	Type	Measurement range, accuracy and errors	Remarks
Inertial Measurement Unit (IMU)	iMAR iVRU-FQ	± 800°/s ± 20 g Rate of turn bias: 0.03°/s Linearity:< 0.2% Scale error:< 0.2% Acceleration bias: 0.003g Linearity: < 0.03%	Port: RS 232 Electrical data: Input voltage 12 - 34 V Input power max. 15 W Mechanical data: Mass 1.7 KG Dimensions: see drawings above

		Scale error:< 0.03% Orientation angle: Pitch and roll: ca. ± 0.6° (during moderate dynamic motions) Yaw influenced by wind	
GPS	µBlox Antares 4	-----	Data rate 1 Hz
Absolute pressure sensor	Setra 270	0 – 1100 hPa ± 0.03% FSO (e.g.: 0.33 hPa ~ 2.5 m at MSL for 0 – 1100 hPa range)	Connected to the on board pitot static system Output: analogue voltage 0 – 5 V Electrical data: Input voltage 22 - 30 V Input power 0.2 W Mechanical data: Mass 0.25 KG Dimensions: see drawings above
Difference pressure sensor	Setra D 239	± 37 hPa ± 0.14% FSO (e.g.: 0.1 hPa ~ 0.3 kt at 50 kts within ± 37 hPa range)	Connected to the on board pitot static system Output: analogue voltage 0 – 10 V Electrical data: Input voltage 22 - 30 V Input power 0.2 W Mechanical data: Mass 0.23 KG Dimensions: see drawings above

Control inputs: Elevator, Aileron, Rudder	Trip wire displacement sensors Micro-Eqsilon WPS 250-MK30	250 mm, optional 500 mm Linearity: ± 0.25% FSO	Output: analogue voltage 0 – 10 V Electrical data: Input voltage 10 V Input power 0.1 W Mechanical data: Mass 0.15 KG Dimensions: see drawings above
Wind vanes	messWERK	Range: ± 90° Accuracy: 3% of range	Wind vanes for Angle of Attack and Angle of Sideslip measurement: electrical angle sensors Output voltage: 3 – 7 V Electrical data: Input voltage 10 V (stabilized) Input power 0.1 W Mechanical data: Mass 0.2 KG per vane Dimensions: see drawings above
Thermometer (PT100, class A)		Range: ± 50°C	Need of constant current

Table 3.3: Applied sensors

The different sensors are described and shown:

1.) Inertial Measurement Unit (IMU) for aeroplane's attitude, turn rates and accelerations

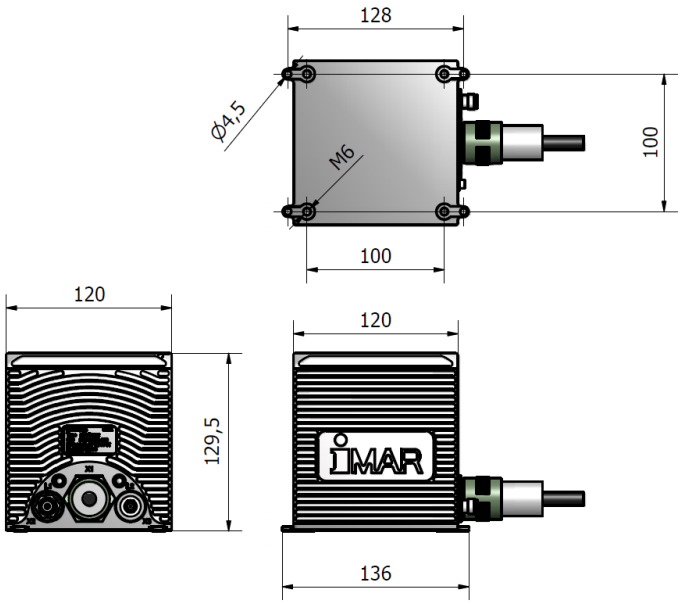

Figure 3.2: IMU iVRU-FQ (dimensions in mm) (Cremer, 2016g)

2.) Air–Data-Boom head for measurement of angle of attack and angle of sideslip at each wing tip (wind vanes) including thermometer

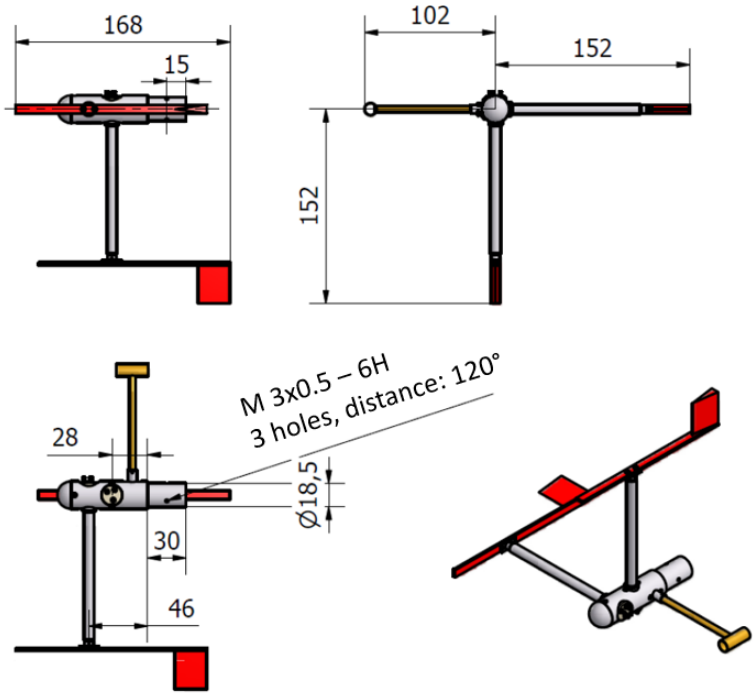

Figure 3.3: messWERK wind vanes and thermometer (dimensions in mm) (Cremer, 2016g)

3.) Absolute pressure sensor

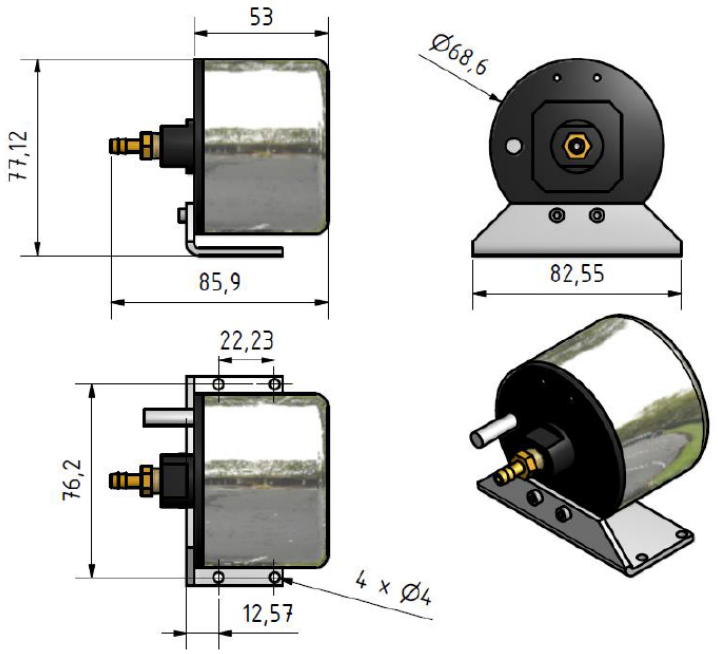

Figure 3.4: Absolute pressure sensors Setra 270 (dimensions in mm) (Cremer, 2016g)

4.) Difference pressure sensor

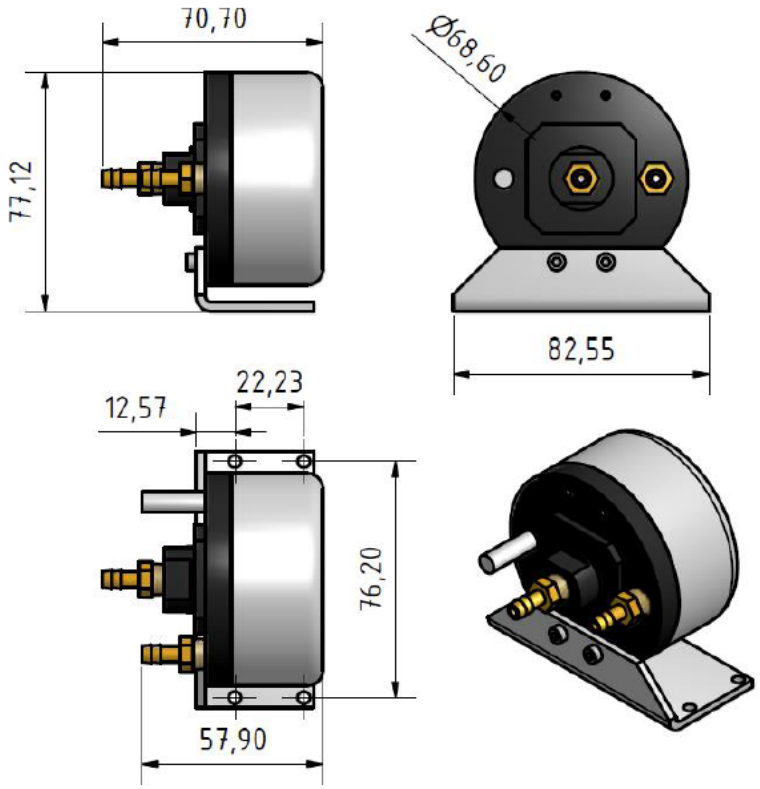

Figure 3.5: Difference pressure sensor Setra D 239 (dimensions in mm) (Cremer, 2016g)

5.) Trip wire displacement sensors for elevator, aileron and rudder displacements (each)

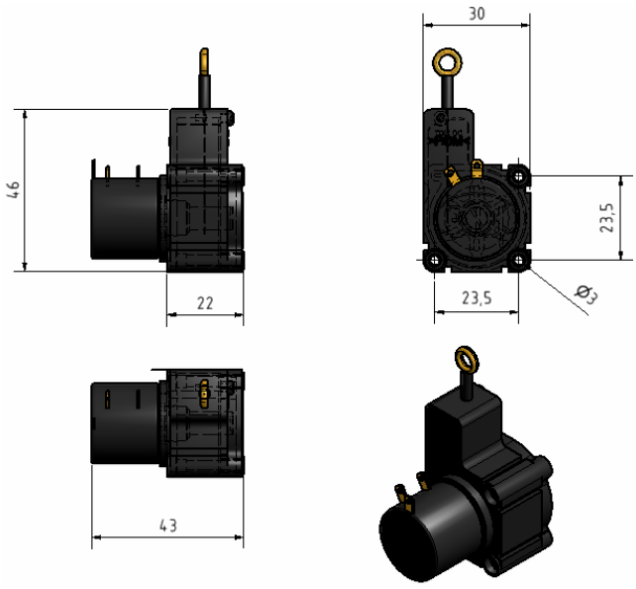

Figure 3.6: Trip wire displacement sensors Micro-Eqsilon WPS 250-MK30 (dim. in mm) (Cremer, 2016g)

In addition, a GPS receiver (with two antennas to avoid shielding GPS signals) for the aeroplane's 3D-position and ground speed is installed inside the mR computer main body box.

The uninterrupted power supply (UPS) is connected to the 12 V on-board power supply of the aeroplane (Figure 3.1).

The corresponding parameter acronym list can be found in the Glossary which is attached to the Table of Contents.

3.4 Data acquisition

The data acquisition system core module is the 'messWERK mR-12' computer (see Figure 3.8). It has the following features:

Ports:

2 x RS 232, max 115200 Baud

16 x analogue input ± 10 V, 16 Bit

(Anti-aliasing cutoff frequency 33 Hz, error type 0.05%; maximum error 0.1%)

16 x digital I/O

1 x analogue output

10 V reference output voltage at D-SUB 37

1 x constant current for PT 100
VGA
1 x LAN
2 x USB
1 x PPS Input (SMA plug)
1 x PPS Output (SMA plug)

Data storage:
Data rate 100 Hz (Standard, configurable)
Type of storage: 64 GB Compact Flash Card (Scan Disk)
Sensors:
1 x GPS µBlox Antares 4 with external Antenna via SMA plug
Optional with internal IMU for turn rates and accelerations about all 3 axis

Electrical data:
Input voltage 11 – 36 V
Output voltage ± 12 V and 5 V
Input power max. 30 W

Mechanical data:
Mass 2 kg

The system has been switched on and the corresponding IMU has been aligned shortly after the aeroplane's engine was started. From that point on data have been determined and stowed until shortly before the aeroplane's engine has been shut off after the specific flight.

Further data acquisition has been conducted via two video cameras, one installed at the vertical fin of the aeroplane and one at the headset of the pilot. The camera at the headset has also been used to record the pilot's comments via its audio channel.

3.5 Installation of the measurement system in the research aeroplane

During a 5-week period, the above described measurement system has been installed by the author in the utilised aeroplane as follows.

3.5.1 Installation of displacement sensor system

For data reproduction reasons the trip wire displacement sensors are, in all cases, mounted and orientated in a way that the outlet for the sensor cable is parallel to the control surface steering cable. The eyelet rings at the end of the sensor cables are fixed to the control surface steering cables with screwed joints. The sensor cables are very thin and thus easily tearable so that in case of a sensor blockage the control system of the aeroplane will not be influenced. The measurement system records the voltage output of the trip wire displacement sensors which is linear to the sensor cable displacement (acronym: eta_rd, xi_rd, zeta_rd). The corresponding calibration protocols can be found in Appendix 6.

3.5.2 Installation of the Inertial Measurement Unit (IMU)

The Inertial Measurement Unit is installed on a mounting plate in the back of the aeroplane (see Figure 3.7).

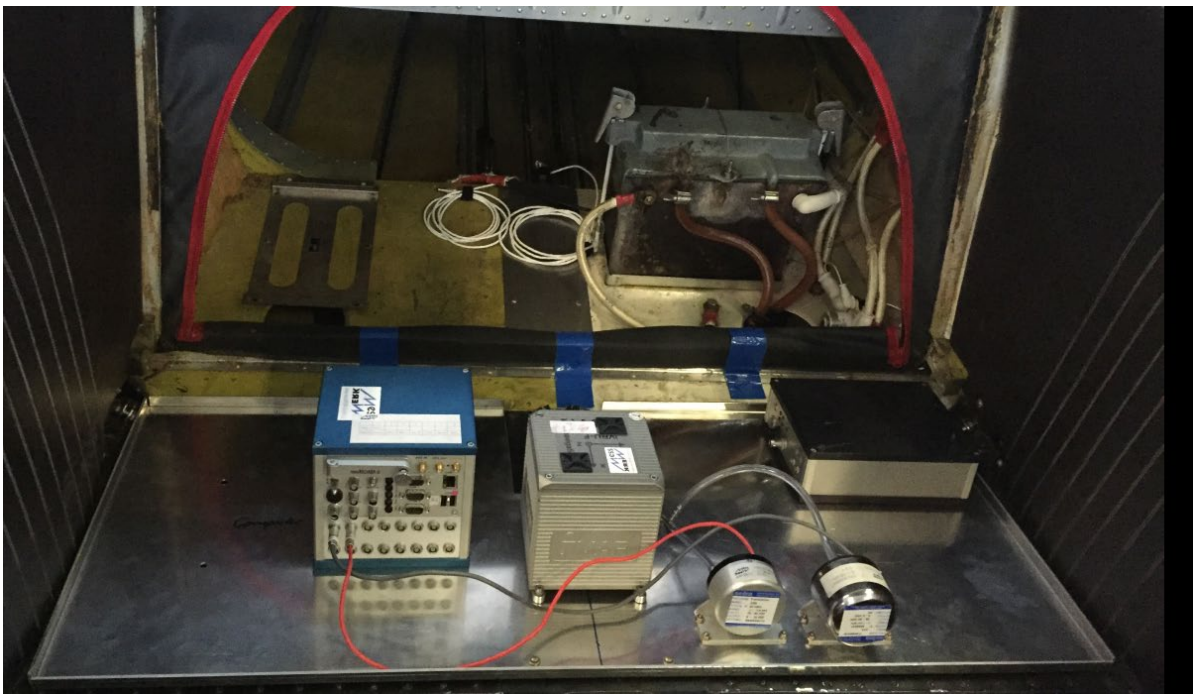

Figure 3.7: Installation of the Inertial Measurement Unit

It is oriented with the connecting plugs pointing against the aeroplane's longitudinal axis. As the mounting plate is tilted against a horizontal line because it is fixed on the aeroplane's structure, the recorded data need to be corrected by a calibration. The calibration protocol can be found in Appendix 6. The IMU - including the accelerometer - is mounted at the position of the aeroplane's CG position. This is also the position where the origin of the aeroplane's coordinate system is located.

3.5.3 Installation of the wing booms and wind vanes

The wing booms can be rotated about their longitudinal axis. The wind vanes are calibrated relative to the wing boom's longitudinal axis. In order to receive the correct sign according to the engineering standard LN 9300, the wind vanes at both boom-heads need to be oriented: one inboard (for angle-of-attack) and one downward pointing (for sideslip angle). The downward pointing wind vanes need to be aligned vertically against a plumb-line. A potential tilt angle can be seen and later cancelled out by calibration and the subsequent adjustment of the data. The corresponding calibration protocols can be found in Appendix 6.

3.5.4 Installation of the data acquisition computer, pressure sensors and Uninterrupted Power Supply (UPS)

To make sure that the data acquisition computer, the total pressure sensor, the difference pressure sensor and the UPS will not be influenced by the rapid movements during the spin trials all four devices are screwed onto the same mounting plate on which the IMU is installed. The corresponding tubes and wires are fixed inside the front and rear parts of the cockpit, inside the wings and inside the fuselage of the aeroplane. All wires and tubes are fixed to the aeroplane's structure or fairings and located so that they do not influence the aeroplane's aerodynamic or control systems even in case of a failure (Figure 3.7).

3.5.5 Wiring of the measurement system

The wiring of the measurement system has been conducted as follows (see Figure 3.8 and Table 3.2 below):

- Uninterrupted Power Supply
  - On board power supply connection cable to 'VDC In' of the UPS
  - External main switch to connection 'Remote' of the UPS
- Connection UPS with mR data acquisition computer
  - Power cable from 'VDC Out' of the UPS to mR
  - RS 232-cable from 'RS232' of the UPS to mR
- mR data acquisition computer
  - External control unit to 'Remote' of the mR
  - GPS cable to upper right connection of the mR
- IMU
  - Connection cable with Lemo-plug from mR to 'DC out'
  - Cable with 'COM1' – plug from mR to 'COM1'

PPS – cable from mR to ‘PPS OUT’

GPS – cable from IMU to ‘L2’

- Sensors

  The three trip wire displacement sensors cables eta_rd, xi_rd and zeta_rd to mR

  The two pressure sensors Pstat_r and Pstau_r to mR

  Wind vane (left wing):

  i) Cable from ‘alpha_le’ and ‘beta_le’ to mR

  ii) Connection cable (yellow) to adapter cable connection (yellow)

  iii) Connection ‘left wing’ from adapter cable to sensor left wing

  Wind vane (right wing):

  i) Cable 1 from ‘alpha_ri’ and beta_ri’ to mR

  ii) Plug ‘Ttotal_r’ from cable 2 to mR

  iii) Plug (yellow) of cable 1 to connection (yellow) of adapter cable

  iv) Plug (blue) of cable 2 to connection (blue) of adapter cable

  v) Connection ‘right wing’ from adapter cable to sensor right wing

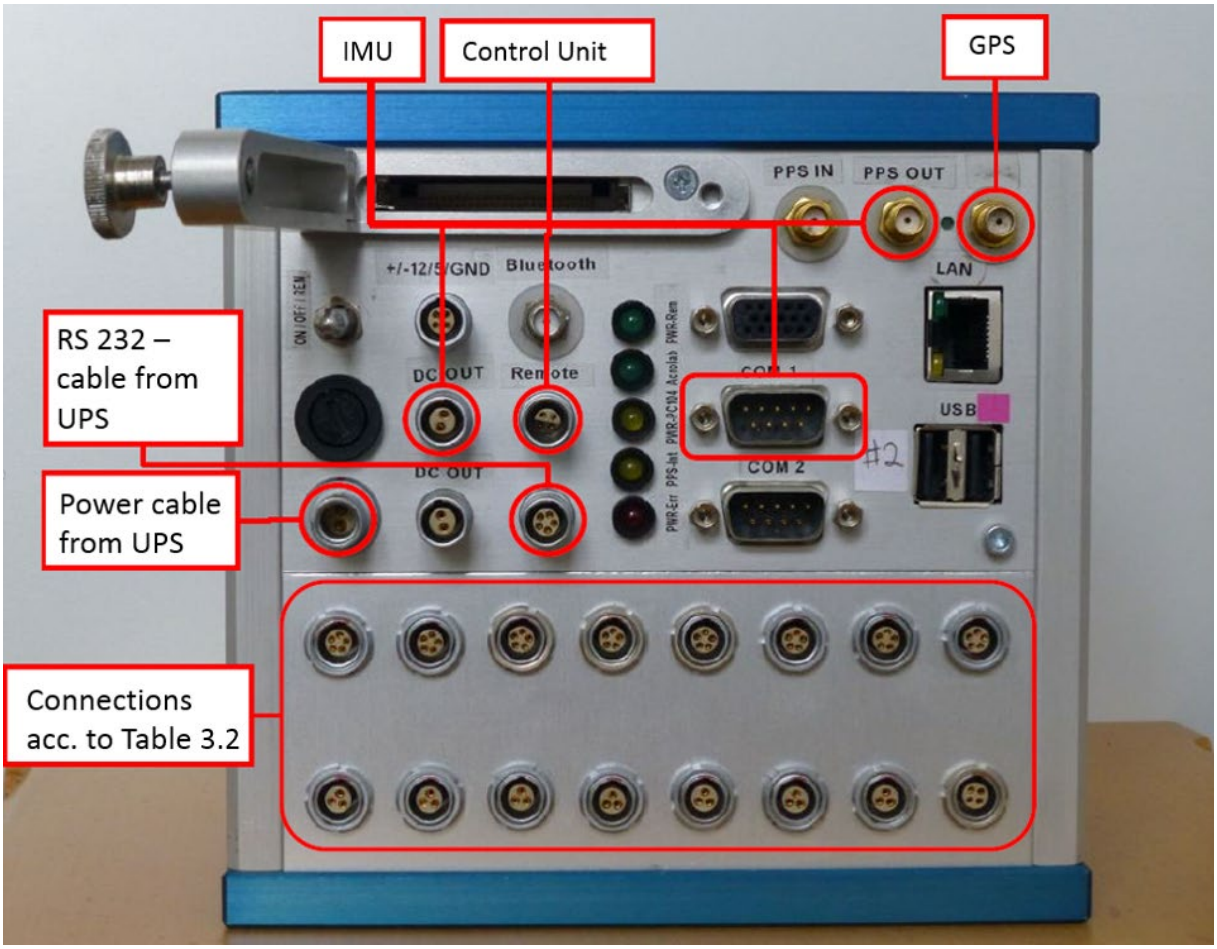

Figure 3.8: mR data acquisition computer front view

1	2	3	4	5	6	7	8
Pstat_r	Pstau_r						
alpha_le	beta_le	alpha_ri	beta_ri	eta_rd	xi_rd	zeta_rd	Ttotal_r

Table 3.4: Pin configuration at the mR data acquisition computer for the sensor connections

3.6 Calibration and data validation of the sensor system

With the measured data from the first flight, a calibration – and by that a validation - of the measurement system has been conducted.

3.6.1 IMU data calibration

Due to the aeroplane´s structure at the position where the IMU has been installed, the coordinate system of the IMU had to be tilted. After approximately a 1 hour calibration flight - conducted by the Author - at a cruising speed of 103 kts (53 m/s) at which the aeroplane´s longitudinal axis is mostly in a 0° pitch attitude, the IMU pitch data set has been shifted to 0°. This has been done by a subtraction of 17° from the original data set. Consequently the 17° backwards inclination of the mounting plate has been adjusted. The bias of the IMU itself are given in Table 3.1 above. The corresponding calibration plot can be found in Appendix 6.

3.6.2 Wind vane sensor calibration

Originally the angle difference between the aeroplane´s longitudinal axis and the longitudinal axes of both air data booms have not been known exactly. The booms have been installed and later adjusted roughly parallel to the aeroplane´s longitudinal axis. Due to that there is an x- and y-axis data off-set for the yaw angle and the angle of attack. As the IMU calibration has been conducted, data from the aeroplane's average cruising attitude (at the speed point of 53 m/s) has been taken by the Author to adjust the corresponding data to eliminate erroneous data off-sets of the sensors.

Thus (see Figure A6.14 in Appendix 6) the following correlations can be written:

$$alpha\_le\_c = alpha\_le\_m + 0.5$$

$$alpha\_ri\_c = alpha\_ri\_m - 5.1$$

The off-sets of both sideslip angles have been determined by a data plot (see Appendix 6, Figure A6.15) with the assumption that whenever the lateral acceleration of the aeroplane is 0 g the aeroplane's sideslip angle is 0°.

Thus the following correlations can be written

$$beta\_le\_c = beta\_le\_m - 2.6$$

$$beta\_ri\_c = beta\_ri\_m + 3.1$$

3.6.3 Static pressure sensor calibration

The calibration of the static pressure sensor has been conducted by comparing the data set of the utilised sensor with a calibrated pressure sensor – which has been calibrated officially by a gauge. The following calibration protocol has been determined during that process:

	name	unit		
			date	29.09.2014
in acro	Pstat_r	V	aircraft type	Fuji
out acro	Pstat_r	hPa		

sensor		reference sensor	
type	B270	type	DPM7885
sensor no.	DA-03	sensor no.	Weston2

description of calibration:

zero refe-	
rence:	n/a
positive:	n/a
remark:	
data file:	Fuji-cal_20140929_1.mat
events:	1 2 3

coefficients to compute Pstat_r:
[219.979761,-0.315]

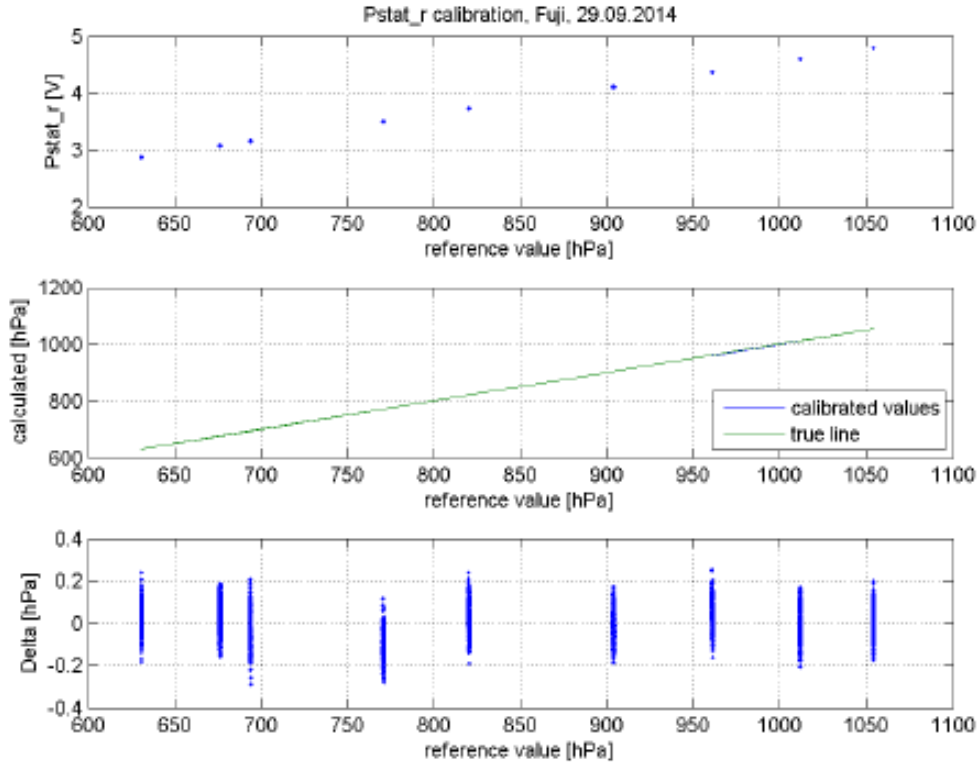

Figure 3.9: Static pressure sensor calibration

In the figure above the first graph shows the output voltage Pstat_r [V] versus the reference static pressure [hPa] within a range of 600 – 1100 hPa measured several times at 9 different values.

The second graph shows that the connection of these 9 measured reference pressure values and a trend line (linear function, calculated [hPa]) do follow nearly the same line.

The third graph shows the variation about the measured pressure value ([Delta [hPa] versus reference value [hPa]). This graph shows that the reference pressure values have a variation of approximately +/- 0.2 hPa, which means an error of around +/- 1.6 m of altitude. This error value meets the necessary altitude precision of +/- 2 m (see also section 3.2.2).

The calibration protocols for all other utilised sensors can be found in Appendix 6.

3.6.4 Calibration of fuel gauges

Because of the expected high influence of the position of the centre of gravity (CG) on the aeroplane´s spin characteristics and resulting spin behaviour, a thorough weighing has been conducted to define the empty mass and the position of the CG under empty mass conditions. Therefore the fuel tanks have been completely drained before the weighing has been conducted. While refuelling the aeroplane a fuel gauge calibration in increments of three litres has been conducted (Table 3.5). The data have been determined by the author at the right fuel tank of the Fuji FA-200–160 on 23-02-2014. The measured fuel temperature of 16°C the specific mass of the aviation gasoline AVGAS 100 LL is 0.72 kg / litre.

scale marking [cm]	litre [L]	mass [KG]
zero marking	15	10.8
1.0	18	12.96
1.8	21	15.12
2.4	24	17.28
3.0	27	19.44
3.5	30	21.6
4.2	33	23.76
4.7	36	25.92
5.3	39	28.08
5.9	42	30.24
6.4	45	32.4
6.9	48	34.56
7.5	51	36.72
8.0	54	38.88
8.6	57	41.04
9.1	60	43.2
9.7	63	45.36
10.2	66	47.52
10.8	69	49.68
11.5	72	51.84
12.0	75	54.54
12.5	78	56.16
13.3	81	58.32
13.9	84	60.48
14.5	87	62.64
15.4	90	64.8
16.0	93	66.96
17.0	96	69.12
18.0	99	71.28
19.4	102	73.44
upper marking	105	75.6

Table 3.5: Fuel gauge calibration (by the author)

With this information the longitudinal and lateral positions of the aeroplane's centre of gravity position can be determined.

3.7 Conclusions

By using a professional, rugged measurement system, spinning can be measured with high accuracy throughout the required sensor ranges. The corresponding sensor calibration and validation have been conducted with the support of the company 'messWerk'. Thereby the later data analysis is based on data which are essential for an interpretation of the measurement results.

After the system set-up the preparation of the aeroplane and the specific flights have now be performed.

Chapter 4 Preparation of the aeroplane and the spin trials

In the following section the preparation of the utilised aeroplane for the spin trials is described.

4.1 Introduction

Especially in a safety critical field like flight-testing the preparation of the aeroplane, the corresponding measurement system and the required trials are imperative. In addition to that the pilot needs to be physically and mentally prepared; his or her piloting skills must be trained and at an appropriated professional level for the planned flight tests. The necessary emergency equipment must be available, the operational reliability must be checked and its usage must be familiar to the crew.

Within this Chapter the aeroplane modification and special inspections are explained followed by the choice of the relevant and measured parameters and the selection of the flight envelope. For clarification reasons that the conducted flight tests are conducted against a legal background of the current air law regulations and the trial procedures are illustrated.

4.2 Modification and inspection of the utilized aeroplane

Due to the expectation that spin tests will cause a higher stress on the aeroplane's gyroscopic systems and the aircraft's structure, the suction system has been modified and a wing spar inspection has been conducted before the trials. In addition to this the responsible Maintenance Organization together with the Author has conducted an in-depth inspection of the aeroplane´s structure – including a sound control cable tension examination and adjustment.

4.3 Suction system modification

The test aeroplane is equipped with a standard suction system to drive the artificial horizon and the directional gyroscope system. These instruments are not designed for aerobatic or spin use. High turn rates as well as pitch and bank angles in excess of 60° may destroy these fragile and expensive devices. To avoid such a destruction the suction system – which is driven by the aeroplane's engine and thus by a drive shaft – had to be modified in a way that the artificial horizon and the directional gyroscope system can be disconnected from it. This is possible by redirecting the suction airflow so that it is not fed through the corresponding instruments. (See valve No. 10 of Figure 4.1, and Figure 4.2)

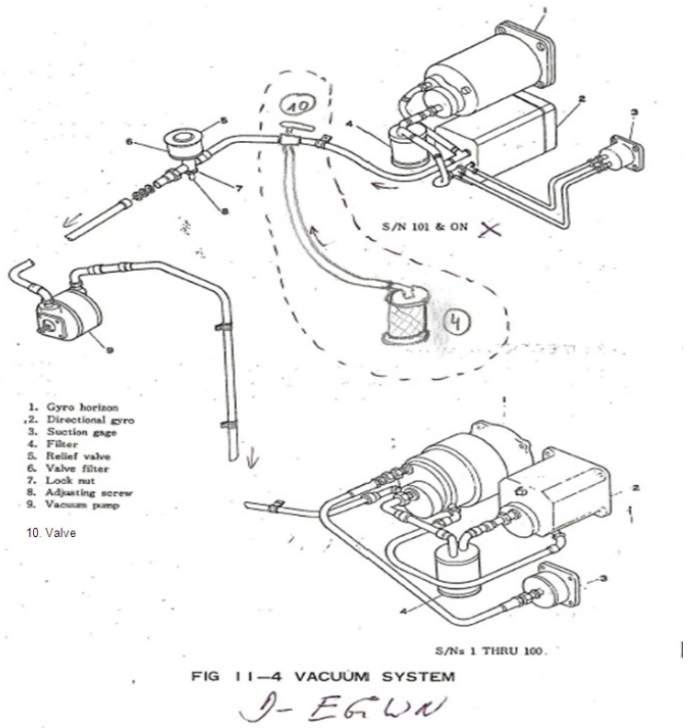

Figure 4.1: Modified suction system of the test aeroplane (original sketch above has been taken from Service Manual of the Fuji FA-200 (Fuji Heavy Industries, 1971) and has been modified by the Author)

Figure 4.2: Part of the modified suction system located in the right-hand leg room of the cockpit (photograph taken by the Author)

By tilting the handle by 90° the airflow is bypassed and thus both gyroscope systems do not work.

4.4 Wing spar inspection

Especially in this kind of research project, safety is of major importance. Due to this the Author conducted inspections of the test aeroplane; especially a thorough wing spar inspection has been performed - because this is the most stressed part of the aeroplane during the spin recovery. The aeroplane is certified for accelerations in the direction of the z–axis (vertical) between +6 g and -4 g. During a spin recovery the aeroplane needs to be recovered from a vertical dive. During this recovery manoeuvre, the airframe will experience accelerations of up to around +3.5 g. Although the aircraft will be always flown well within the aeroplane's certified g-limits, it is essential that the aeroplane can cope with the increased loads.

By using a borescope together with a connected camera system the Author conducted the entire wing spar inspection in February 2014.

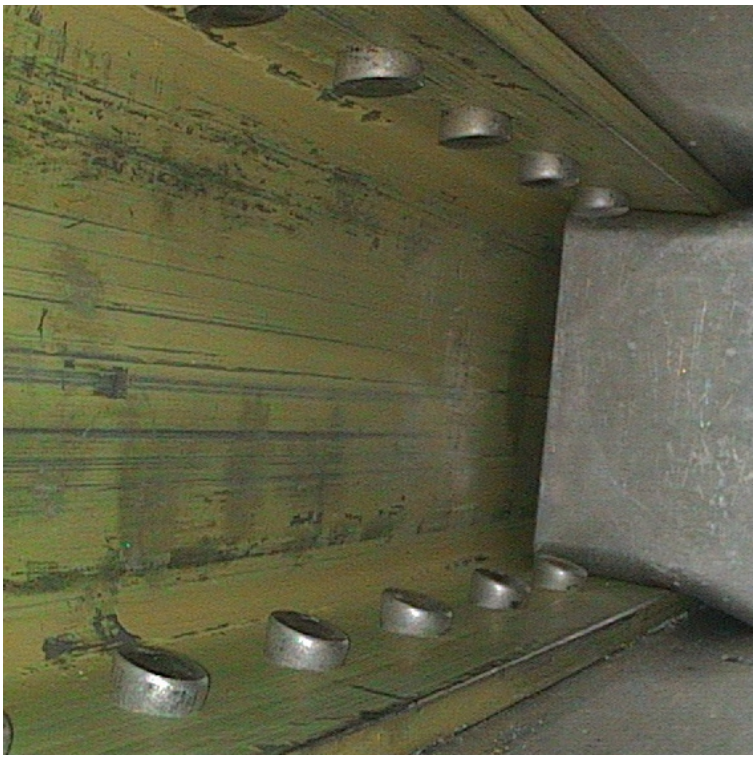

Figure 4.3: A wing spar of the test aircraft (photographed during inspection in February 2014)

It can be seen in Figure 4.3 that the wing spar of the aeroplane is in a very good condition. No corrosion or other damage has been detected during the entire inspection process. After a detailed consultation together with the responsible Maintenance Organization (Air-Service Klausheide, located at the home base of the aeroplane), a team of certifying staff decided, together with the Author, that spin trials can be conducted safely.

After the aeroplane has been inspected the preparation of the actual trials are required. For that the relevant spin parameters need to be determined, the flight envelope and a detailed trial schedule has to be defined.

4.5 Choice of the relevant and investigated parameters

As spinning is a highly complex type of movement, its description and analysis is also complex. During a spin an aeroplane is rolling, pitching, yawing and its vertical speed is quickly varying. Furthermore the airflow (the relative wind) - while moving downwards about a vertical axis - will encounter the aeroplane's geometry from various directions and speeds. Influenced by this airflow and the mass distribution of the aeroplane, forces (including lift and drag) and moments are created and change with time as the aeroplane's attitude changes with time. Through these forces and moments, the aeroplane will be accelerated in all three directions and about all three axes. Thus the roll-, pitch-, and yaw rates will vary as the vertical speed changes. The value of the atmospheric density of the air (damping properties) is needed and for that the barometric altitude and outside air temperature is measured. Because spinning is additionally influenced by the aeroplane geometry, the positions of the control surfaces need to be documented.

The utilised measurement system has been developed at the Technische Universität Braunschweig together with the company Messwerk (Cremer, 2016g). It has been proven during several certification flight test programmes in recent years and it measures 78 different parameters.

For feasibility reasons not all of the 78 parameters and combinations of them have been analyzed and evaluated within this work. But to cover the main spin influencing factors from those 78 parameters (see parameter acronym list after the Glossary) the following have been chosen for the investigation of the spin dynamics of the utilised single-engine low-wing aeroplane:

Parameter acronym	Unit	Parameter description
Alpha_le_c	[°]	Angle of attack at the left wing boom head
Alpha_ri_c	[°]	Angle of attack at the right wing boom head
Beta_le_c	[°]	Angle of side slip at the left wing boom head
Beta_ri_c	[°]	Angle of side slip at the right wing boom head

Table 4.1: Airflow parameters

Parameter acronym	Unit	Parameter description
Hpunkt	[m/s]	Vertical speed based on Hbaro, positive when upwards (climbing)

Table 4.2: Altitude parameters

Parameter acronym	Unit	Parameter description
In_Phi	[°]	roll angle
In_Theta	[°]	pitch angle
In_Psi	[°]	yaw angle (heading)

Table 4.3: Angular attitude parameters

Parameter acronym	Unit	Parameter description
In_p	[°/s]	roll rate
In_q	[°/s]	pitch rate
In_r	[°/s]	yaw rate

Table 4.4: Angular velocity parameters

Parameter acronym	Unit	Parameter description
Accelerations	[m/s^2]	x, y, z direction

Table: 4.5: Accelerations parameter

Parameter acronym	Unit	Parameter description
Eta_ca	[°]	elevator control surface deflection, positive when surface down
Xi_le_ca	[°]	left aileron control surface deflection, positive when surface down
Xi_ri_ca	[°]	right aileron control surface deflection, positive when surface down
Zeta_ca	[°]	rudder control surface deflection, positive when surface deflected to the left

Table 4.6: Control surface parameters

The reason for this choice is that with this set of parameters the aerodynamic situations (Alpha, Beta, all control surface deflections), the altitude losses (Hpunkt), the attitude and angular rates of the aeroplane (Phi, Theta, Psi, p, q, r), 3D-accelerations, and recovery times (by rudder deflection angle Zeta) can be determined and thus a spin can be described and analysed in-depth.

Other parameters like Mach numbers or airspeeds and the corresponding static and dynamic pressures, air density and the corresponding temperatures and atmospheric (static) pressures, etc. can be used for future investigations. GPS data could be used for the validation of barometric and density altitude data. System data like cycle number, pps (pulse per second) or the power supply values (see unit column in the acronym list) are not relevant for spin analysis but necessary to document the consistency of the data.

4.6 Flight envelope determination regarding masses and Centre of Gravity positions, limit of the tests and choice of the test points within the defined flight envelope

In this context a flight envelope is a value field consisting of the aeroplane mass and the position of its Centre of Gravity (CG).

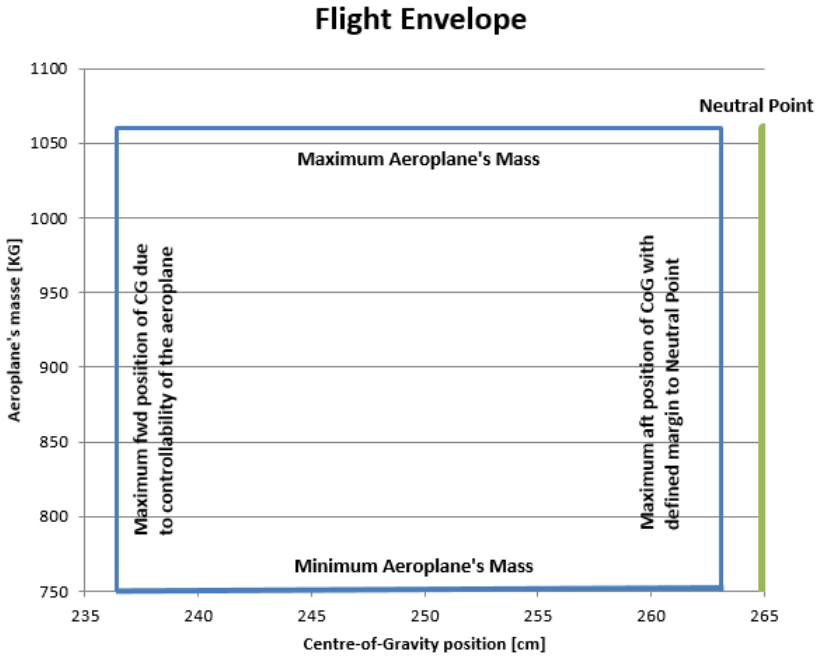

Figure 4.4: Example of a generic flight envelope (by the Author)

The upper and lower boundaries of such an envelope consist of the minimum and maximum aeroplane’s mass - which is defined by the corresponding Design Organisation.

The left and right boundaries are based on flight test results and their analysis which establish sufficient static and dynamic stability as well as control authority and thus controllability about the aeroplane (EASA, 2012).

By shifting the CG backwards along the x-axis (e.g. by “trim” masses), it will reach a certain point on the longitudinal axis which is defined as the Neutral Point. At that point the aeroplane shows neutral static and dynamic stability about the y-axis (longitudinal motions).
If the aeroplane’s CG is shifted further backwards the aeroplane will become unstable and manually uncontrollable. Such a condition must be avoided. The corresponding Design Organisation needs to define a minimum margin between the maximum allowed aft CG position – which is then the right boundary of the flight envelope - and the Neutral Point.

The left limit is based on the trim flap capability to substitute the longitudinal control in case of an elevator failure (elevator in a free-moving condition). If the aeroplane is too nose heavy so that it cannot be recovered or de-rotated from a 3° descent flight path only by using the trim flap installed at the elevator for a safe landing the ‘technical’ CG limit is reached (EASA, 2012). The Design Organisation needs again to define a minimum margin between the technical limit and the operational limit of the aeroplane.

Both margins need to be approved by the certifying Authority.
By these flight tests the aeroplane’s flight stability and thus its controllability within the defined flight envelope is ensured. Within such a flight envelope the aeroplane needs to comply with all requirements of the corresponding Certification Specifications including spin recovery capability. Further explanation in this context can be found in Appendix A2 ‘Example of a certification spin test planning’.
One of the most important requirements which have to be met within this research project is flight safety. Hence a series of trials have been started in a known and safe area of the certified flight envelope which is the central section of the value field.
Within that particular part of the flight envelope there is no conflict with both CG limits. Starting with an aeroplane’s mass, which is above the medium mass (Flight 1), it was possible to leave the utility category envelope and move into the normal category envelope quickly with small mass steps. With that the known spin area has been left. So an expansion of the conducted and possible future trials in all directions of the flight envelope is easily feasible.
As this research project opens up a new approach to a research field which contains flight safety risks and which has limited other scientific work, the author decided to conduct the spins with a maximum of 6 turns as it is defined by the corresponding Certification Specification of this aeroplane.

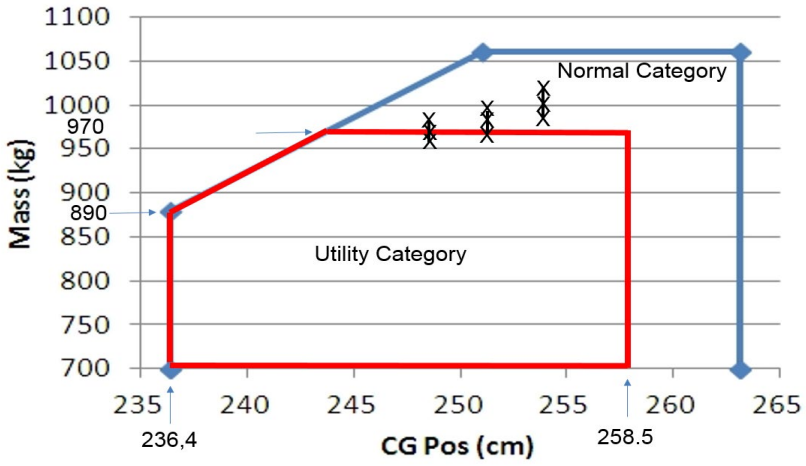

Figure 4.5: Flight envelope of the research aeroplane Fuji FA-200-160 including the chosen test points (by the Author)

Within such a value field – a flight envelope which meets the above conditions and requirements – systematic scientific spin tests can be conducted without a higher risk of losing the aeroplane and / or the flight test crew because the aeroplane is within the stability and mass limits and thus we can expect controllable and recoverable aeroplane behaviour. Outside this value field the aeroplane may behave very differently.
During the flight test phase of an aeroplane's design process, spin tests are only approved to go ahead for certification reasons within an EASA or FAA approved Design Organisation.

The conducted spin flight tests for this project have been carried out for pure research rather than certification reasons and thus are not as strictly controlled (as explained below). The Fuji FA-200–160 is certified as a normal (N), utility (U) and aerobatic (A) category aeroplane. Due to that the aeroplane has three different certified flight envelopes.

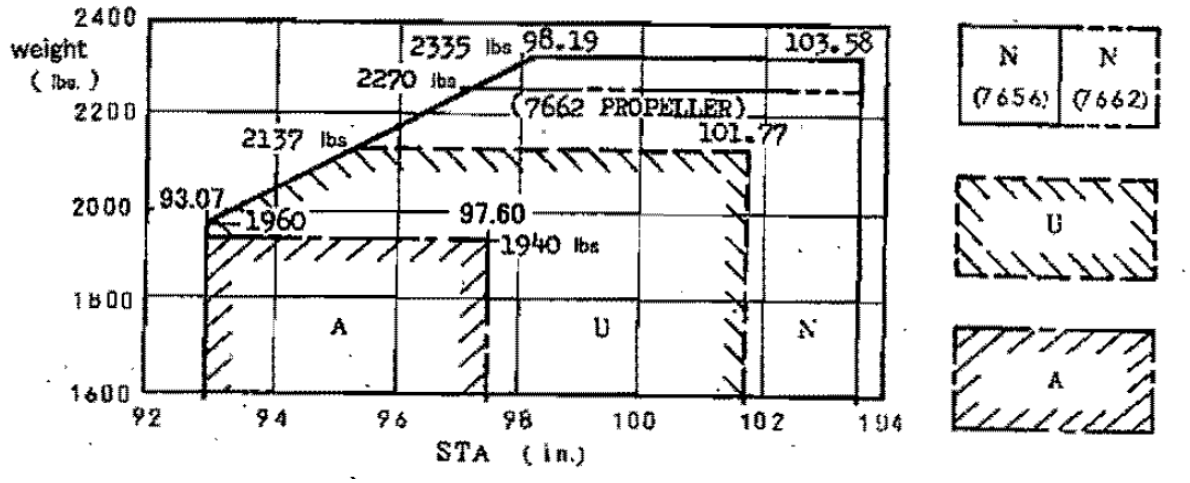

Figure 4.6: Three flight envelopes of the Fuji FA-200–160, (Fuji Heavy Industries, 2011)

Within the normal category flight envelope (indicated by N in Figure 4.6) the aeroplane is not approved for spinning. Within the utility and aerobatic category flight envelopes the aeroplane is approved for a maximum of six spin turns during one spin run.

For the planned flight tests the spins are conducted at high, medium and low masses combined with forward, middle and aft centre of gravity positions.

The centre of gravity position can be shifted by installing different trim masses in the back of the aeroplane's fuselage (maximum forward CG position without trim masses, aft shift of CG by adding trim masses at Station 404, see figure below). The change in the aeroplane's mass is conducted by burning fuel during the corresponding climb phases between the spins.

The total mass of the aeroplane during the spins consists of the:

- Aeroplane´s Basic Empty Mass (including basic equipment according to the 'Airplane Flight Manual' (Fuji Heavy Industries, 2011) (see page 17 – 28) and unusable fuel and oil)
- Mass of the Crew (including Parachutes)
- Mass of the usable fuel onboard (including 35 kg minimum fuel on-board) – see note 1 below
- Mass of the measurement system
- Trim mass

Note 4.1: The Fuji aeroplane is normally operated within an 'Approved Training Organization' (ATO) which is certified according the European Aviation Safety Agency (EASA) regulations. For safety reasons it is defined within the corresponding Operation Manual (OM) of the ATO that the aeroplane needs, at the end of any flight, at least 35 kg of fuel on-board. This consists of the Alternate fuel (fuel for a potential flight to an alternate aerodrome after an aborted approach for landing) and a reserve fuel of at least 30 minutes flight time.

The aerobatic flight envelope cannot be used for the test flights because its maximum defined mass of 890 kg (1960 lbs) is far below the actual total mass of the aeroplane. The maximum defined mass of the utility category flight envelope is 970 kg.

Within the limits of the spin certified flight envelopes of the aeroplane, it is expected that the spin behaviour of the aeroplane is basically known and safe. In addition to that, spinning in these envelopes has been done by the Fuji Test Pilot during the certification phase of the aeroplane. For this reason the corresponding spin tests within this research project have been conducted mainly outside the known and certified flight envelope (which is permitted as the tests are for research purposes and performed by a qualified test pilot).

The corresponding CG positions, masses, moment arms (from datum line) and moments are given in Tables 4.7 to 4.9. (From 'Airplane Flight Manual', Fuji Heavy Industries, 2011).

		MASS [KG]	MASS [LBS]	*	ARM [CM]	ARM [INCH]	=	MOMENT [KGcm]	MOMENT [LBSINCH]
	Litre								
AC BEM		681,5	1501,101		246,2	96,92913		167785,3	145500,5
CREW (incl. Parachutes)		216	475,7709		250	98,4252		54000	46827,85
Fuel O/B	108	77,76	171,2775		239	94,09449		18584,64	16116,27
EQUIPMENT		10	22,02643		342	134,6457		3420	2965,764
TRIM MASS		0	0		0	0		0	0
GM / CG / MOM Cond. 1		985,26	2170,176		247,4372	97,41621		243789,9	211410,3
FUEL BURN OFF		15	33,03965		239	94,09449		3585	3108,849
GM / CG / MOM Cond. 2		970,26	2137,137		247,5676	97,46756		240204,9	208301,5
FUEL BURN OFF		15	33,03965		239	94,09449		3585	3108,849
GM / CG / MOM Cond. 3		955,26	2104,097		247,7021	97,52052		236619,9	205192,6

Table 4.7: CG-position calculations for conditions 1 – 3 (forward CG positions)

		MASS [KG]	MASS [LBS]	*	ARM [CM]	ARM [INCH]	=	MOMENT [KGcm]	MOMENT [LBSINCH]
	Litre								
AC BEM		681,5	1501,101		246,2	96,92913		167785,3	145500,5
CREW (incl. Parachutes)		216	475,7709		250	98,4252		54000	46827,85
Fuel O/B	91	65,52	144,3172		239	94,09449		15659,28	13579,45
EQUIPMENT		10	22,02643		342	134,6457		3420	2965,764
TRIM MASS		25	55,06608		404	159,0551		10100	8758,542
GM / CG / MOM Cond. 4		998,02	2198,282		251,4625	99,00097		250964,6	217632,1
FUEL BURN OFF		15	33,03965		239	94,09449		3585	3108,849
GM / CG / MOM Cond. 5		983,02	2165,242		251,6526	99,07584		247379,6	214523,2
FUEL BURN OFF		15	33,03965		239	94,09449		3585	3108,849
GM / CG / MOM Cond. 6		968,02	2132,203		251,8487	99,15303		243794,6	211414,4

Table 4.8: CG-position calculations for conditions 4 – 6 (middle CG positions)

		MASS [KG]	MASS [LBS]	*	ARM [CM]	ARM [INCH]	=	MOMENT [KGcm]	MOMENT [LBSINCH]
	Litre								
AC BEM		681,5	1501,101		246,2	96,92913		167785,3	145500,5
CREW (incl. Parachutes)		216	475,7709		250	98,4252		54000	46827,85
Fuel O/B	95	68,4	150,6608		239	94,09449		16347,6	14176,35
EQUIPMENT		10	22,02643		342	134,6457		3420	2965,764
TRIM MASS		40	88,10573		404	159,0551		16160	14013,67
GM / CG / MOM Cond. 7		1015,9	2237,665		253,6794	99,87378		257712,9	223484,1
FUEL BURN OFF		15	33,03965		239	94,09449		3585	3108,849
GM / CG / MOM Cond. 8		1000,9	2204,626		253,8994	99,96039		254127,9	220375,2
FUEL BURN OFF		15	33,03965		239	94,09449		3585	3108,849
GM / CG / MOM Cond. 9		985,9	2171,586		254,1261	100,0496		250542,9	217266,4

Table 4.9: CG-position calculations for Condition 7 – 9 (aft CG positions)

4.7 Legal basis for test flights

The following text is reproduced from the European Commission Regulation (EU) No. 1178 / 2011

The legal regulations for research test flying - which includes the leaving of certified flight envelopes - are:

1.) European Commission Regulation (EU) No. 1178 / 2011, § FCL.820 Flight test rating

(a) The Holder of a pilot licence for aeroplanes or helicopters shall only act as a Pilot–In–Command in category 1 or 2 flight tests, when they hold a flight test rating

(b) The obligation to hold a flight test rating established in (a) shall only apply to flights tests conducted on:

(1) Helicopter certificated or to be certificated in accordance with the standards of CS-27 or CS-29 or equivalent airworthiness codes; or

(2) Aeroplanes certificated or to be certificated in accordance with:

(i) The standards of CS–25 or equivalent airworthiness codes; or

(ii) The standards of CS-23 or equivalent airworthiness codes, except for aeroplanes with an maximum take-off mass of less than 2000 kg

(c) The privileges of the holder of a flight test rating are to, within the relevant aircraft category:

(1) In the case of a category 1 flight test rating, conduct all categories of flight test, as defined in Part-21, either as Pilot-In-Command or Co-pilot;

(2) In the case of a category 2 flight test rating:

(i) Conduct category 1 flight tests, as defined in Part-21

-As a Co-pilot, or

-as a Pilot-In-Command, in the case of aeroplanes to in (b)(2)(ii), except for those within the commuter category or having a design diving speed above 0.6 Mach or a maximum ceiling above 25.000 feet

(ii) Conduct all other categories of flight tests, as defined in Part-21, either

as Pilot-In-Command or Co-pilot

(3) In addition, for both category 1 or 2 flight test ratings, to conduct flights specifically related to the activity of design and production organisations, within the scope of their privileges, when the requirements of EASA FCL Subpart H (Class and Type Ratings) may not be complied with.

And additionally:

2.) European Commission Regulation (EU) No. 748 / 2012, Appendix XII,

(b) Categories of flight tests

Flight tests include the following four categories:

(1) Category 1

- Initial flight(s) of a new type of aircraft or of an aircraft of which flight and/or piloting characteristics may have been significantly modified.
- Flights to investigate novel or unusual aircraft design features or techniques.
- Flights to determine or expand the flight envelope.
- Flights to determine the regulatory performances, flight characteristics and handling qualities in extreme conditions.

(2) Category 2

- Flights done in the part of the flight envelope already opened and comprising manoeuvres, during which it is not envisaged to encounter flight and/or handling characteristics (performance and flying qualities) significantly different from those already known.
- Display flights and demonstration flights of a non-type-certified aircraft.
- Flights conducted for the purpose of determining whether there is reasonable assurance that the aircraft, its parts and appliances are reliable and function properly.

(3) and (4) not applicable to this investigation

It can be seen from the European Commission Regulations above – which can be found in the current version at the webpage https://www.easa.europa.eu/regulations - that a certified test pilot is allowed to conduct the necessary category 1 flight tests for spin research reasons on an aeroplane which belongs to the same category as the Fuji FA-200-160.

4.8 Flight trial procedures and conditions

The spin flight tests are performed with the use of a procedure which has been defined for this research project. With this procedure, further spin tests can be conducted and repeated in a way that the corresponding data can be collected similarly and thus systematically compared to the data recorded within this work.

Procedure 1 (Spin Entry):

Prior to start a particular spin the aeroplane has to be flown to at least 5000 feet above ground level, the engine power has to be set to idle while the flaps are retracted (set to 0°). All spins are to be performed to the left.

5 knots before the aeroplane enters a fully developed stall:

- The elevator has to be deflected into the full up position
- The rudder has to be deflected into the full left position
- The ailerons have to be kept in the neutral position
- This control input configuration has to be kept until the recovery procedure (see procedure 2 below) will be applied (no change of aeroplane geometry during the spins)
- Entering the specific stall and subsequent spin must be conducted with a slow deceleration rate (1 kt / second) (see Certification Specification CS 23.201)
- The spin run consists of six spin turns (see Certification Specification CS 23 for Utility Category aeroplanes CS 23.221) with a subsequent recovery

Conditions on the flight tests:

Before setting off, the measurement system must be switched on and aligned before starting the aeroplane's engine. The aircraft is then flown to the test area.

The spin trials have to be conducted over an unpopulated area: in this case over the North Sea coastline, and in an airspace next to an aerodrome (Jade - Weser Airport, Wilhelmshaven) to ensure a successful potential power-off forced landing.

During the spin, the atmosphere should be as clear of turbulence as possible, VMC (visual meteorological conditions) must be met and the ground must be in sight all of the time. In addition to that the ambient atmospheric conditions must be similar to make sure that the later results are not influenced significantly. To ensure that the different flights have been conducted at days with very similar weather conditions (air pressures, air temperatures,

humidities and thus air densities). The corresponding air densities can be found in Figure 4.8 below.

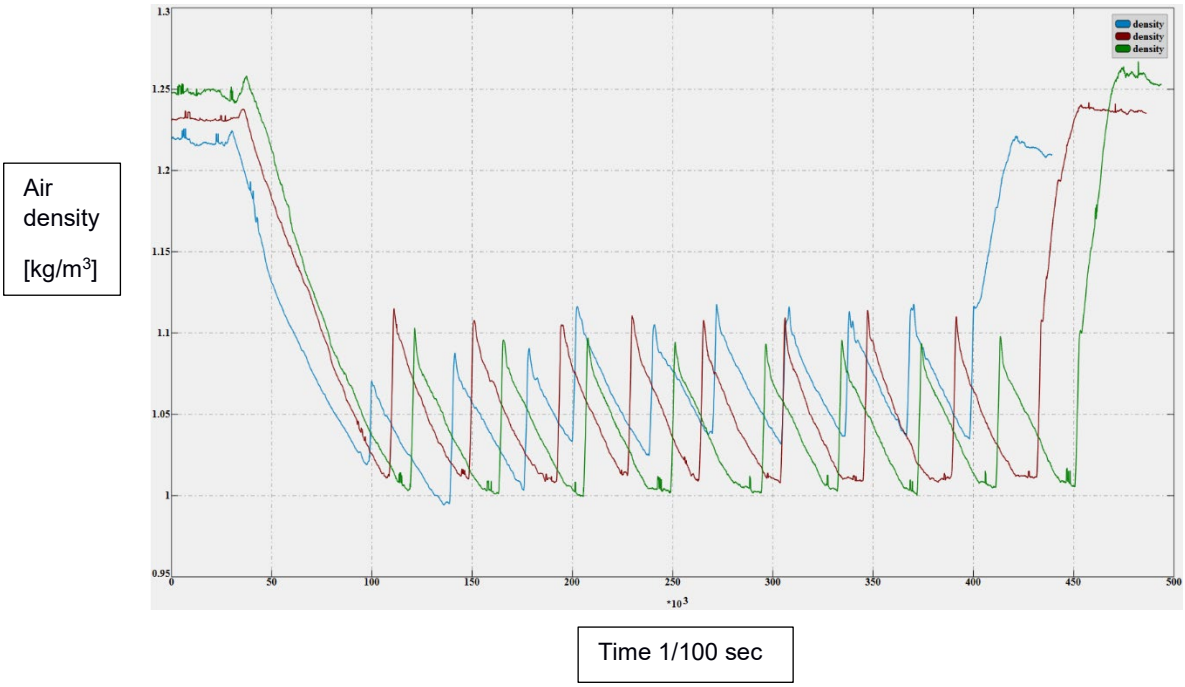

Figure 4.7: Air densities during the 3 spin flights (blue line: 1. flight, brown line: 2. flight, green line: 3. flight).

During the spin runs the air densities changed almost identically between 1.0 kg/m^3 and 1.1 kg/m^3 so that not influences on the results can be seen.

The crew need to wear parachutes all of the time and the pilot has a head-set mounted camera. The pilot also comments on the spin manoeuvre and these audio notes are recorded as part of the head-set mounted camera system. An additional camera system mounted on the aircraft tail (vertical fin) records the entire aeroplane's movements from that location.

The spin trials begin with the CG position as forward as possible and are subsequently continued with trials in the mid and aft position of the CG range. As mentioned above the aeroplane is operated mainly outside of the certified spin flight envelope (see section 4.6).

The aeroplane's centre of gravity shift is conducted by installing trim masses at station 404 cm aft of the aeroplane's datum line (Fuji Heavy Industries, 2011), 'Airplane Flight Manual').

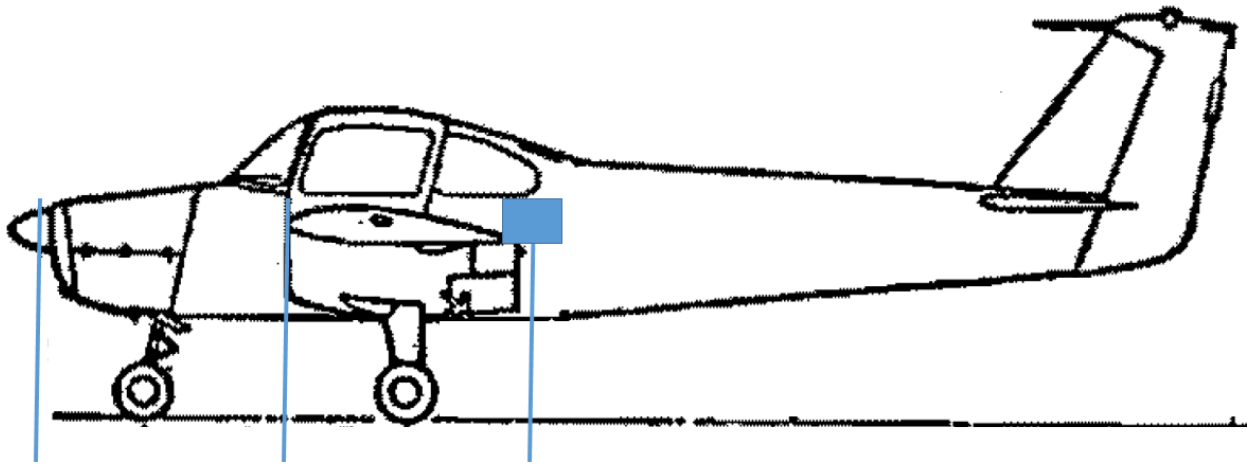

Figure 4.8: Position of the reference position, datum line and trim mass (by the author)

The reduction of the aeroplane's mass is due solely to its engine's fuel consumption. During an entire flight, which contains nine spins, the engine fuel supply is changed every 15 minutes by using fuel from the right and left tank alternatively. This keeps the fuel distribution within the aeroplane nearly in balance, with the maximum fuel imbalance around 7.5 kg. The control inputs for the elevator and rudder are conducted with a rapid motion (less than one second) so as not to produce aerodynamic transient conditions. No anti-spin-parachute has been installed so as not to change the spin characteristics of the aeroplane by mass or aerodynamic changes due to the parachute and its installation on the aircraft.

Note that all spins are conducted to the left due to the:

1.) Torque effect of the propeller
2.) Propeller wash effect
3.) Precession effect of the propeller during pitching
4.) Asymmetric propeller thrust during pitch-up/down flight conditions

For statistical reasons, in all nine spin conditions, three spins will be flown (so the same experiment is conducted three times for comparison and consistency purposes) so that 27 spins are conducted in total.

Procedure 2 (Spin Recovery): standard spin recovery procedure according to the 'Airplane Flight Manual' (Fuji Heavy Industries, 2011):

1.) Rudder full right position (opposite of the spin direction)

2.) Immediately following rudder application, move the elevator control slightly forward of neutral position in a brisk motion
3.) As the rotation stops, neutralize rudder and elevator control
4.) Roll the aeroplane to 0° bank
5.) Pull the aeroplane out of the dive within certified G – limits

This procedure corresponds with that applied by Stough et al. (1985).

4.9 Conclusions

Within this Chapter the modifications (e.g. of the suction system) and inspections (e.g. of the wing spar) of the utilised aeroplane, before the test flights have been conducted, are explained. The reasons for the chosen parameters and the flight envelope (including the aeroplane's CG determination) are presented. In addition, the legal background for the test flights and the corresponding trial procedures are given.

After the above preparations, the practical flights have been performed on the 11th, 14th and 21st of April 2015.

As the experiments have been conducted in the real (natural) atmosphere, influences of the atmosphere on the measurements cannot be eliminated or excluded, although the atmosphere had low turbulence during the time of the flights.
Unintentional control inputs (during the spin entry phase or during the developed spin phase), the engine in idle power, unknown changes of the horizontal wind, etc. may have influenced the spins and thus the data.

For a scientific evaluation of the experiments the measured data need to be analysed by applying mathematical methods. The applied methods can be found in the Chapter 6 and Appendix 7.

Chapter 5 Spin description

In the following section, the physical mechanisms of spinning are described in-depth.

At each state of the spin sequence the aeroplane's attitude, airflow, control deflection, turn rate, vertical speed and acceleration behaviour due to the acting forces and moments are illustrated and described. The description explains a spin as detailed as possible on the basis of the measured data using flight mechanical principles which will be introduced in turn during the text below. The tests and measured parameters are limited to aeroplane mass distributions where the centre of gravity is located in front of the Neutral Point of the aeroplane. This must be taken into consideration when testing the limits of the test data.

5.1 Introduction

For a more complete understanding of a spin it is essential to explain the aeroplane's behaviour during an entire spin run: that means from spin entry until full recovery from it. The following measured parameters will be taken into account:

Parameter	Notation	Notation	Notation	Notation
Altitude related	Hpunkt			
Relative wind related	Alpha_le_c	Alpha_ri_c	Beta_le_c	Beta_ri_c
Acceleration related	X direction	Y direction	Z direction	
Angular related	In_Phi	In_Theta	In_Psi	
Angular rate related	In_p	In_q	In_r	
Control surface related	Eta_ca	Xi_le_ca	Xi_ri_ca	Zeta_ca

Table 5.1: Parameters used for spin description. (For descriptions and definitions, see Glossary Table 1 and 2)

The above listed parameters are all aeroplane related parameters which have been measured in the course of this research project. In addition to those above, system parameters like system time, power supply data or GPS related parameters (like GPS altitude, GPS vertical speed, etc.) have been collected but not analysed within this context. Although they are not spin relevant, this has been done - to ensure that the measurement systems work constantly and properly.

Control forces could not been determined because measuring such forces through the instrumentation system would interfere with the flight control system or the structure of the aeroplane. This is not permitted by EASA.

5.2 Spin description on the basis of the measured flight test data

For conducting a spin the aeroplane's aerofoil needs to be stalled asymmetrically to create an asymmetrical lift and drag on both sides of the aeroplane's centreline and centre of gravity respectively.

Therefore, and in all conducted cases, to induce stall, the aeroplane needs to be slowed down whilst maintaining a selected altitude. Airspeed reduction will reduce the overall lift according to the following expression:

$$F_{Lift} = \frac{1}{2}\rho\, v^2\, S\, c_l \qquad (1)$$

Wherein:

F_{Lift} = Lifting force [N], created by the wing - fuselage combination of the aeroplane

ρ = Density of the air [Kg / m^3]

v = True airspeed of the aeroplane [m/s]

S = Surface of the lift creating wing - fuselage combination of the aeroplane [m^2]

c_l = Lift coefficient of the wing-fuselage [-]

After rearranging equation (1) to

$$v_{min} = \sqrt{\frac{2\, F_{Lift}}{\rho\, S\, c_l}}$$

It can be seen that for a fixed aeroplane mass, fixed altitude (and thus fixed density), and fixed geometry (e.g. no flap extension while approaching a stall), the minimum lift (vector) F_{Lift} depends only on the c_l value which varies with aeroplane attitude.

5.3 Example of a spin entry

As an example of the spin entry behaviour of the Fuji aeroplane, Flight 1, Spin 1 (i.e. the first spin within condition 1) in a time frame between 1370 – 1390 seconds after the system start, has been selected. This is the very first spin flown for this research project. The reason for

this choice is that the Author had at this particular moment - during this particular spin - the lowest ‘spin training’ status within the entire project. Due to that this spin resembles that which may occur during an aircraft accident or during a situation where an unintentional spin is entered.

Before stalling c_l is a quasi-linear function of the angle of attack (α) of an aerofoil – see Figure 5.1.

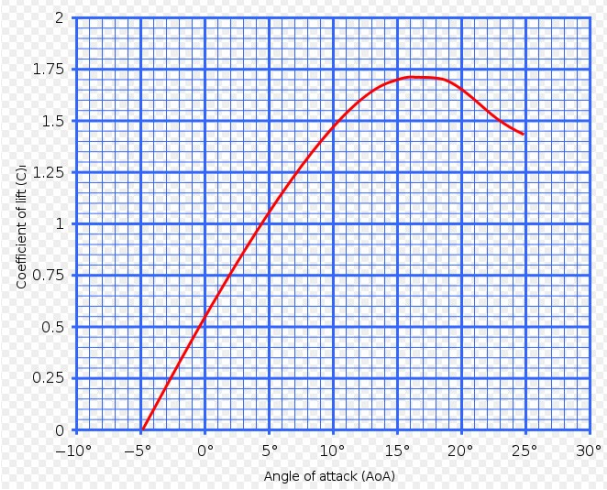

Figure 5.1: Example of a typical aerofoil lift coefficient c_l versus angle of attack, α behaviour (FAA, 2004)

c_l can be varied by changing the aeroplane’s angle of attack directly by increasing the elevator deflection η, e.g. increasing α leads to an increased value of c_l and vice versa. This leads to a characteristic stalling speed v_{min} of a wing and thus to a characteristic angle of attack where a stall occurs around a given aerofoil.

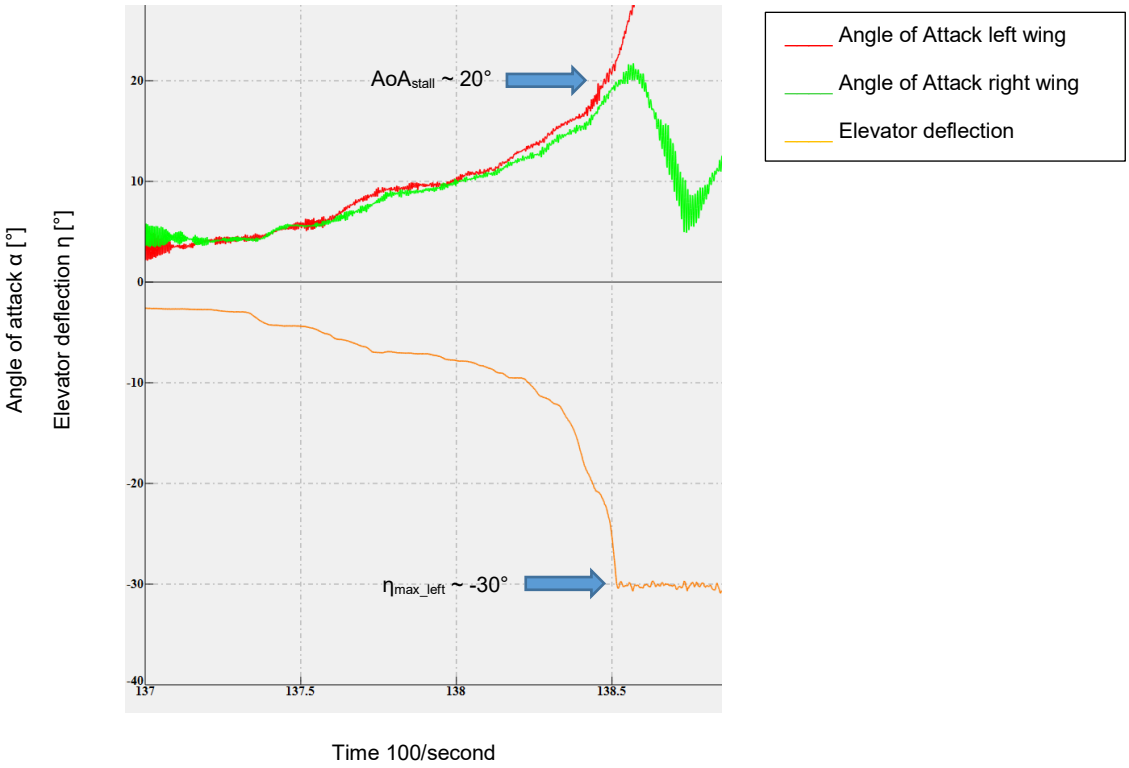

Figure 5.2: left wing (red) and right wing (green) angle of attack behaviour of the Fuji aerofoil, Elevator deflection η (orange) - η is constant during the entire spin (i.e. from 1385 seconds), later reversed for spin recovery (this is not plotted).

The Fuji aerofoil stalls at $\alpha \sim +20°$ (Figure 5.2) and because this is an asymmetric stall, the left wing has stalled (red line) but the right wing (green line) has not.

The asymmetric stall is initiated by the wing developing a non-zero yaw angle and consequential sideslip angle (yaw and sideslip have opposite signs). This is achieved by deflecting the rudder to one side. The amount of rudder deflection to achieve an asymmetric stall depends on the aeroplane's geometry (e.g. fuselage length, fuselage shape, position of wings at the fuselage, etc.), power settings (e.g. propeller RPM, manifold air pressure, propeller blade pitch angle), the aeroplane configurations (e.g. flap setting, landing gear in up or down position), etc. - on the size of the rudder surface (and thus the absolute value of the laterally pointing lifting vector of the tail section), and hence by the turning moment created about the z-axis.

In the 27 considered cases all spins have been conducted to the left hand side (the reason is discussed in Section 4.8) as the rudder has been fully deflected to the left side as indicated by the blue line in Figure 5.3.

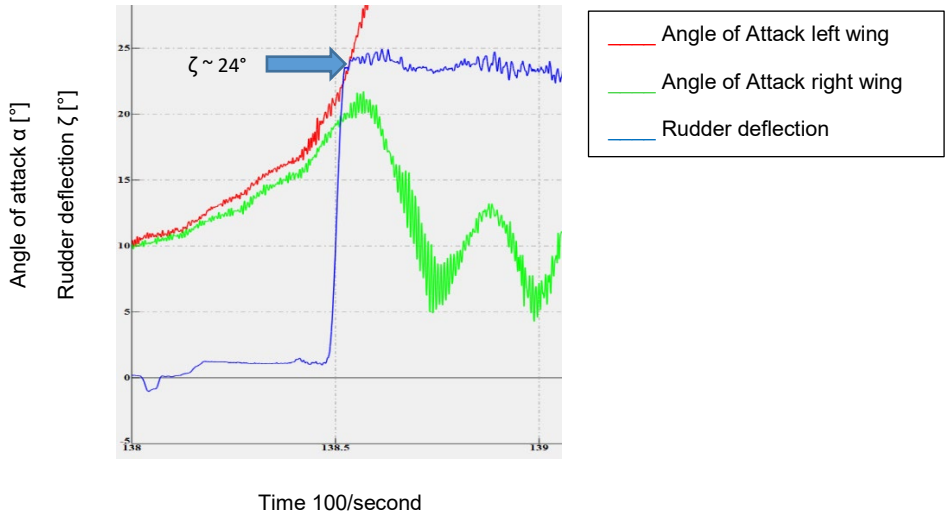

Figure 5.3: The rudder deflection angle ζ (blue) is constant during the spin before recovery.

By deflecting the rudder to one side the vertical tail – i.e. the combination of the fixed vertical fin together with the rudder itself - creates a non-zero side force vector - due to a higher c_l - and hence a corresponding anticlockwise yawing moment about the z-axis.

To maintain the aeroplane's geometry between the spin initiation and the recovery constant the ailerons are kept nearly fixed in the neutral (undeflected) position as can be seen in Figure 5.4. Due to the high turning rates about all axes during a spin it is very difficult for the pilot to keep the ailerons precisely at 0° deflection. Based on the Author's experience it can be said that small aileron deflections of up to χ = ±10° do not influence the aerodynamic behaviour of the aeroplane much during a period of a spin run.

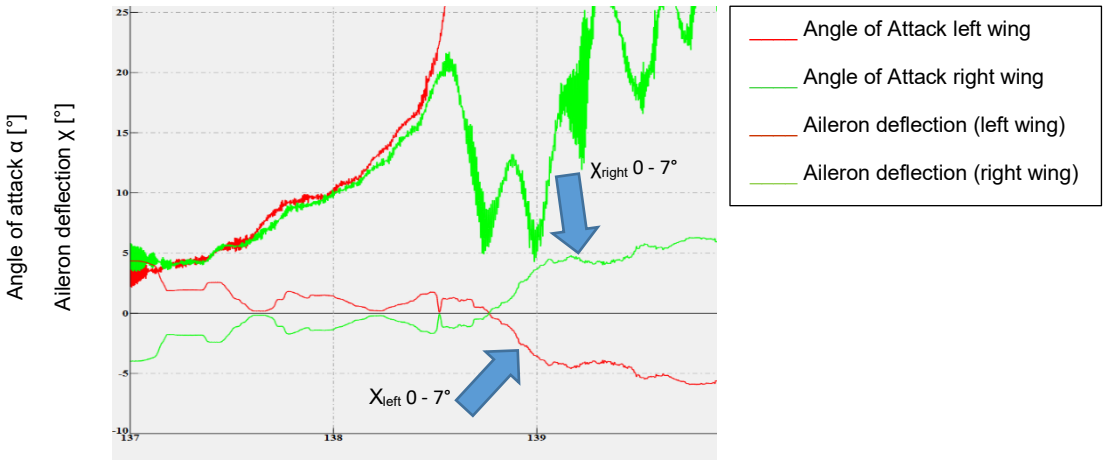

Figure 5.4: In addition to the Figure 5.2 above, aileron deflection angle χ (Xi) for both wings is nearly constant during the entire spin and later spin recovery

Elevator and rudder deflections reach their full deflection at nearly the same time (see Figure 5.5) and thus the slowest reachable airspeed. This ensures that the aeroplane rolls in a defined way into the spin and not due to unduly high different wing speeds while initiating the full rudder deflection at higher airspeeds. The roll behaviour due to the rudder deflection can be seen in Figure 5.7.

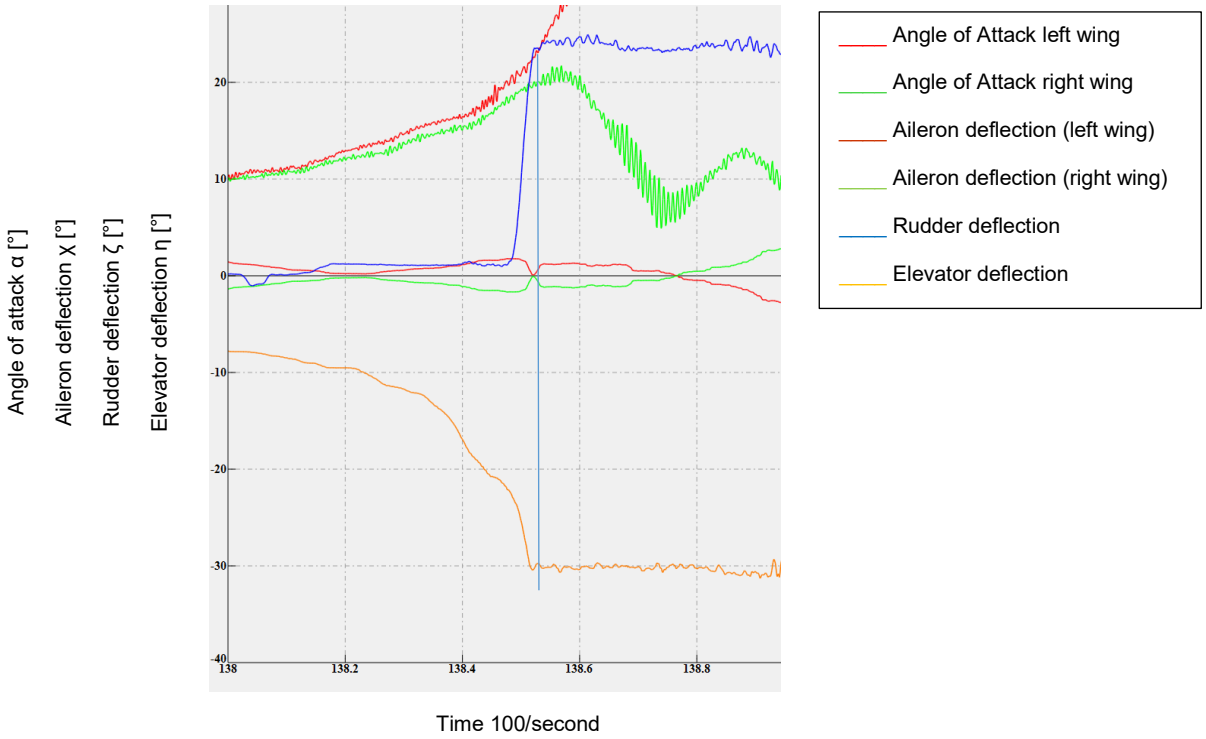

Figure 5.5: Elevator, η, (orange) and rudder, ζ, (blue) deflections reach their maximum values at the same time (see vertical light blue line at around 1385 s) – both control deflections are nearly constant during the spin.

Due to the rudder deflection ζ to the left (positive sign) the aeroplane enters an asymmetric stall, anticlockwise yaw (aeroplane nose to left as tail rotates to the right) and hence a positive sideslip angle (relative wind from the right hand side, see Figure 5.6).

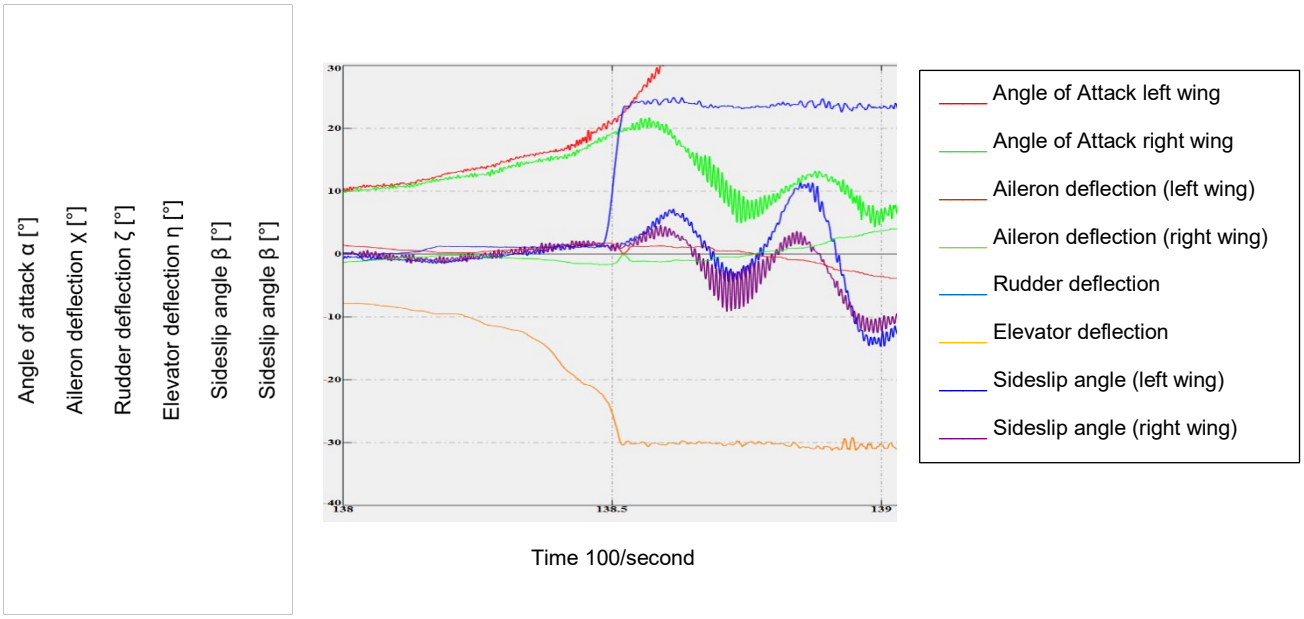

Figure 5.6: in addition to Figure 5.5, left (dark blue) and right (purple) sideslip angle β during the spin entry phase

Due to the rudder deflection, the aeroplane experiences different airspeeds at each wing. Thus both wings create a different amount of lift. The left (slower) wing creates less lift as the right (faster) wing. Hence the aeroplane rolls to the left while yawing to the left. The roll behaviour during the spin entry phase can be seen in the Figure 5.7.

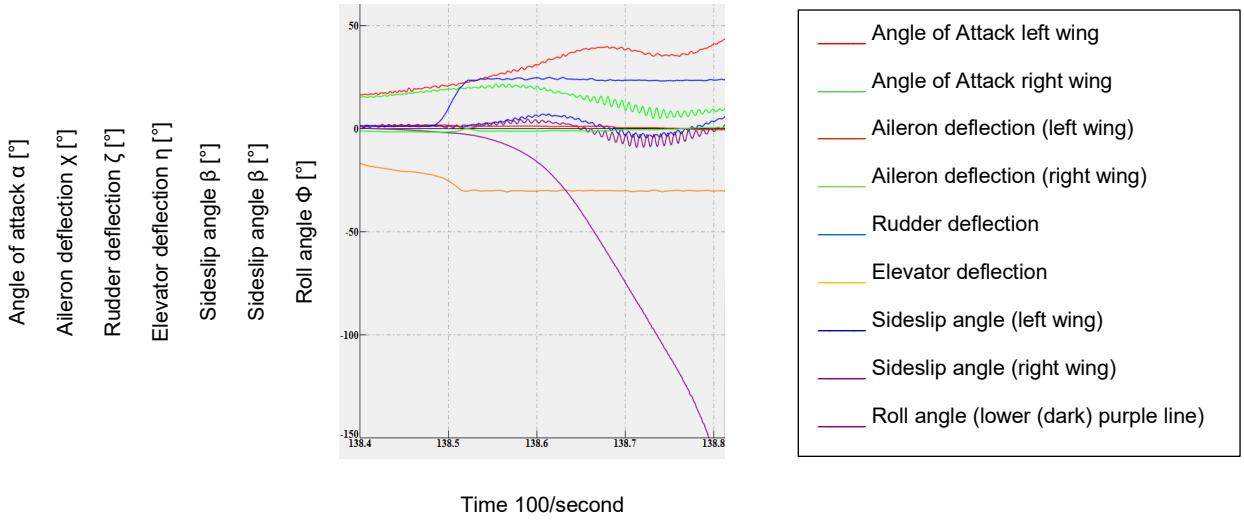

Figure 5.7: in addition to 5.6 above, roll behaviour during the spin entry phase

By deflecting the rudder to the left, the aeroplane will yaw to the left; this means the aeroplane will change its heading to the left. This can be seen in the Figure 5.8 (yellow line). By deflecting the rudder to the left the aeroplane will expose its fuselage and vertical tail behind its pivot point – the centre of gravity - into the airstream. This leads to a back-swing of

the aeroplane's longitudinal axis (heading) to the right. Due to the constant rudder deflection the aeroplane will again yaw to the left.

The horizontal airstream will slow down very quickly as the aeroplane starts to follow its vertical spin axis in a kind of parabolic trajectory. This leads to the reduction of the resetting force (airstream) which produces the initial back-swing.

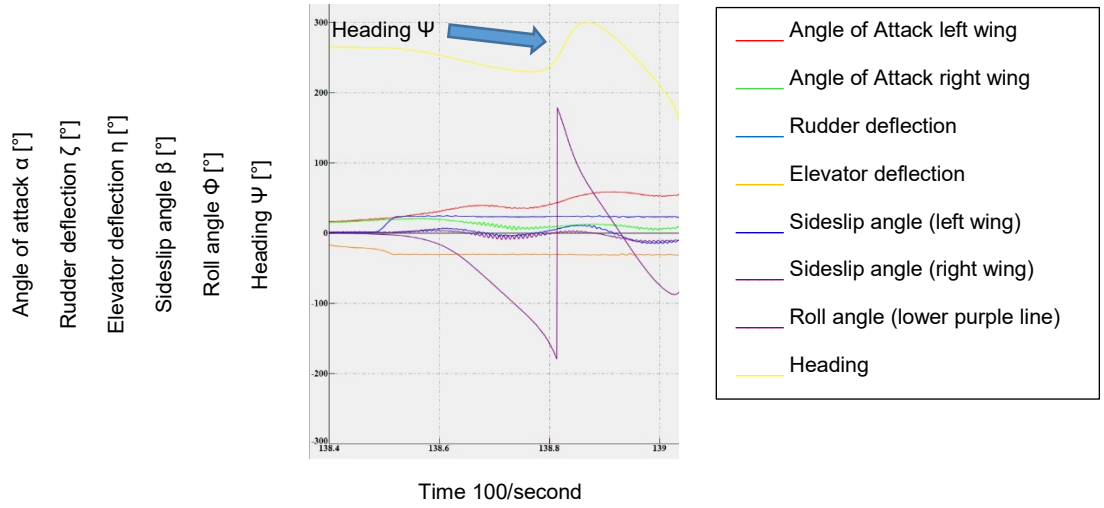

Figure 5.8: (in addition to Figure 5.7 above) yaw behaviour during the spin entry phase

This effect can be recognized with the data in Figure 5.9.

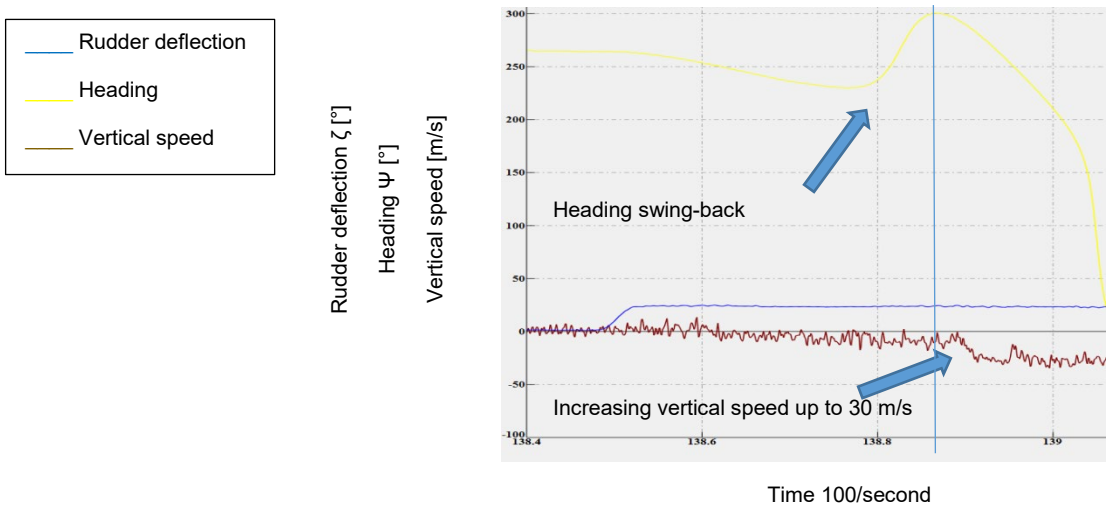

Figure 5.9: (in addition to Figure 5.8) heading swing-back and increasing vertical speed during the spin entry phase

The vertical speed is up to the moment when the heading swing-back to the right is reversed to the ‘second’ yaw to the left low (around 3-7 m/s) but as the aeroplane accelerates its vertical speed and thus a vertical spin trajectory is about to be reached, the aerodynamic force on the rear part of the fuselage of the aeroplane (which was generated by the horizontal airstream) is reduced significantly. Hence the aeroplane will not experience a heading swing-back of this amount again during one spin run. Later in this section it can be seen that the following heading swings are much less than the first one and that this effect only influences the corresponding yaw rate (non-linear behaviour of the data).

The aeroplane and its aerofoil must attain a characteristic angle of attack in order to reach the stall condition. Whilst maintaining a selected altitude, and assuming the aeroplane is in an undisturbed atmosphere, the angle of attack is linked to a characteristic pitch angle Θ (here 13.5°, see Figure 5.10).

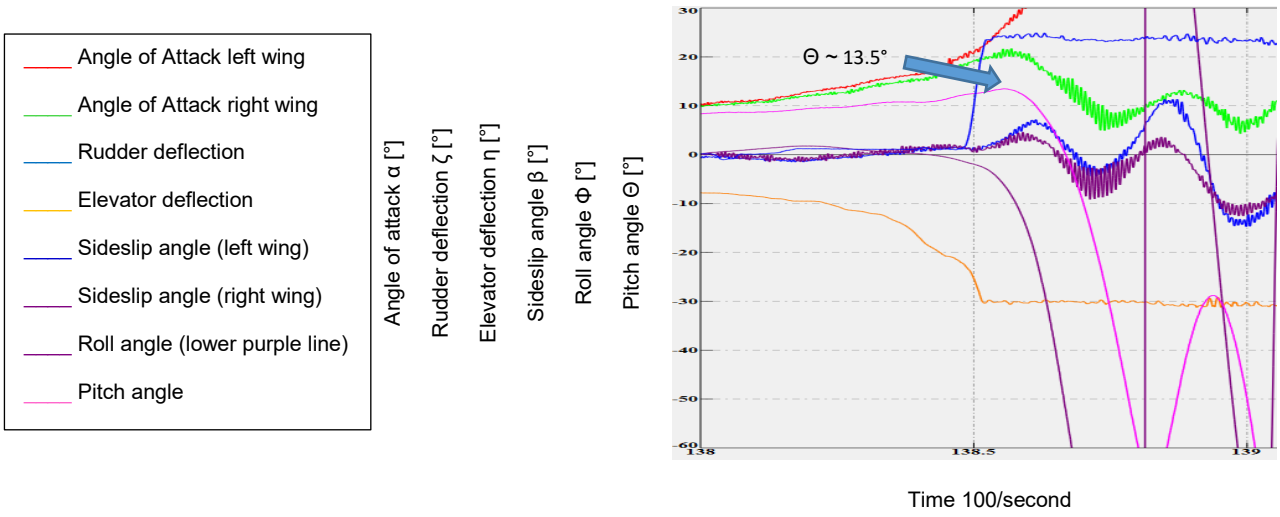

Figure 5.10: (in addition to 5.8 above) pitch behaviour during the spin entry phase

The maximum pitch angle is reached shortly after the maximum angle of attack (Figure 5.11). This time delay (of around 0.2 seconds) is because the aeroplane’s inertia about the y-axis pitches the aeroplane a little further than it would be pitched up by aerodynamic forces alone.

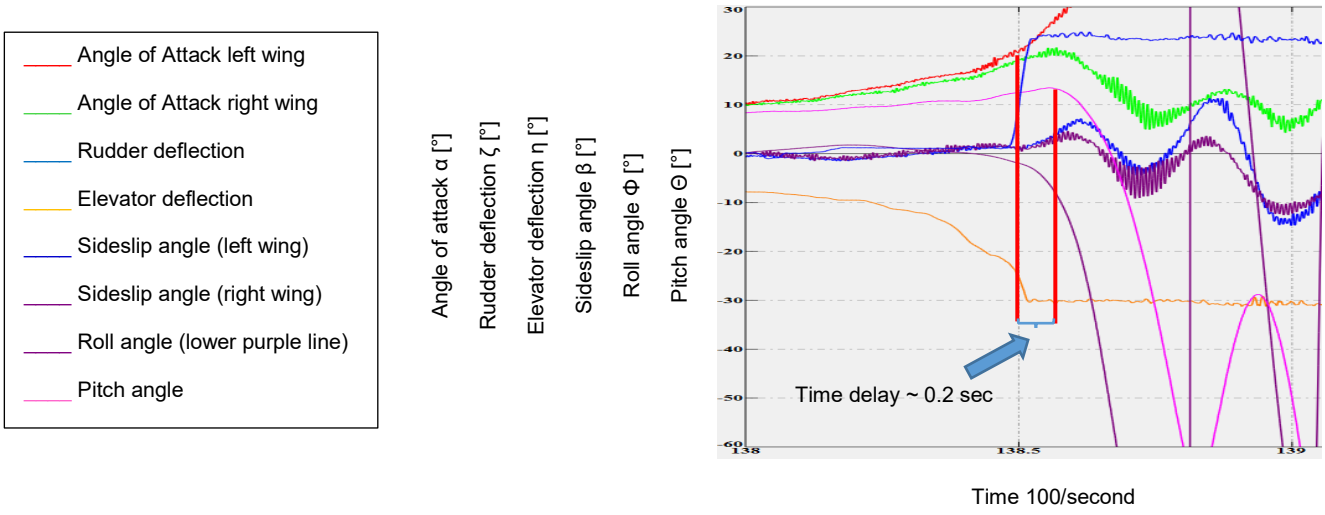

Figure 5.11: (in addition to 5.10 above) maximum pitch up, time delay during the spin entry phase

During the spin entry phase the aeroplane starts to turn about all three axes as explained above. Due to this motion the acceleration in the z-direction is increasing from 1g to around 1.8 – 2.2 g. During a spin run the roll, pitch and yaw angle of the aeroplane change constantly thus the aeroplane-fixed z-axis points constantly in a different direction so that the values for the z-acceleration also change accordingly (Figure 5.12).

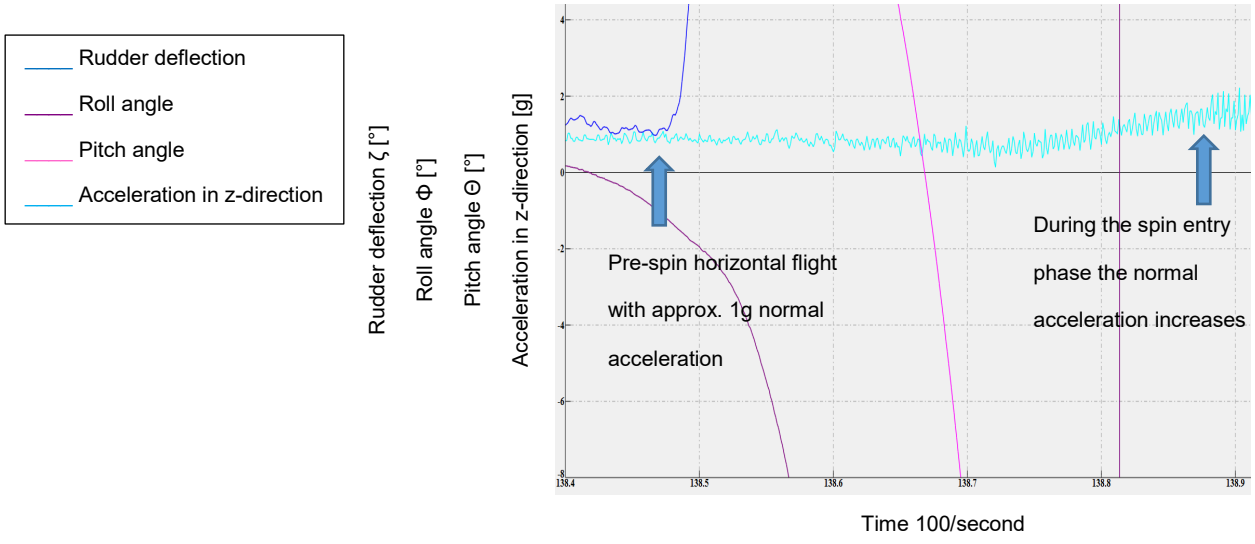

Figure 5.12: Increase of the normal acceleration during the spin entry phase

Note that the acceleration into the aeroplane's z-direction is not the acceleration towards the geographical Earth centre; hence it is above 1 g during a spin although the aeroplane travels along a vertical trajectory.

The accelerations into the x and y-axes directions are not as much affected as the acceleration into the z-direction (Figure 5.13). Due to the fact that the aeroplane is rolling and pitching, the aeroplane-fixed x and y-axes are tilted against the horizontal plane and thus the x and y-accelerometers are influenced by the gravitational acceleration. This influence affects the acceleration in the z-axis as well, but as the aeroplane travels about a vertical spin axis with a non-zero angle of bank, the gravitational acceleration affects the acceleration measurement in this direction much less and the acceleration resulting from a bank angle is much stronger.

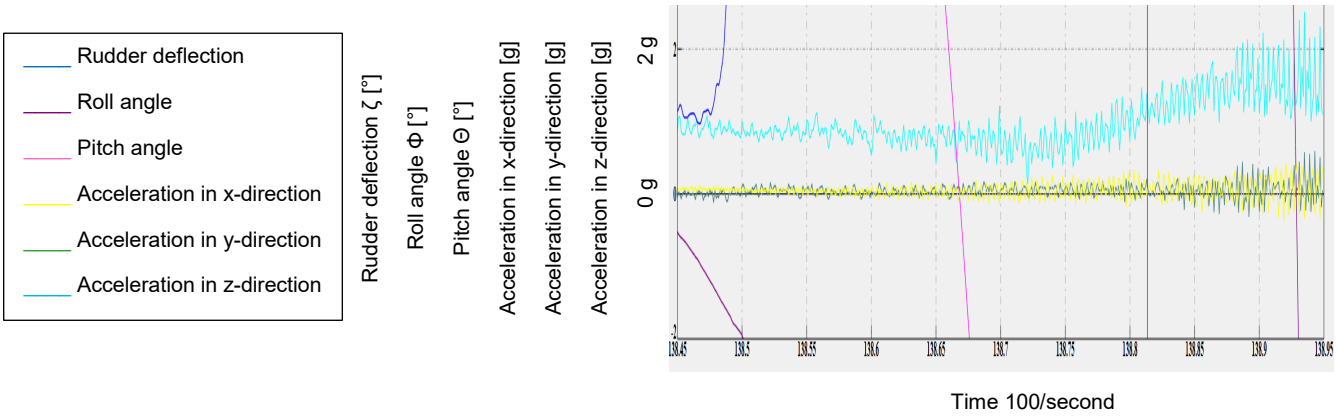

Figure 5.13: Quasi-constant accelerations in the x and y-axes during the spin entry phase

(Note: 1 g = 9.81 m s^{-2})

5.4 Example of a developed spin

The entry phase ends when all described parameters experience a significant change compared to the original undisturbed horizontal flight (here after 3 seconds).

As an example of a developed spin behaviour of the Fuji, the same spin as in section 5.3 has been taken (for the same reasons as described above). For this phase of a spin, a time frame of 1388 – 1399 seconds (i.e. 23:08 minutes and 23:19 minutes and 11 seconds duration) after the system start has been taken. This time frame follows the first time frame in

the section 5.3 (spin entry) without a time gap, and the order of the described parameters are basically the same.

The behaviour of the turning rates p, q, and r about the x, y, and z axes are described here. This was not done in the previous section because the turning rate behaviour is straight forward, i.e. the turning rates increase as the roll, pitch and yaw angle values increase.

5.4.1 Angle-of-Attack and Angle-of-Sideslip behaviour

Figure 5.14 below shows the angle of attack behaviour after the spin entry phase. The control surfaces for elevator, η, and rudder, ζ, are held fixed at their control stops or kept neutral (χ) as much as possible.

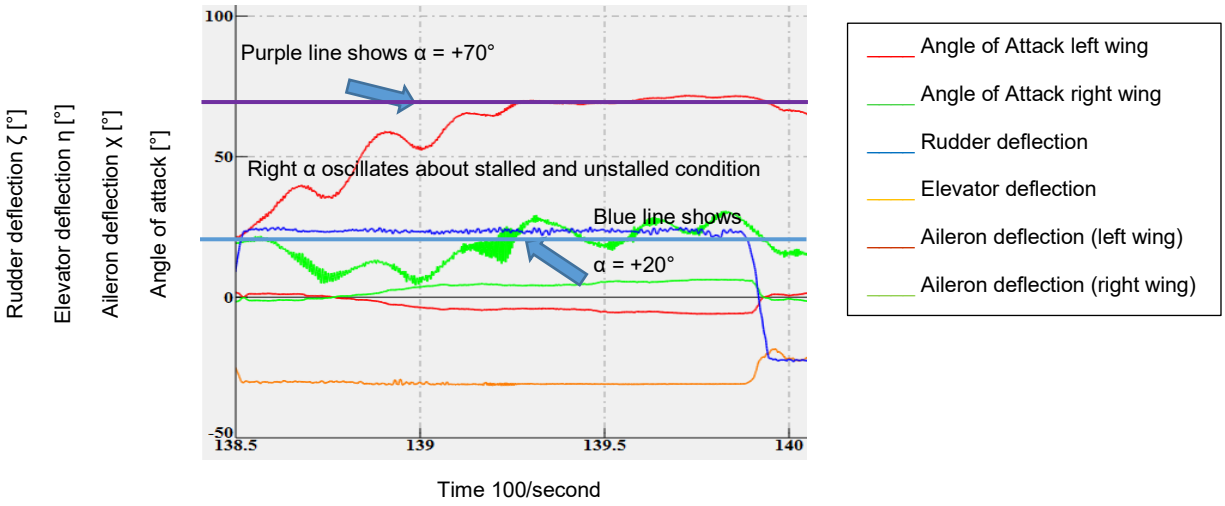

Figure 5.14: Left α (upper red line) and right α (upper green line) behaviour of the Fuji aerofoil during a spin. Elevator deflection η, Rudder deflection ζ and Aileron deflection χ (lower red line left and lower green line right) are constant during the entire spin, η later neutralized, ζ later reversed and χ still neutral for spin recovery (not in the Figure above)

The aerofoil of the FA 200 stalls at ~ +20°. Thus as seen from the Figure 5.14, the left wing is 'deeply' stalled during a developed spin as it approaches a final α value of around +70°

including some local peaks. The data of the right wing α shows an oscillating course about stalled and unstalled conditions in the second half of the spin. In the first half of the plot the right wing α values are well below +20°, in the second half of the plot values are about +20°.

Why is there oscillation in the α data and thus oscillation of the left and right wing α values? After the rudder is fully deflected to the left, the aeroplane yaws to the left and by this it swings about its new aerodynamic or force equilibrium.

This oscillation is conditioned by the aeroplane's inertia (which causes a certain over-swing of the final yaw angle) and the (resulting) aerodynamic forces on the rear fuselage. These cause a certain reversal of the yaw (back to the right) because the tail section of the fuselage is exposed into the airstream going from upstream.

The same aeroplane behaviour can be observed while flying on a selected heading and the pilot commands a sole rudder pulse input to one side. The aeroplane yaws to the corresponding side and the rudder is released to its neutral position, the Fuji oscillates three times (according to the Author's experience on that aeroplane, no particular measurements have been conducted) about the initial heading until the aeroplane's oscillation is damped down to zero. Here again the aeroplane's inertia and the resetting aerodynamic force on the rear fuselage are the causes for this damped oscillation.

The independent superpositions of movements can be observed in the α data in Figure 5.15. After full rudder deflection to the left (upper blue line), both sideslip angles, β (left side lower blue line and right side lower purple line) show positive values. This indicates that the airstream hits the sensors and thus the wings from the right. The asymmetric stall occurs at this time so that the left wing drops and hence the aeroplane rolls to the left.

Initially both sideslip angle values behave similarly (they are both in phase and damped oscillations) as the aeroplane oscillates about its new aerodynamic or force equilibrium, like after a sole rudder pulse control input. After (again) three turns, the left sideslip angle behaviour is excited. Although both β oscillations are still in phase, the amplitude of the left β values increases strongly.

This behaviour sets in when the right α approaches stall for the first time and then oscillates about ~+20° (stalled – unstalled condition of the right wing).

It can be observed from the data that while the right α increases into a stalled condition; the left β starts to be excited.

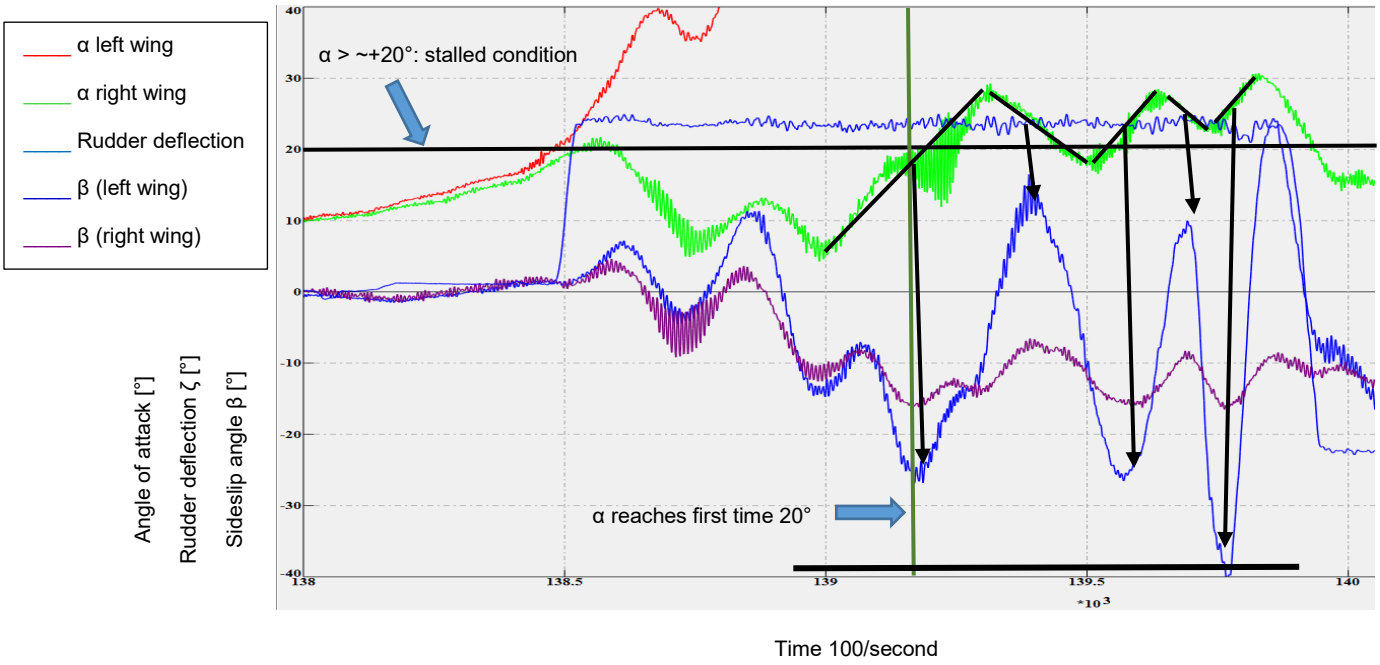

Figure 5.15: Left α (upper red line) and right α (upper green line), rudder deflection ζ, left β (lower blue line) and right β (lower purple line) behaviour of the Fuji during developed spin

In other words: if the right wing's drag increases (positive gradient of the right α) and thus the aeroplane yaws to the right, it slips to the left (negative peak of the left β values, see first black arrow in Figure 5.15 above) and if the right wing decreases its α value and hence its drag (negative gradient of the right α, see second arrow in Figure 5.15) the aeroplane yaws to the left and thus slips to the right (positive peak of the left β values).

As the wing tip of the outer wing (here the right wing tip) is much faster during a spin (and consequently the right β sensor) than the inner wing tip, the outer wing receives more relative wind from ahead and thus the outer wing tip β values do not fluctuate as much as the inner (left) wing tip values.

The reason for the changes in the α values in the region about the stalled / unstalled condition of the right wing is the vertical speed of the aeroplane. The faster it travels vertically the higher the value of α becomes. This can be seen in Figure 5.16.

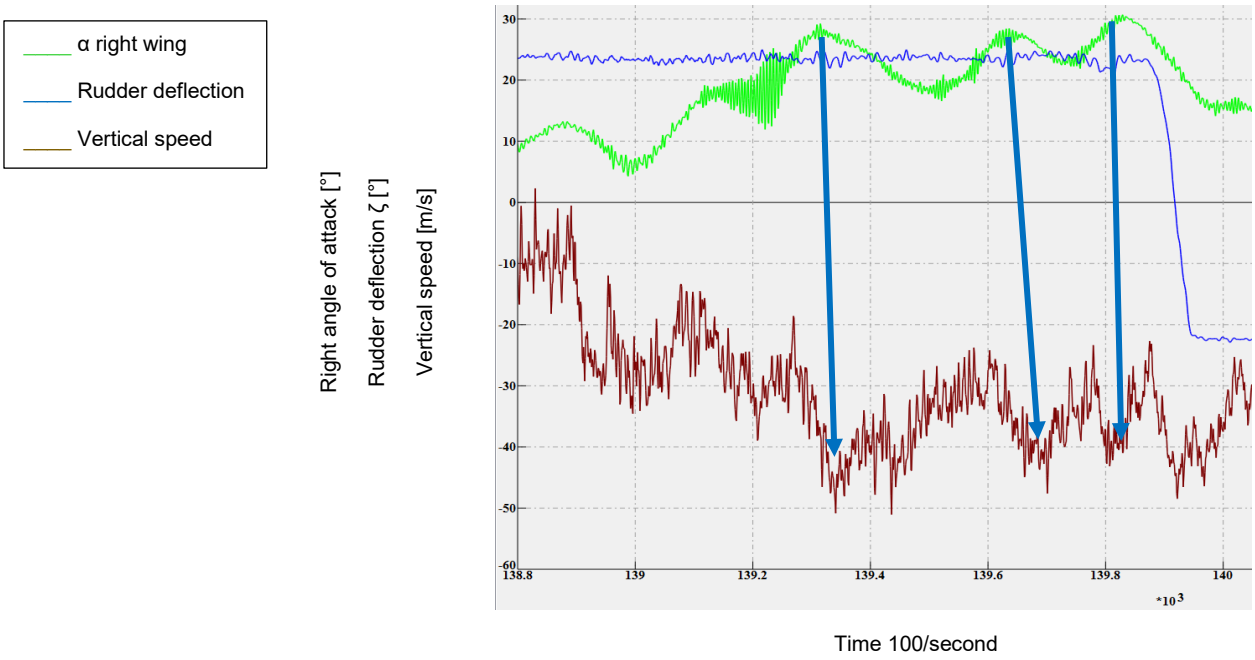

Figure 5.16: Vertical speed, right α and ζ. Note: Static pressure has been taken from the normal production Pitot-Static-System; time delays between α peaks and vertical speed peaks are due to pressure transmission time delays through a four metre long static pressure tube. The high data fluctuation is caused by the position of the static pressure port which is located on both sides of the aeroplane's fuselage which lies in the path of the vortices created by the presence of the wings and front part of the fuselage.

The reason that the left α is not fluctuating like the right is that the aeroplane travels much more in the direction that the left wing is pointing to (see Figure 5.14).

5.4.2 Acceleration behaviour around all three axes

Due to the aeroplane's rotation about all axes during a spin the acceleration measurement in the x, y and z – axes directions is influenced by the current roll, pitch and yaw angles of the aeroplane. An example can be seen in Figure 5.17.

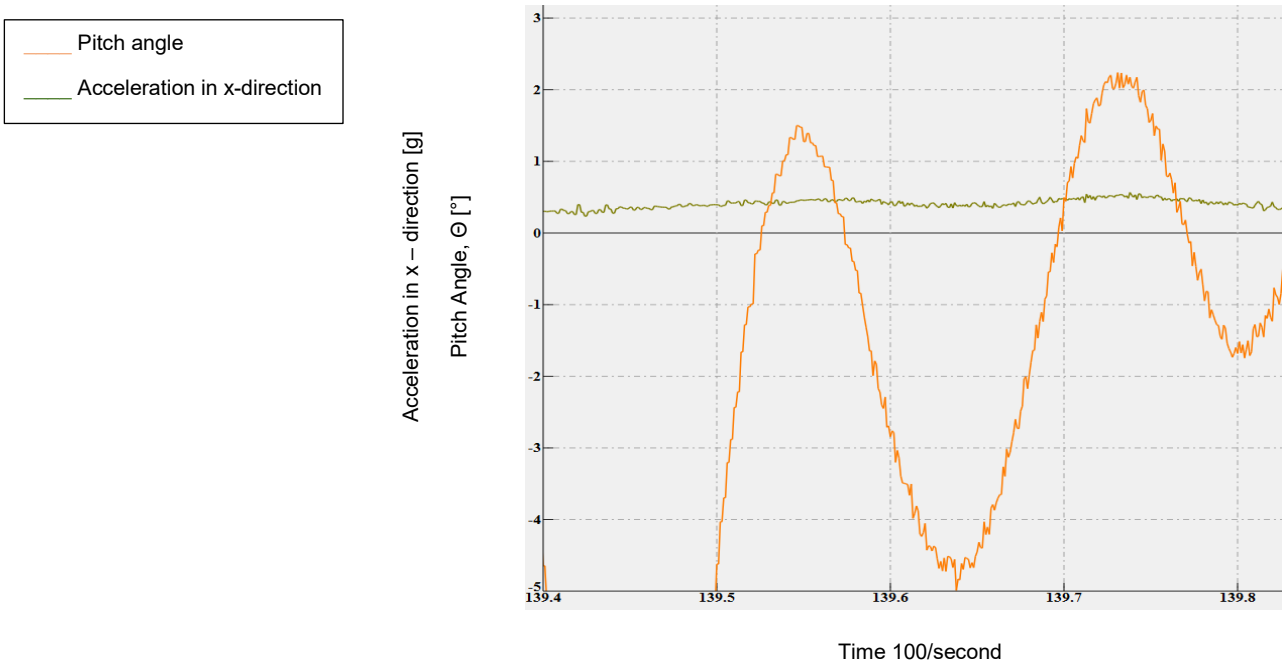

Figure 5.17: Acceleration in x-direction and pitch angle run. Note: The pitch angle, Θ, values have been shifted by +45° (upwards) for comparison reasons

The entry phase and the very first part of a spin cannot be used for this discussion as the acceleration values are strongly disturbed by a high degree of vibration of the IMU which is caused by the strong stall buffet of the aeroplane and the engine vibrations (which is transmitted via the aeroplane's structure to the IMU) as one can see in Figure 5.18.

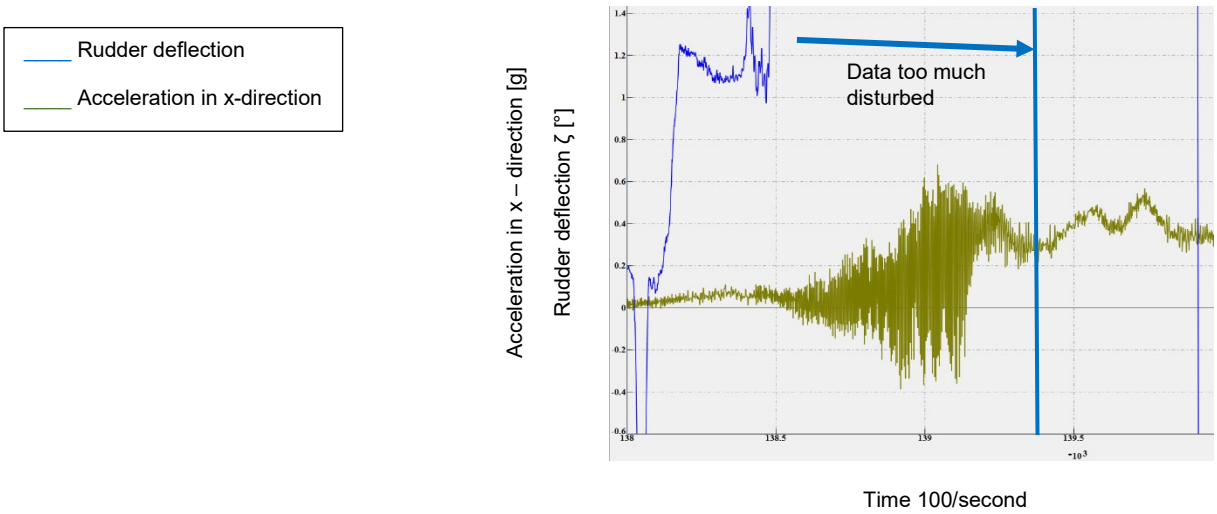

Figure 5.18: Acceleration in x-direction and rudder deflection during the entire spin procedure. Between spin entry and 1394 seconds after system start, the x-direction acceleration data cannot be used due to the high level of data disturbance

Later in the spin manoeuvre, the stall buffet calms down because the aeroplane gains airspeed and thus moves more smoothly.

Due to the nose down attitude of the aeroplane during a spin, the acceleration values for the x-direction are above zero g (while flying unaccelerated horizontally it is zero in the x-direction). The aeroplane oscillates about its final pitch value of approximately - 45°. Thus a mean acceleration of 1g * sin 45° = 0.707 g should be seen in the data but which is actually (Figure 5.18) not the case. (The acceleration values are between 0.3 to 0.5 g).

From the data of the aeroplane's vertical speed one can see that the aeroplane is nearly constantly accelerating downwards until reaching a certain plateau about which the vertical speed values are oscillating (Figure 5.19).

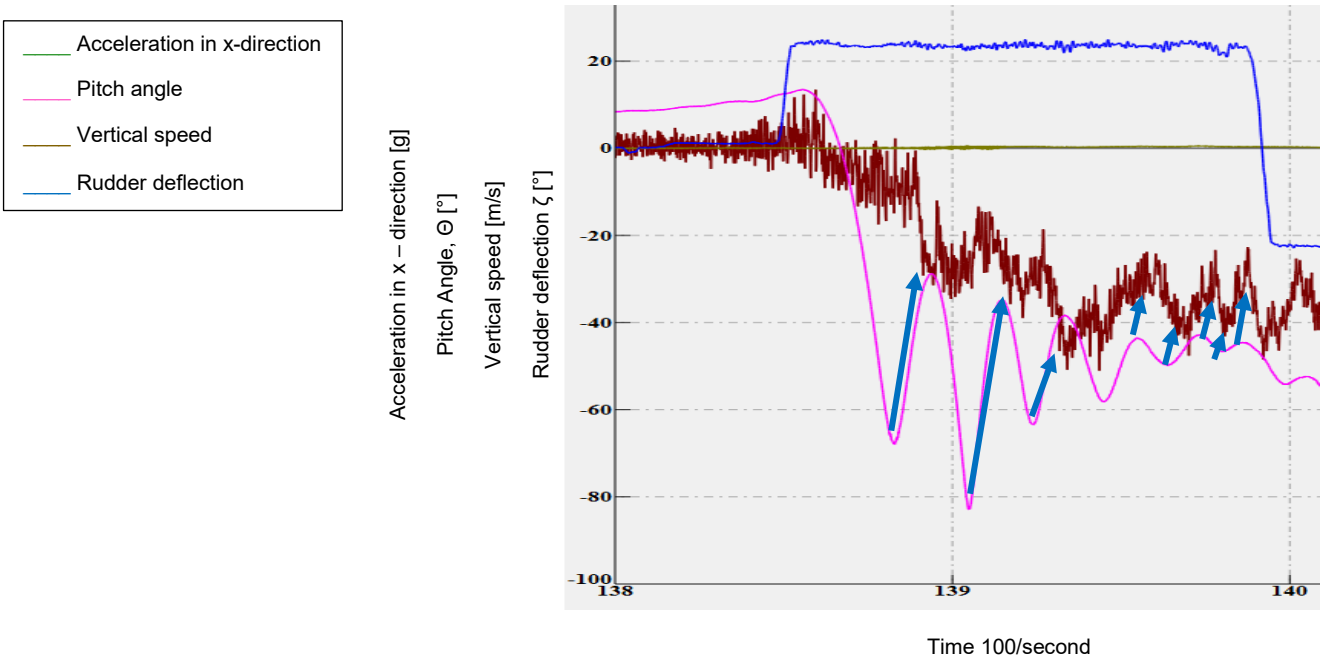

Figure 5.19: The vertical speed increases until it reaches a final plateau. It depends on Θ and the vertical drag vector (airstream hits the aeroplane vertically from below). The time delay of the vertical speed with respect to Θ is caused by the pressure transmission through the static line

Due to the fluctuation of the pitch angle, Θ, the vertical velocity and thus the vertical acceleration is changing. Thus the acceleration in the x-direction does not just depend on the aeroplane's pitch angle (Figure 5.20).

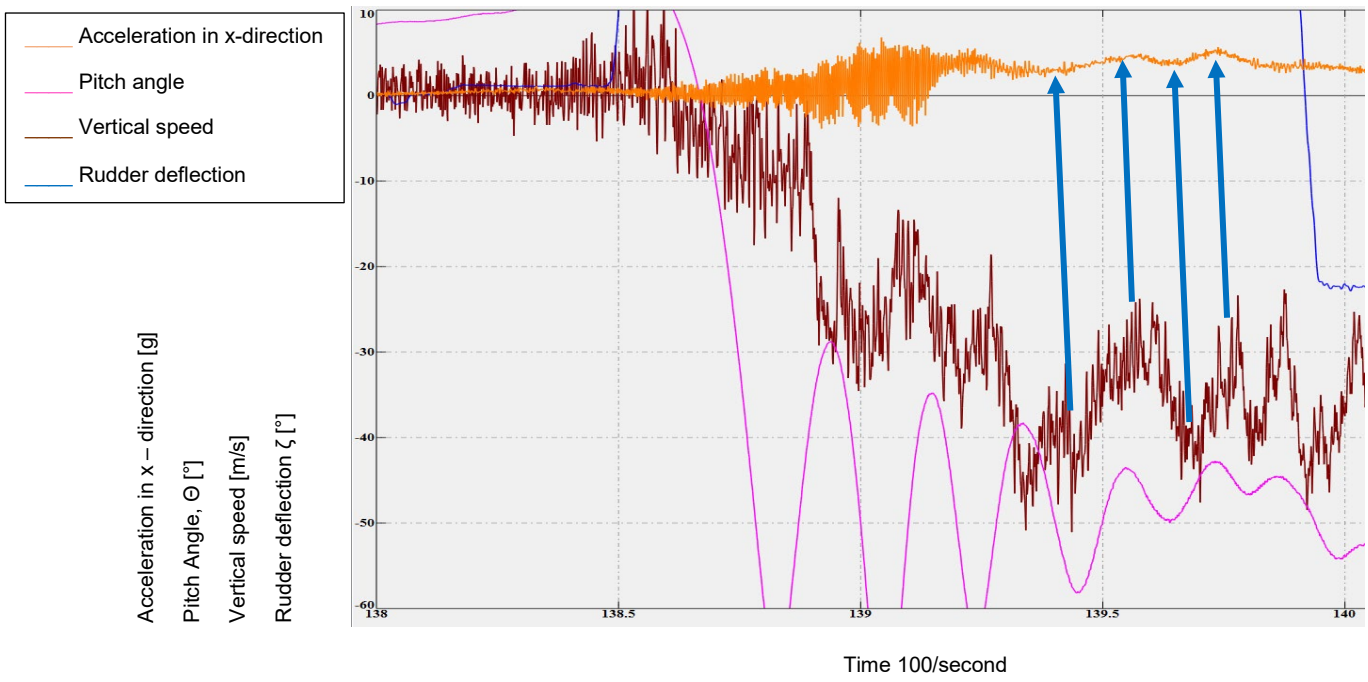

Figure 5.20: Pitch Angle, vertical speed and x-acceleration. Note: x-acceleration values are multiplied by 10 for demonstration reasons. Blue arrows show the dependency between vertical speed and x-acceleration

The acceleration in the y-direction (to the right) is mainly influenced by the roll to the left. In the case of the airflow staying attached to the right wing and thus a relevant amount of lift is created on that side, the aeroplane rolls to the left. The roll creates acceleration in the y-direction of the aeroplane's fixed coordinate system. It is shown in Figure 5.21 that this corresponding slight acceleration is up to around 0.3 g.

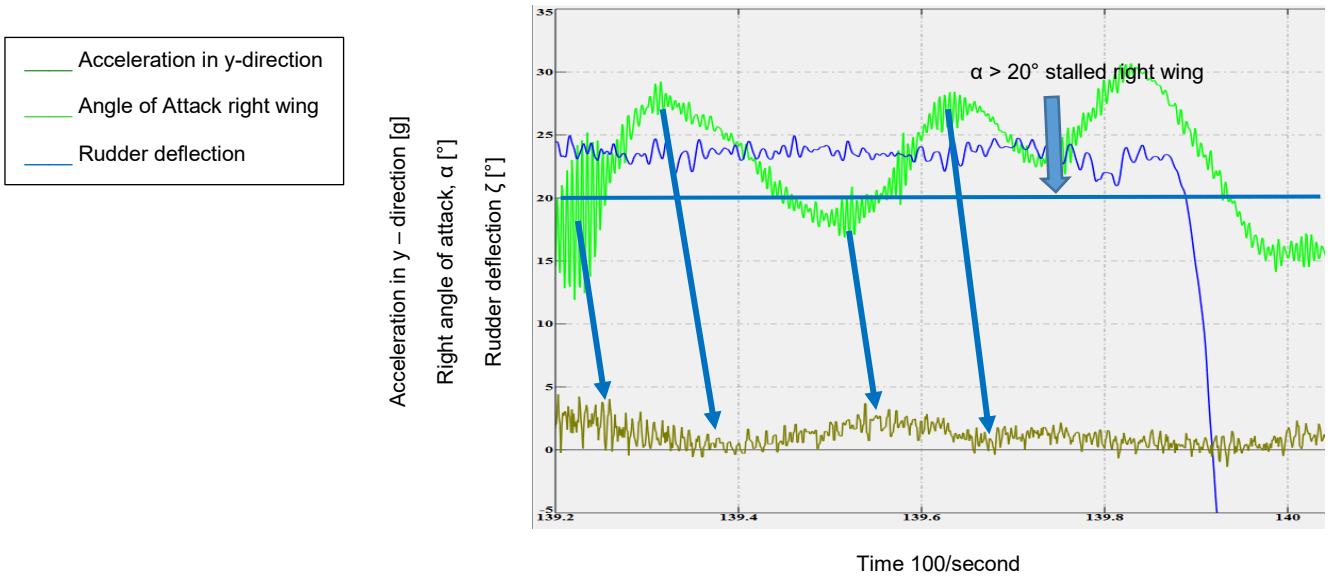

Figure 5.21: Right angle of attack, α, rudder deflection, ζ and acceleration in y-direction (due to aeroplane's roll). Note: y-acceleration values are multiplied by 10 for comparison reasons

The time delay is caused by the acceleration of the aeroplane's (laterally distributed) mass (around 980 kg gross mass of the aeroplane with approximately 75 kg of fuel in the wing tanks within this flight condition plus the mass of the wings, landing gear, etc.). The lifting force of the right wing needs a certain (small) time to start the aeroplane rolling to the left. This can be recognized by the corresponding arrows in Figure 5.21.

The current aeroplane bank angle - and thus the tilt angle of the y-direction accelerometer – contributes to the resulting y-acceleration. But, as Figure 5.22 shows, this influence is overridden by the roll acceleration and cannot be recognized in the recorded data.

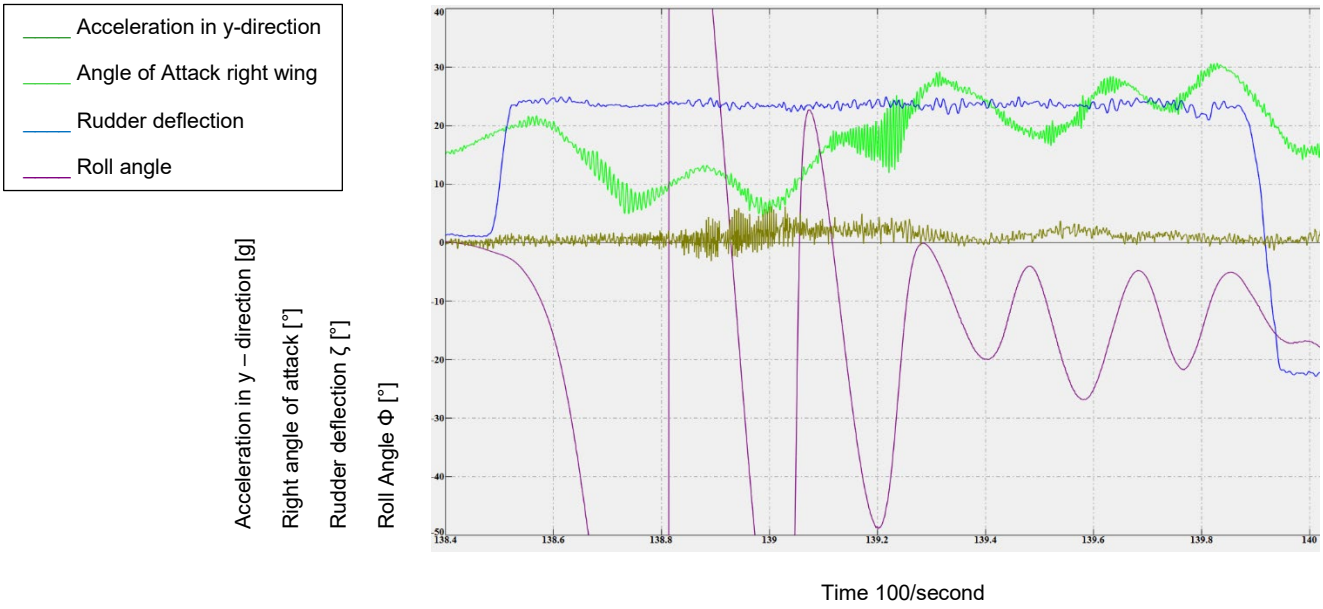

Figure 5.22: The roll angle influence on the resulting y-acceleration cannot be recognized

In Figure 5.23 the dependency of the z-acceleration on the yaw rate is shown.

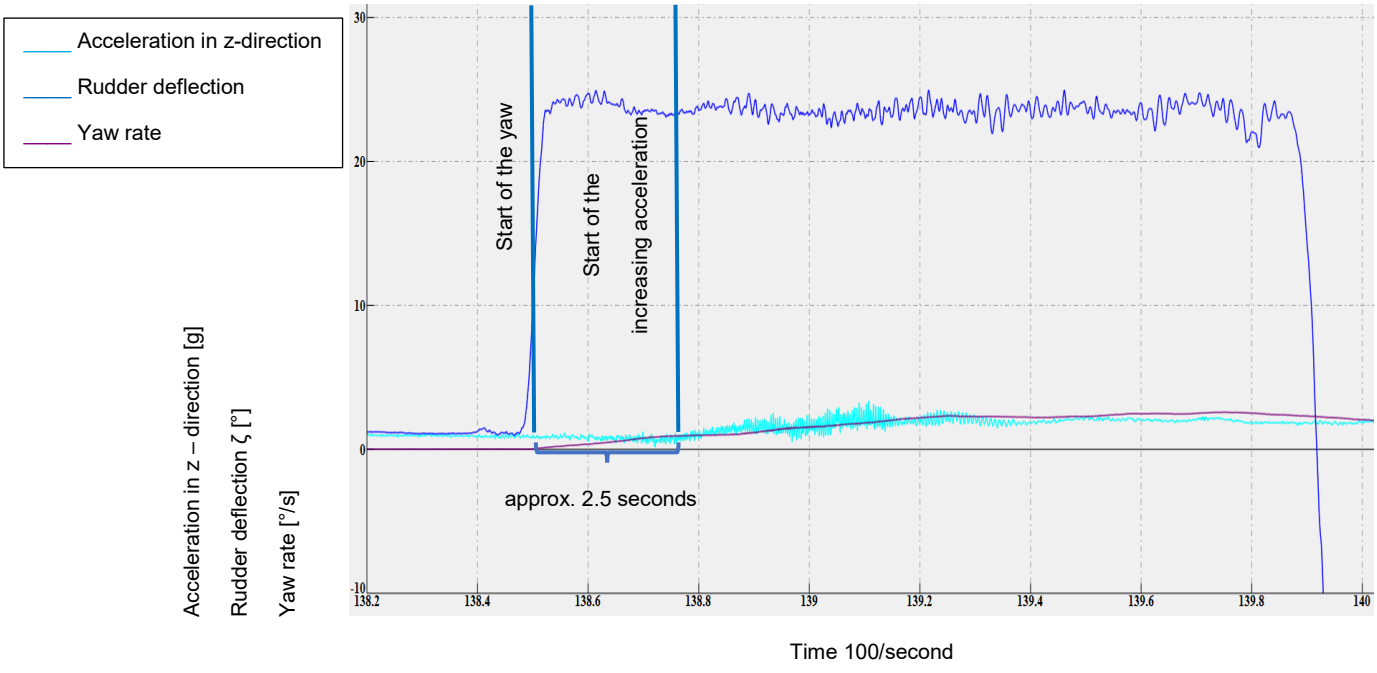

Figure 5.23: Acceleration in z-direction, rudder deflection and yaw rate. Note: for comparison purposes, absolute yaw rate values divided by 50 are shown. This is so that the values are presented at the same order as the z-acceleration

As the yaw rate values are much higher (in the area of 100 – 130 °/s) than the z-acceleration values (1 – 2.5 g), the dependency of the z-acceleration on the yaw rate cannot be seen in

the first instance. Thus the yaw rate values have been scaled to a similar order as the z-acceleration values. This enables the yaw rate dependency of the z-acceleration of the rolling and pitching aeroplane to be seen.

Due to the moment created by the rudder deflection, the aeroplane starts yawing to the left. This induces a roll to the left because of the yaw – roll coupling (of all aircraft and explained more fully in the next section). Since the aircraft is in stall, the aeroplane then pitches downwards. This superposition of the three motions causes a constant change of the z-axis tilt and a corresponding influence on the z-acceleration.

At the very first moment the aeroplane yaws, the roll and pitch motions are small and thus the z-axis tilt is small. This is the reason for the time delay shown in Figure 5.23. While the spin motion is developing, the z-acceleration increases to around 2.5 g.

5.4.3 Aeroplane's attitude and turn rate behaviour (Φ with p, Θ with q, Ψ with r)

(roll angle = **Φ,** roll rate = p, pitch angle = **Θ,** pitch rate = q, yaw angle = **Ψ,** yaw rate = r)

When applying the rudder the aeroplane yaws to the same side. While yawing to one side the outside wing (here the right wing) is increasing its local airspeed and thus the inside wing is decreasing its local airspeed. Due to that difference in airspeed the faster wing creates more lift then the slower and hence the aeroplane starts rolling. These both motions cannot be separated from each other. This phenomenon is called the 'yaw-roll-coupling'.

In order to always create the same magnitude of the yaw-roll-coupling effect, the rudder is always fully-deflected at the same airspeed of 55 KIAS (Knots Indicated Airspeed) or about 28 m/s. This is 2 knots or 1 m/s above the stalling speed of the aeroplane's clean (i.e. flaps up) configuration. This leads to a roll behaviour which is shown in Figure 5.24.

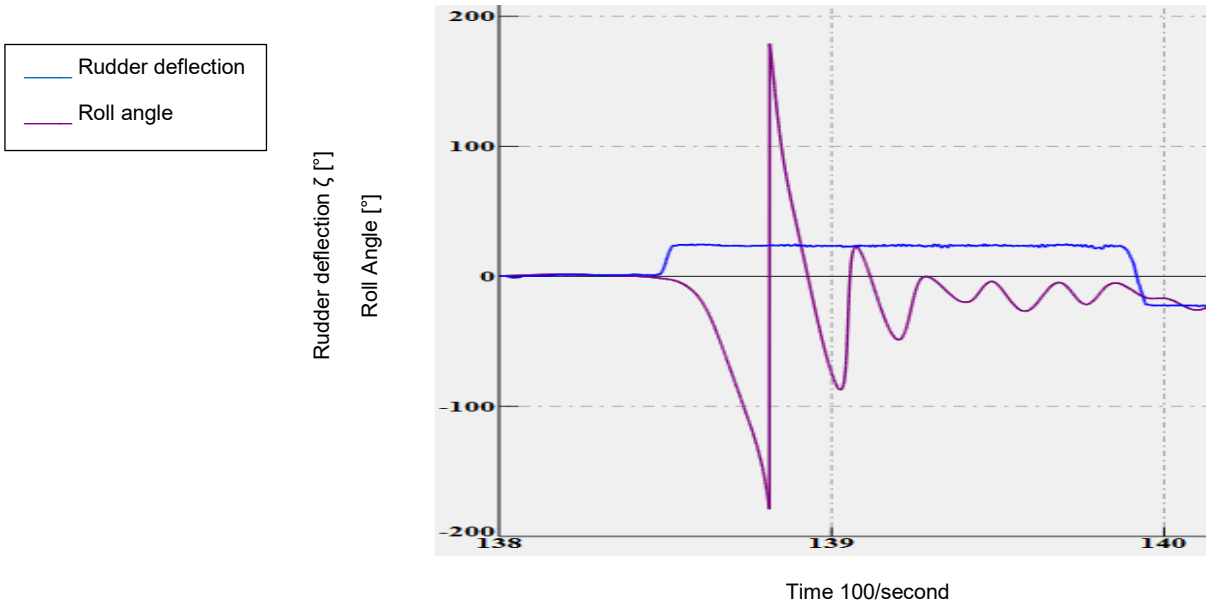

Figure 5.24: Rudder deflection and roll angle. Note: the aeroplane completes initially a full roll through a bank angle of 180° (indicated by the first negative and positive peak)

Rolling of an aeroplane is driven by asymmetric lift on both side of the aeroplane's x-axis. This can be seen in Figure 5.25.

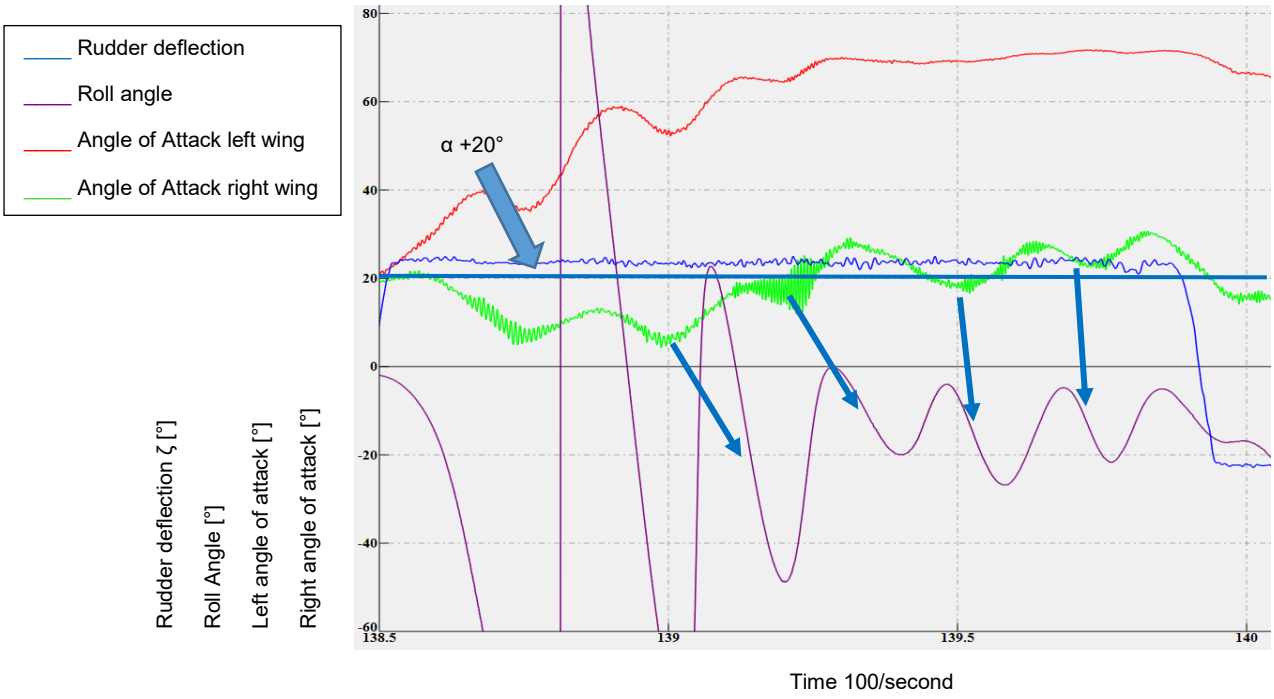

Figure 5.25: Rolling of the aeroplane is caused by asymmetric lift of the wings. Note: as soon as the right wing creates no relevant amount of lift (stalled condition, α_{right} > around +20°) the roll is damped

The small blue arrows on Figure 5.25 show that if the right α is low (wing is creating lift) the aeroplane rolls to the left with a time delay due to the aeroplane's inertia. In the case that the right α is higher than +20° then roll to the left decreases. This can also be seen with the corresponding roll rate (see Figure 5.26).

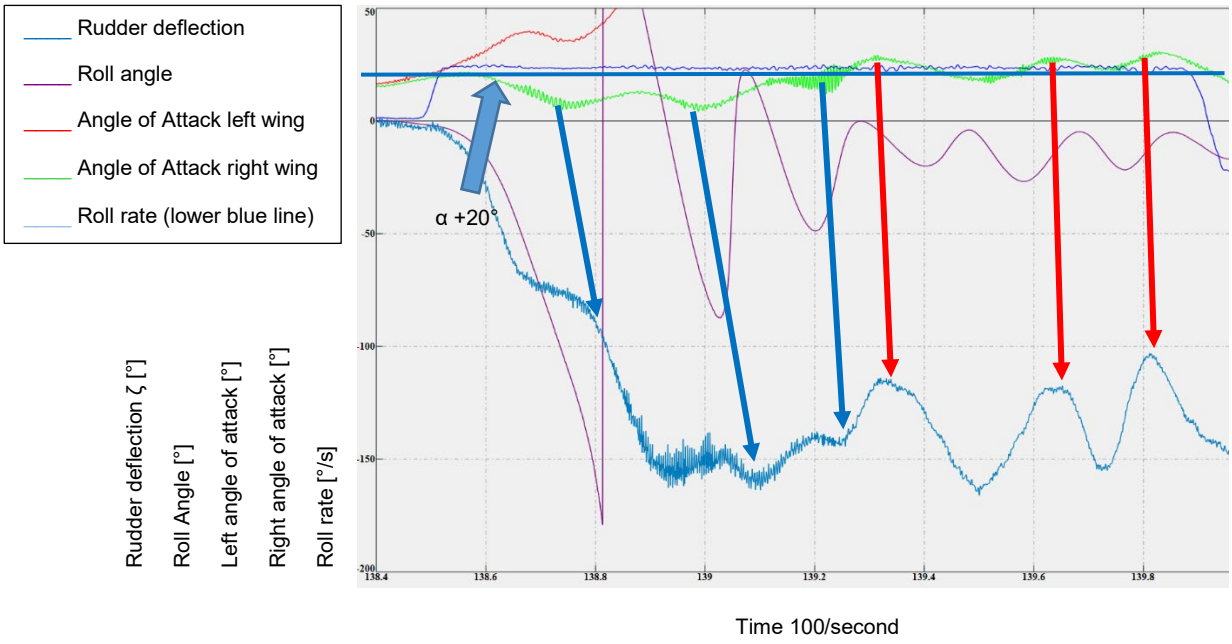

Figure 5.26: (In addition to Figure 5.25 above) Roll rate is driven by asymmetric lift of both wings

As soon as the right wing creates lift due to a lower α, the aeroplane increases its roll rate to the left (see small blue arrows in Figure 5.26). As soon as the right wing enters a stalled condition the roll rate runs basically (see red arrows in Figure 5.26) together with the α value.

In the following section the pitch angle run and the corresponding pitch rate run are analysed.

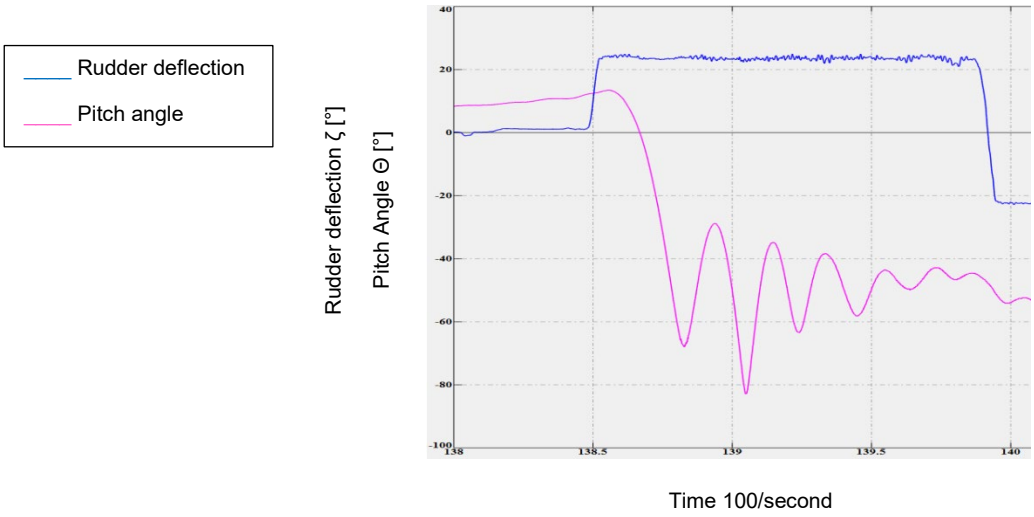

Figure 5.27: Rudder deflection and pitch angle run. Note: In all 27 observed cases the second pitch down peak shows the maximum pitch down value

Based on the Author's experience in stalling the Fuji, a clean (flaps up) stall according to the current Certification Specification (1 kt/s speed reduction in a horizontal flight without a bank angle) produces pitch down angles of around -5 to -10°. During a spin run the aeroplane shows maximum pitch down angles of ~85° while rolling and yawing into the spin.

This 'yaw-roll-coupling' induces a tilt of the lifting vector (up to a bank angle of 180° as shown above) which is, during a horizontal flight, pointing vertical upwards. This vector tilt, combined with the pitch down of the stall leads to a strong pitch down attitude.

From the moment of the rudder deflection the aeroplane yaws to the corresponding side. The yaw rate is increasing during the first part of the spin while the rate of descent is increasing as well. This can be observed in Figure 5.28.

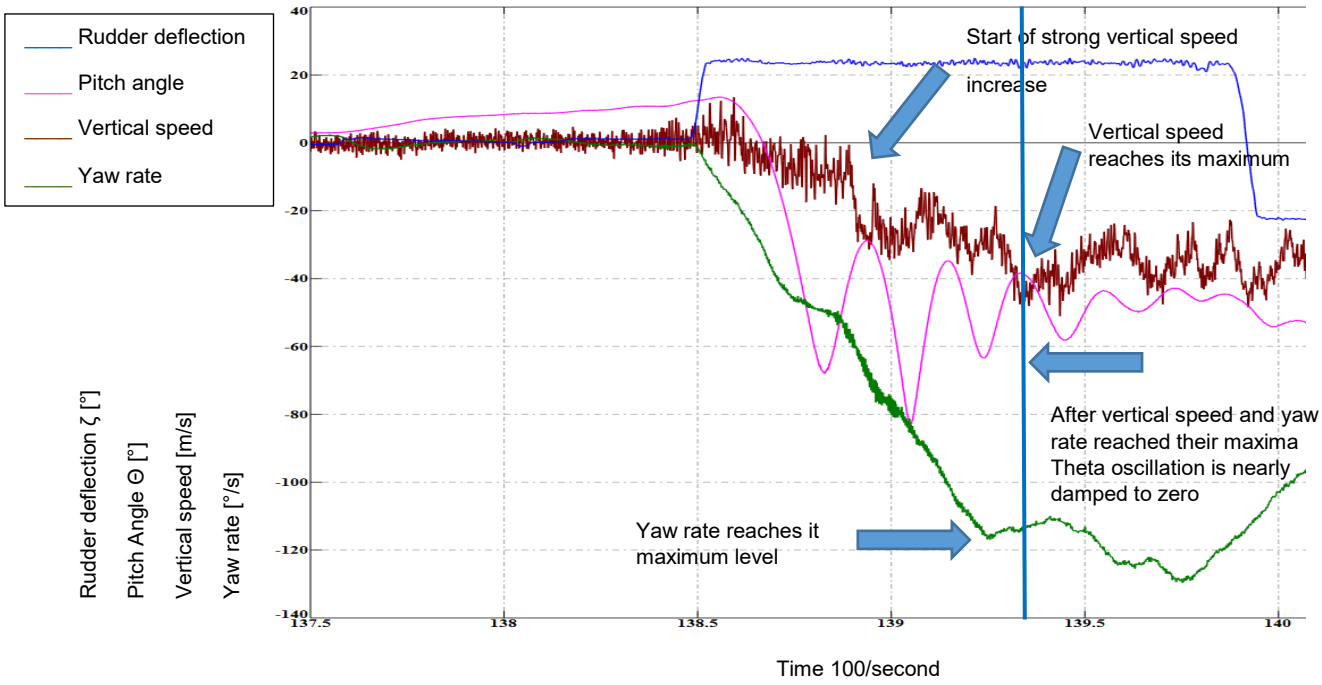

Figure 5.28: Rudder deflection, vertical speed, pitch angle and yaw rate

The position of the Centre of Gravity (CG) lies between 247.4 cm to 254.1 cm behind the corresponding aeroplane's datum line (see Chapter 4). Due to this the main surface area of the aeroplane is located behind the CG. The main contribution to the aeroplane's mass is the engine which lies ahead of the CG.

The airstream which hits the aeroplane from below leads to a pitch down motion due to the main surface area position. The (increasing) yaw rate leads to a pitch up motion of the aeroplane due to the position of the engine.

Thus the aeroplane oscillates about a final pitch angle while approaching a fully developed spin.

The first pitch down motion is not the strongest because the vertical speed is not very high. The second pitch down motion is the strongest because the vertical speed increases strongly due to the moment in which the yaw rate is still relatively low.

While the yaw rate increases the pitch up tendency increases.

Both forces – the aerodynamic force which pitches the aeroplane downwards and the centrifugal force which pitches the aeroplane upwards – are slowly balancing and thus the aeroplane's pitch oscillation is damping down to zero.

During the first part of the spin (see Figure 5.29) the corresponding pitch rate is in phase with the pitch angle (red arrows). After the vertical speed and the yaw rate have reached their maximum level and the pitch oscillation is nearly damped to zero (right of the blue vertical line) the pitch angle and the pitch rate are not as clear in phase as before. This is due to the small pitch angle changes (< 5°) and the (still) high pitch rates about the final pitch angle.

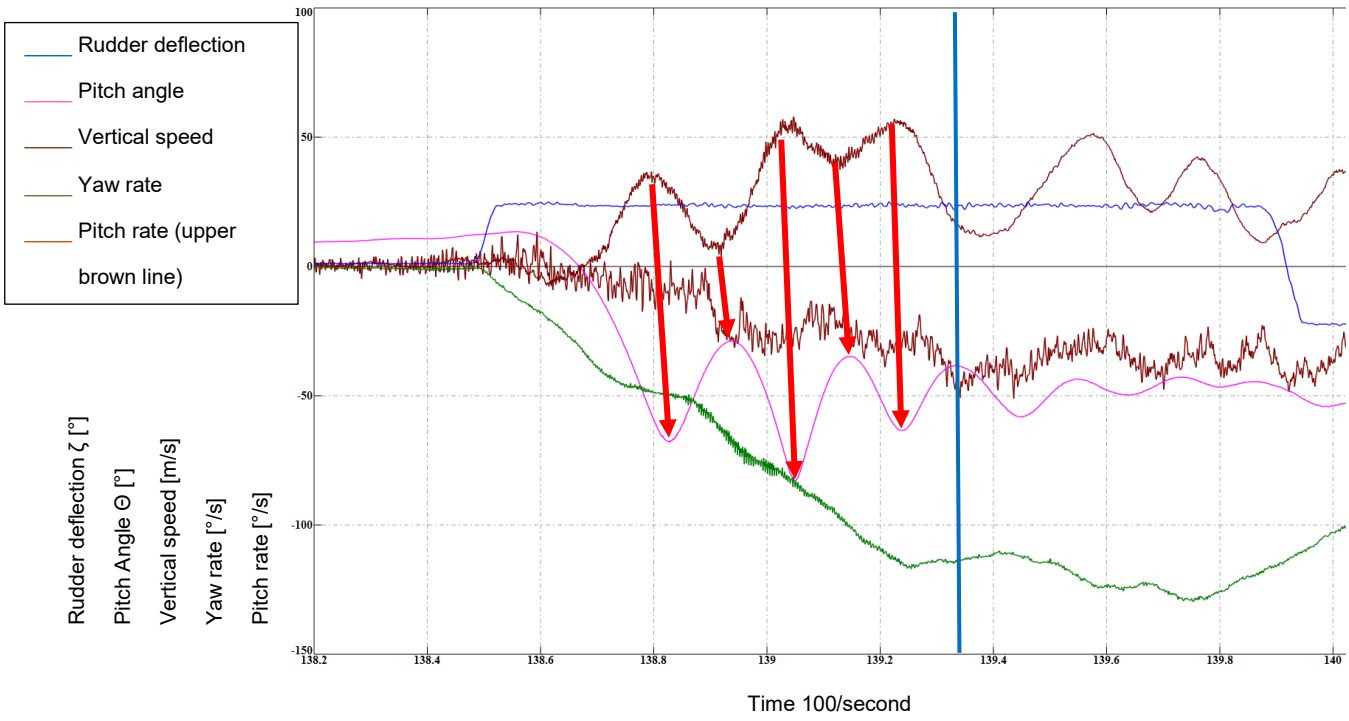

Figure 5.29: Pitch rate run showing additionally the changes in time of the rudder deflection, pitch angle, vertical speed and yaw rates

The yaw behaviour of the aeroplane is mainly influenced by the rudder deflection (Figure 5.30). After the rudder is fully deflected, the yaw angle (heading) starts to change in the corresponding direction. The spin entry behaviour has been described above.

The yaw rate increases with a quasi-linear function until it reaches a plateau.

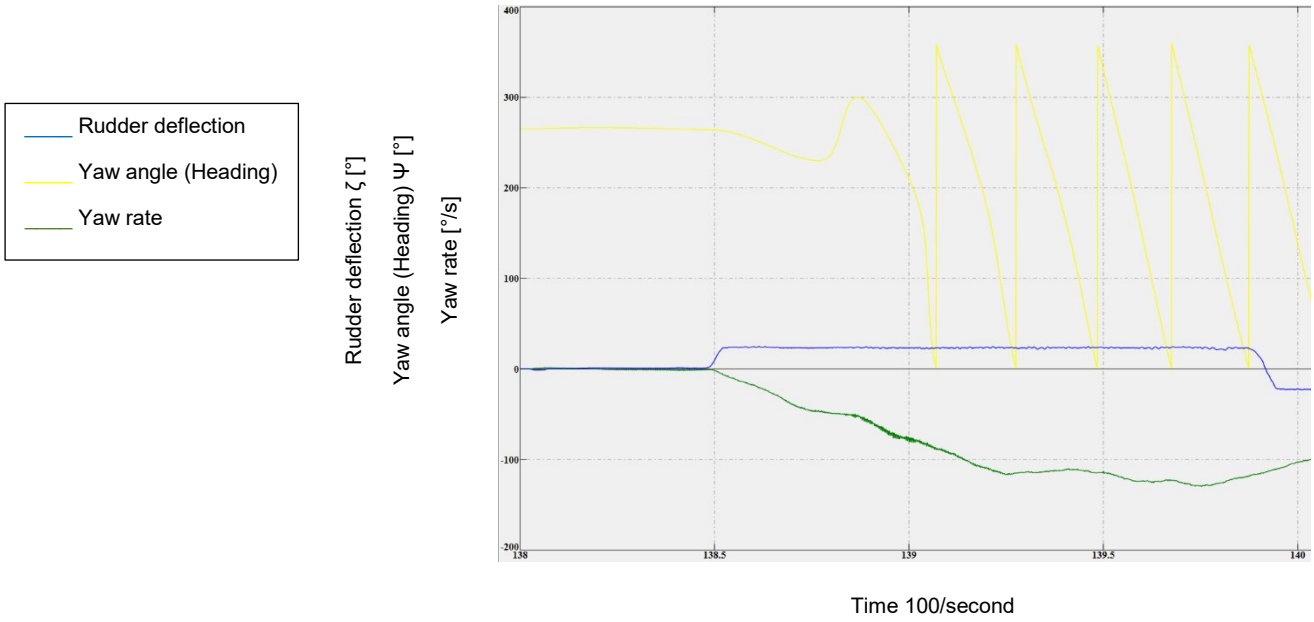

Figure 5.30: Rudder deflection, yaw angle (heading) and yaw rate behaviour of the Fuji FA 200 during the entire spin run

As the aeroplane starts its descent and reaches a vertical trajectory, both the vertical speed and the speed of the corresponding airflow increase. This increase of freestream wind speed drives up the yaw rate (wind milling effect). This can be seen in Figure 5.31.

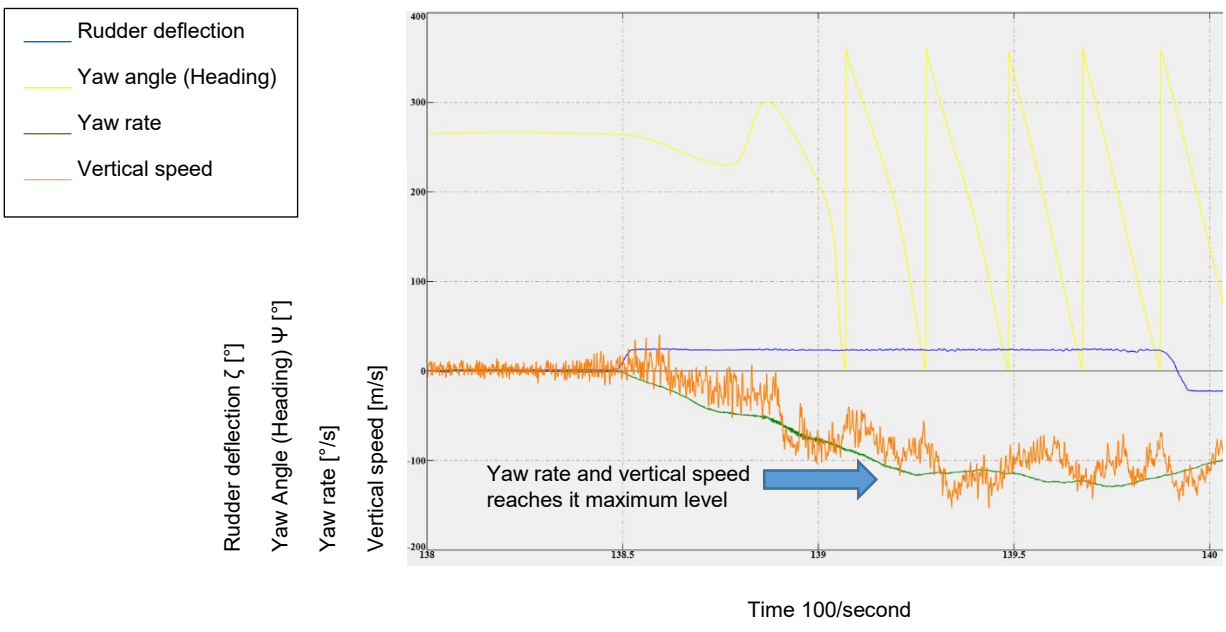

Figure 5.31: Vertical speed and yaw rate run of the Fuji FA 200 during an entire spin run. Note: the values of the vertical speed are multiplied by 3 for comparison purposes

Basically, the yaw rate follows the vertical speed when the aeroplane travels on a vertical trajectory. Both data sets reach a plateau when the spin is fully developed.

5.5 Example of a spin recovery

Within this spin discussion the recovery phase starts when the rudder deflection is reversed and thus the spin is influenced by the pilot significantly. From this point onwards all parameter behaviour is disturbed by the defined recovery procedure which can be found in Chapter 4.

As an example of Fuji spin recovery behaviour, the same spin as in Section 5.4 has been taken (for the same reasons as before). For this phase of a spin, a time frame of 1399 – 1410 seconds (i.e. 11 second duration) after the system start has been taken. This time frame follows the second time period as discussed in the sections above (after spin entry and developed spin) without a time gap.

The main observation during this spin phase is that the aeroplane stops its rotation to the left and while reducing the elevator deflection to about zero, the aeroplane enters a vertical dive. Hence it loses altitude rapidly, quickly gains airspeed and the pilot recovers the aeroplane from the vertical dive by pulling the elevator until horizontal flight is regained.

Figure 5.32 shows all the discussed parameter in one diagram during the recovery phase of the spin.

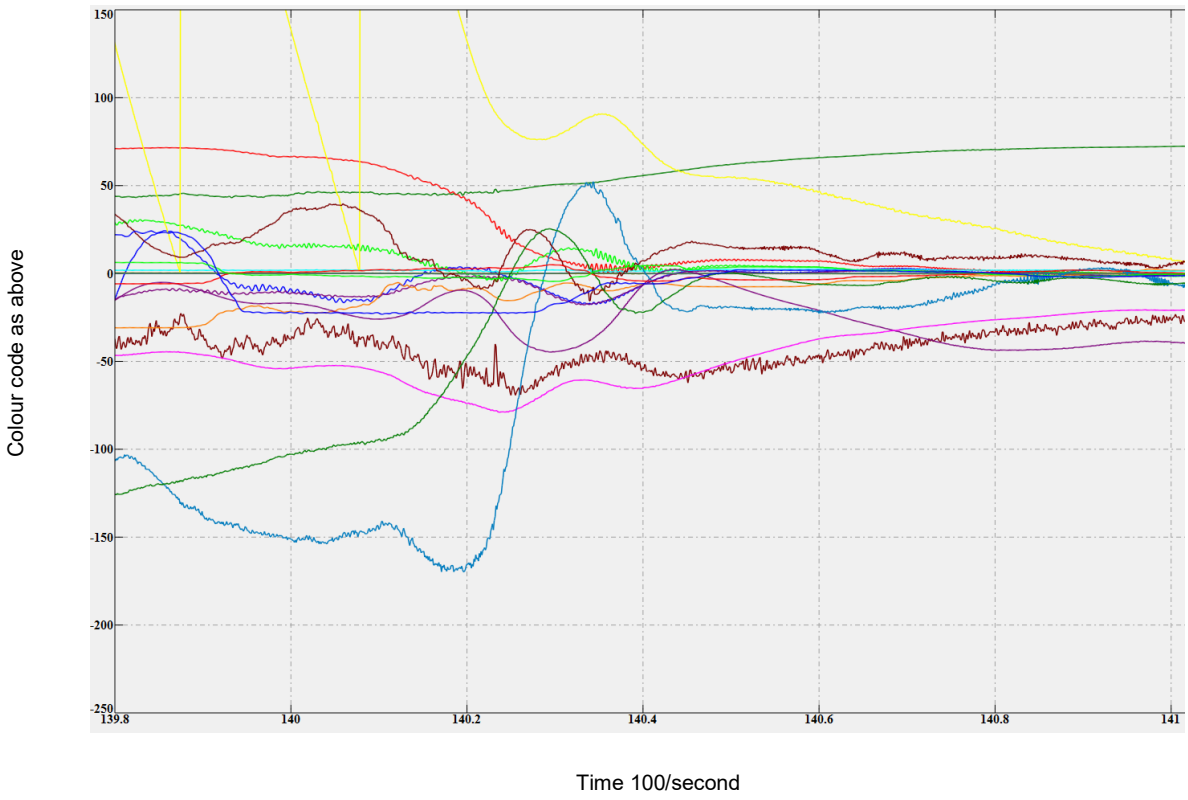

Figure 5.32: Spin recovery data example

As this phase of the spin is influenced by a standardized and defined recovery procedure that the pilot has to follow or apply, the main interest lies in the recovery time.

Within this spin discussion the spin recovery starts when the rudder deflection is reversed – in the present case from maximum positive to maximum negative values – and it ends when the turn direction is reversed – in the present case from left to right.

The recovery time is – as is the entire spin – influenced very strongly by the aeroplane's mass and Centre of Gravity position. These influences will be discussed later in this Chapter.

5.6 High frequency data fluctuation

One reason for the high frequency oscillations of some of these parameters is the sensor interference with the aeroplane's structure (e.g. the rudder touches the rudder stop which is part of the tail structure and which is excited by the airflow and the engine vibration. This vibration is transmitted via the control cables to the displacement sensor for the rudder deflection measurement – see Figure 5.33).

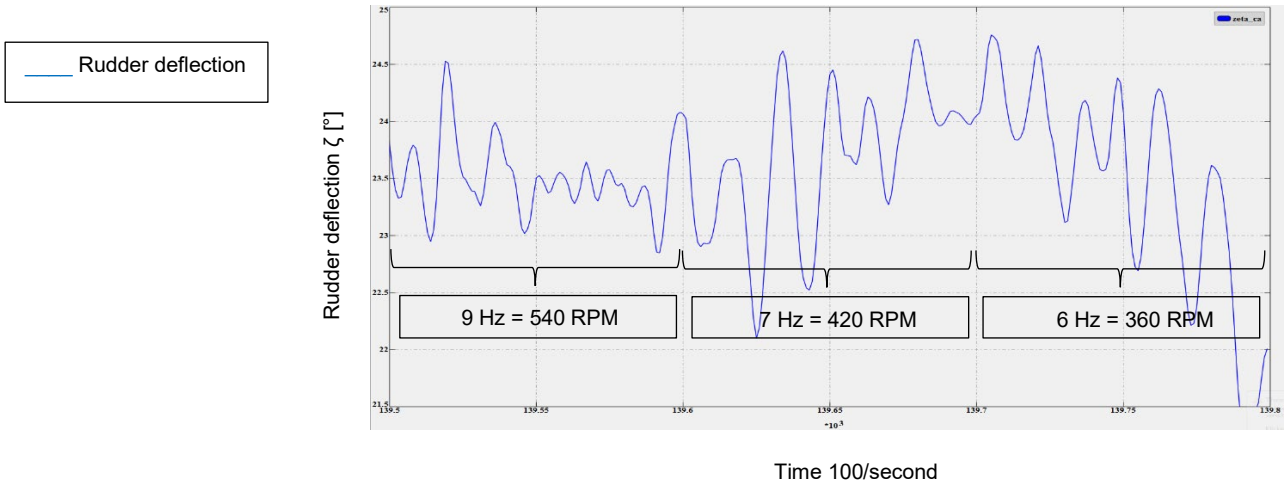

Figure 5.33: High frequency oscillation due to engine vibration. Note: engine RPM drops due to fuel starvation during the course of the spin (fuel sloshes away from the fuel withdrawal point due to the aeroplane's rotation). Amplitude changes are due to the inhomogeneous swing of the corresponding control cable.

Another reason for high frequency oscillations of some of these values is the eigenvalue frequency of the sensors itself, which are mounted on a wing-boom. Those sensors (e.g. for α and β measurements) are excited by the energy from the surrounding airflow, as can be the boom itself (Figure 5.34). Although the parameter frequencies do not change significantly over the observed example time frame, the amplitudes undergo changes due to the superposition of the eigenvalue frequencies of the sensor and boom.

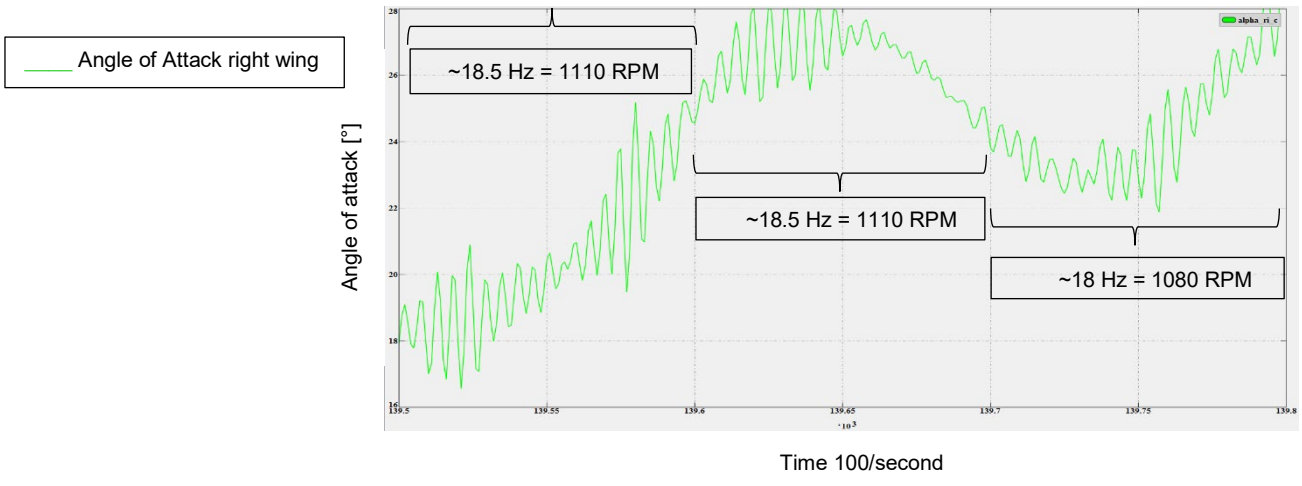

Figure 5.34: High frequency oscillations due to the angle of attack sensor eigenvalue frequency. Changes in amplitude occur due to in-flight oscillations of the sensor and interference from the wing-boom

5.7 Conclusions of the spin description

In this Chapter a typical spin sequence – from entry to a full recovery – is described. The depth of the explanations and how the discussed parameters interact give a detailed insight into this flight mechanics phenomenon. Such a discussion has not been found in the literature for this aeroplane category.

From the above findings: aeroplane designers, flight testers, flying instructors and pilots can derive principles, tests and training procedures which are flight safety relevant. These could be e.g. aeroplane attitudes – and thus moments during a spin - from which spins can be recovered faster, more precisely or safer than from other moments during a spin.

This spin description helps to start modelling this flight dynamic phenomenon for other aeroplanes, to validate CFD software based simulations or dynamic spin model data from wind tunnels. It is a new basis from which to describe this flight mode to the mathematician, physicist and computer scientists in order to develop future models within a computational environment.

In the next Chapter, methods are applied to show how the investigated spin parameters develop and behave when changing the aeroplane's mass and CG position. Such investigations have not been conducted in the past in such a great detail, or covering such a big part of the aeroplane's stability envelope.

Chapter 6 Mathematical spin test data analysis

As discussed in Chapter 2 (Literature Review) the aeroplane's pitch angle, θ, (and its behaviour over time) is an important characteristic spin parameter. According to 'traditional' pilot thinking an aeroplane enters a flat spin and by that, control surfaces are likely to be shielded when the CG is moved backwards. This means the crew and the aeroplane are in danger. By analysing this particular parameter, a straight and effective approach to a scientific spin investigation is conducted and a starting point for a modern spin analysis is laid. Because of its significance and potential complexity the author focused on this main spin parameter and a mathematical model is derived in this Chapter. As far as the author knows, this is the first time that a mathematical model of θ has been presented. Many other parameters are analysed in the next Chapters. Space and time does not permit at this stage to model all of the other parameters in addition to the conducted work.

In addition to the description of spin analysis in Chapter 5, the following a mathematical spin test data analysis can be found.

6.1 Introduction into the mathematical spin test data analysis

After a detailed description of the aeroplane's behaviour during a spin – based on the measured data – in Chapter 5 some selected flight mechanical parameters will now be considered mathematically.
Because of the complexity of the cross-dependency of the measured parameter the modelling within the sections below will concentrate on the data runs of the specific parameter. The modelling of cross-dependencies and further parameter is a subject for further work.
The measured spin data has been numerically analysed for each of the parameters listed below. Note that inside each square bracket the name used within the measurement system software is stated:

Parameter	Flight mechanical notation	Measurement system notation
Pitch Angle	θ	[ln_Theta]
Pitch rate	q (for frequency analysis)	[ln_q]
Total Angular Velocity	Ω	[(ln_p^2 + ln_q^2 + ln_r^2)^1/2]

Left and Right Angle of Attack	*α*	[alpha_le_c; alpha_ri_c]
Yaw rate	*r*	[ln_r]
Roll rate	*p*	[ln_p]
Recovery time	*t*	---

Table 6.1.1: Analysed flight mechanics parameters

The results of the data analysis were obtained using MATLAB scripts developed for this research project. In the following sections flight test data are investigated and dependencies of data sets and influencing factors are discussed.
For a clear categorization of the results the level of dependencies or sensitivities are divided into three grades which are:

Grade	Dependency
strong / high	100 – 70%
Moderate	69 – 30%
weak / low to none	29 – 0%

Table 6.1.2: Dependency levels

This categorization is recognized in different disciplines and used within several scientific projects (Biermann, 2015). These grades are reasonable for the spin data analysis on hand.

6.2 Evaluation and processing of the θ-Values

Within the following section the mathematical model for the description, evaluation and processing of the pitch angle (θ) behaviour of the utilised aeroplane is explained. This model has been created during the course of this research project on the basis of the flight test data which have been collected during the above described 27 spin runs. In addition to this, Appendix 7 explains the general mathematical methods including statistical methods which have been applied for the analysis of θ and the other measured parameters.

Three csv-files are read in; each of them containing data from one flight and thus each of them containing data for nine spin runs. From each flight a time series of θ is obtained.
The processing of these θ-values during the single spin runs are performed by the following mathematical steps:

1.) Detection and storing of the θ-values which belong to spin runs:

Each spin run is a maximal coherent sub-series consisting of θ-values with

$$\theta \leq -20°$$

θ ≤ -20° makes sure that the aeroplane has definitely left the normal pitch range of an ordinary flight situation. There are 27 spin runs, each of them being a small time series (θ_i), which are stored separately. Each value θ_i has been taken at time values t_i. The time series (θ_i) are processed in two ways:

- Each spin run is processed individually
- Averages of groups of three spins are calculated. The processing is performed with these groups. Each group consists of spins with (nearly) the same values for the mass and the position of the centre of gravity of the aeroplane (same conditions).

Within one group the time series must have the same length. Therefore at some spin runs a (very) small number of values at the end of the time series has to be cut off.
The next steps are executed for both the individual and the averaged time series.

2.) Finding relative minima and relative maxima:

(a) The values are smoothed by a moving average of order 21 (see equation (A2) in Appendix 7). Figure 6.1 shows the raw and smoothed data.

(b) After smoothing, one searches for θ-values which are bigger or smaller than its 20 predecessors and its 20 successors (see equation (A3) in Appendix 7):
$\theta_{i-20}, \ldots, \theta_{i-1} \leq \theta_i \geq \theta_{i+1}, \ldots, \theta_{i+20}$ (relative maximum)
$\theta_{i-20}, \ldots, \theta_{i-1} \geq \theta_i \leq \theta_{i+1}, \ldots, \theta_{i+20}$ (relative minimum)

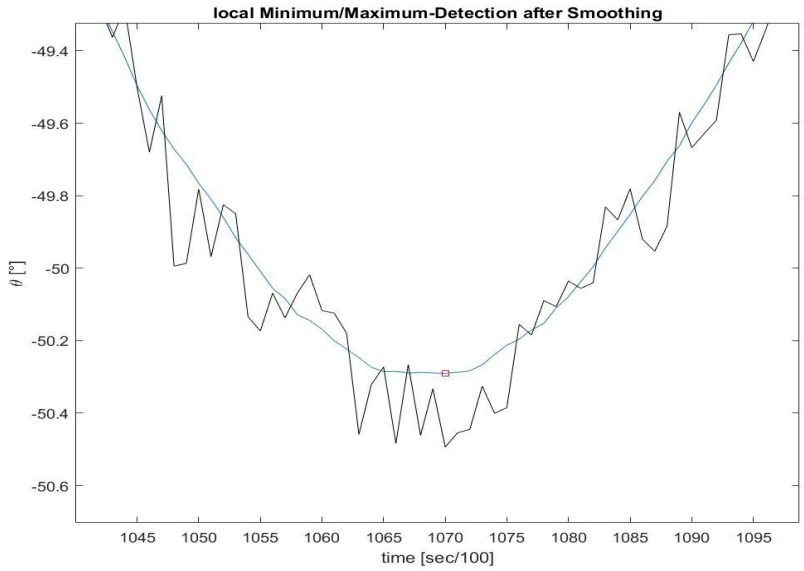

Figure 6.1 Black line: θ-Values, blue line: smoothed θ-values, red square: detected relative minimum of value at 10.7 seconds

The positions (index values) of the minimum and maximum – values are stored. It is known that there are six minimum and six maximum values within one spin run (as there are 6 turns).

3.) Calculation of the numerical derivatives (for the averages):

The numerical derivatives are calculated using a second order central differencing scheme and plotted. For the calculation, equation (A4) in Appendix 7 is used. This calculation is done by using the smoothed time series which has already been used for finding the relative minima and relative maxima (see above).

For the rear part of the time series, a mathematical model has been established. It is assumed that the corresponding rear parts of the time series (now beginning at the position of the third relative minimum) can approximately be described by the model formula:

$$\Theta \approx \Theta_{limit} + \sin(\omega \cdot t + \delta) \cdot e^{-d \cdot t + a} \qquad (1)$$

The aims of the following steps are

- to find the damping coefficient d
- to find the limit value Θ_{limit}

- to find the angular frequency ω

4.) Obtaining estimations for Θ_{limit} and d in formula (1)

For this calculation formula (1) is only considered at the minimum and the maximum – values found above.
There are six relative minima and six relative maxima. Out of these twelve min. / max.-values the last eight are taken, i.e. the first two minima and the first two maxima are not taken into account.
Let Θ_{m1}, Θ_{m2}, …, Θ_{m8} be the last eight minima and maxima and t_{m1}, t_{m2}, …, t_{m8} the corresponding time positions. Putting this into formula (1) one gets

$$\Theta_{mj} \approx \Theta_{limit} \pm e^{-d \cdot t_{mj} + a} \qquad \text{for j = 1, …, 8} \qquad (2)$$

If Θ_{mj} is a maximum value, there is a positive sign, otherwise there is a negative sign. Using the natural logarithm one gets from the formula (2)

$$\ln \left| \theta_{mj} - \theta_{limit} \right| \approx -d \cdot t_{mj} + a \qquad \text{for j = 1, …, 8} \qquad (3)$$

In order to get an appropriate value for d (and a value for a) a linear regression has to be done using the known values t_{m1}, t_{m2}, …, t_{m8} and Θ_{m1}, Θ_{m2}, …, Θ_{m8}.
However for the unknown value Θ_{limit}, an estimation has to be conducted as well. Therefore, the following steps are performed:

a) Getting an initial guess for θ_{limit}, calling it θ_g

b) Performing the linear regression with the value

$$t_{mj}, \ln \left| \theta_{mj} - \theta \right| \qquad \text{with } \theta = \theta_g \text{ and for j = 1, …, 8} \qquad (4)$$

i.e. first of all, the initial guess θ_g for θ is taken.

c) In order to get an improvement of this first estimation of θ_{limit} the squared error of the regression is considered as the function of θ, and a value for θ is found at which this function will be minimal. This value for θ will be taken as final estimation of θ_{limit} and will be considered as the limit pitch angle. This is the pitch angle the aeroplane will reach when the θ oscillations are totally damped out (has stopped).

After that the regression with the values from (3) is done again, using the final estimation value θ_{limit}. By this regression an estimation of the damping coefficient is obtained.

These three sub-steps have been performed in the following way:

a) For θ_g, the initial guess of θ_{limit}, the mean of the lowest maximum and the highest minimum among the considered extreme values $\theta_{m1}, \theta_{m2}, \dots, \theta_{m8}$ is taken

b) For the linear regression, a matrix R is used which corresponds to that in equation (A16) of Appendix 7 (for the case p = 1), the matrix V is needed in the next sub-step:

$$R = \begin{pmatrix} t_{m1} & 1 \\ \vdots & \vdots \\ t_{m8} & 1 \end{pmatrix} \qquad V = R \circ (R^t \circ R)^{-1} \circ R^t \tag{5}$$

c) By defining and calculating (using the natural logarithm)

$$\vec{y}(\theta) = \begin{pmatrix} ln|\Theta_{m1} - \theta| \\ \vdots \\ ln|\Theta_{m8} - \theta| \end{pmatrix} \qquad \frac{d}{d\theta}\vec{y}(\theta) = \begin{pmatrix} \frac{1}{\theta - \Theta_{m1}} \\ \vdots \\ \frac{1}{\theta - \Theta_{m8}} \end{pmatrix} \tag{6}$$

One obtains the quadratic error e(θ) of the regression as a function of θ and the derivative of that function:

$$e(\theta) = \vec{y}^t(\theta) \circ \vec{y}(\theta) - \vec{y}^t(\theta) \circ V \circ \vec{y}(\theta) \tag{7}$$

$$\frac{d}{d\theta} e(\theta) = 2 \cdot (\vec{y}(\theta) - V \circ \vec{y}(\theta))^t \circ \frac{d}{d\theta}\vec{y}(\theta) \tag{8}$$

The minimization of $e(\theta)$ is conducted by several gradient descent procedures (done like in procedure (1a) of Appendix 7, using formulae (7) and (8)). The starting points of these gradient descent procedures were those mean values of neighboured extreme values, which do not differ from the initial guess Θ_g by more than 3°. Among the results of these gradient descent procedures that one is taken for the final estimation of Θ_{limit} which gives the smallest error value of $e(\theta)$ (see formula (7) and Figure 6.2) and which does not differ from the initial guess Θ_g by more than 2°. This is due to the behaviour of the logarithm function (to avoid zero or very high values to be put into the logarithm). The values 2° (for final estimations) and 3° (starting

point for gradient descents) are based on trials which lead to reasonable results (see the corresponding plots).

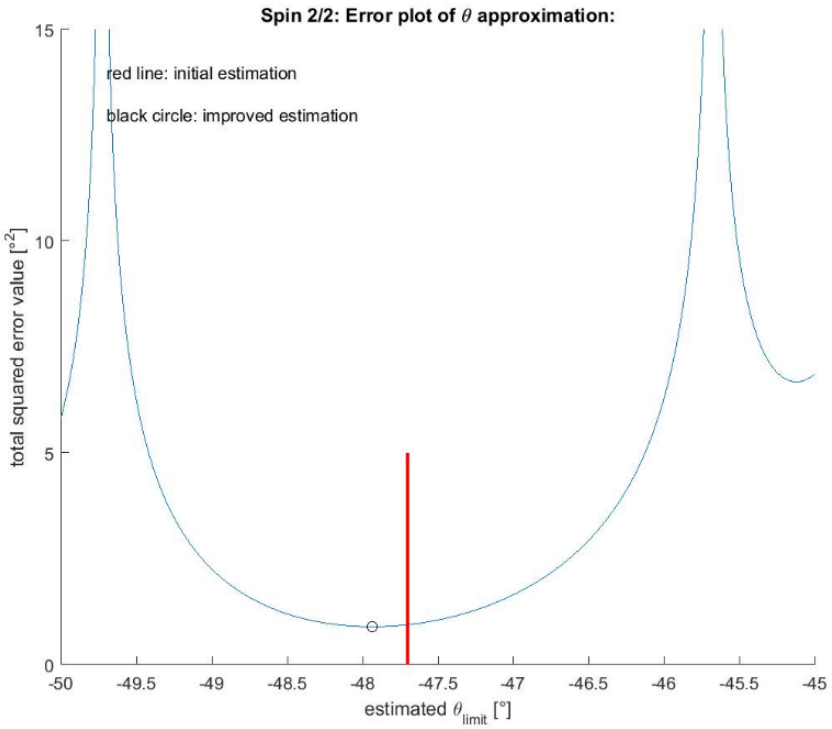

Figure 6.2: Example for a small adjustment of the initial guess (position noted by the red line) to obtain the final estimate for Θ_{limit} (denoted by the black circle)

6.) Detection of the main frequencies and ω in formula (1):

The frequencies of the oscillating parts of the time series, which belong to the highest amplitudes, are calculated. Therefore in a preparing step the damping factors are removed from the sample values (Θ_i) of the rear part of a spin run with $\Theta \leq -20°$, getting with that a new time series $\left(\Theta^{(u)}{}_i\right)$ ('undamped Θ') consisting of the values:

$$\Theta^{(u)}{}_i = \frac{\Theta_i - \Theta_{limit}}{e^{-d \cdot t_i + a}} + \Theta_{limit} \qquad (9)$$

The values Θ_{limit}, d and a have been calculated in step 5. The values t_i are the time values at which the sample values Θ_i are taken. A fast Fourier transform (FFT) (see equation (A11)

in Appendix 7) is applied to the time series $\left(\Theta^{(u)}{}_i\right)$. The absolute values of the FFT are sorted, the first six values and the corresponding frequency values are taken. As mentioned above this has only been done for the rear part of the values from the Θ - function.

The separation between the front and the rear part of the function is done by taking the position of the third relative minimum. The detected frequency values and the corresponding amplitudes A (with A = 2· $|F_j|$ with a FFT – value F_j) are stored.
For the angular frequency, ω, appearing in (1) the value $\omega = 2 \cdot \pi \cdot f_{max}$ is taken with the frequency f_{max} belonging to the maximal amplitude of the rear part.

The implication of the model established in this section and further results of the data analysis including the corresponding interpretation can be found in the following sections.

6.3 Pitch Angle data analysis

The analysis for the pitch angle values has been conducted as follows:

Procedure 6.3.1: Pitch Angle data processing ('it_bereiche_einlesen'):
This procedure has been described in the previous section. Its outcome is an estimation of the damping coefficient d, and the θ limiting value θ_{limit}. These values are parts of the model

$$\Theta \approx \Theta_{limit} + \sin(\omega \cdot t + \delta) \cdot e^{-d \cdot t + a} \qquad (10)$$

which has been gained by taking the values behind the third minimum into account (see the vertical line in the graphs, e.g. Figure 6.3 below)

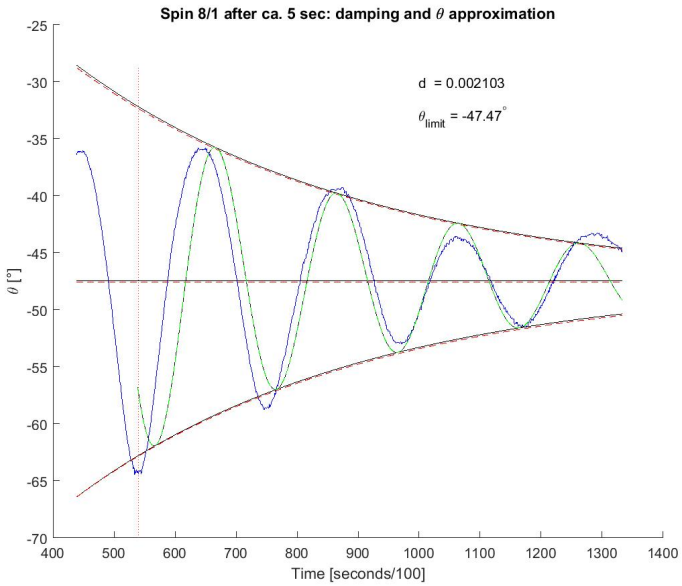

Figure 6.3: Example for a determination of the damping coefficient d and θ limiting value

For each spin condition - flown with the utilized aeroplane - such a model together with the corresponding limit value θ_{limit} is established from the measured data.

For model testing reasons, in addition to Procedure 6.3.1 the analysis has also been conducted with averaged θ-values of a specific flight condition which led to better model fits and additionally the results were changed only slightly.

Procedure 6.3.2 ('it_evaluation_theta_limit_R_export')

Tasks of this procedure:

1. Interpolation of the aeroplane's mass values for each CG-mass condition (section 4.6).
2. Processing and output of the aeroplane's mass values and CG positions for each spin run, together with the corresponding θ function limit values (θ_l). These values are used for conducting linear regressions for the adjustment of the linear model. Figures 6.4 - 6.6 illustrate the results obtained.

$$\theta_{limit} \sim a_0 + a_1 \cdot \mathrm{mass} + a_2 \cdot \mathrm{Cpos}$$
$$\theta_{limit} \sim b_0 + b_1 \cdot \mathrm{mass}$$
$$\theta_{limit} \sim c_0 + c_1 \cdot \mathrm{Cpos}$$

   Including the calculation of the coefficient of determination R^2

3. Exporting data to the statistical software package, R.

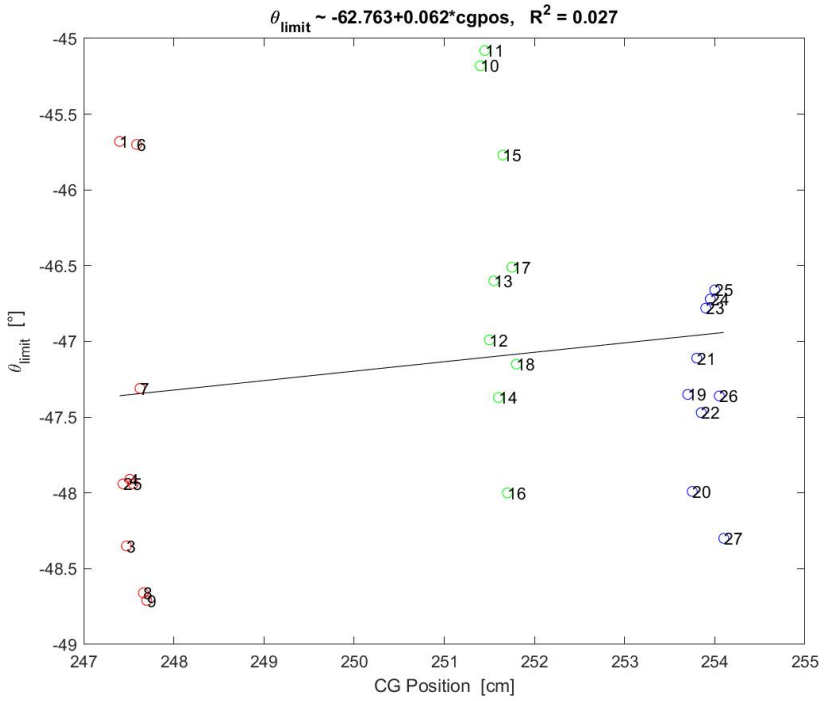

Figure 6.4: θ_{limit} versus CG position for all 27 spin runs. Conditions 1 – 3 are on the left hand side (red circles = flight 1), conditions 4 – 6 (green circles = flight 2) on the middle column, and conditions 7 – 9 (blue circles = flight 3) are on the right hand side of the plot

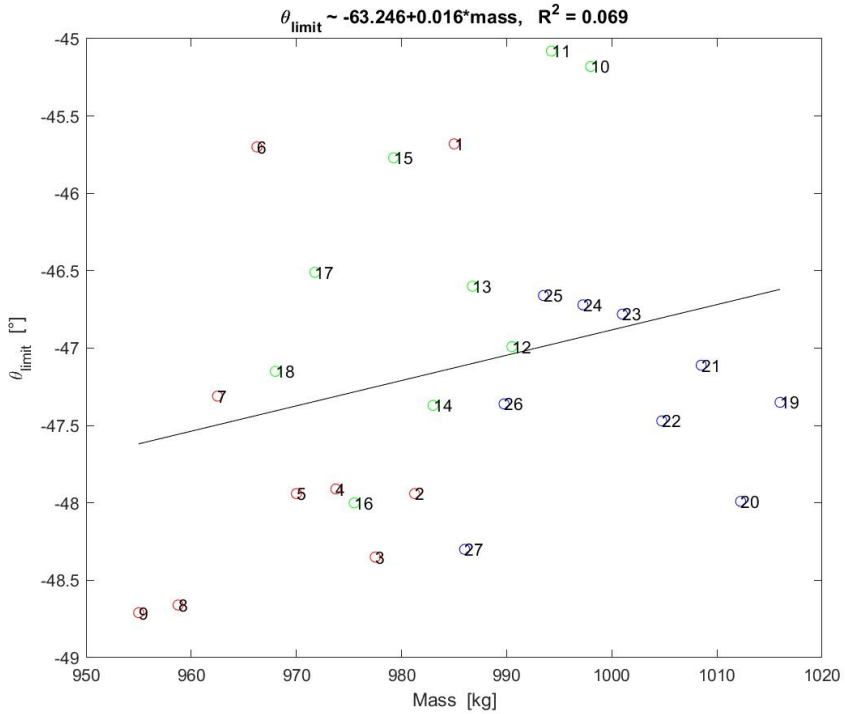

Figure 6.5: θ_{limit} versus aeroplane's mass for all 27 spin runs

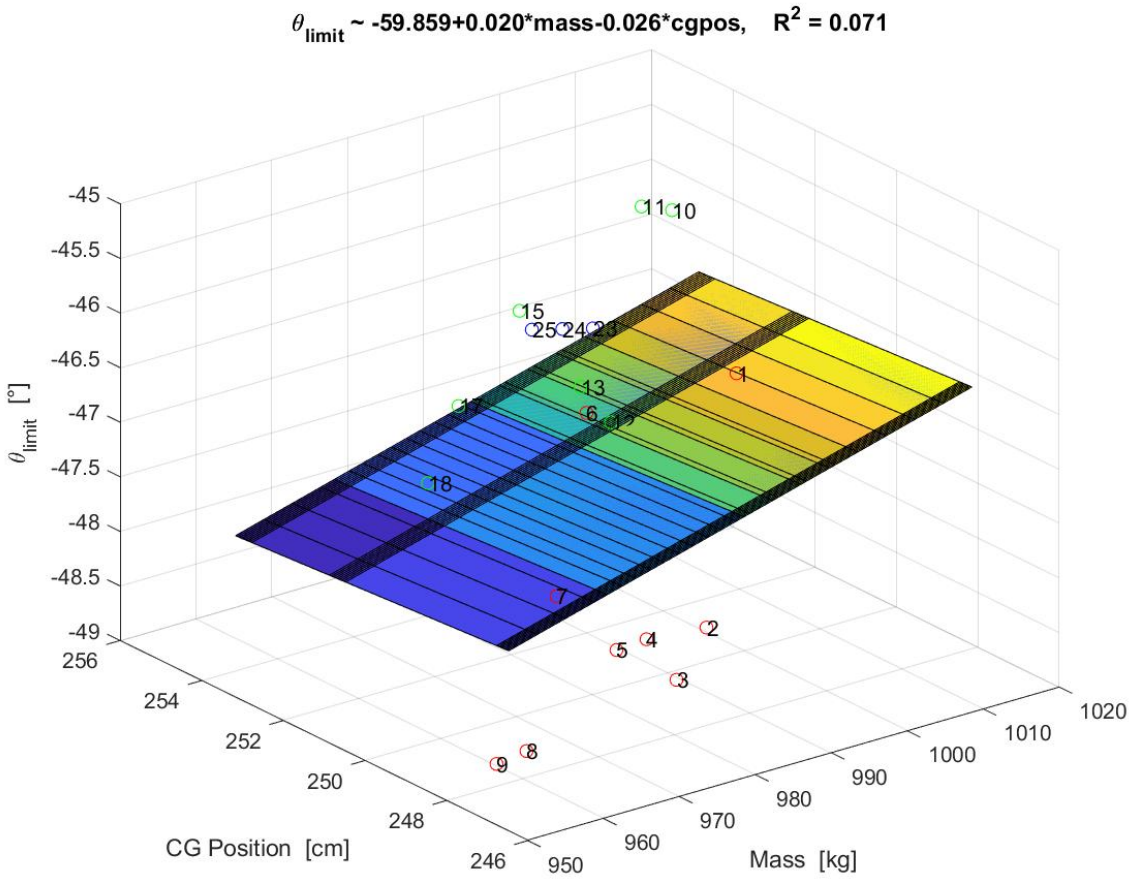

Figure 6.6: Response surface 3D plot of θ_{limit} versus CG position and aeroplane's mass using all 27 spin runs.

In the following sections, the corresponding results of the data analysis are presented in relation to proving observations 1 to 9.

6.4 Observation 1: The second minimum value of the pitch down (In_Theta) function always produces the highest negative value.

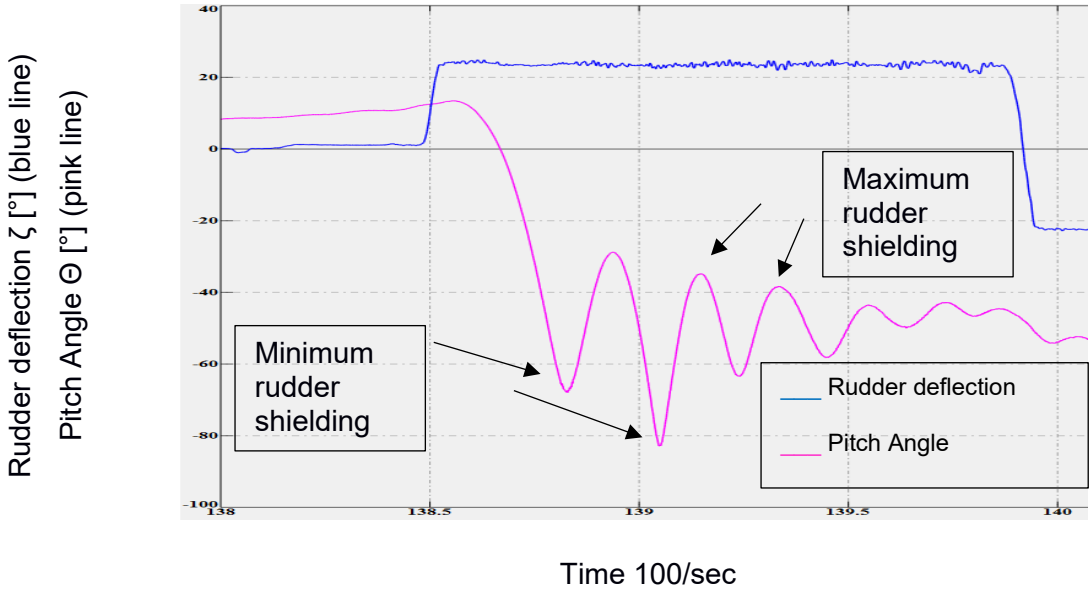

Figure 6.7: Pitch angle Θ [°] and rudder deflection ζ [°] versus time for spin 1 of condition 1.

The plot above (Figure 6.7) shows typical pitch angle behaviour (based on data from spin 1 of condition 1) of the chosen aeroplane. The data indicate that the second pitch down motion produces the largest negative pitch angle followed by a damping of the pitch oscillation. The pitch angle reaches a characteristic final value (see sub-section 6.5). All spin runs show a similar pattern. The position of the second minimum indicates that at that point spin recovery is the easiest to perform.

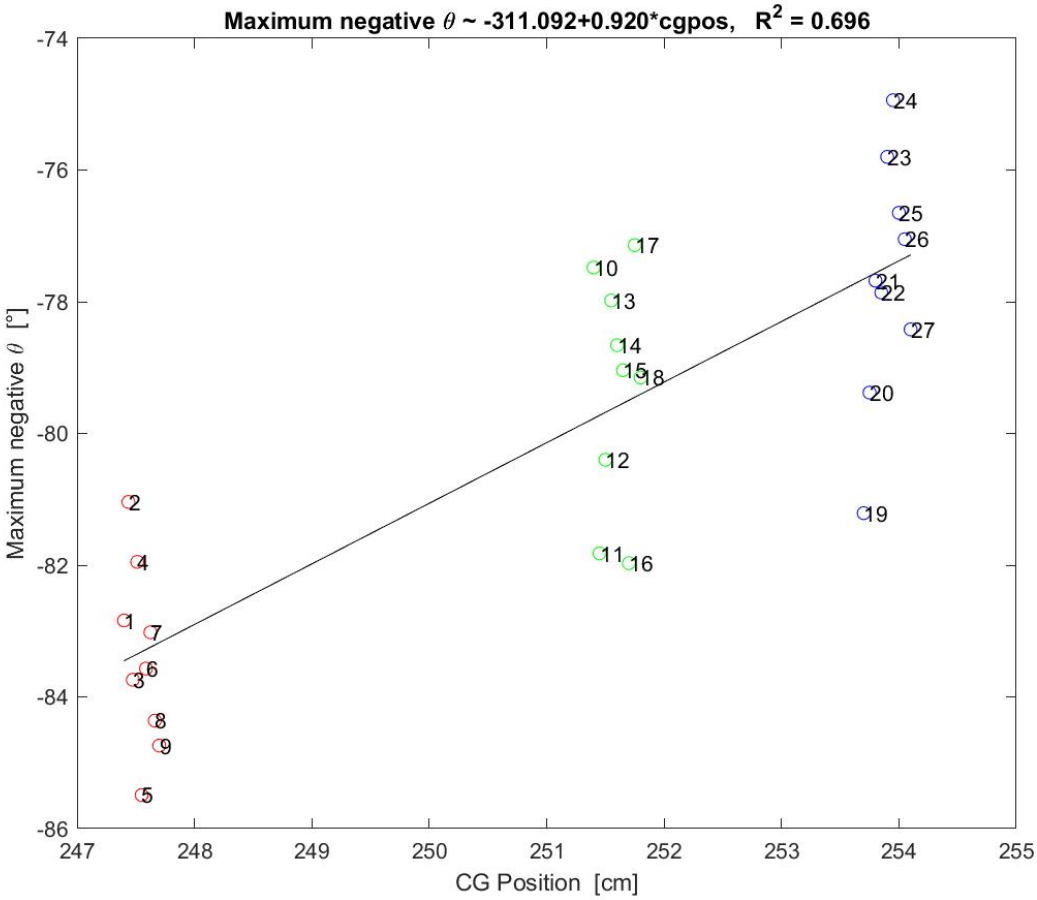

Figure 6.8: Maximum negative pitch angle versus CG position for all 27 spin runs.

Note: To distinguish between the different flights the following colour code is used throughout this Chapter: red circles = flight 1 = condition 1 – 3; green circles = flight 2 = condition 4 – 6; blue circles = flight 3 = condition 7 - 9

The positive slope of the plotted regression line (Figure 6.8) shows that the largest negative pitch angles are measured with forward located CG positions. The change of the maximum negative pitch angle follows a moderate to strong dependency (coefficient of determination, R^2) of 69.5% when changing the CG position. Taking the regression line into consideration, the pitch angle values range from around – 83.7° to -78°, which is a pitch angle change of 9.3% when shifting the CG position by 7 cm. Thus the trend, as the pitch angle moves towards -78°, is of increased difficulty in spin recovery and the amount of tail shielding is increasing, so the manoeuvre is less safe for the pilot.

The influence of gusts and / or sloshing fuel during the spin entry phase increases the scatter in the data points parallel to the y-axis.

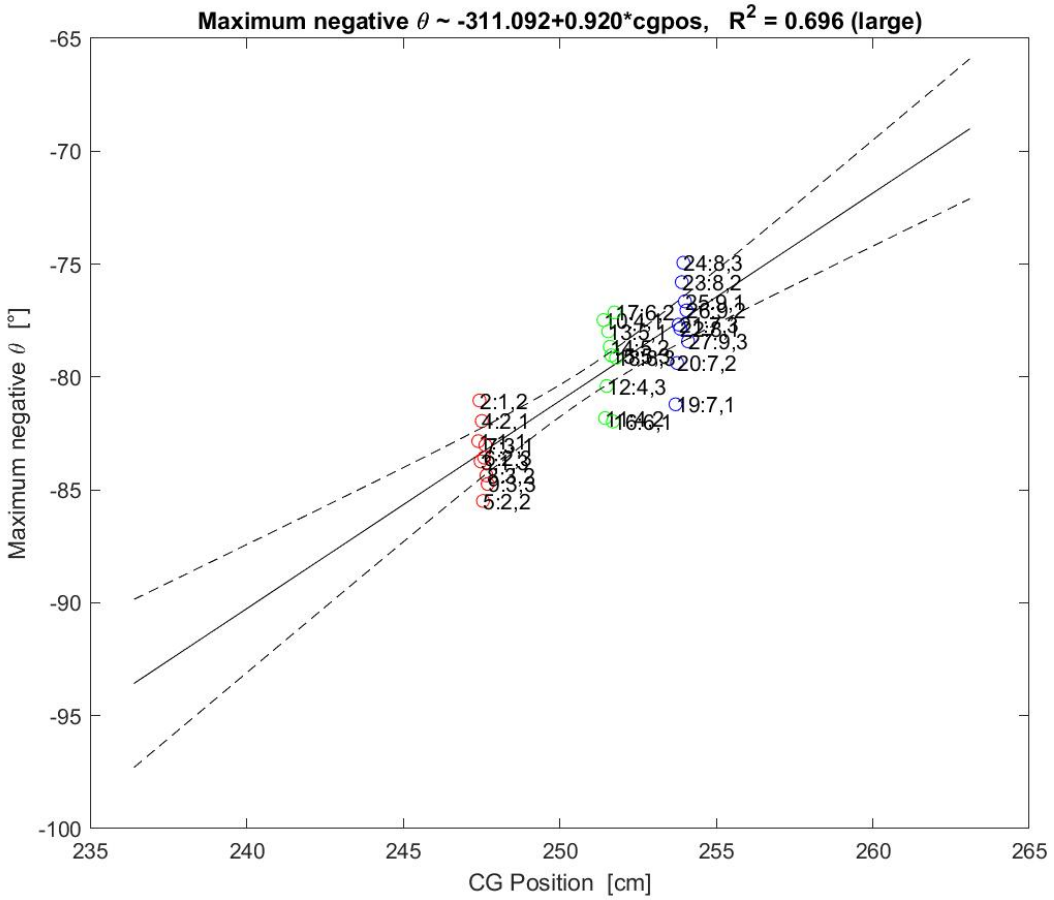

Figure 6.9: Maximum negative pitch angle versus CG position for the 27 spin runs. Extrapolation to the left and right boundaries of the flight envelope, including confidence intervals

The x-axis range limits (Figure 6.9) are the left and right boundaries of the flight envelope. The straight line is the linear regression; the dashed lines are the 95% confidence intervals.

The extreme left of the flight envelope (i.e. nose heavy) will lead to pitch angles of more than 90° down. Not only is the aeroplane's nose pointing towards the ground this attitude causes negative G forces on the pilot, which is disorientating.

At the extreme right of the flight envelope the pitch angle is shallower, which indicates that the aeroplane would be harder to recover from a spin.

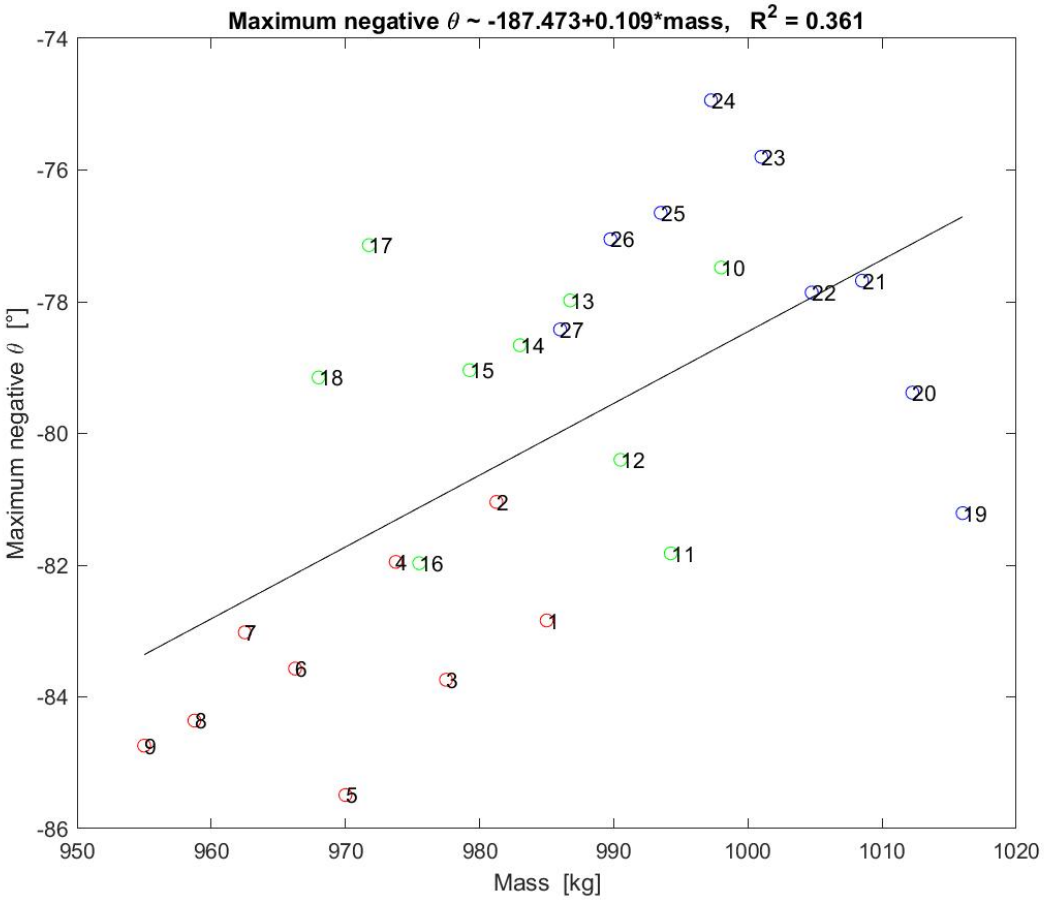

Figure 6.10: Maximum negative pitch angle versus aeroplane mass for all 27 spin runs.

With a positive slope of the regression line, the maximum negative pitch angle decreases with increasing aeroplane mass. This dependency has an R^2 value of 36.1%, which is much lower than seen in Figure 6.8 and can be understood as moderate. The data points in Figure 6.10 are distributed much more over the entire field. This is because the aeroplane mass has less influence on the maximum negative pitch angle than changing the CG position. In this case, the pitch angle values change by around 8.5% with changes in the aeroplane mass of 60 kg. Therefore higher masses produce less safe conditions for aeroplane recovery.

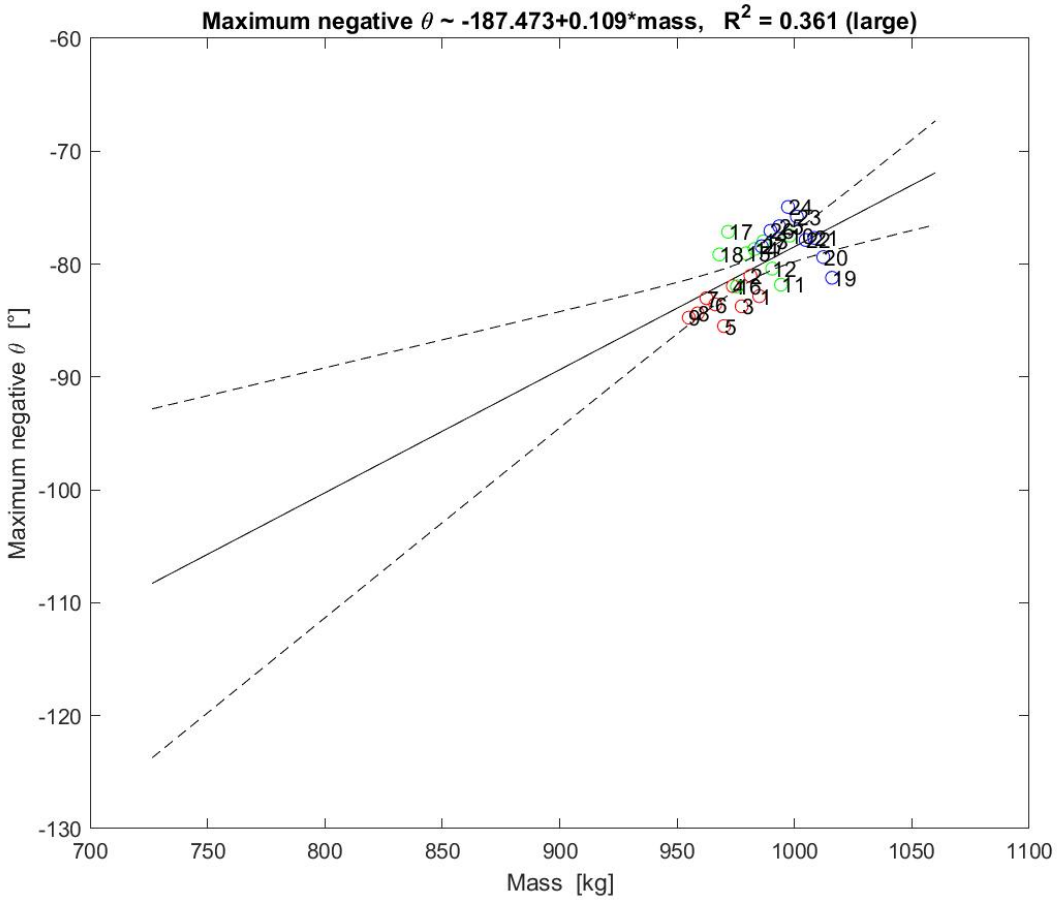

Figure 6.11: Maximum negative pitch angle versus aeroplane mass (for all 27 spin cases).

At the left hand x-boundary of Figure 6.11, i.e. when fuel is low, if the aircraft enters a spin at that point, the resulting aircraft behaviour will be harsh (i.e. the extreme attitude of the aircraft and pilot) and therefore disorientating. The low pitch angles on the right hand x-axis boundary imply that spin recovery would be longer and the altitude loss greater.

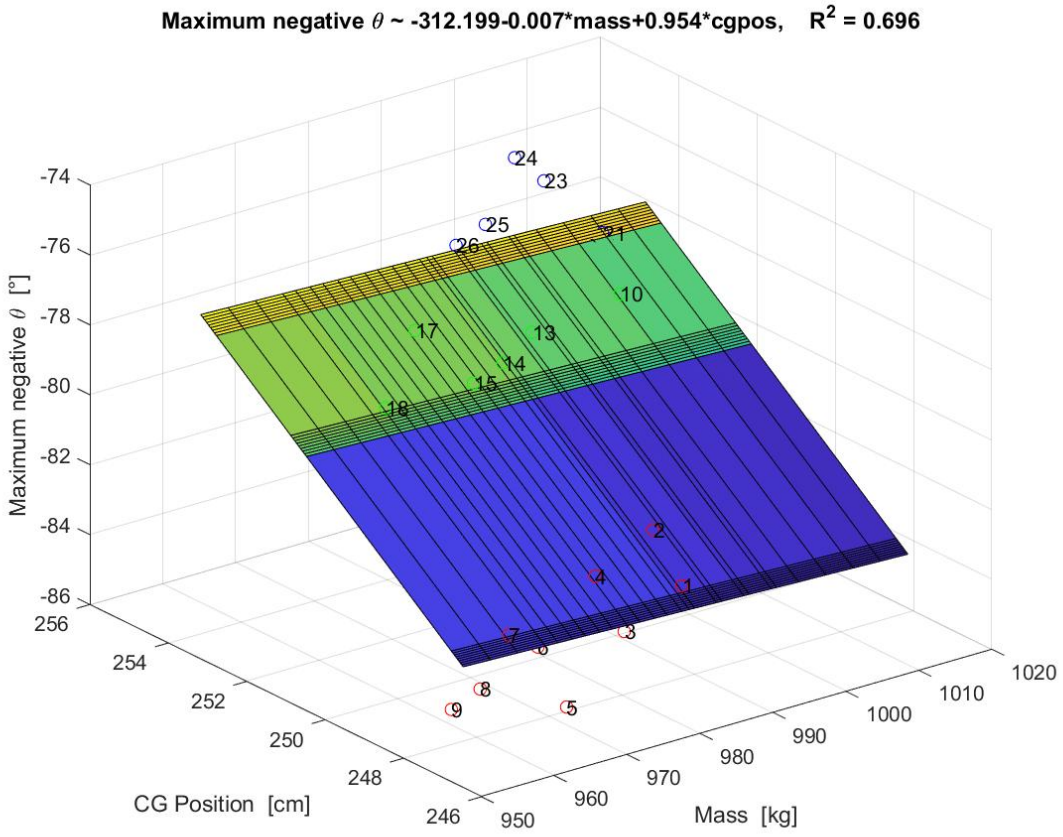

Figure 6.12: Maximum negative pitch angle versus aeroplane mass and CG Position

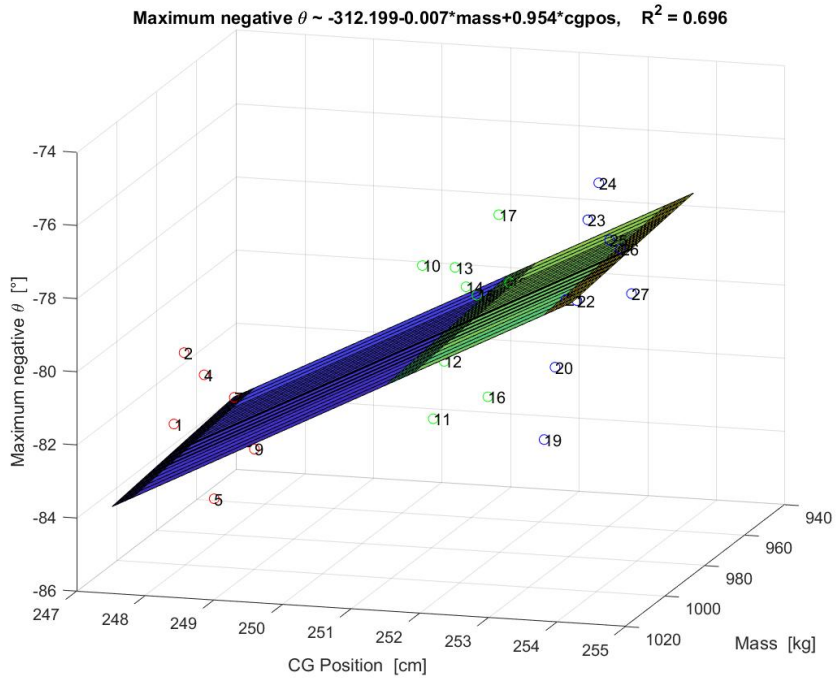

Figure 6.13: Maximum negative pitch angle versus aeroplane mass and CG Position (tilted view)

Figure 6.12 and 6.13 show the cross-coupling of both parameter changes and its influence on the largest negative pitch angle of the aeroplane. The R^2 dependency of 69.6% is nearly the same value as it can be shown in Figure 6.9 (maximum negative pitch angle versus CG position change). Therefore there is no cross-coupling between the CG and mass parameters.

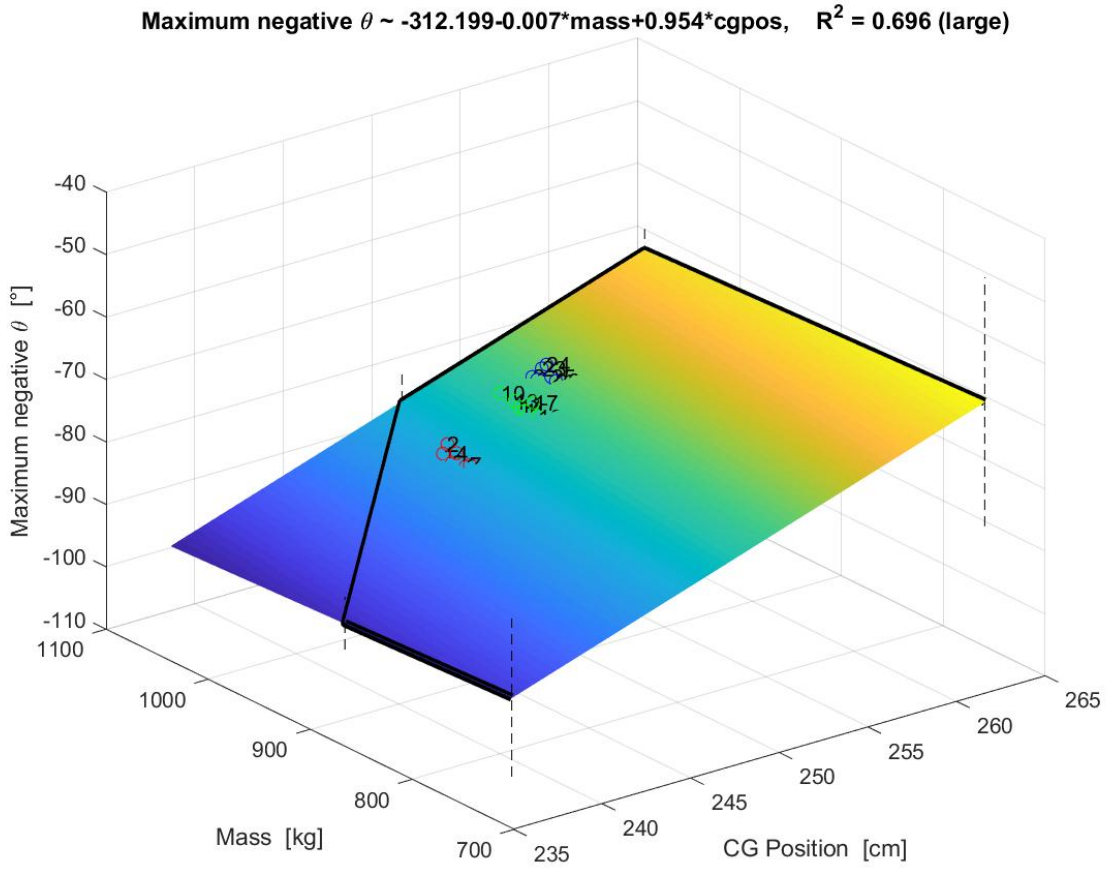

Figure 6.14 Maximum negative pitch angle versus aeroplane mass and CG Position (extended view) including confidence intervals of 95%.

The effect that always the second pitch down motion during a spin of a single-engine low-wing basic training aeroplane is the situation in which the aeroplane shows the maximum negative pitch angle (it is in the most vertical nose down attitude) has not been mentioned in the reviewed literature. This effect can be used in different scenarios which will be explained in Chapter 8.

6.5 Observation 2: Independent of the aeroplane's mass and CG position, the pitch angle (In_Theta) approximates to a characteristic value

In the following section, the pitch angle approximation of the aeroplane is investigated. After the initiation of a spin, the aeroplane shows a damped oscillation of its pitch angle. This damping leads to a final pitch angle (θ_{limit}) with which the aeroplane will rotate about its spin axis after a certain amount of time (after approximately 30 seconds). In Figures 6.15 and 6.16, the values for θ_{limit} are distributed between around -45° to -49° over the range of flown CG positions. Note that this theta range is contrary to that defined by Kredel (1998).

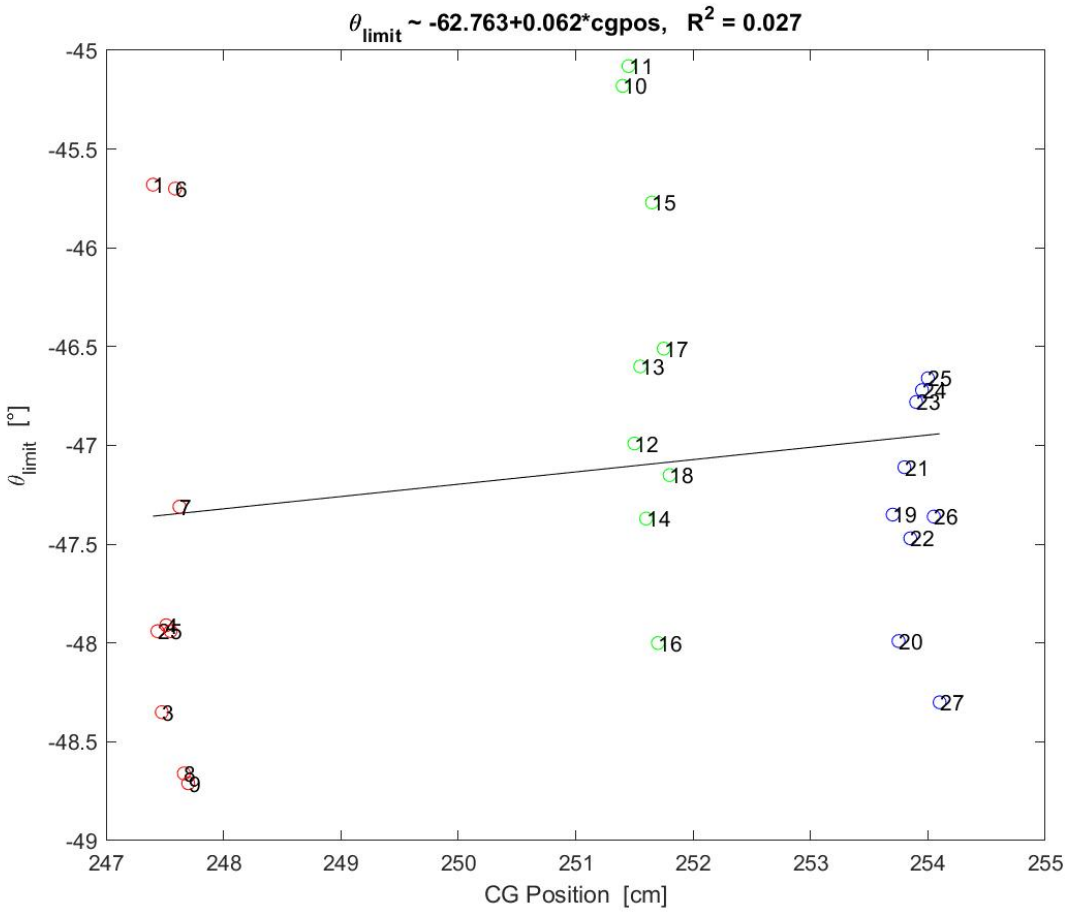

Figure 6.15: Limit value of Theta (pitch angle) versus Centre of Gravity position (for all spin cases).

The corresponding regression line shows a very small positive rise and a dependency of θ_{limit} on the CG positions is approximately 2.72 %, which is remarkably small considering the amount of CG change from nose heavy to tail heavy (see Figure 6.16).

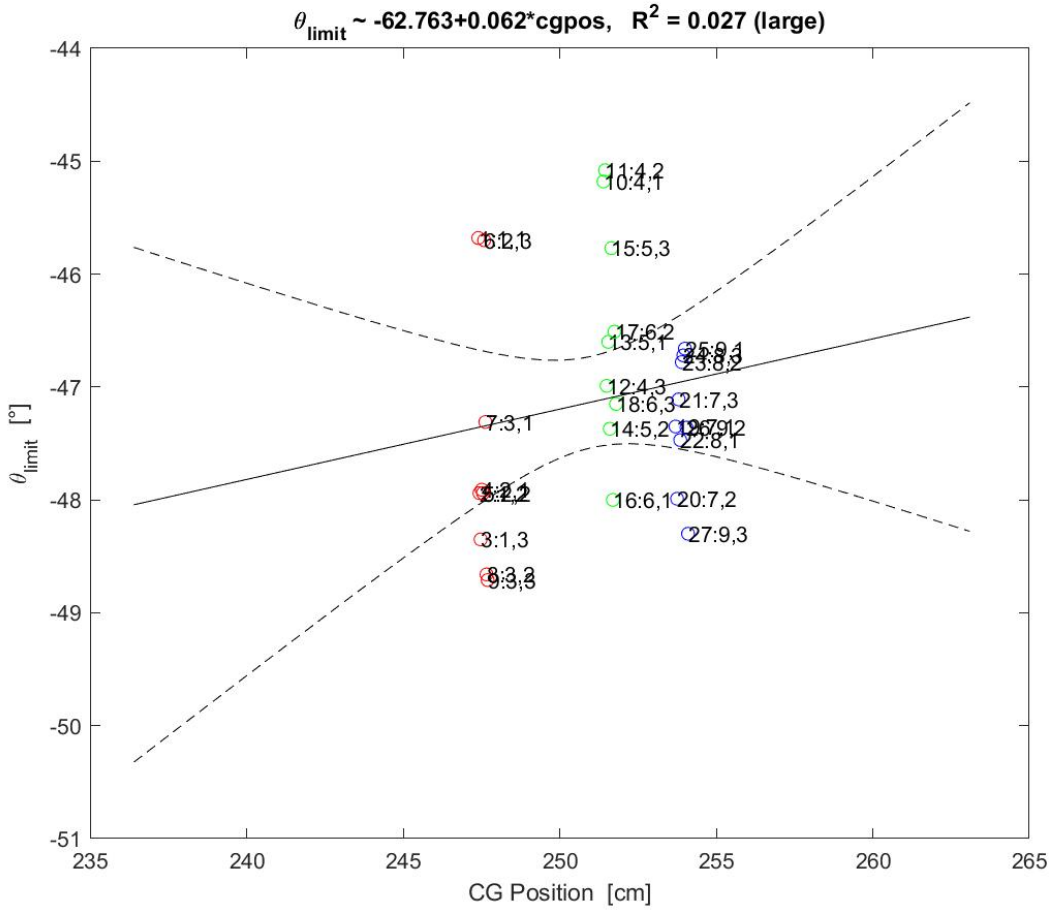

Figure 6.16: Limit value of Theta (pitch angle) versus Centre of Gravity position over the complete CG range (for all spin cases).

Hence even at the extremities of the flight envelope (Figure 6.16), the theta limit is still in close proximity to the original 47 degree limit. Therefore, no matter how much rudder shielding the Fuji FA-200-160 has, during any spin in its CG flight range; there is little effect on the final limit of the pitch angle.

A very small dependency of the θ_{limit} on the aeroplane's mass of around 6.93 % can be found in the Figure 6.17 below.

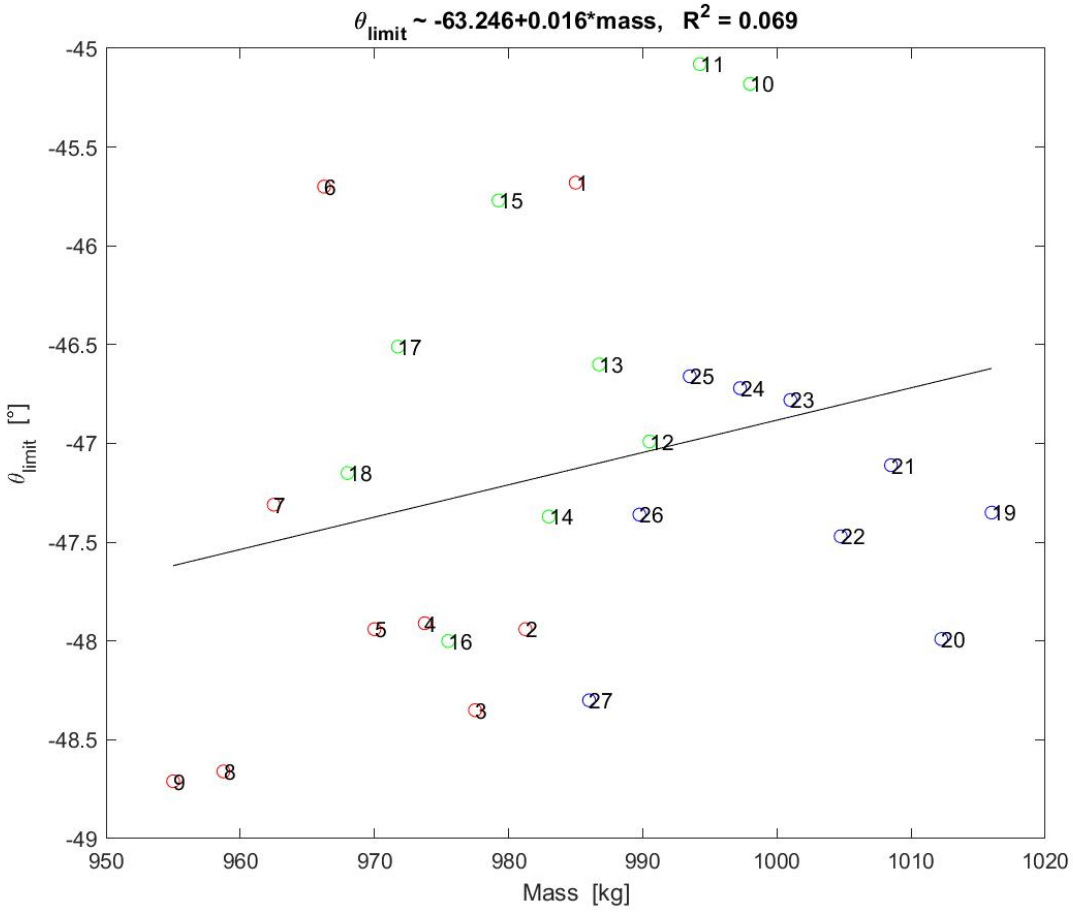

Figure 6.17: Limit value of Theta (pitch angle) versus the aeroplane's mass

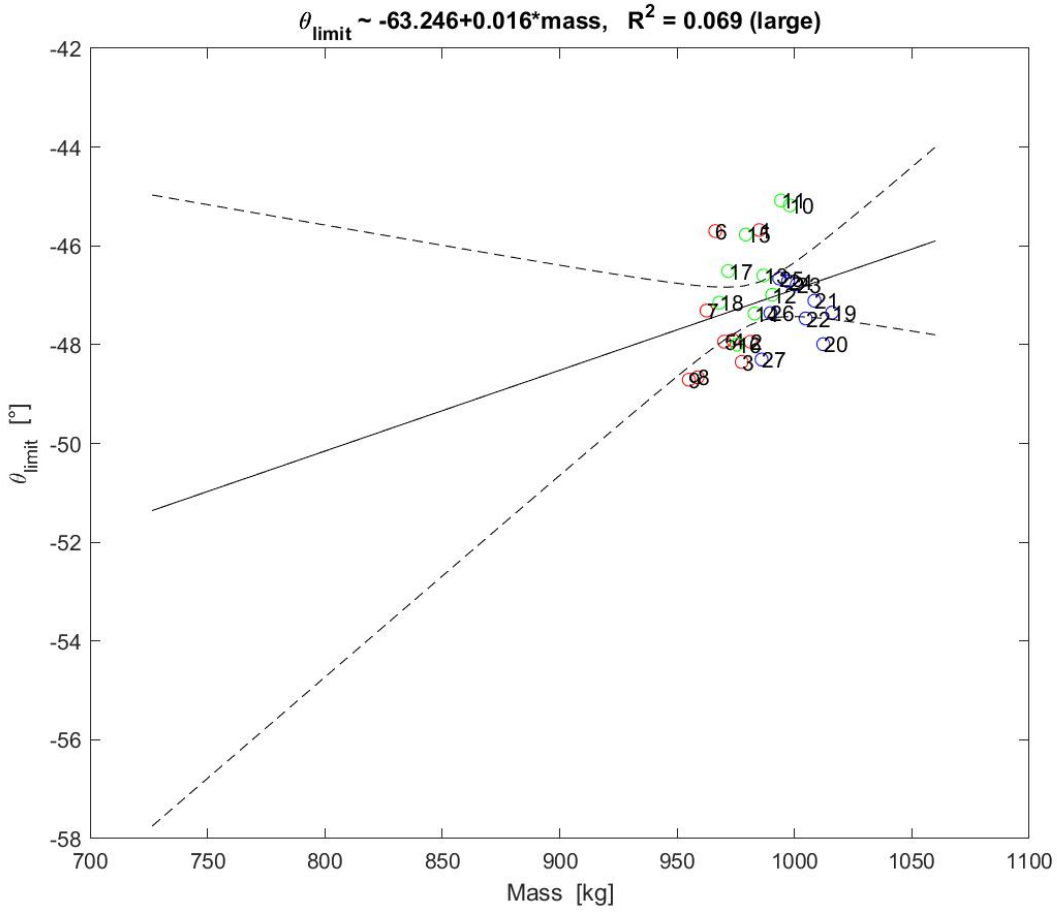

Figure 6.18: Limit value of Theta (pitch angle) versus aeroplane mass, extended to the boundaries of the flight envelope, for all spin runs, with confidence intervals (dashed lines) of 95%

Due to the measured values being taken within a small region (955 to 1015 kg) of the total mass value range (700 to 1060 kg) in the flight envelope (i.e. one-sixth of the range), extrapolation of the theta limit leads to a wider area of possible theta limit values. Figure 6.18 shows two 95% confidence limit (dashed) lines. At the minimum permitted mass of the flight envelope, the theta limit value is expected to lie between -58 and -44.5 degrees, i.e. almost 14 degrees. Hence although the conclusion of little dependency can be drawn between the theta limit and mass in the original spin runs, no such conclusion can be drawn on the extended range.

In Figure 6.19 below, it is shown that even a possible cross-coupling of both CG position and aeroplane's mass will only influence the θ_{limit} value by approximately 7.15 %.

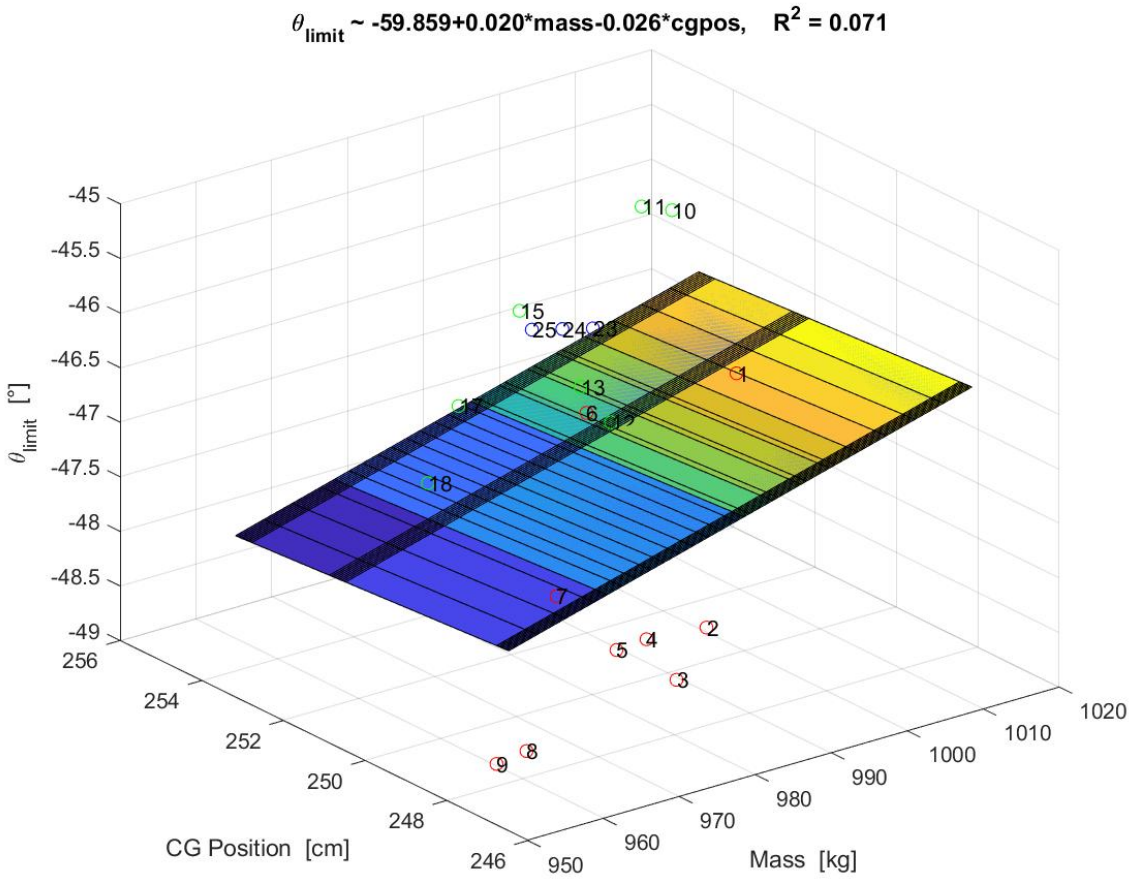

Figure 6.19: Response surface plot of the limit value of Theta (pitch angle) versus aeroplane's mass and CG position

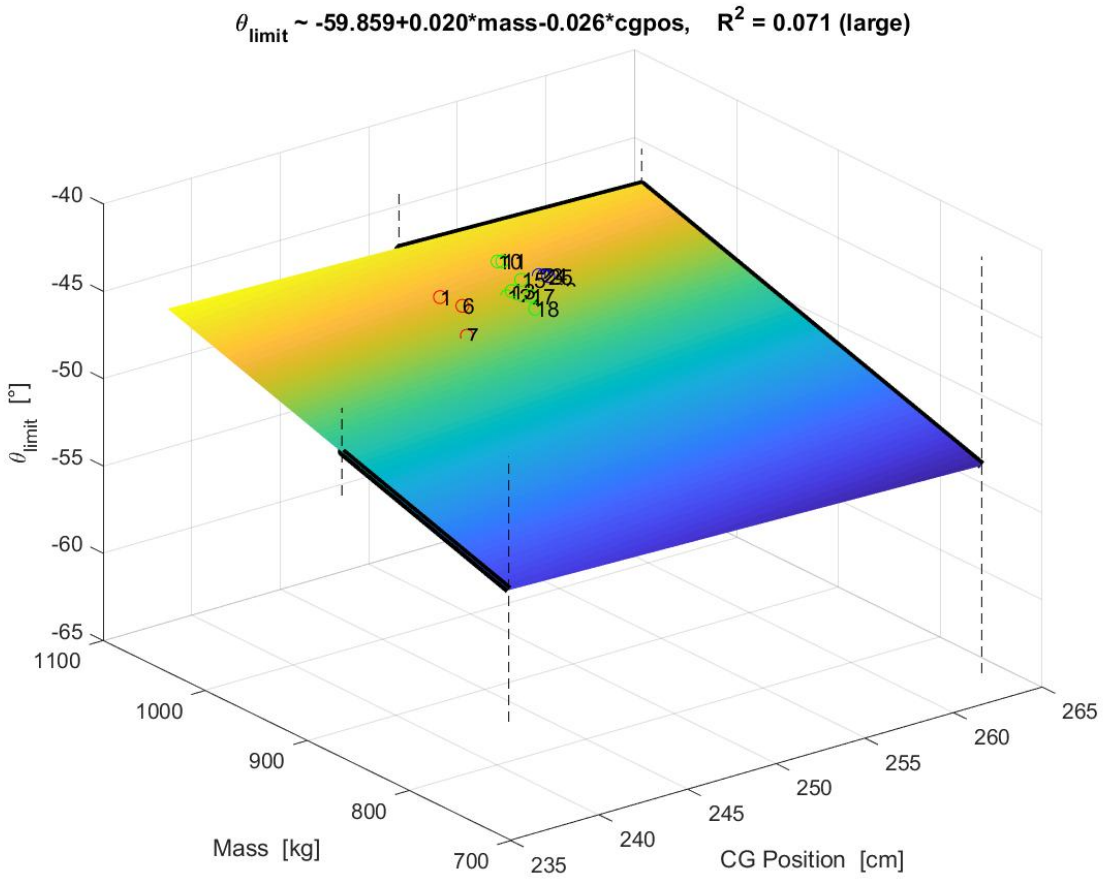

Figure 6.20: Limit value of Theta (pitch angle) versus aeroplane's mass and CG position

The mean value of all θ_{limit} values is -47.13° and its relative standard deviation is 2.15% (see figure 6.21).

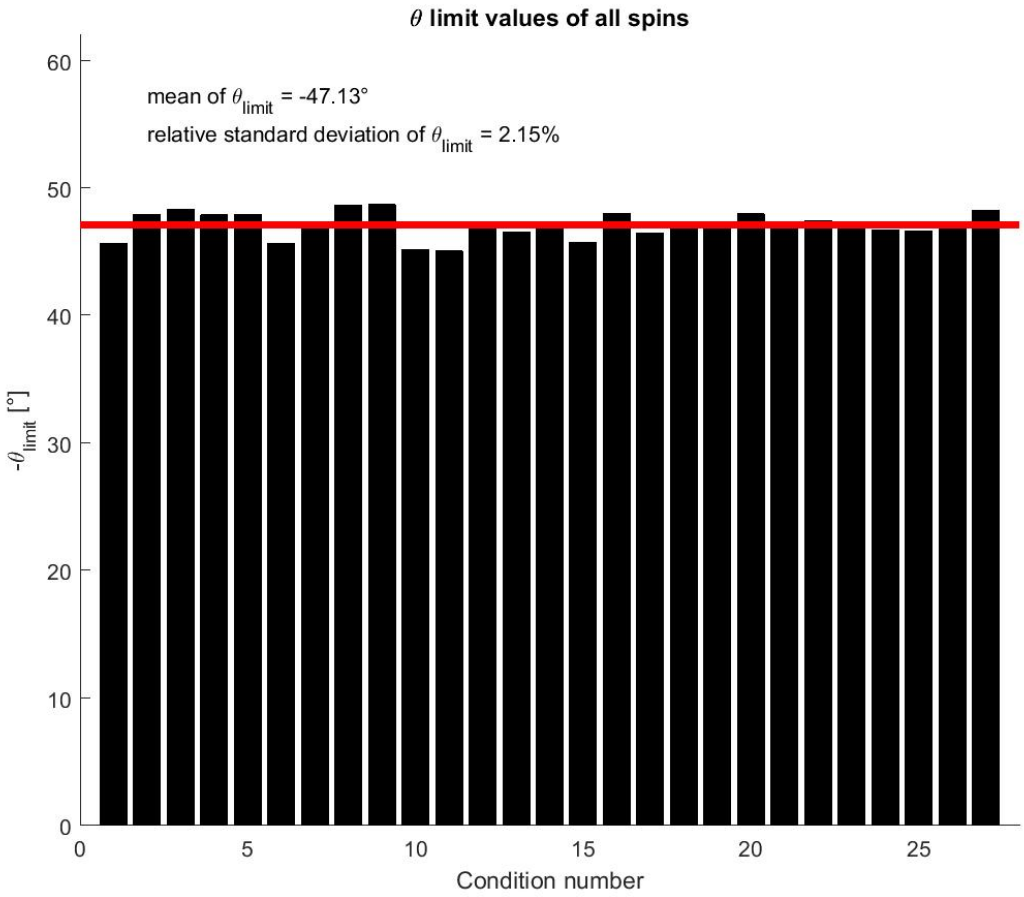

Figure 6.21: Limit value of Theta (pitch angle) of every single spin

Taking into account that errors (from atmospheric disturbances and control inputs) can influence theta values, an averaged value of theta in a single condition (1 – 9, see Tables 4.7 to 4.9) will smooth the errors and lead to more representative results. The corresponding averaged values can be found in Figure 6.22 below. The average mean value is 47.18° and the corresponding relative standard deviation decreases to 1.5 %.

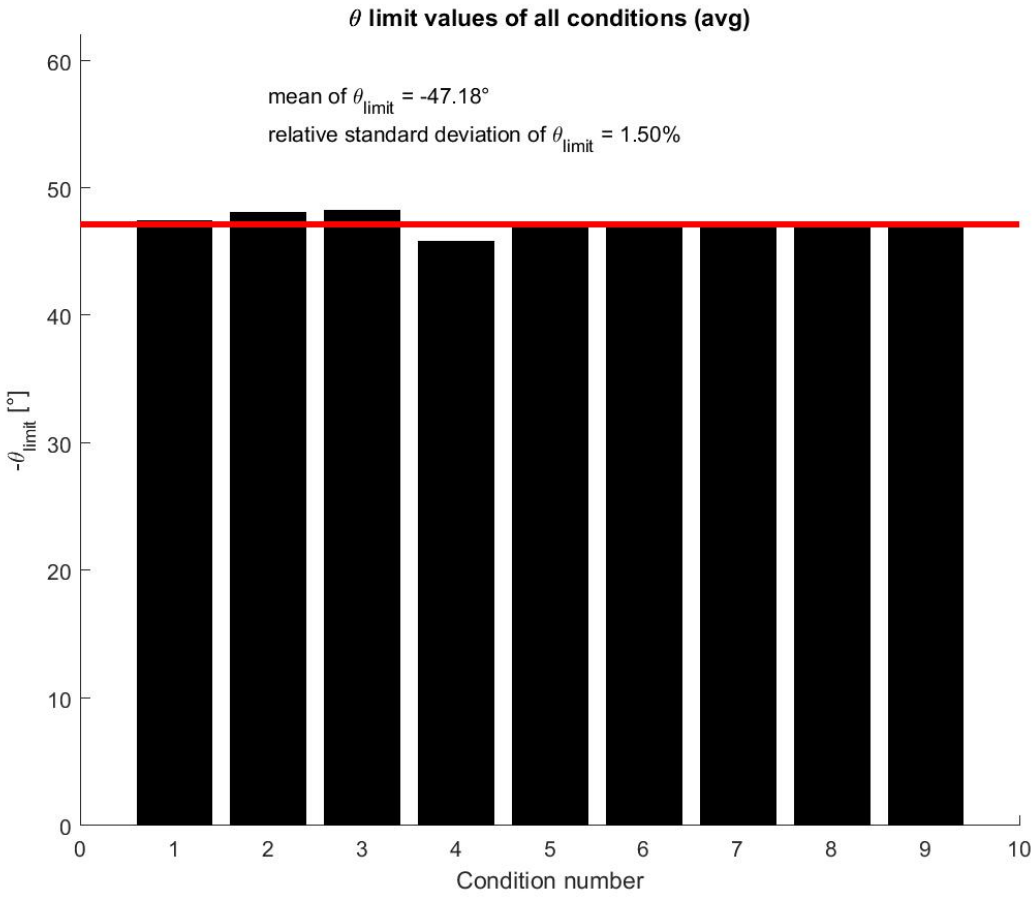

Figure 6.22: Averaged limit value of Theta (pitch angle) of every single spin condition

Based on these results it can be said that independent of the aeroplane's mass and CG position for the flown values, the pitch angle approximates to a characteristic value. Across the whole flight envelope, the value of theta limit would vary by at less than 4 degrees for CG changes but might vary by up to 11 degrees for the aircraft mass.

Once the value of θ_{limit} is known, this can be used to calculate the amount of tail shielding that the aircraft has in this spin situation. The 47 degree angle can be projected onto the side view of the aircraft so that the unshielded area can be found. Then the side force can be evaluated using this known area. Thus the ability to recover from a spin and the expected recovery time can be estimated.

Using Procedure 6.3.2, the final θ_{limit} values have been determined. Figure 6.23 presents a particular example of the time dependent motion for theta. The entire set of plots including the corresponding damping coefficients and values of θ_{limit} can be found in an electronic Appendix (USB drive) to this work.

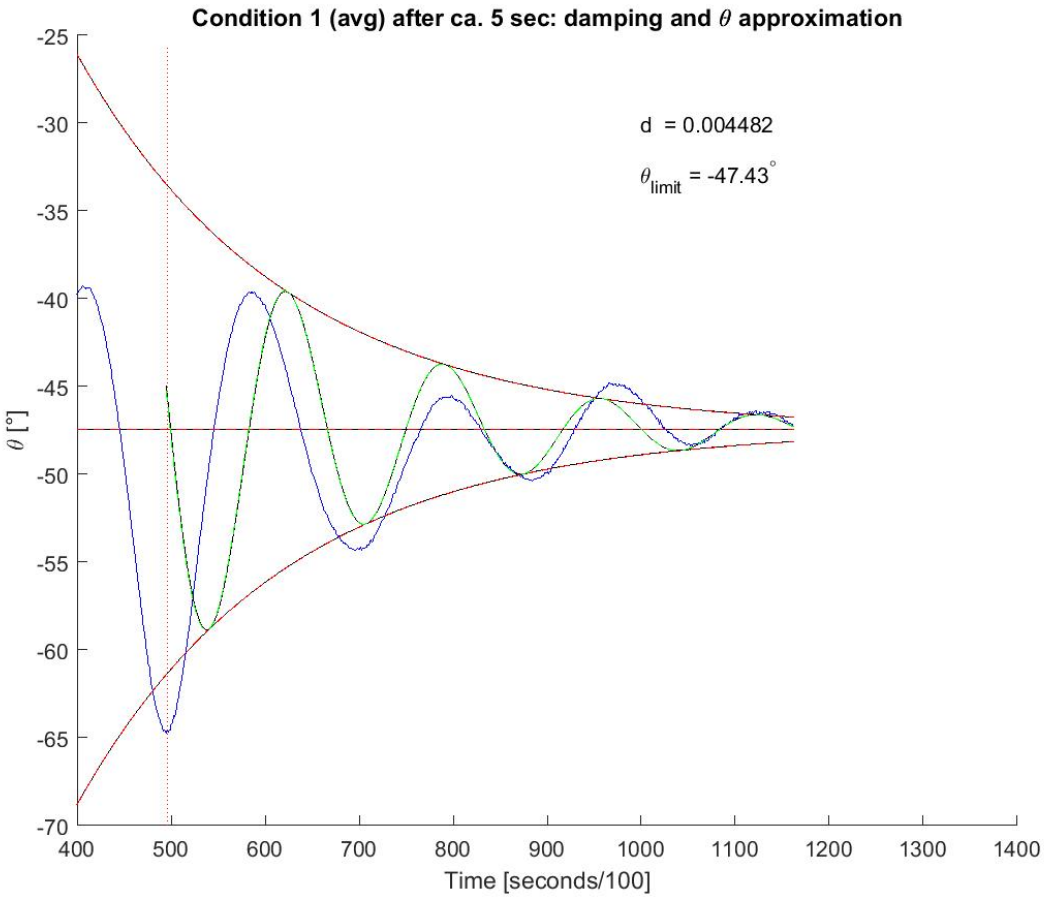

Figure 6.23: Example for the averaged theta values of a spin condition (here condition 1) including the damping coefficient and the resulting θ_{limit} value.

The results presented above are in contradiction to the traditional spin explanations in terms of the effect of CG position. For example, Air Ministry (1995) states that: 'The attitude of the aircraft at this stage will depend on the aerodynamic shape of the aircraft, the position of the controls and the distribution of mass throughout the aircraft'. And according to Bowman (1971) that: 'Experience has shown that in most cases, an airplane will spin flatter as the center of gravity is moved rearward.' Neumann (2003) also expressed the same opinion. Similarly Zimmerman (1936) and Seidman et al (1939) state that the centre of gravity position can significantly affect the spin and recovery characteristics.

6.6 Observation 3: Maximum Yaw rate (ln_r) changes with CG position and mass

In the following section the aeroplane's yaw behaviour is investigated which has been influenced by a shift of the CG position and the mass of the aeroplane.

The reason for the interest in maximum yaw rate is that the faster an aeroplane spins the more likely a pilot is to become disorientated.

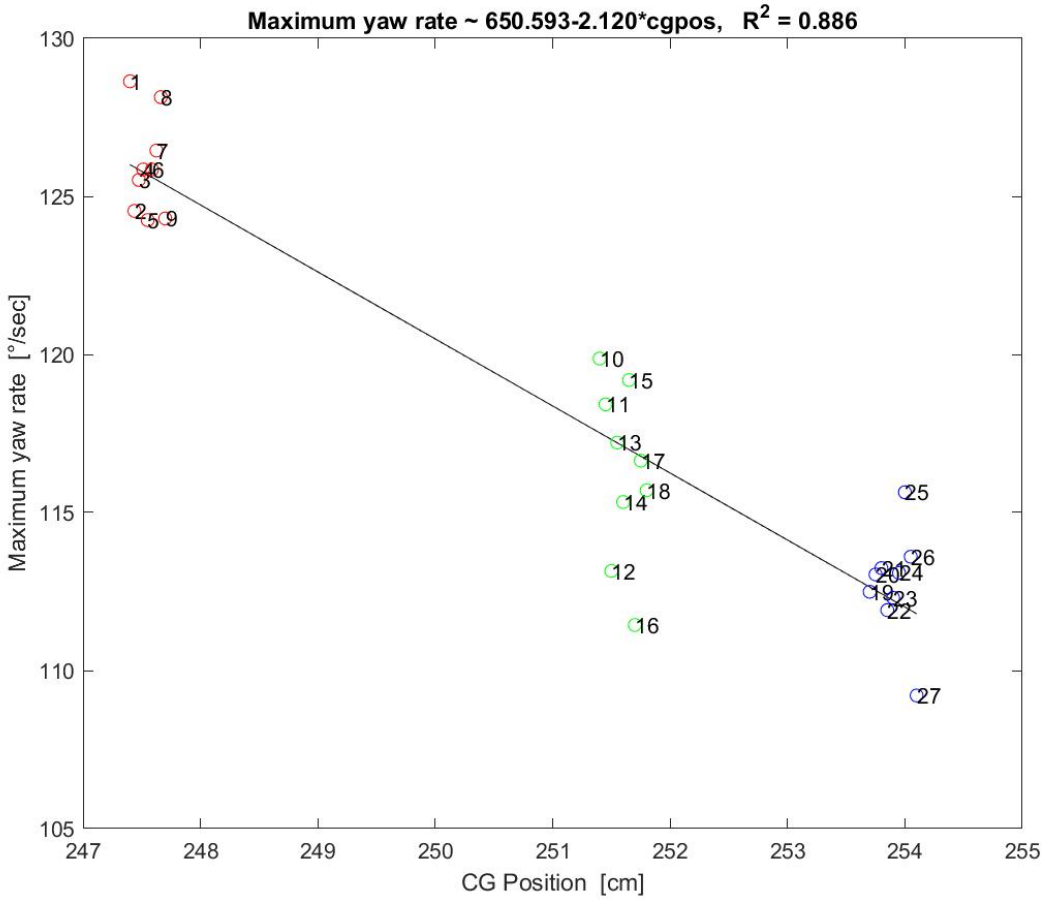

Figure 6.24: Maximum yaw rate versus CG position (for all 27 spin cases)

As Figure 6.24 shows, the maximum yaw rate changes significantly when the CG position is moved backwards. Sloshing fuel and gust effects lead to the scattering of the measured data points in the corresponding plots within this section. The variation of the yaw rate change follows an 88.6 % R^2 dependency on the variation of the CG position. Forward CG positions result in faster yaw rates than aft CG positions which are shown on the plot above. With values between around 126°/second and 114°/second the yaw rate changes by approximately. 9.5%.

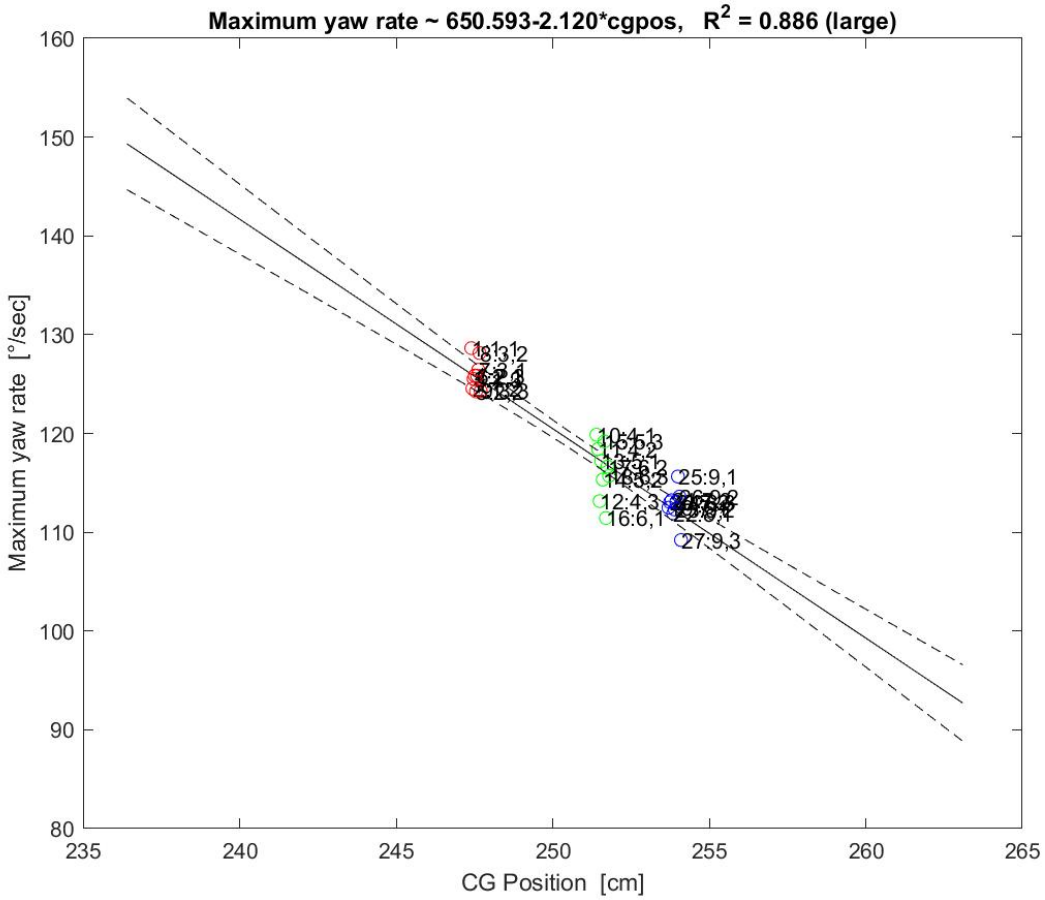

Figure 6.25: Maximum yaw rate versus CG position (for all 27 spin cases) for the extended flight envelope for CG, with 95% confidence interval lines (dashed)

Therefore at minimum values of permitted CG position (see the left hand side of Figure 6.25), the aircraft spins faster, undergoes greater stresses during the spin, and for the pilot there is a greater probability of disorientation. The closeness of the confidence interval lines implies that the information could be used for predictive values of the maximum yaw rate against CG for mission planning. Thus the loading of an aircraft (passenger, fuel and payload) would ensure that certain forward CG positions were not adopted.

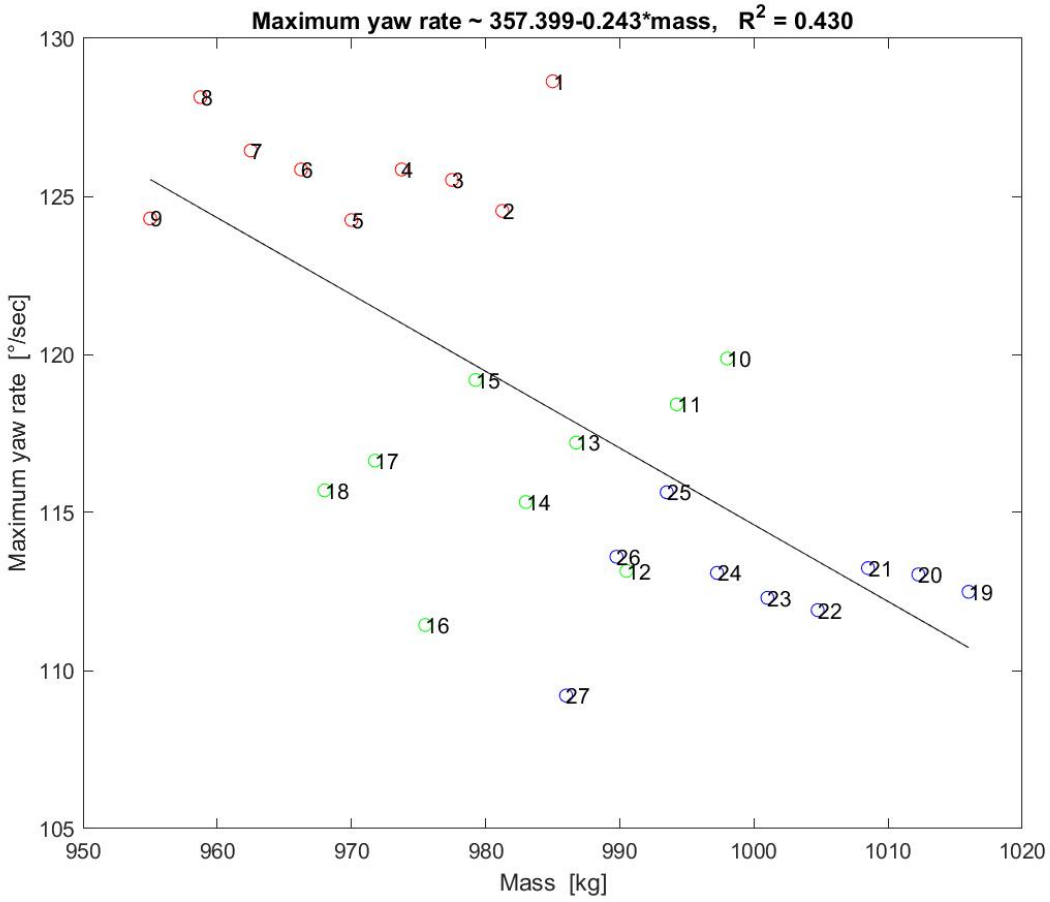

Figure 6.26: Maximum yaw rate versus mass for all 27 spin cases

The mass of the aeroplane does not influence the yaw rate as significantly as CG. The change in the yaw rate due to a change in the aircraft's mass shows a dependency of 43% - again with a negative slope of the regression line (Figure 6.26). Lower masses result in faster yaw rates than higher masses. With a data range between around.125°/sec and 113°/sec, the yaw rate changes by approximately 9.5% (as for the CG effect in Figure 6.24)

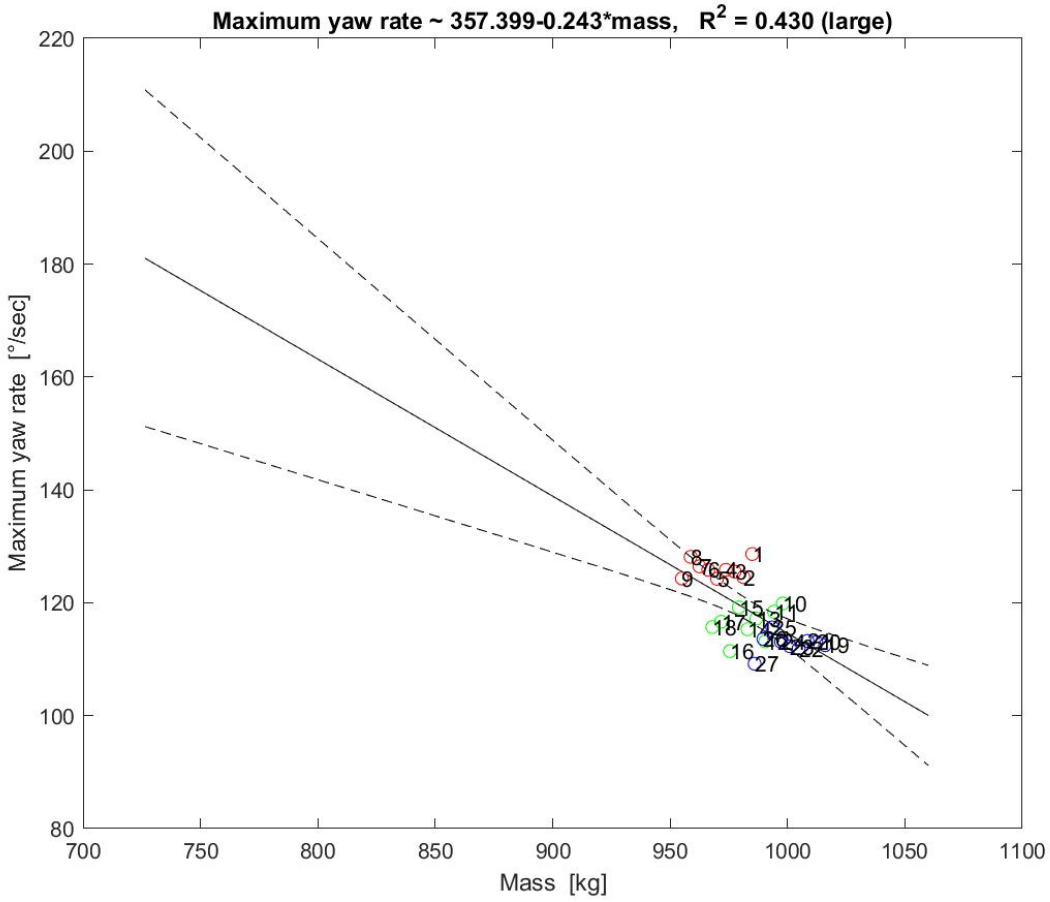

Figure 6.27: Maximum yaw rate versus mass for all 27 spin cases across the full mass range with 95% confidence interval lines (dashed)

Once the data is extrapolated to the full range of permitted mass values, the possible maximum yaw rates predicted can be up to 220 °/second (compared with 155°/second for the effect of CG). Thus mass changes in the aircraft affect the pilot and aircraft more strongly.

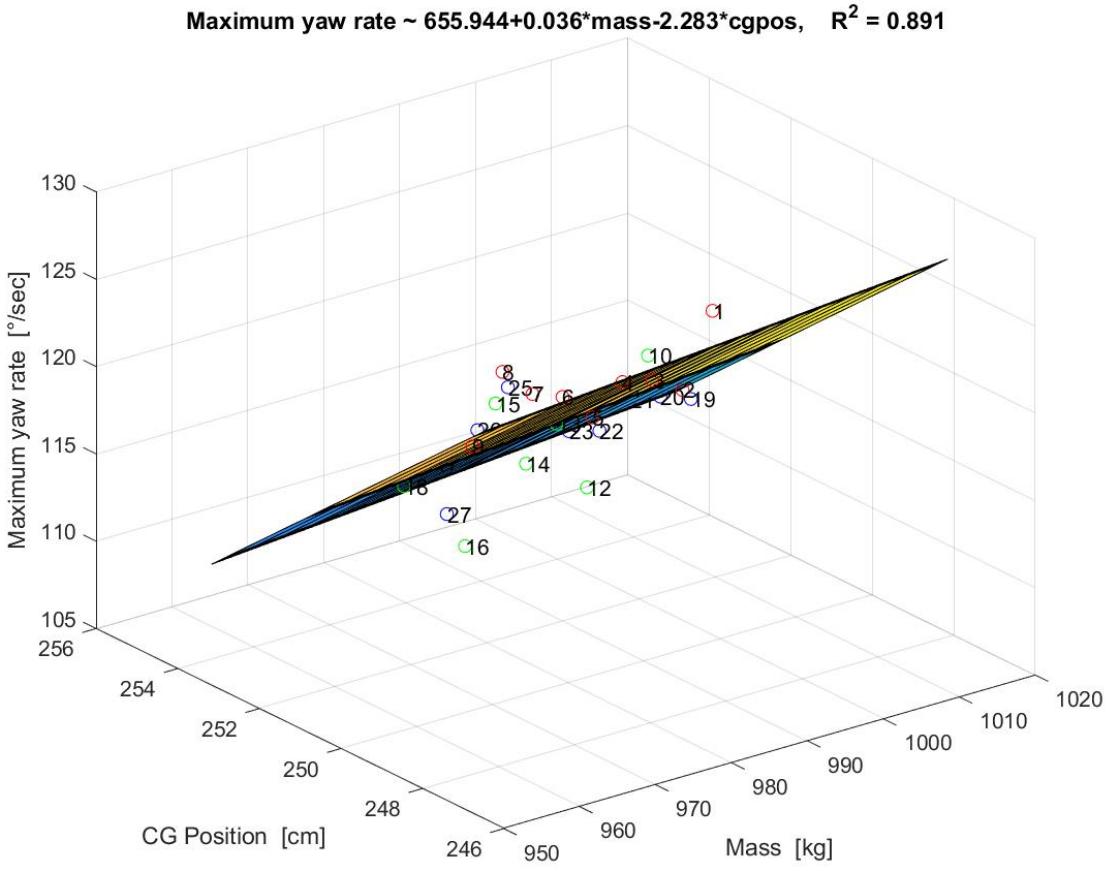

Figure 6.28a: Response surface for the Maximum yaw rate versus CG position and mass for the 27 spin cases

There is no significant cross-coupling of the influences of the CG position change and the mass change. Figure 6.28a and 6.28b shows that the overall influence of both parameters is an R^2 value of 89.1 % which is nearly the same value as the CG position influence alone (Figure 6.24). In the reviewed literature a corresponding finding cannot be found.

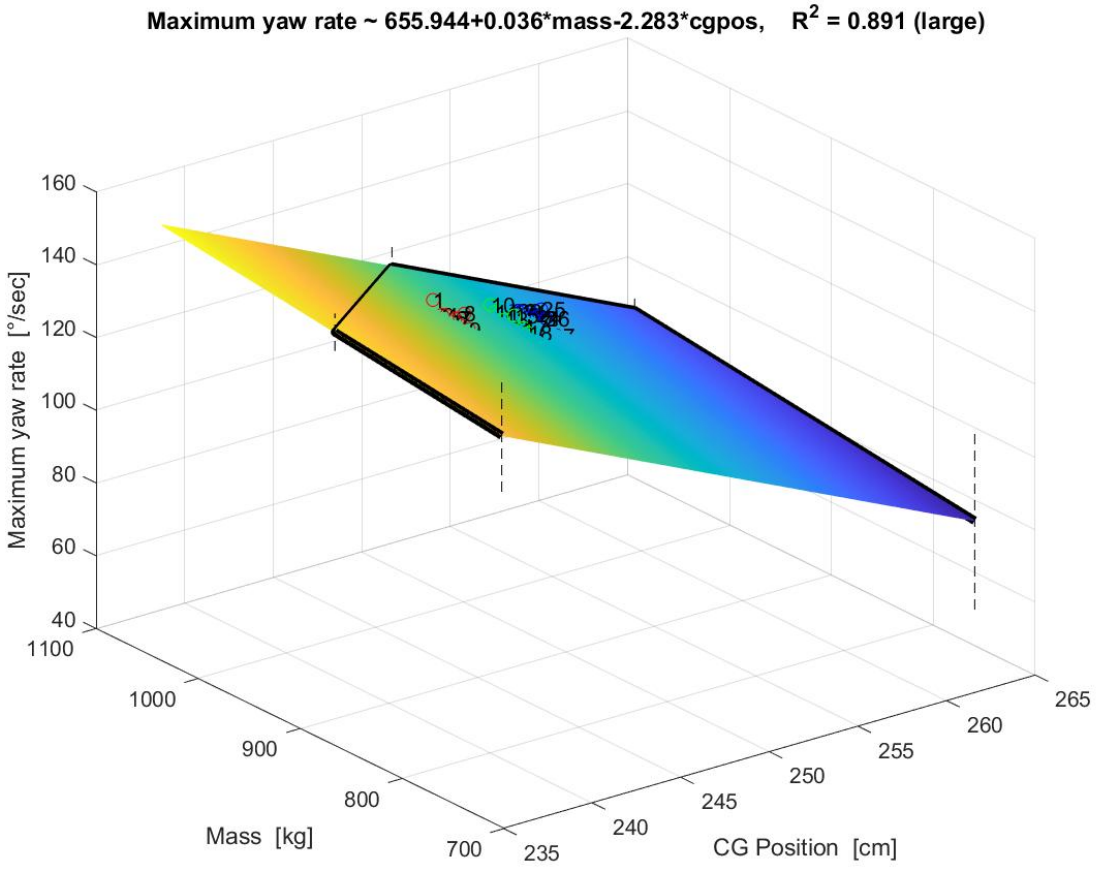

Figure 6.28b: Response surface for the Maximum yaw rate versus CG position and mass for the 27 spin cases (extended range). The dashed lines indicate the 95% confidence intervals

One of the conclusions of the work of Stough, et al. (1987b) was that 'A center-of-gravity shift of nine percent of the mean aerodynamic chord had little effect on spin characteristics'. In the case of the Fuji, with a mean aerodynamic chord of 1.524 m (from Table A4.2); a 9% change would be 14 cm. From the Fuji results in Figure 6.25, a 14 cm change in CG provides a change in the maximum yaw rate of approximately 25°/second (=130-105), or a rise of a 24% (25/105) in the maximum yaw rate. This is a definite change in spin characteristics, and thus the Fuji results disagree with the conclusions of Stough et al. (1987b) which are not derived from a systematic set of data.

6.7 Observation 4: The yaw rate (ln_r) oscillation changes with CG position or mass

This section focusses on the second derivative of yaw angle with respect to the CG or mass values. The second derivative was calculated in Matlab as a first order difference of the measured values.

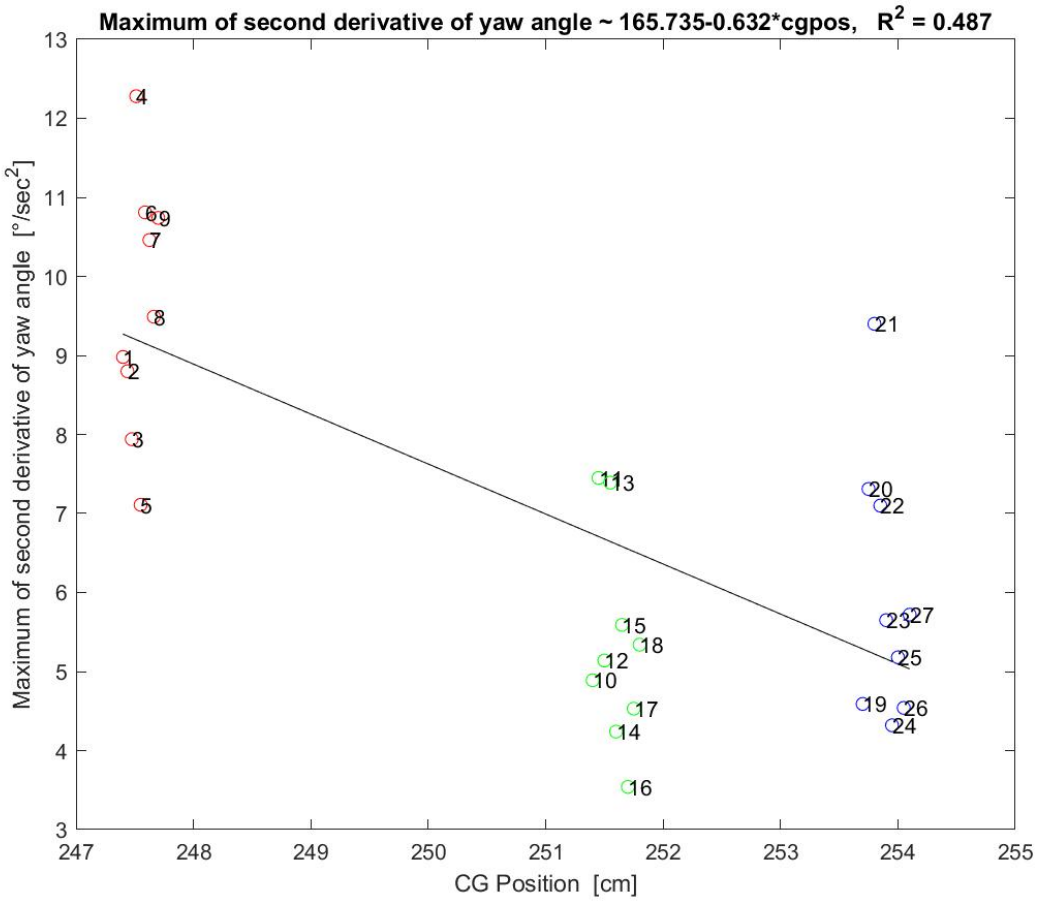

Figure 6.29: Maximum of second derivative of yaw angle versus CG position for all 27 spin runs

Figure 6.29 shows that the oscillation of the yaw rate changes is only moderate with the shift of the CG position. The regression line represents a 48.7% value which has a negative slope. During the CG position change the values for the second derivative of the yaw angle changed from around 9.2 °/sec^2 to 5.1 °/sec^2 which is a change of approximately 55.4%. This means that spins with forward CG positions are changing their yaw rate more than spins with aft CG positions. The higher the spin acceleration the more stress on the aircraft and the pilot. The second derivative of the yaw angle is sensitive to random disturbances like gusts, control inputs and sloshing fuel. This is evidenced by the left hand set of data being distributed fairly evenly about the regression line, whereas the data for the second set are mainly below and for the third set mainly above.

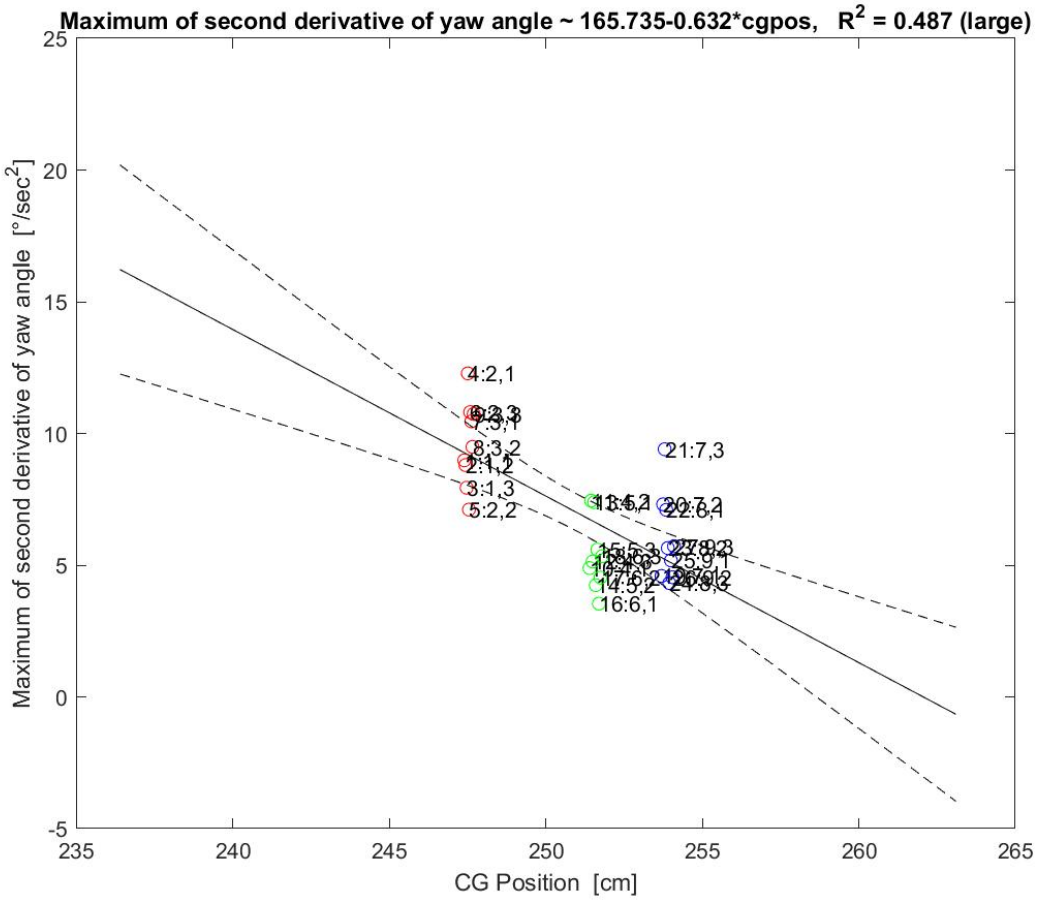

Figure 6.30: Maximum of second derivative of yaw angle versus CG position for the 27 spin runs and 95% confidence intervals (dashed lines) across the maximum range of the CG in the flight envelope

The randomness of the data in each of the three sets is demonstrated in the Figure 6.30. For the 27 spin runs there were 9 experiments repeated three times each. For example runs 1, 2, 3 are the same case and 10, 11, 12 are three runs of a different case. The left hand column of the data on the graph shows the first 9 runs. The order from top to bottom is 4, 6, 9, 7, 8, 1, 2, 3, and 5 therefore it can be seen that run 5 is at the opposite end from runs 4 and 6. For the middle and right columns the data are arranged in a different order for each column, hence showing the randomness.

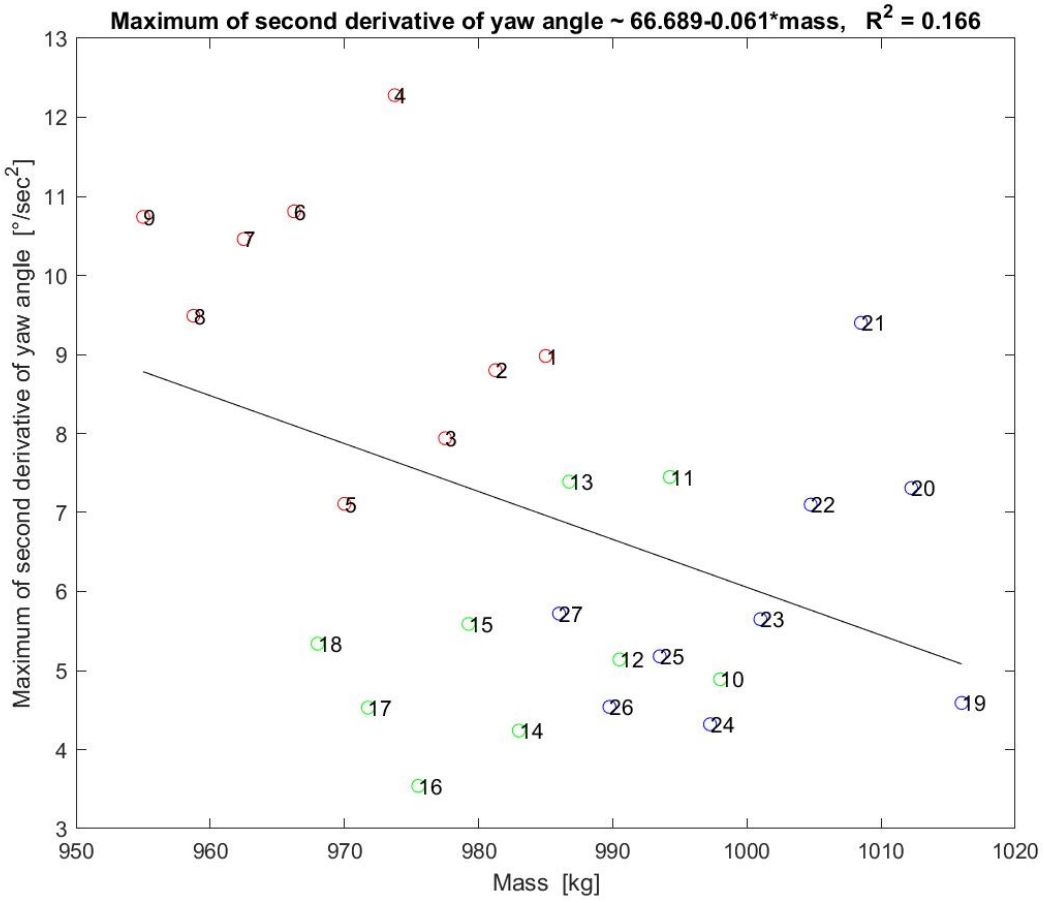

Figure 6.31: Maximum of second derivative of yaw angle versus mass for the 27 spin runs

The oscillation of the yaw rates with mass (Figure 6.31) has an R^2 value of 16.6%, therefore a low dependency. Based on the regression line – which shows a negative slope - the values of the second derivative of the yaw rate lie between 8.9 °/sec^2 to 5.0 °/sec^2.

The results indicate that lower aeroplane masses will lead to larger angular accelerations about the z-axis.

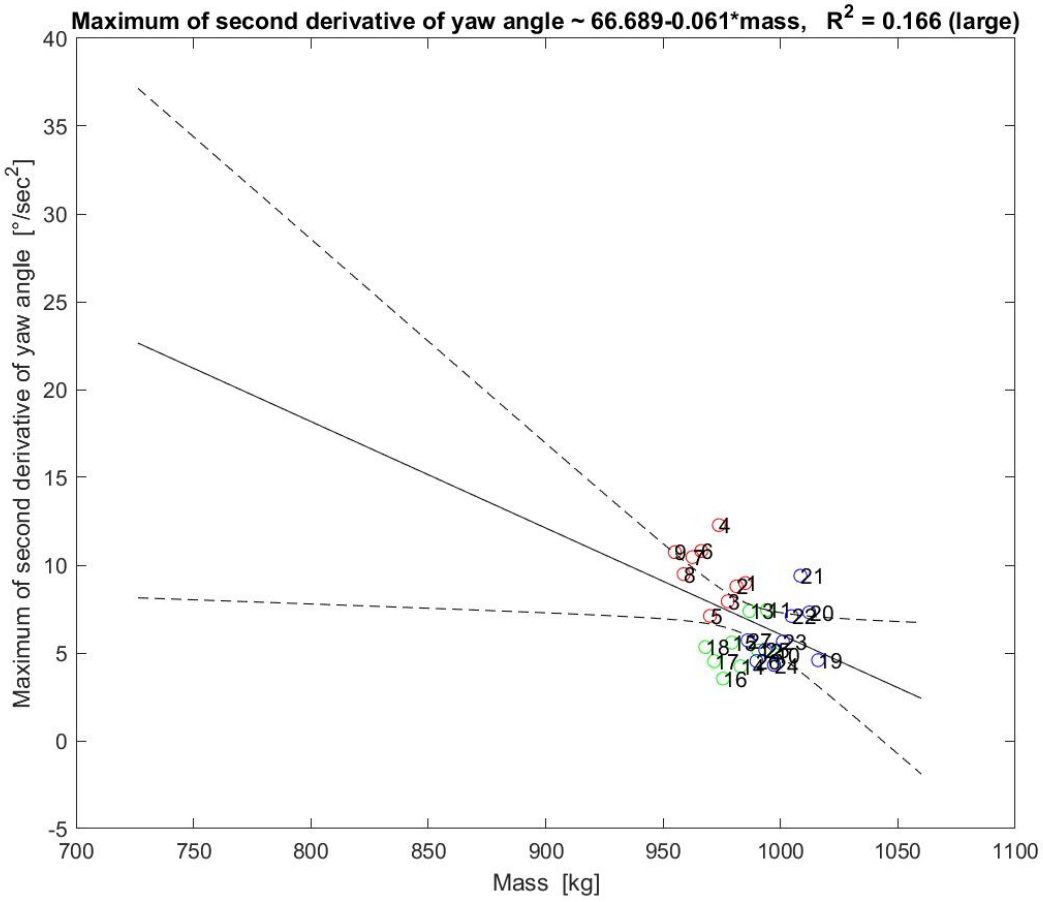

Figure 6.32: Maximum of second derivative of yaw angle versus mass for the 27 spin runs for the maximum range of mass in the flight envelope. The dashed lines indicate the 95% confidence intervals

Due to the small value of R^2 for this parameter relation when the 95% confidence interval lines are applied to the graph (Figure 6.32) the left hand side range is too large for reliable predictions. At the higher mass boundary on the right hand side of the graph, the predictions are more useful. Therefore the only way to make the prediction more reliable would be to have more data points, especially to the left hand side of the graph.

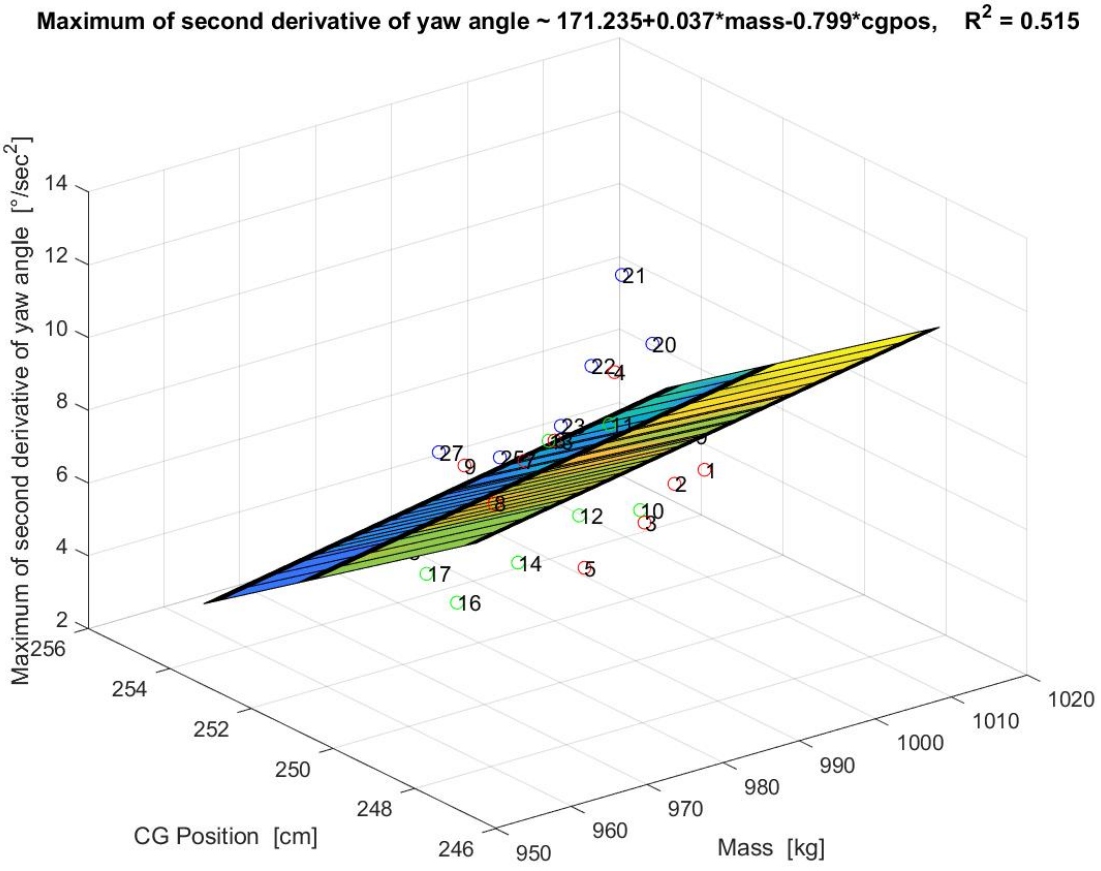

Figure 6.33: Maximum of second derivative of yaw angle versus CG position and mass

A significant cross-coupling of both parameters cannot be seen either in Figure 6.33 or Figure 6.34 as the dependency of the yaw rate oscillation only follows 51.5% a linear model which is according to the definition (see Table 6.1.2) above a moderate degree of sensitivity.

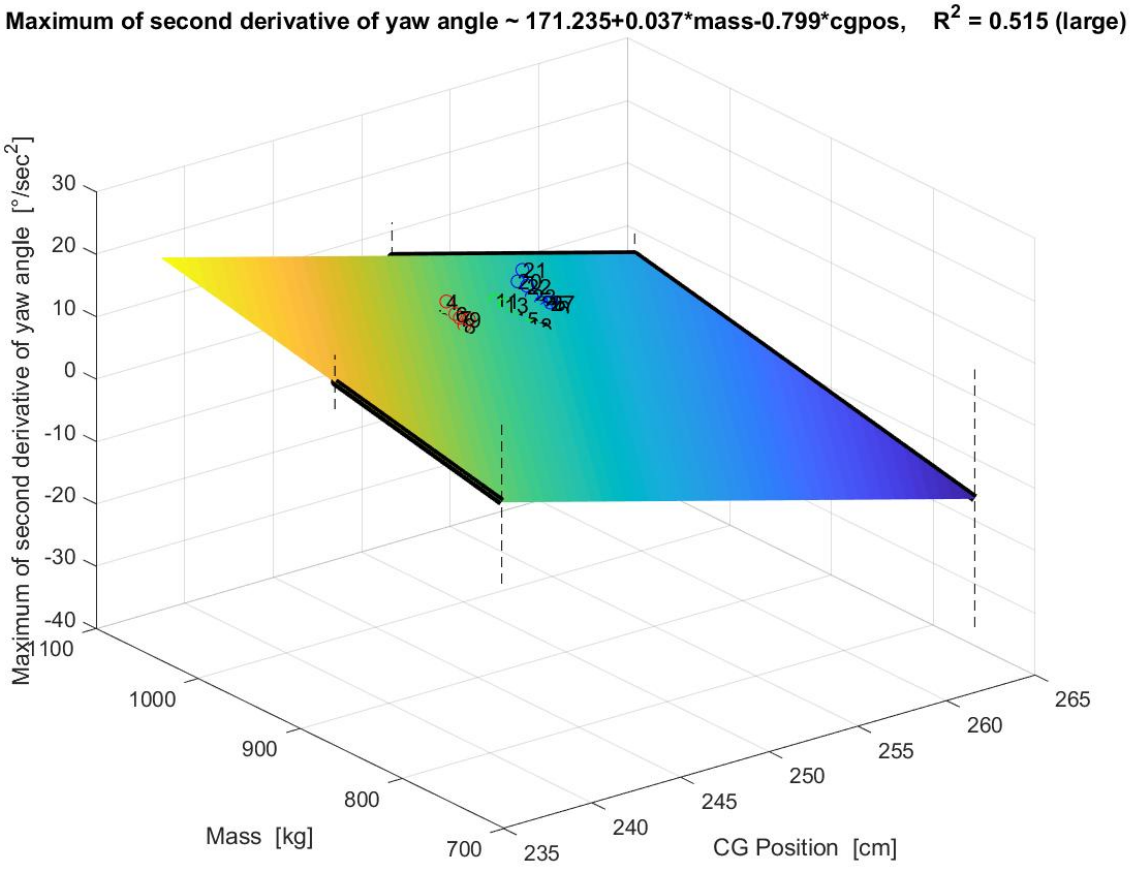

Figure 6.34: Maximum of second derivative of yaw angle versus CG position and mass for the 27 spin runs for the maximum range of mass and CG in the flight envelope. The dashed lines indicate the 95% confidence intervals

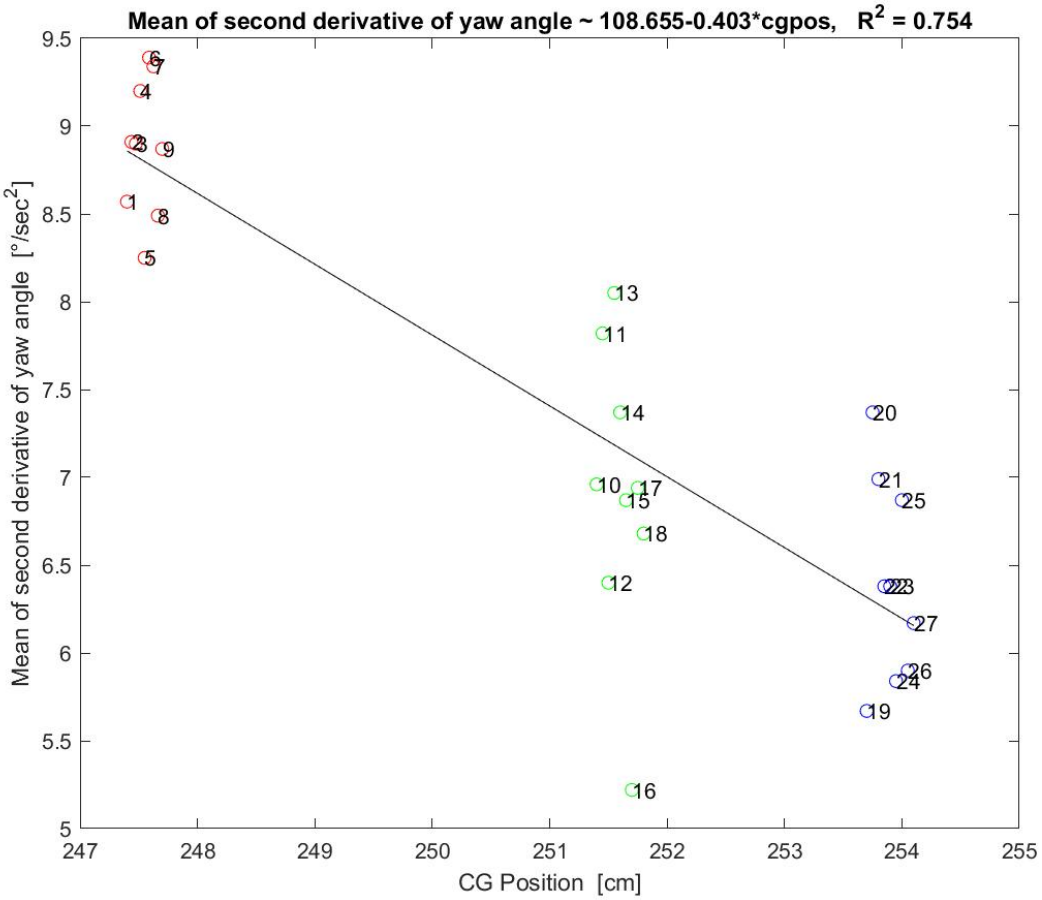

Figure 6.35: Mean of second derivative of yaw angle versus CG position for the 27 spin runs

By averaging the values of the yaw rate change – which aims to minimize the influence of random errors like gust effects or sloshing fuel - the results are clearer than the values of the maximum second derivative of the yaw angle. In Figure 6.35 it can be seen that the mean of the second derivative of the yaw angle shows a strong 75.4% dependency. The data points are scattered for each CG position along the y-direction. The corresponding regression line shows a negative slope, thus it can be seen that a forward CG position will lead to higher angular accelerations about the aircraft's z-axis. From the most forward CG position to the most rearward CG position, there are rapid angular acceleration rates between 8.9 °/sec^2 to 6.1 °/sec^2.

Aviation medicine sources record that in rotational tests subject experienced a lack of positional awareness when subjected to rotational accelerations above 2°/s^2 for more than 30 seconds. A typical time for one of the spin cases in this thesis from entry to recovery is around 20 seconds.

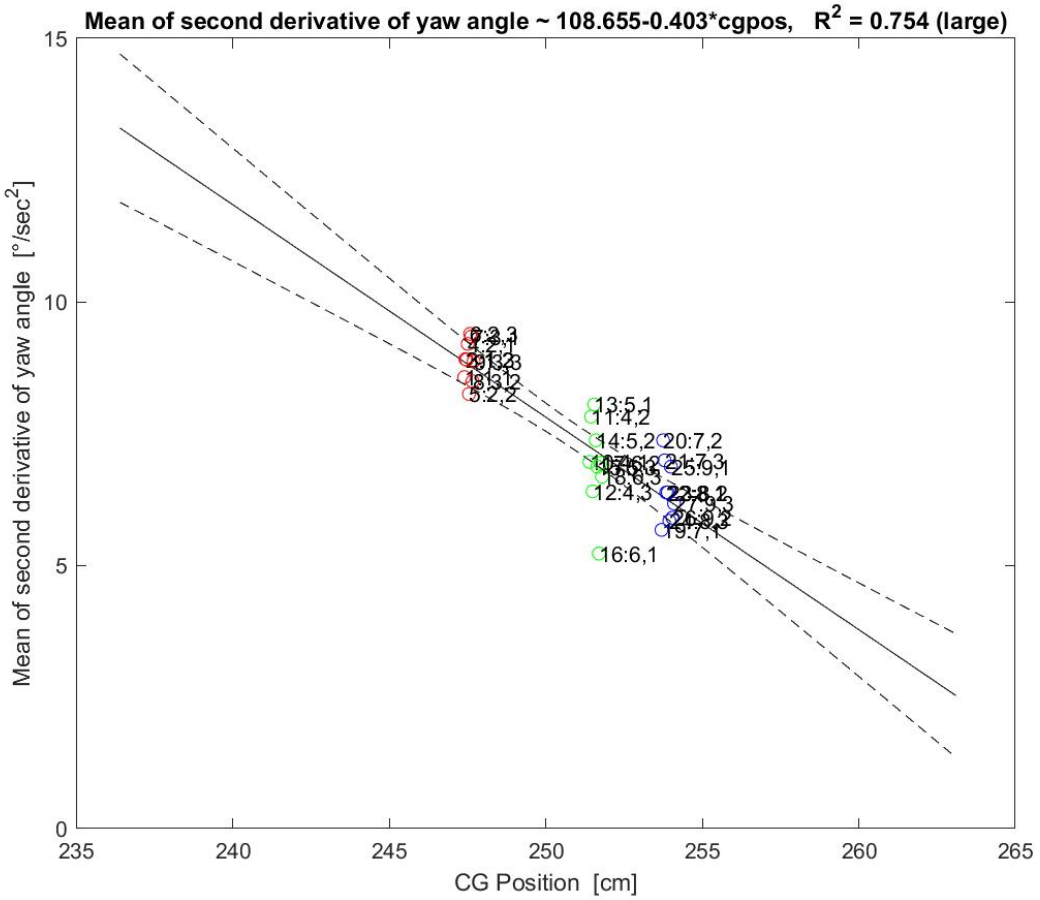

Figure 6.36: Mean of second derivative of yaw angle versus CG position for the 27 spin runs for the maximum range of CG in the flight envelope. The dashed lines indicate the 95% confidence intervals

Although recovery is possible at the left hand boundary a pilot was to enter a spin condition the mean second derivative of yaw angle is certainly a cause for concern from the safety point of view for both pilot and aircraft.

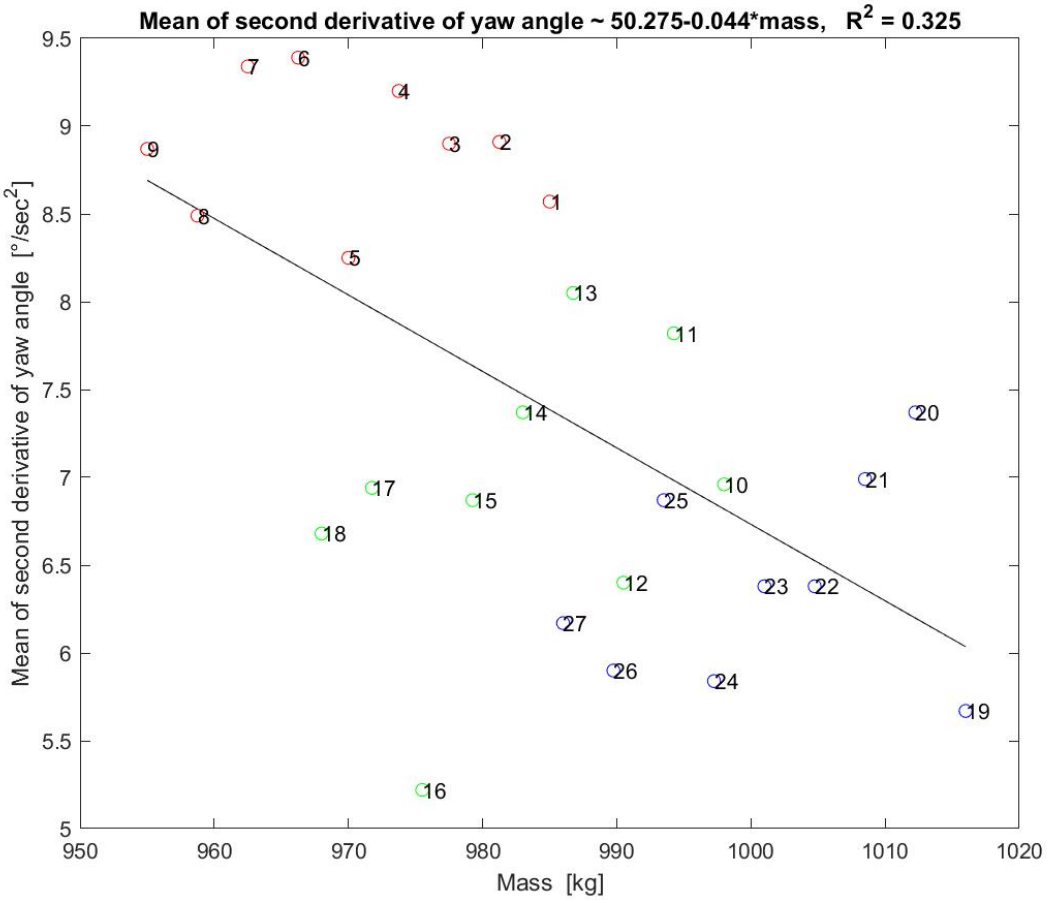

Figure 6.37: Mean of second derivative of yaw angle versus mass

The almost random distribution of the data points in Figure 6.37 (and Figure 6.38) shows that there is a low dependency of 32.5% between the mean of the second derivative of the yaw angle and the mass. A data range from 8.7 °/sec^2 to 6.0 °/sec^2 can be found. The mass of the aeroplane influences the spin behaviour much less than the CG position (see Figure 6.35).

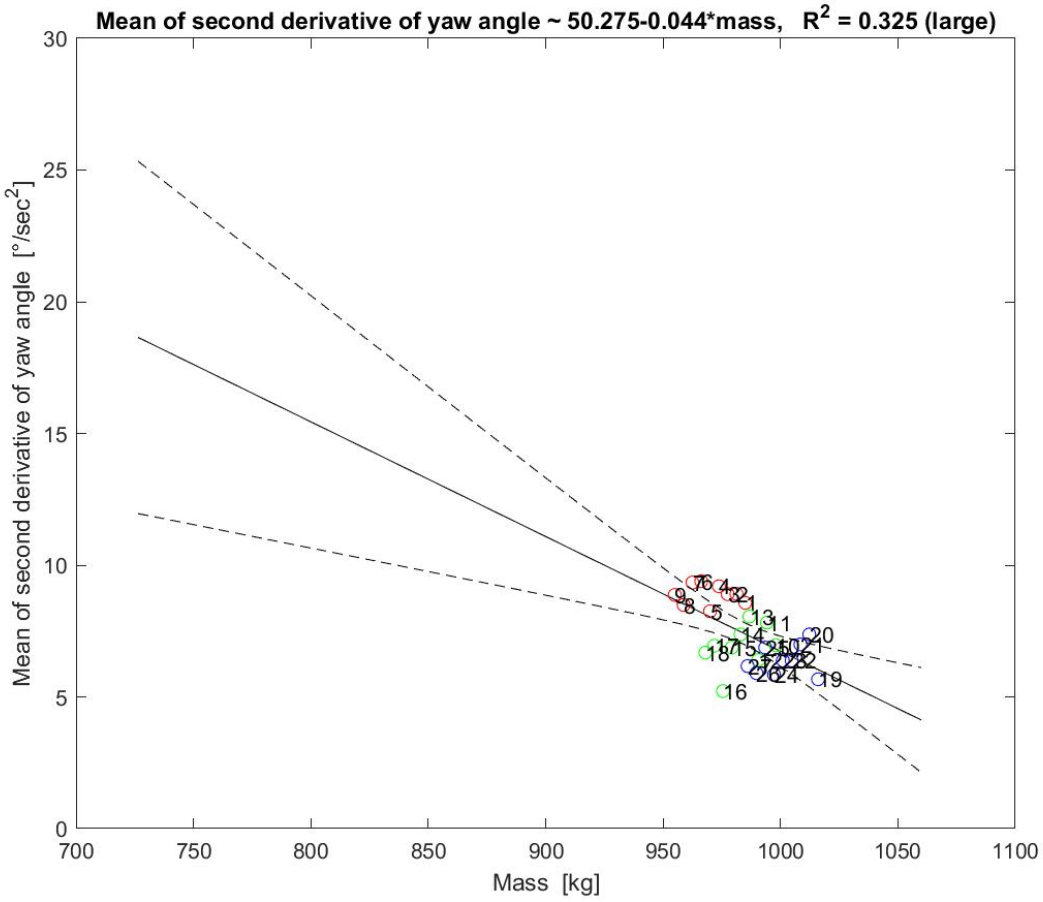

Figure 6.38: Mean of second derivative of yaw angle versus mass for the 27 spin runs for the maximum range of mass in the flight envelope. The dashed lines indicate the 95% confidence intervals

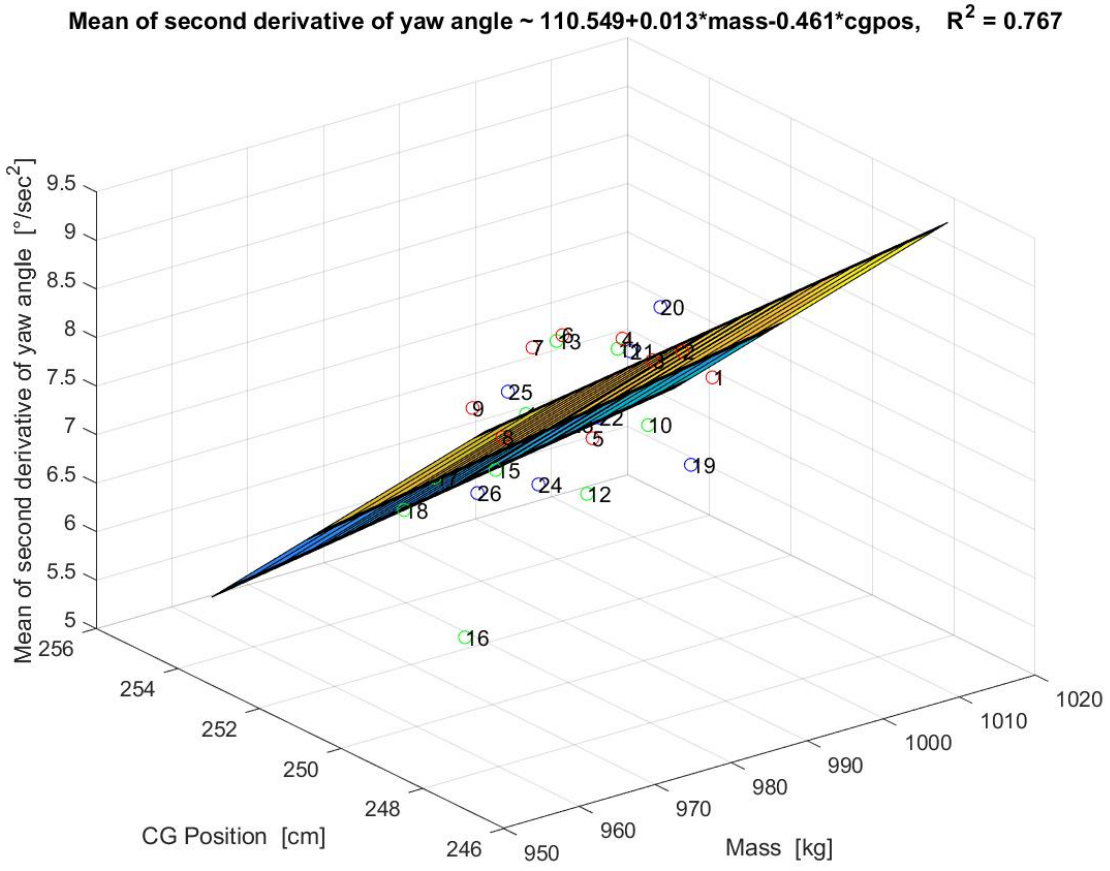

Figure 6.39: Mean of second derivative of yaw angle versus CG position and mass for all 27 spin runs

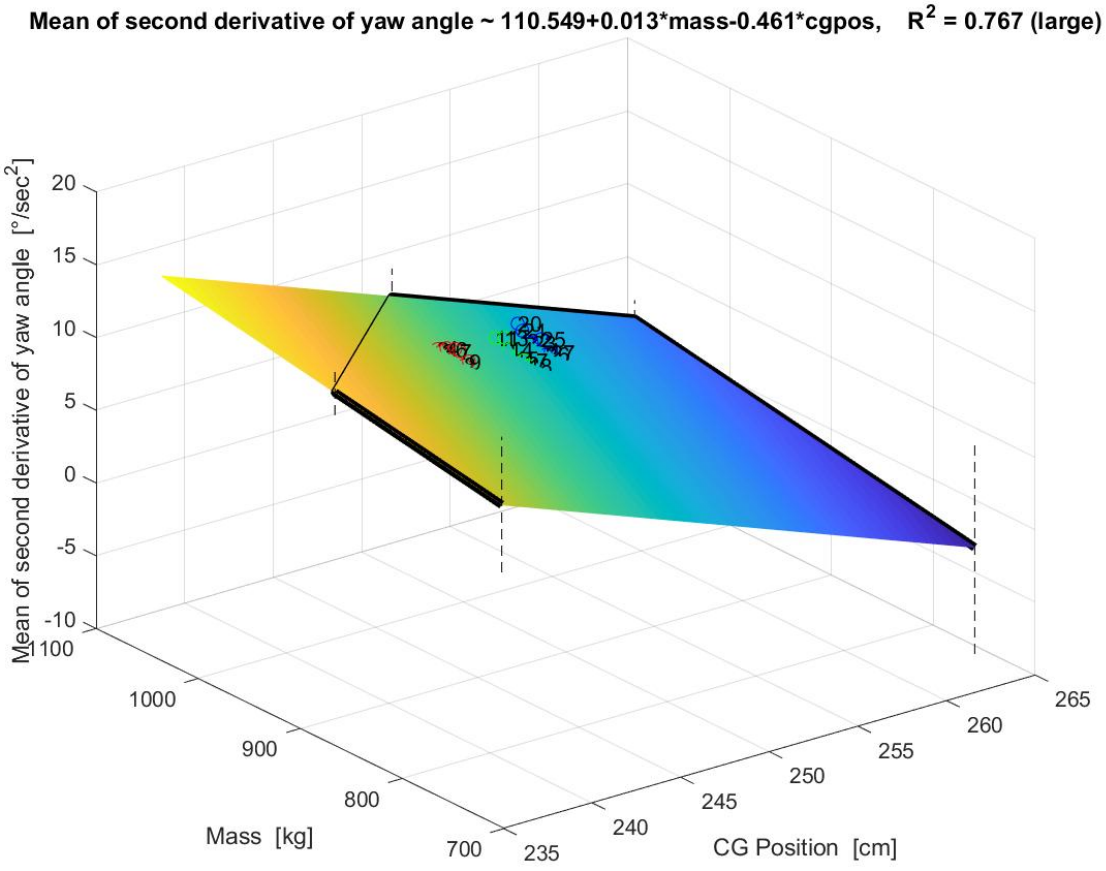

Figure 6.40: Mean of second derivative of yaw angle versus CG position and mass for the 27 spin runs for the maximum range of mass and CG in the flight envelope. The dashed lines indicate the 95% confidence intervals

The R^2 value of 76.7% indicates (Figure 6.39 and 6.40) that cross-coupling of both averaged parameters has a stronger influence on the mean second derivative of yaw angle than the corresponding maximum values shown in Figure 6.33 (R^2 = 51.5%).

As the dependency is higher than the CG alone case in Figure 6.35 (R^2 = 75.4%), this indicates that the mass has a slight positive influence with the CG on the mean of second derivative of yaw angle.

The above described spin behaviour of any aeroplane in the same category as the Fuji has not been found in the reviewed literature. The general pilot´s understanding is in contradiction to the above shown dependencies.

6.8 Observation 5: Maximum difference in angle of attack values between left and right wings leads to a maximum in roll rates (alpha_le_c – alpha_ri_c; ln_p)

The typical understanding within the pilot's community is that when CG position is more aft, spin entries and thus the aeroplane's departure behaviour are more violent and results in faster spins (higher roll rates) due to angle of attack differences between the wings (asymmetric stalling). Furthermore aeroplanes with an aft CG are more unstable and thus the spins are more unstable and hence faster.

During a spin to the left, the left wing (lower) produces much higher angle of attack values than the right wing (upper). The measured flight test data show that the maximum difference in angle of attack values between the wings produces a maximum in the roll rate of the aeroplane (with a certain phase shift). An example is shown in Figure 6.41. The upper line (black) shows the difference of the left and right Angle of Attack values. The lower line (blue) shows the roll rate of the aeroplane. Every maximum of the angle of attack values produces a maximum of the roll rate. The maximum of the roll rate develops with a characteristic phase shift. The (nearly) parallel red dashed lines illustrate that this phase shift is almost constant in a defined flight condition (in this case spin condition 9, spin number 3). For each of the 27 spin runs the averaged phase shift (or Angle of attack-roll rate shift) was determined and plotted in Figure 6.42. Note that the typical time to complete 1 spin is between 2.5 to 3.1 seconds (Table 6.3).

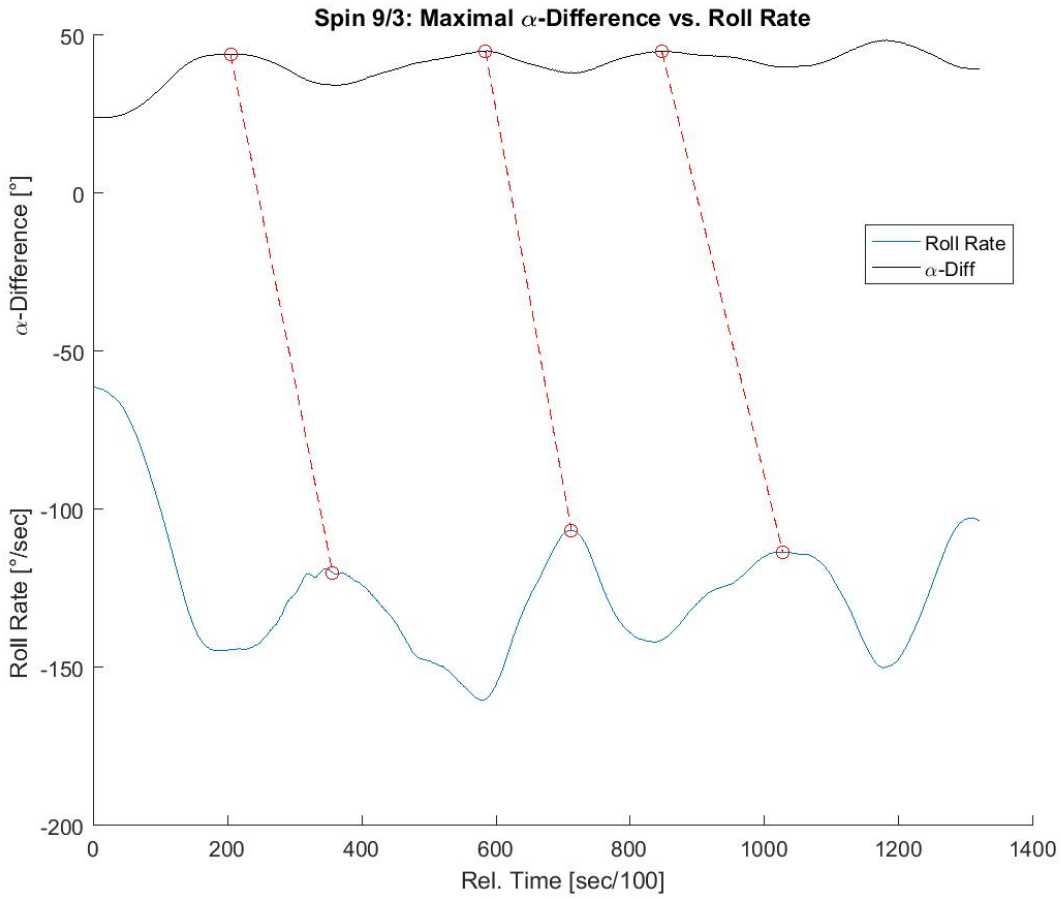

Figure 6.41: Maximum difference in angle of attack values produces a maximum in roll rate. (Case considered spin condition 9, spin number 3)

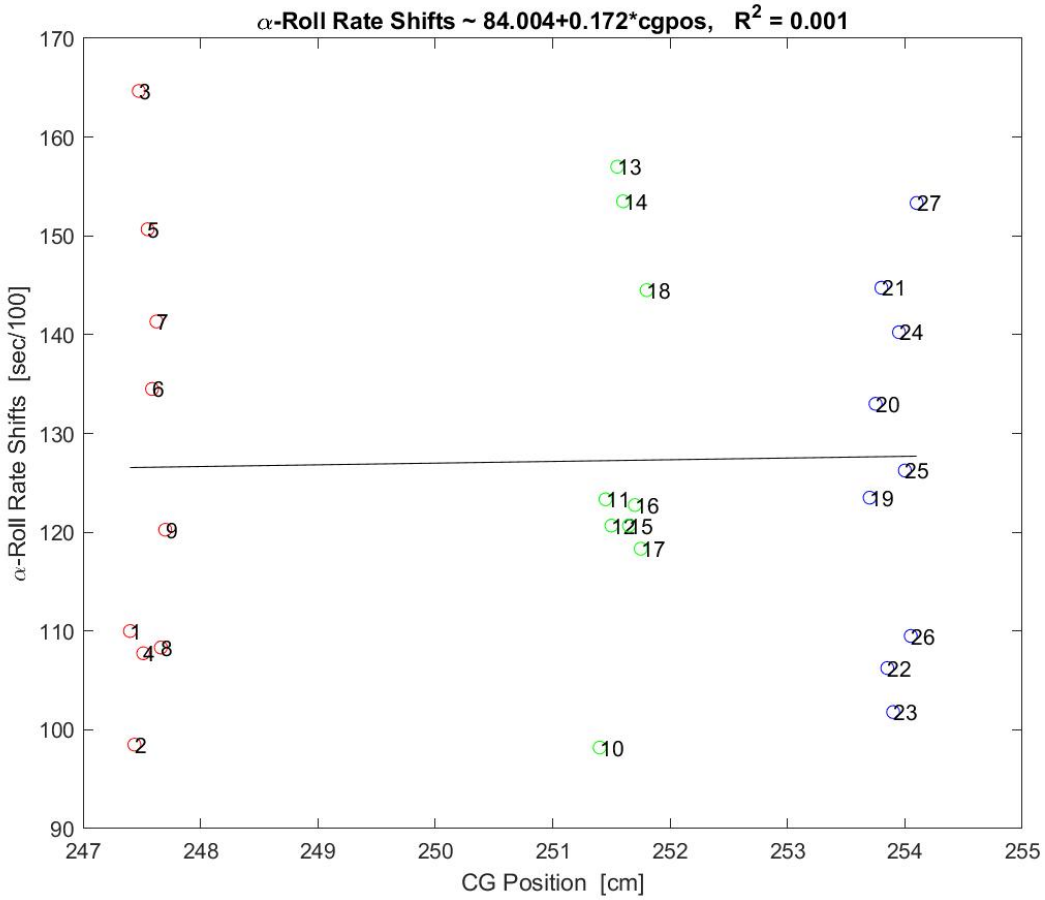

Figure 6.42: Angle of attack-roll rate shift versus CG Position for all 27 spin runs

The change of the CG position has a minimal effect (R^2 = 0.1%) on the Angle of attack-roll rate shift (Figure 6.42). The scattering of the data is due to other influences (e.g. fuel sloshing, atmospheric influences like gusts) but not the CG position change.

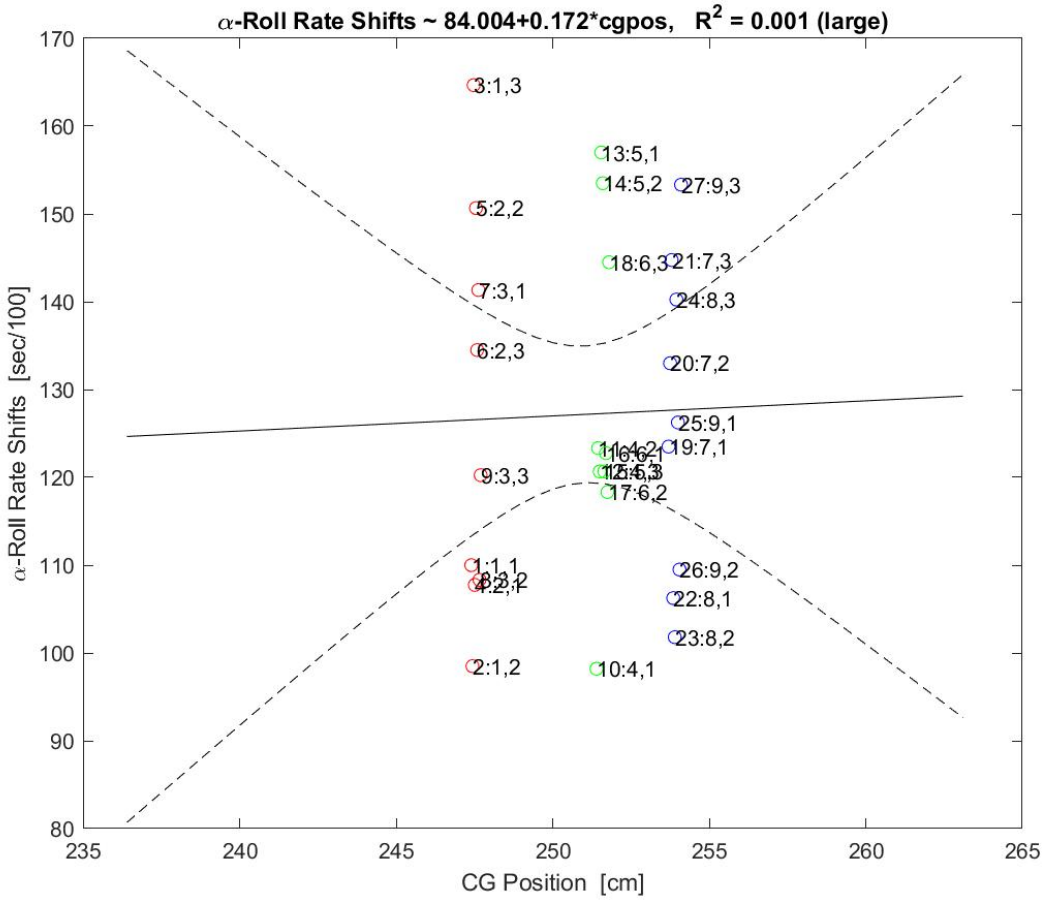

Figure 6.43: Angle of attack-roll rate shift versus CG Position for all 27 spin runs including the 95% confidence intervals

Although the statistical model predicts that there is little to no influence on the phase shift through R^2, the confidence interval model does not produce the same result. In Figure 6.42 the range of values for the phase shift is from 1 to 1.65 seconds for the 27 spin runs (CG from 247 to 255 cm). Figure 6.43 shows the extended CG range covering the flight envelope (235 to 265 cm). Because five out of nine middle-column values are close together, the statistical model predicts that the 95% confidence interval lines are closer for the middle column than for the left and right data columns. Although the phase shift has the same range of values as in Figure 6.42, outside of the flight envelope the model predicts that the phase shift values could vary significantly. A CG shift of 5 cm to the left of the flight envelope would produce a phase shift range of around 50 – 190 [sec/100]. That means that a pilot could experience between 1 and 5 roll rate changes during 1 spin turn. The 5 roll rate changes would be much more disorientating for the pilot and a higher stress is put on the aeroplane's structure.

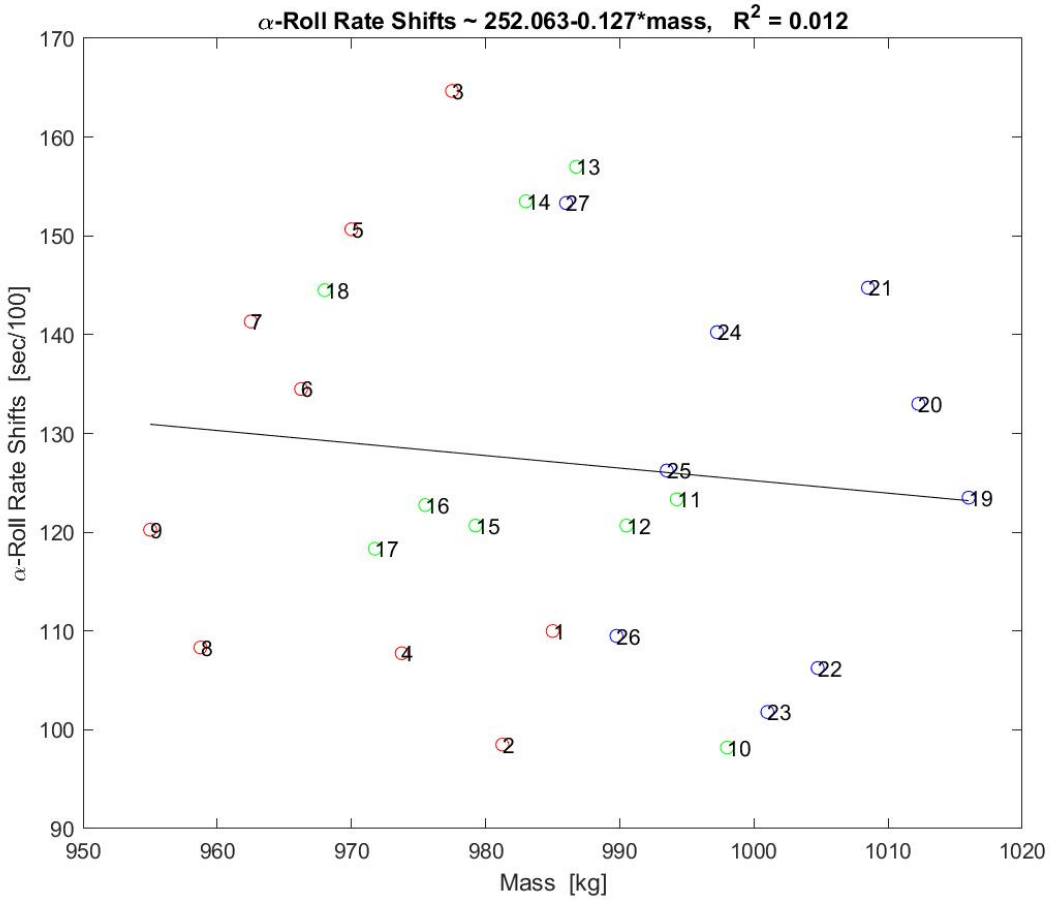

Figure 6.44: Angle of attack-roll rate shift versus mass for all 27 spin runs

Figure 6.44 indicates that mass has also little to no influence on the phase shift (1.2% dependency). The scattering of the data is due to influences other than mass. However, unlike the CG case in Figure 6.43 the extended mass range shows that there could be a high probability in the number of roll rate changes during 1 spin turn within the flight envelope (Figure 6.45).

The statistical model indicates that in the case of Angle of attack-roll rate shift that mass has more influence than CG.

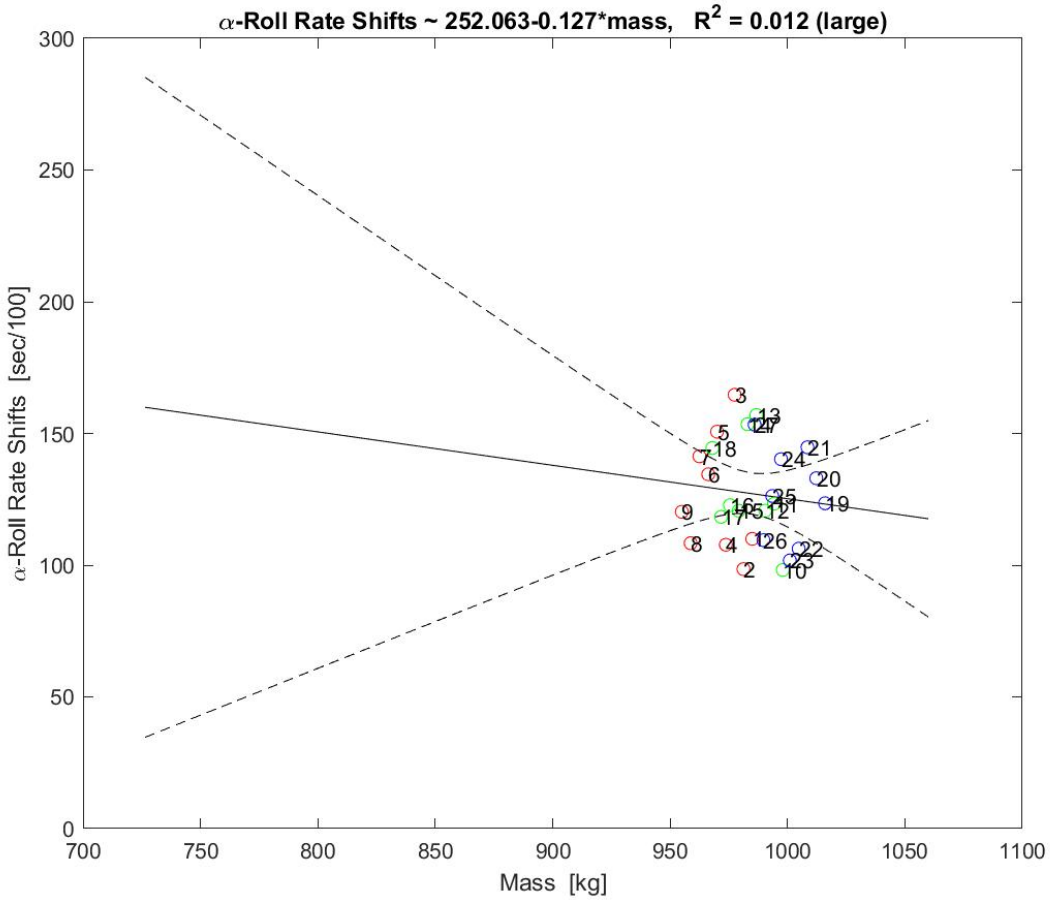

Figure 6.45: Angle of attack-roll rate shift versus mass for all 27 spin runs including the 95% confidence intervals

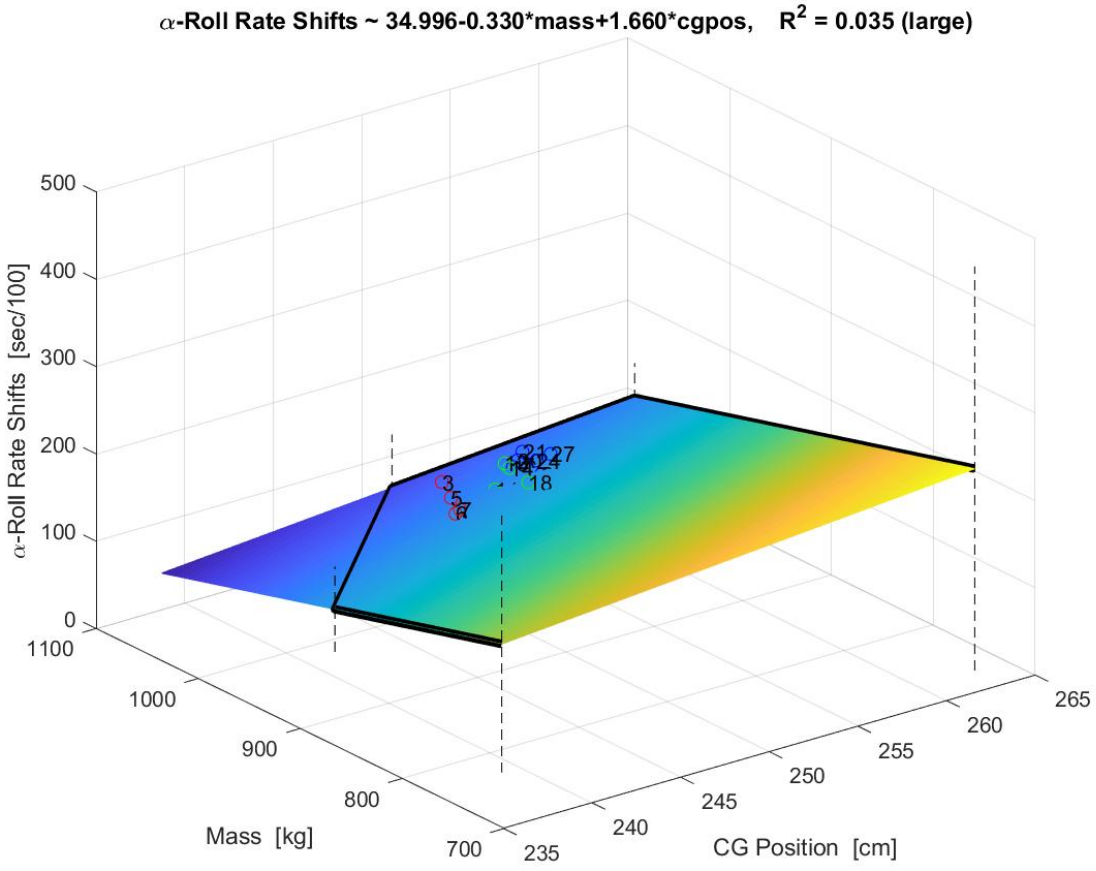

Figure 6.46: Angle of attack-roll rate shift versus CG position and mass for the 27 spin runs for the maximum range of mass and CG in the flight envelope. The dashed lines indicate the 95% confidence intervals

There is little to no cross-coupling of mass and CG position on the phase shift.

Within the data set of the 27 spin cases no dependency on mass or CG position has been shown. However, across the flight envelope the statistical model indicates that mass has an effect, the further one goes to the limits of the flight envelope.

Within the reviewed literature no corresponding statements can be found.

6.9 Observation 6: Rate of roll (ln_p) changes with CG Position and aeroplane's mass

The usual attitude of an aircraft in normal flight is straight and level. However, when an aeroplane enters a spin it banks in the direction of the dropped wing acquiring a non-zero roll rate. This section investigates whether the roll rate changes with CG position and / or the aeroplane's mass. The scattering of the data are based on pilot control inputs, sloshing fuel, different fuel levels and atmospheric influences like gusts during the tests.

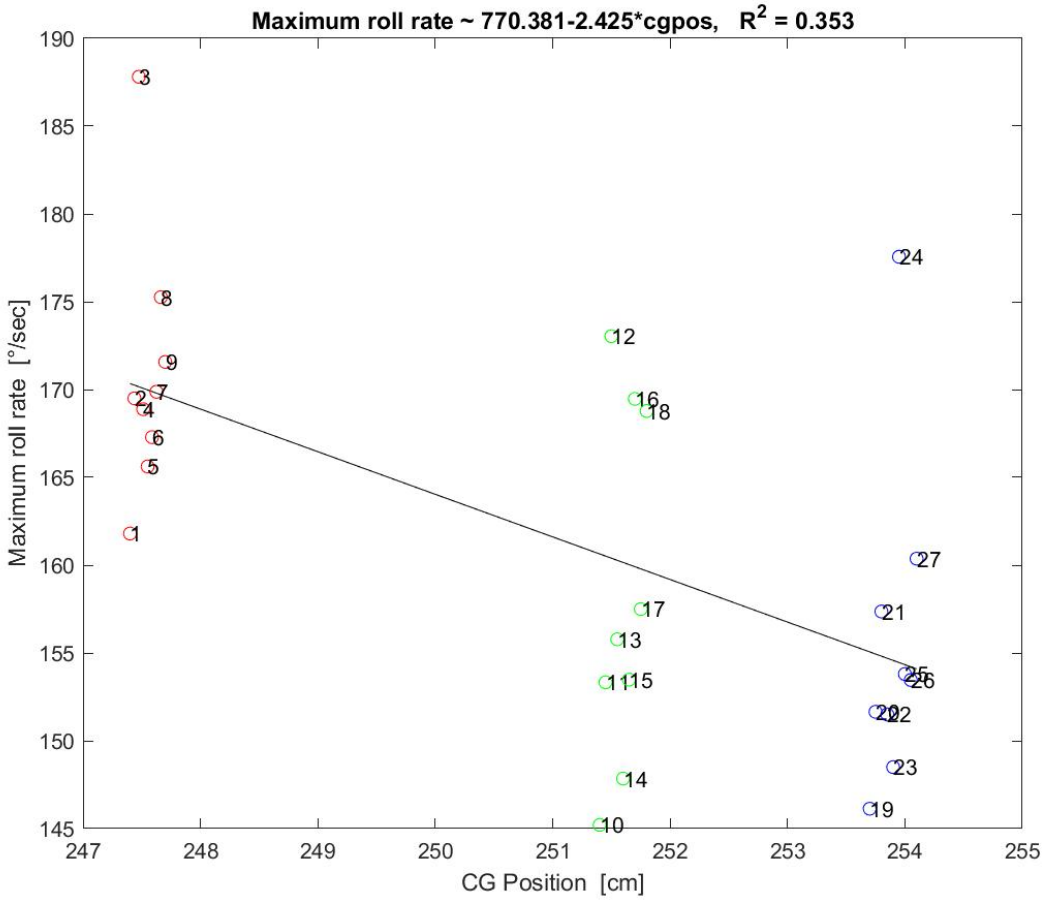

Figure 6.47: Maximum roll rate versus CG position for all 27 spin runs

Figure 6.47 shows that the roll rate increases by shifting the CG position to the front of the aeroplane. This would be increasing uncomfortable for the pilot, who could be more susceptible to disorientation. One interesting case is that seen at the top left hand corner where the roll rate is more than 185° / second. This means that after 1 second, the pilot and aircraft are upside down. A pilot trained for spinning would roll through another 180° of bank angle and recover from the spin. An untrained pilot might try to hold the original altitude and by that, pull the aeroplane into an almost vertical dive and thus into high speeds, which could than lead to structural over-stressing.

The corresponding regression line has a negative slope and the dependency of the roll rate on the CG position is 35.3 % which is a moderate sensitivity. This is similar to that found for the mass change case in Figure 6.49 where the dependency is 36.5%.

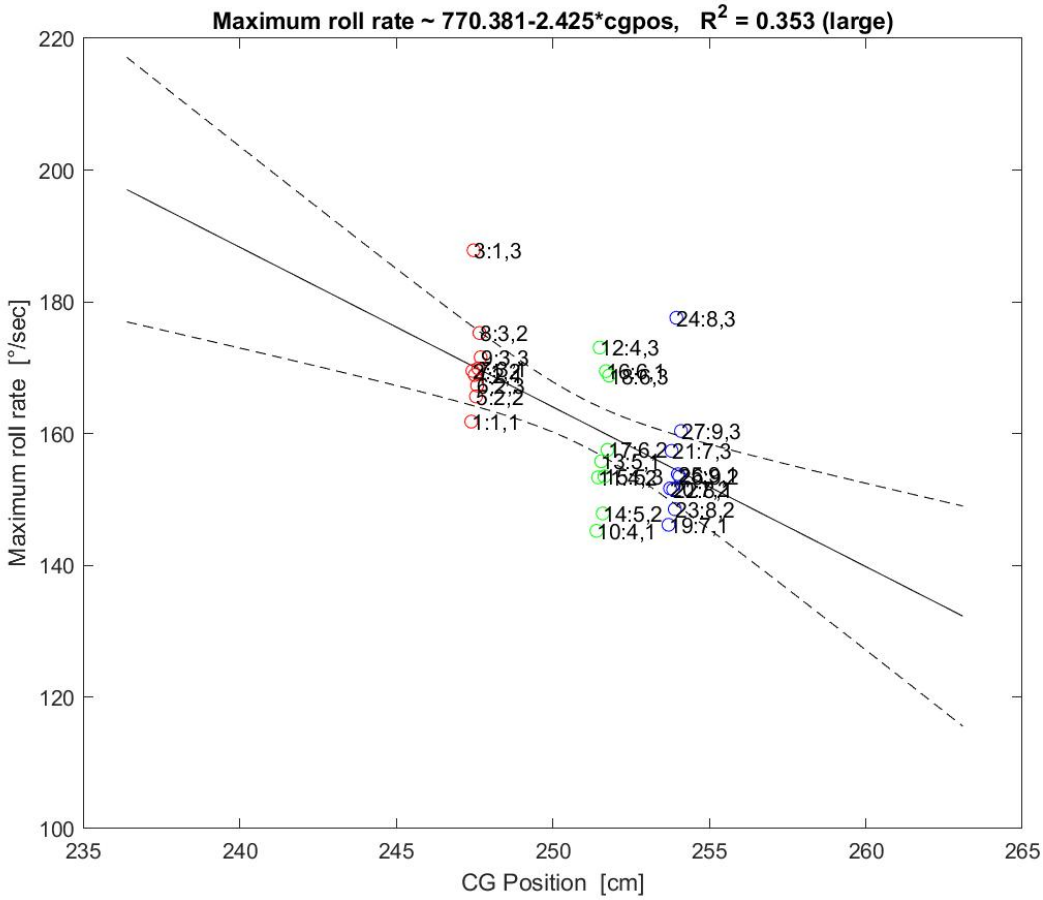

Figure 6.48: Maximum roll rate versus GC position for all 27 spin runs including the 95% confidence intervals

The trends in Figures 6.48 and 6.50 (i.e. the entire flight envelope range) are the same as seen in Figures 6.47 and 6.49. However, the uncertainty in the maximum roll rate value increases towards the outer limits of the flight envelope.

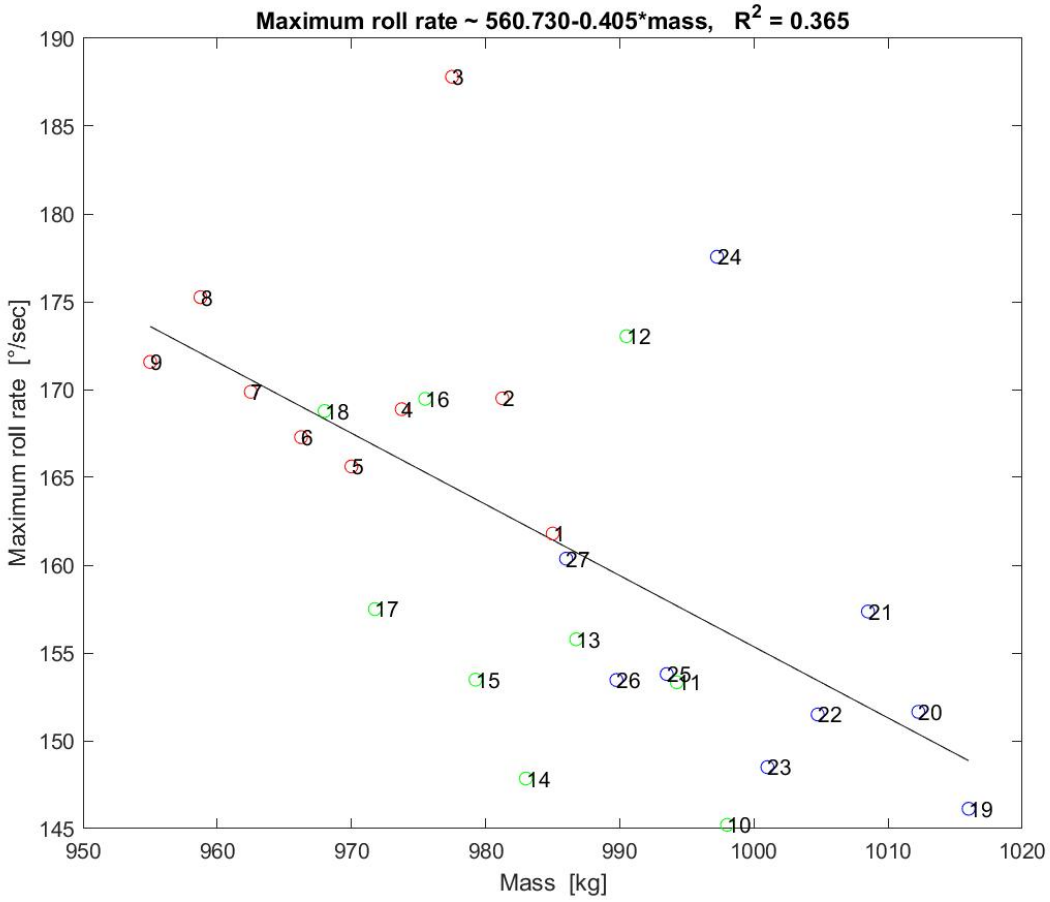

Figure 6.49: Maximum roll rate versus mass for all 27 spin runs

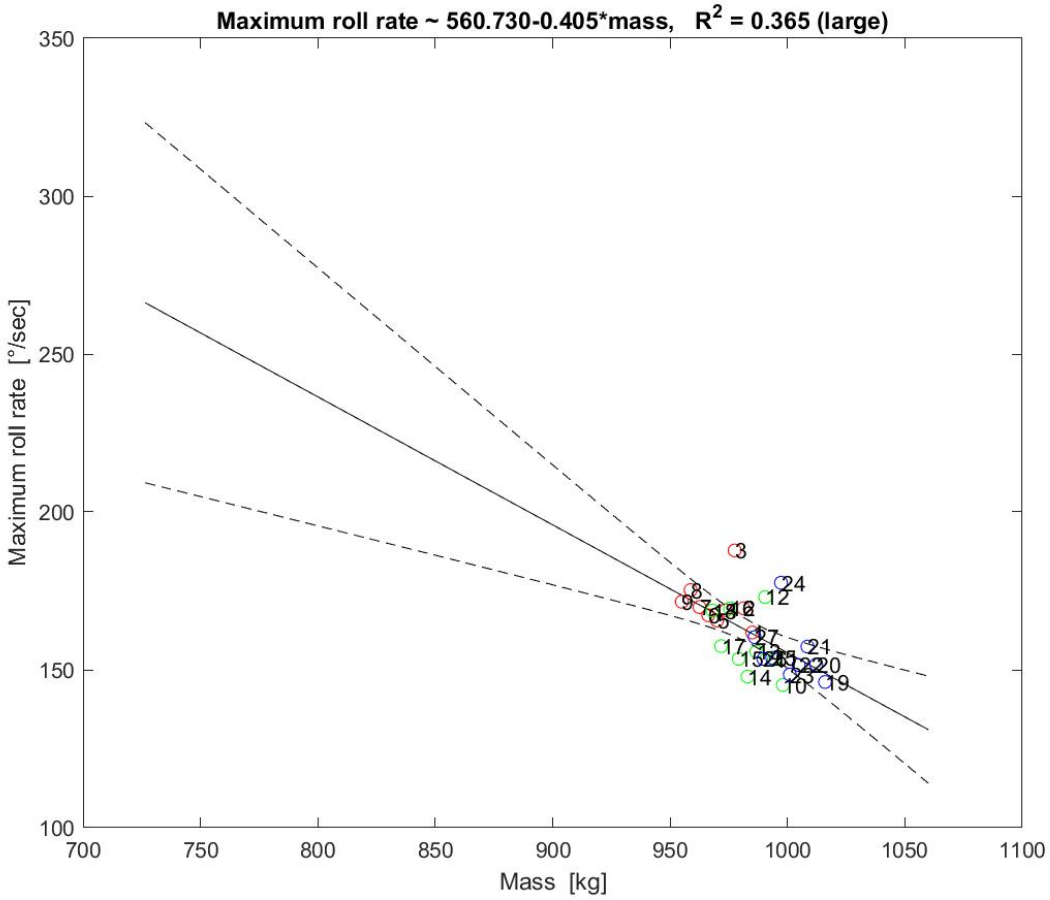

Figure 6.50: Maximum roll rate versus mass for all 27 spin runs including the 95% confidence intervals

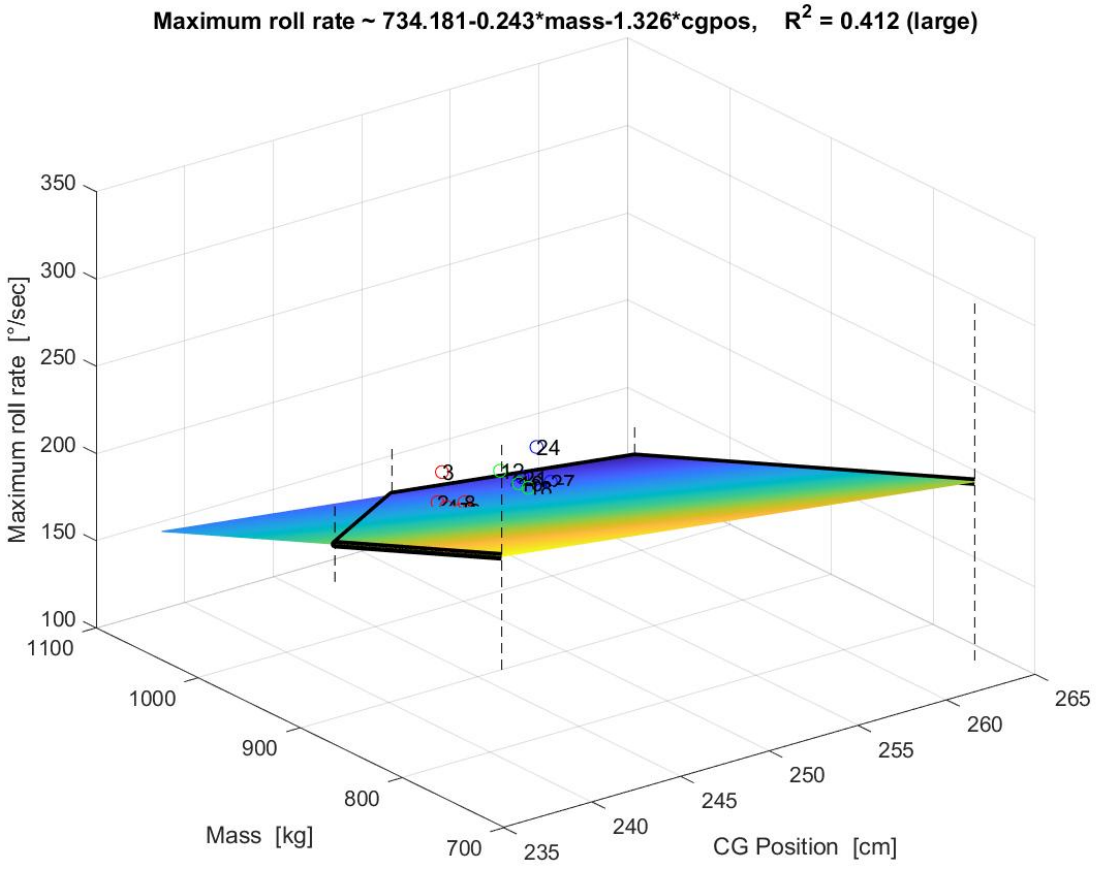

Figure 6.51: Maximum roll rate versus CG position and mass for the 27 spin runs for the maximum range of mass and CG in the flight envelope. The dashed lines indicate the 95% confidence intervals

Even the cross-coupling of both parameter changes can be seen as moderate as the dependency of the roll rate change is with 41.2%, still of the same order as both individual parameter influences shown above. In this case the roll rate values changes from around 149°/s to 174°/s which is a difference of approximately 14%.

In the reviewed literature no comparable statement has been made concerning the roll rate change due to mass and / or CG position changes and its dependencies.

The statistical model indicates that the observation is likely to be satisfied. A CG shift of only 7 cm along the aeroplane's longitudinal axis produces a change in the roll rate by 25° / second. This means that over the course of 1 turn an aeroplane could acquire 75° extra roll angle and therefore over the course of a 6-turn-spin it could acquire an additional 1 ¼ complete rotation about the roll axis.

6.10 Observation 7: Total Angular Velocity Ω changes with CG position and mass

Because spin is a rotational manoeuvre, total angular velocity Ω, is a key parameter of the motion. In this section an investigation is made as to the influence of changes in CG positions and mass on Ω.

$$\Omega = (p^2 + q^2 + r^2)^{1/2}$$

Where p, q and r are the roll, pitch and yaw rates respectively.

Due to the dependency of Ω on p and r, the findings in sections 6.6 and 6.7 for yaw rate and sections 6.8 and 6.9 for roll rate are relevant for this section. The roll rate range change is in the same range as the Ω change which can be found in Figure 6.52.

Figure 6.52 shows also that the total angular velocity changes with the shift of the CG Position. There is little scatter in the measured data and this is found on small areas of the plot.

R^2 gives a nearly perfect match of 94.6% between the linear regression model results and the real measured data. The negative slope of the regression line shows that a forward located CG position will lead to a faster spin and vice versa.

The scatter in the average Ω-values is less than that seen in the maximum values of the yaw and roll rates (sections 6.6 and 6.9).

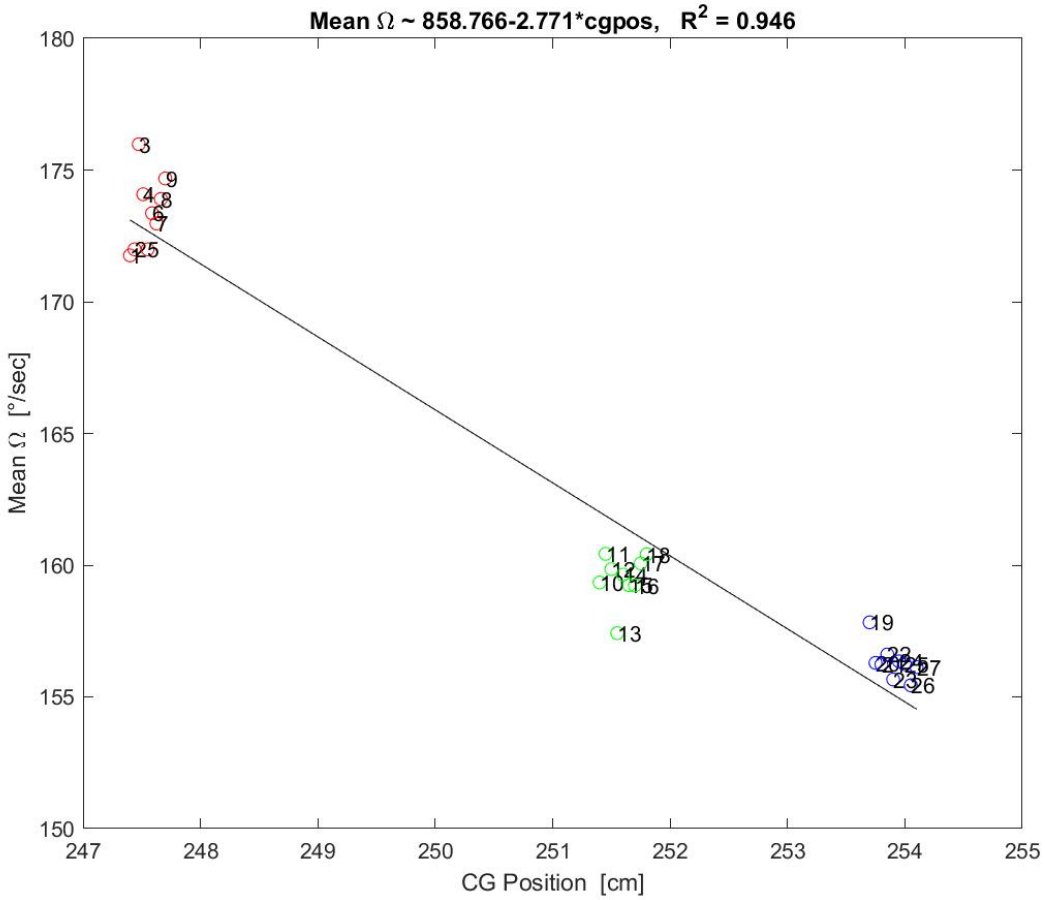

Figure 6.52: Total angular velocity versus CG Position for all 27 spin runs

The total angular velocity changes strongly when changing the CG position.

When the CG of an aircraft is moved to the front the aircraft has a higher static margin and it is more stable in flight, also the spin rate increases. A higher spin rate makes it more likely for the pilot to suffer disorientation.

As the average duration of a spin is around 2.5 to 3.1 seconds (see Table 6.3) a difference in Ω of around 20° / second (see Figure 6.52) due to a change of the CG position of 7 cm can lead to around 60° difference in Ω per turn. Therefore for a 6-turn-spin this leads to a difference of 360°. In other words the aircraft spinning at a point on the left hand side of the diagram will complete one extra rotation compared to it spinning at a point on the right hand side of the diagram. If the full range of CG across the flight envelope is taken into account (see Figure 6.53) the difference between the left and right hand boundaries is now almost 3 extra rotations.

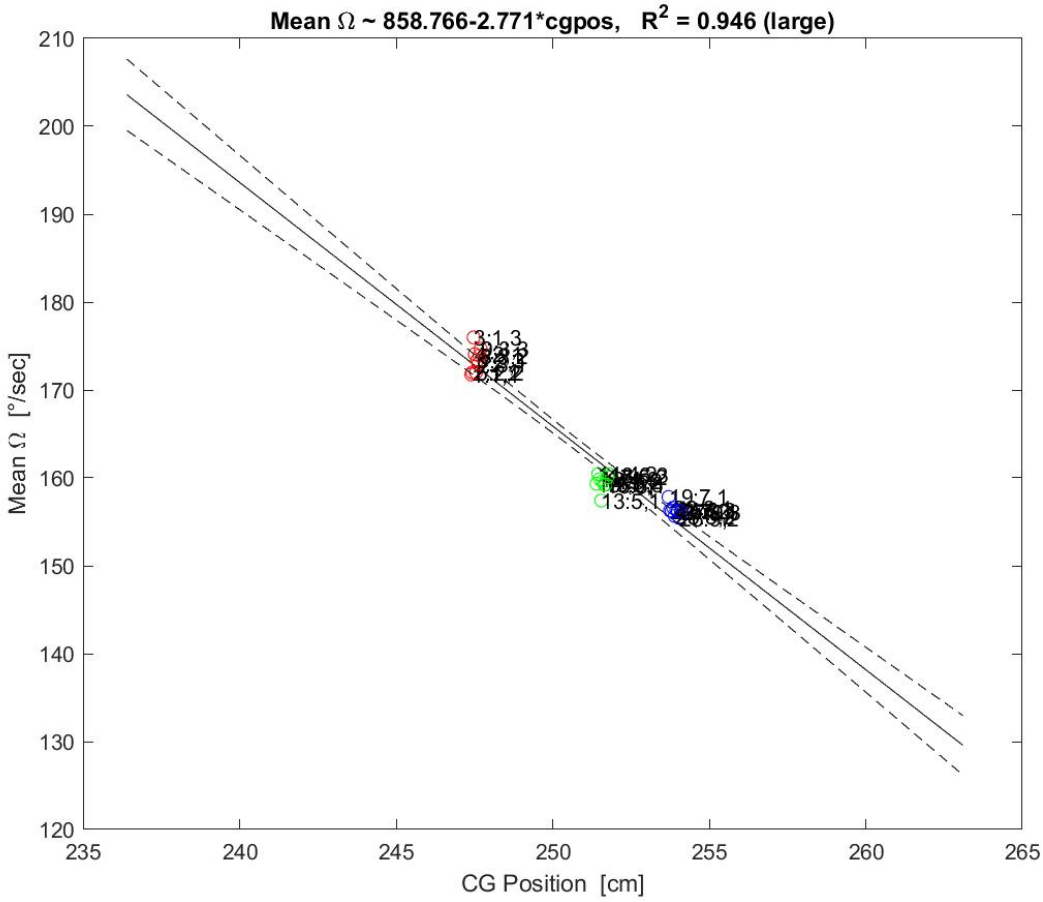

Figure 6.53: Mean of total angular velocity versus CG position for all 27 spin runs including the 95% confidence intervals

Although the pilot could become disorientated since the pilot's seat is located in close proximity of the CG, the rotational accelerations on the body are considerably lower than that of the aeroplane's wing tips.

Ambros & Seidler (2013) state that flat spins lead to a higher value of the total angular velocity. In a flat spin the aircraft is tail heavy i.e. the CG position is towards the tail. Figure 6.52 and 6.53 show that when the CG position is towards the tail, Ω has a lower value which is opposite to Ambros & Seidler (2013)'s findings.

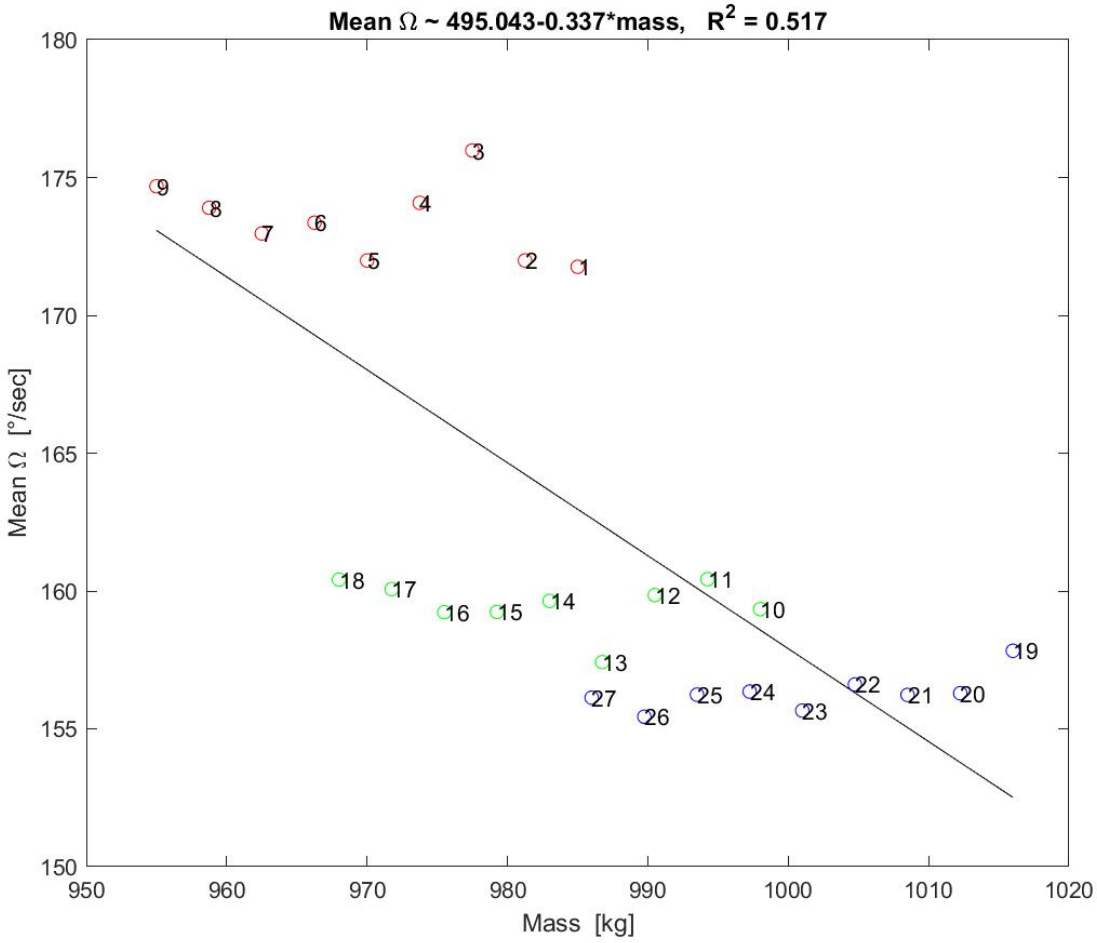

Figure 6.54: Total angular velocity versus mass of the aeroplane for all 27 spin runs

Statistically the influence of the mass on the total angular velocity is much lower than the CG influence because the value of R^2 is 51.7% which can be taken as a moderate dependency. The measured data are much more scattered than in the case above (see Figure 6.52). However, over the mass range presented in Figure 6.54 the change in Ω is 20°/ second which is the same as found as the effect of CG change.

The pilot will become more disorientated with higher spin rates which in the case of Figures 6.54 and 6.55 will occur in lighter aircraft. For an aircraft on a long sortie where the mass of the aircraft will be reduced due to fuel consumption, a pilot entering a spin is more likely to become disorientated towards the end of the sortie compared to entering a spin at a start of the sortie. This is especially true for the approach phase of a flight because the approach speeds are closer to the stalling speed and a stall and corresponding spin can be encountered more easily.

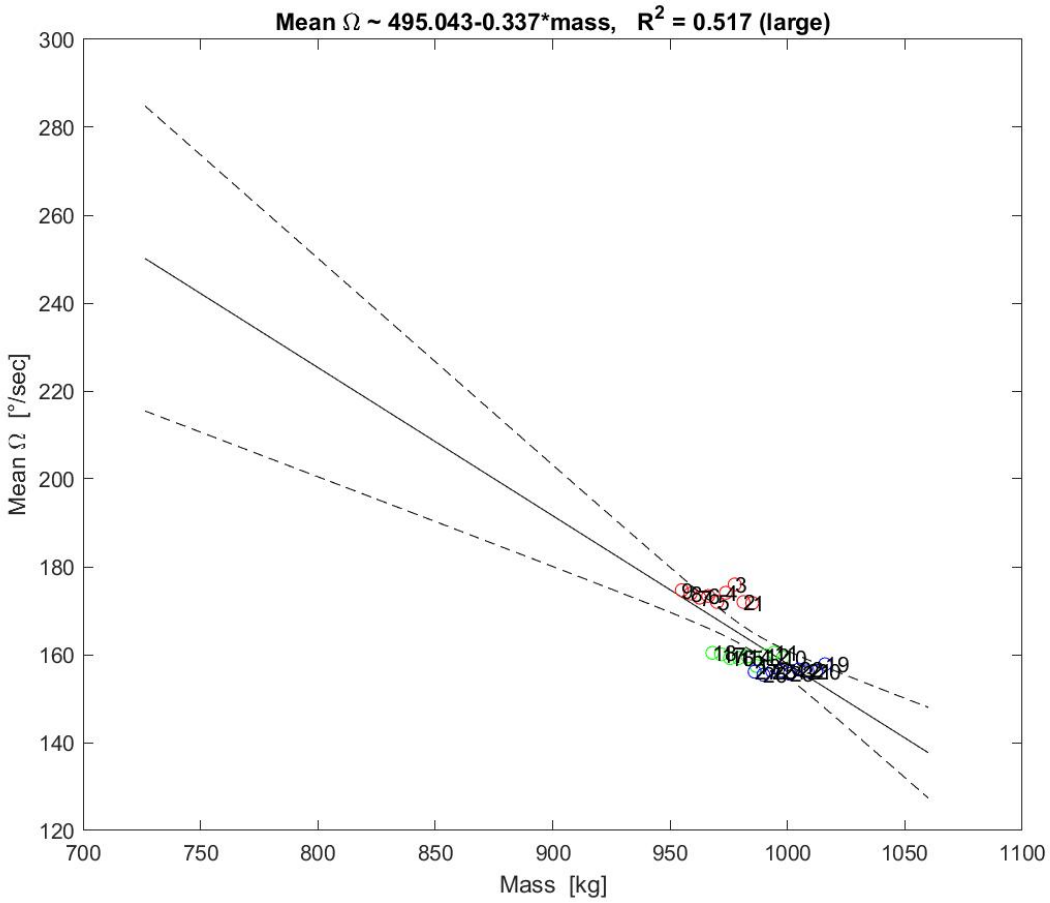

Figure 6.55: Mean of total angular velocity versus mass for all 27 spin runs including the 95% confidence intervals

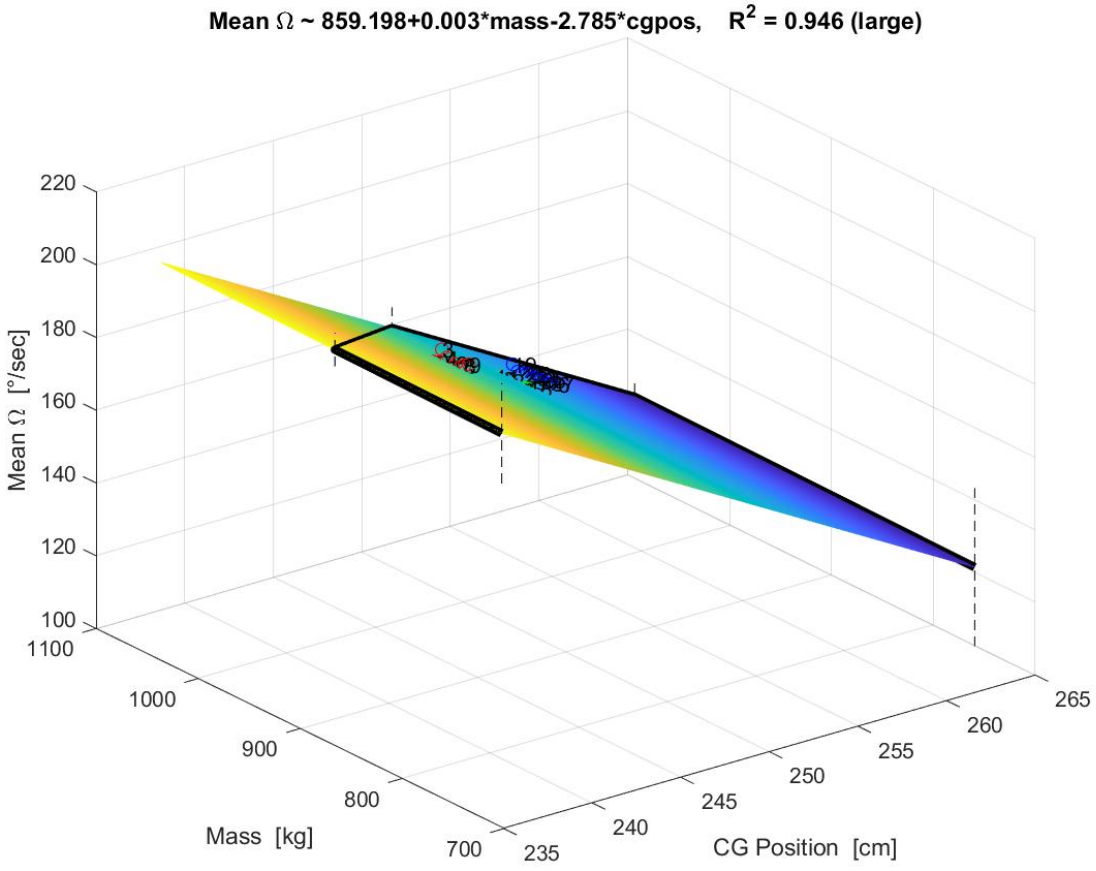

Figure 6.56: Mean of total angular velocity versus CG position and mass for the 27 spin runs for the maximum range of mass and CG in the flight envelope. The dashed lines indicate the 95% confidence intervals

An examination of the corresponding cross-coupling of both parameters shows that the total angular velocity versus CG Position behaviour does not change which leads to exactly the same R^2 value.

The general pilot's opinion of spinning is that as the CG moves towards the tail, Ω increases. This perception is the opposite of what the flight tests above prove.

The only reference found which supports the findings in this section is from Stough, et al. (1987b) who stated 'As the center of gravity was moved aft, the turn rate (Ω) of the fully developed spin decreased'. This statement was not proven since no measured data was provided in that paper.

6.11 Observation 8: Recovery time becomes shorter with CG moving backwards

During this part of the data analysis the spin recovery phase is investigated with reference to the CG position and aeroplane's mass. The variation in the recovery times and thus the corresponding turn angles until the aeroplane stops the spin motion, will be determined and interpreted.

The spin recovery starts when the rudder deflection is reversed from a maximum deflection to the left (positive values) to a maximum deflection to the right (negative values, see data for zeta_ca in Figure 6.57) and when the elevator deflection will be neutralized (i.e. set to around 0° deflection angle, see data for eta_ca also in Figure 6.57). As a result, the turn direction is reversed – in the present case from left to right.

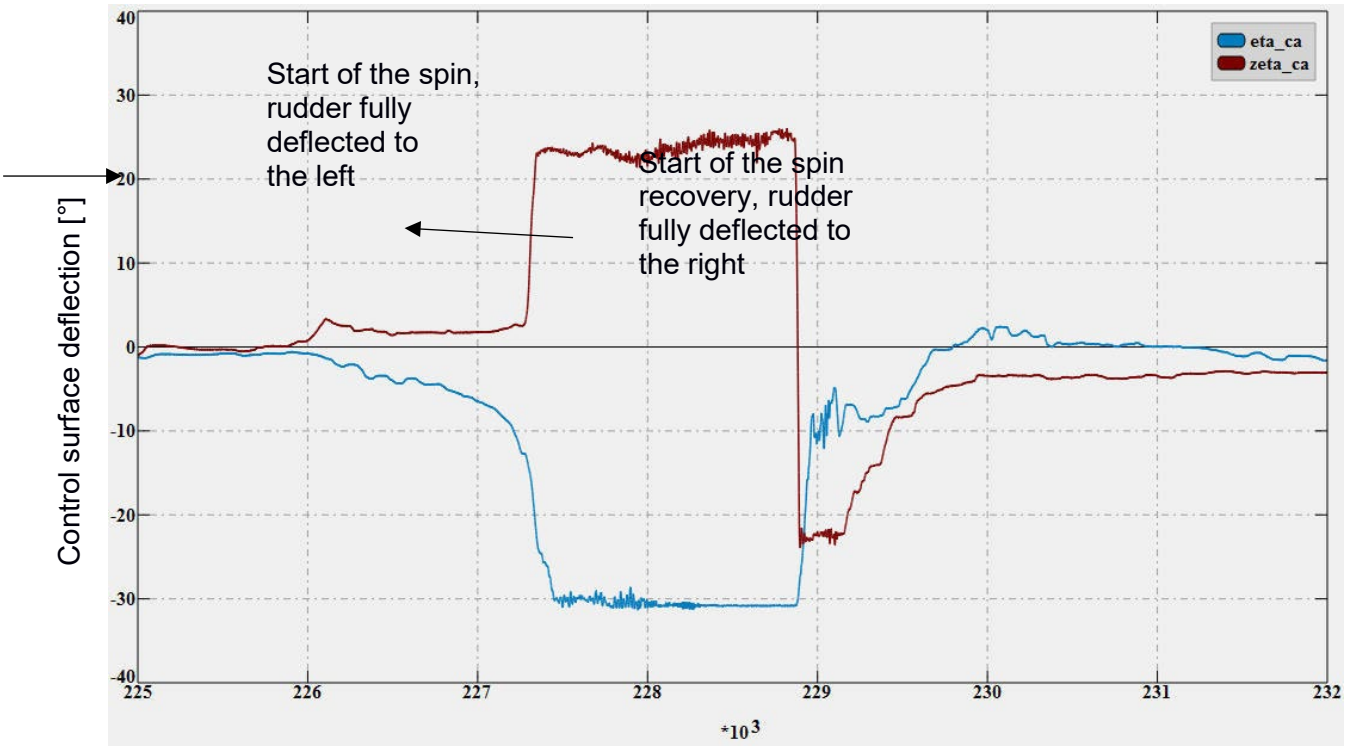

Fig. 6.57: Control surface deflection angles for rudder and elevator for a typical spin run, (shown data: spin run 2nd condition, 4th spin)

All 27 recovery turns and thus the corresponding turn angles from the initiation to the end of the recovery has been investigated on the basis of the aeroplane headings (In_Psi) and the corresponding times.

Figure 6.58 shows an example of a spin recovery time and turn angle investigation. The required time is the time between when the rudder deflection is fully reversed (blue line, point B) and the time at which the turn direction is reversed (red line, point C). The turn angle is also the aircraft heading change.

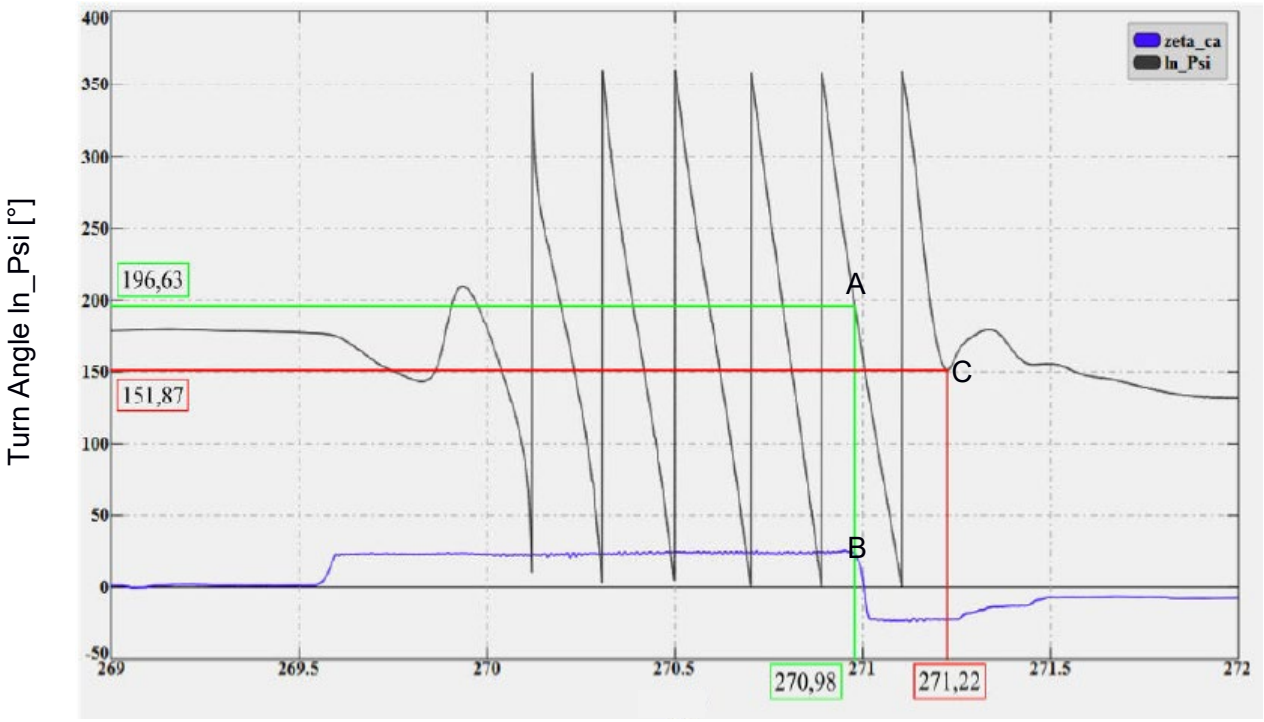

Figure 6.58: Turn Angle (ln_Psi) and rudder deflection (zeta_ca) time history together with examples for required time (points B to C) and turn angle during the recovery of 1st spin, 5th condition

Consider point A: the declining values for the turn angle show that the aeroplane spins to the left. The values in the green and red squares show the measured values for the recovery time (x-axis) and recovery or turn angle (y-axis). In the example in Figure 6.58 the spin recovery started at a time of 270.98 centiseconds ≡ 2709.8 seconds after the measurement system was started with a heading of 197° and it ended at a time of 271.22 centiseconds ≡ 2712.2 seconds, with a heading of 152°. Thus the recovery took 2.4 seconds with a corresponding angle of 405° (= 1.24 turns).

Flight No.	Average CG position (Tables 4.7 to 4.9)	Turn angles		
		Angle [°]	No. of full turns [-]	Time [sec]
1	forward (247 cm)	460.24	1.28	3.09
2	mid (251 cm)	425.58	1.18	2.87
3	aft (254 cm)	376.40	1.05	2.52

Table 6.3: Mean values of the spin recovery time and angles of all 3 flights (27 spin runs)

In Table 6.3 the mean values of the three flights are presented. In each flight 9 spins have been conducted. The CG ranges are 247.4 to 247.7 (forward CG position), 251.4 to 251.8 (middle CG position), 253.7 to 254.1 (aft CG position). The results show that by shifting the CG by approximately 7 cm to the back of the aeroplane, the recovery time and the corresponding recovery angle are both reduced by 18%. This proves observation 8. (Note that the same conclusions are obtained if the individual spin runs are considered instead of the averaged)

Kredel (1998) says (translated from German) that flat spins, with an aft CG position, are very stable and thus dangerous. In the author's experience the more stable the aircraft's behaviour is, in the recovery phase, the longer it takes to complete the recovery phase.

In addition to that source (Bowman, 1971) states that 'Low values of tail-damping power factor and high horizontal-tail positions (for partial-length rudders) were adverse to recoveries and had about the same effect as moving the center of gravity rearward.' which is also in contradiction to the measured values.

The same source (Bowman, 1971) continues with 'In several documented spin test programs, good and rapid recoveries were obtained by rudder reversal and down elevator from spins that were steep and typical of median or forward center-of-gravity positions.' which is also a statement which cannot be generalized and thus used for certification test flights, design advises or flight training.

6.12 Observation 9: The spin behaviour of the Fuji FA 200 – 160 can be generalised for single-engine low-wing aeroplanes

The investigation into this observation is divided into two parts. In the first part the behaviour of the Fuji has been considered. In the second part of the investigation other aircraft in the same category are studied. Those results are presented in Chapter 7.

In Figure 6.59 the averaged pitch values of every spin condition (1 – 9) are very similar. The three red lines represent conditions 1 – 3, the three green lines conditions 4 – 6 and the blue lines conditions 7 – 9.

Initially all 9 runs are in sequence. However, as time progresses there are increasing differences between the values of conditions 1 – 3 (red lines) and the blue and green lines, indicating a shorter period of oscillation.

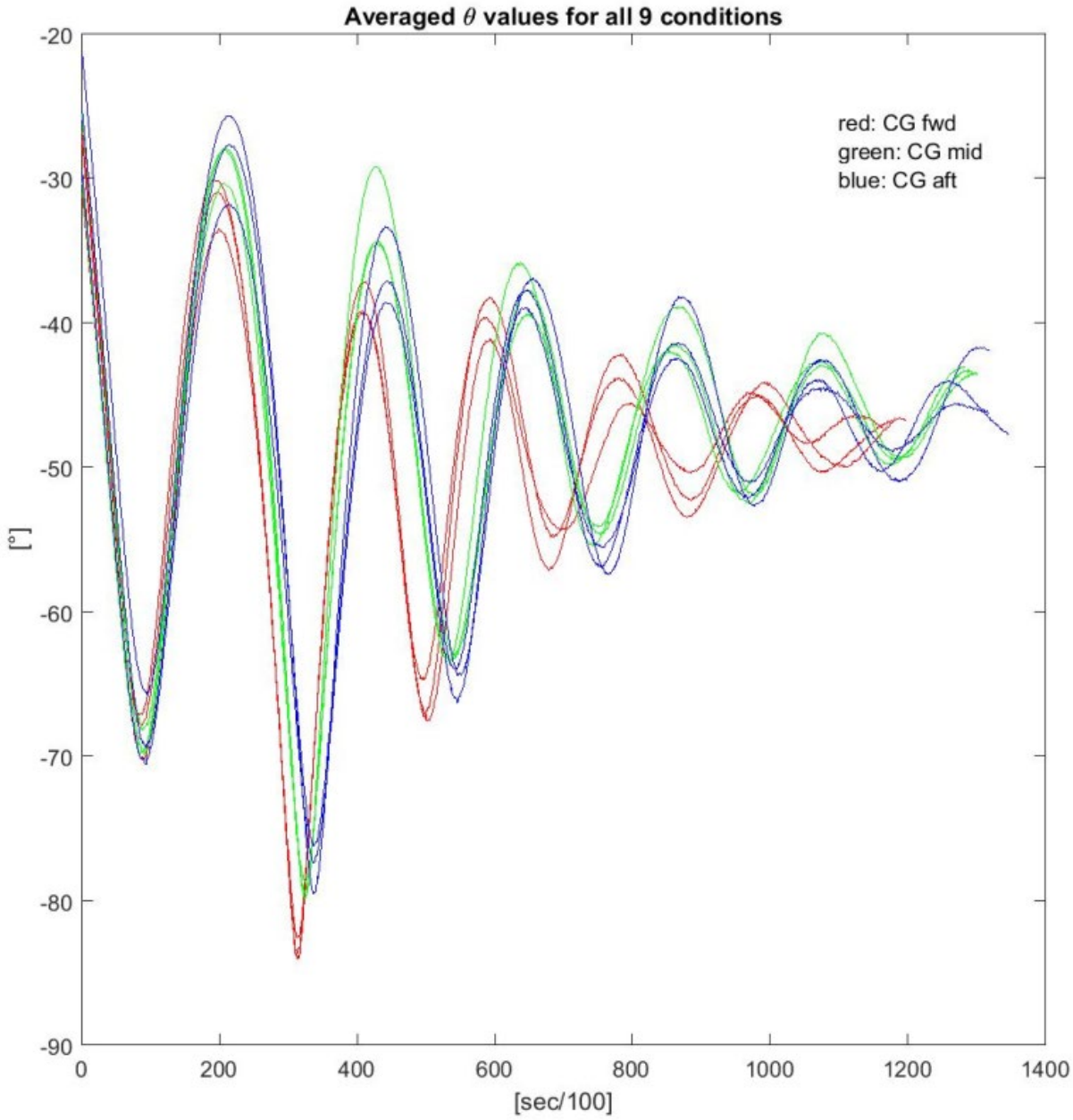

Figure 6.59: Averaged pitch values for every spin condition (Every line represents the averaged pitch values of one condition (i.e. 3 spin runs))

This similarity can be shown very clearly with a spectral analysis for the nine conditions

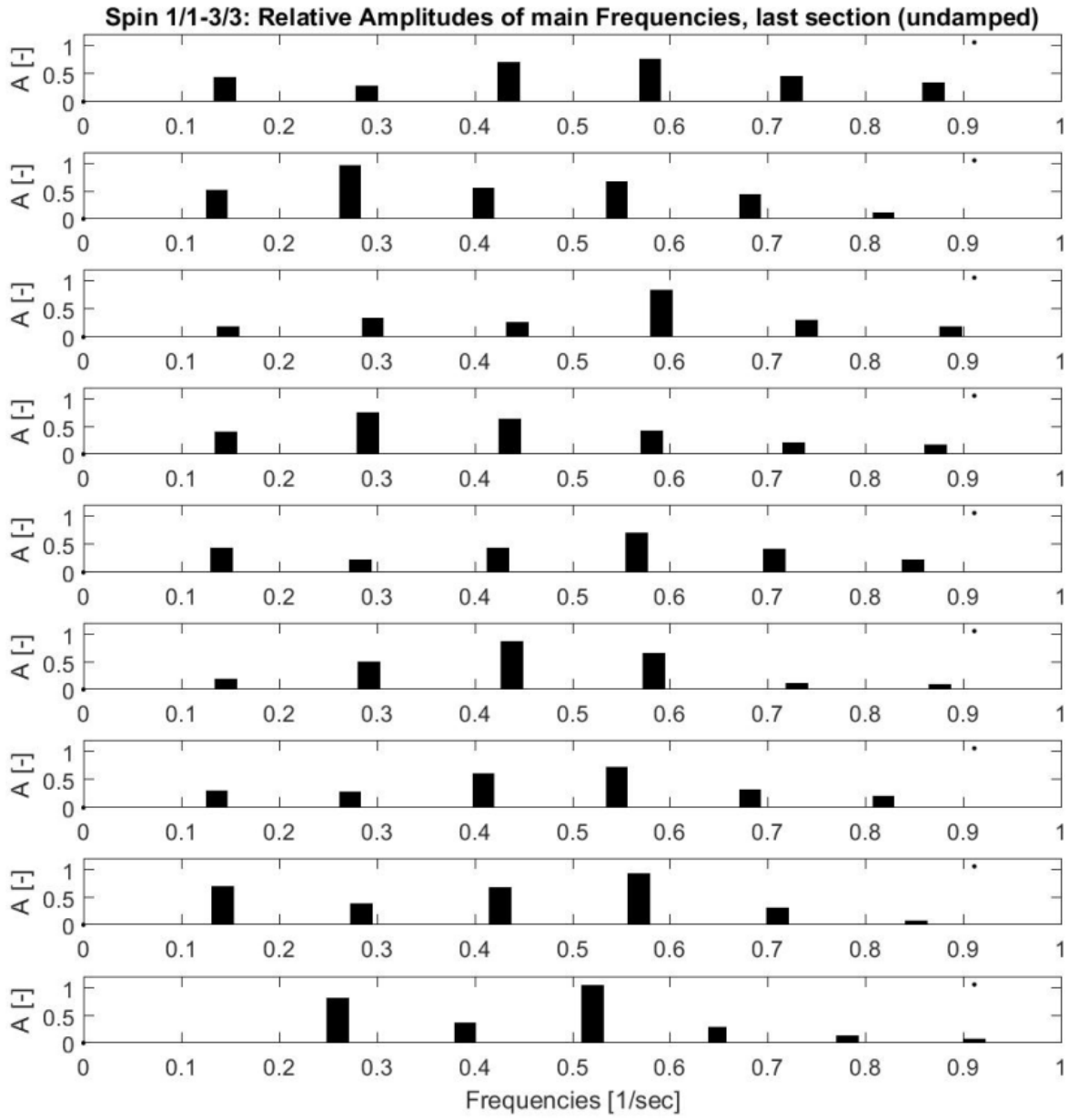

Figure 6.60: Spectrum of spin 1/1 to 3/3 (i.e. first 9 spins)

The spectrum above shows the main frequencies in the region of 0.25 to 0.55 Hz. Under these mass and CG position conditions a certain scattering can be seen. The reason for this scattering is likely to be atmospheric influences as this particular flight took place in high wind conditions which can induce turbulence over the very flat and even topographical conditions (North Sea shore line) where the flights have been conducted. In turbulent flow the aircraft's forces and moments vary suddenly. Such changes induce fuel sloshing. Especially as the fuel tanks are only filled to approximately 50% of their maximum capacity for mass and balance reasons.

The spectrum of the pitch values of the spins 4/1 to 6/3 is more explicit. As one can see in Figure 6.61 the main frequencies of these nine pitch functions are in all cases very close to 0.5 Hz.

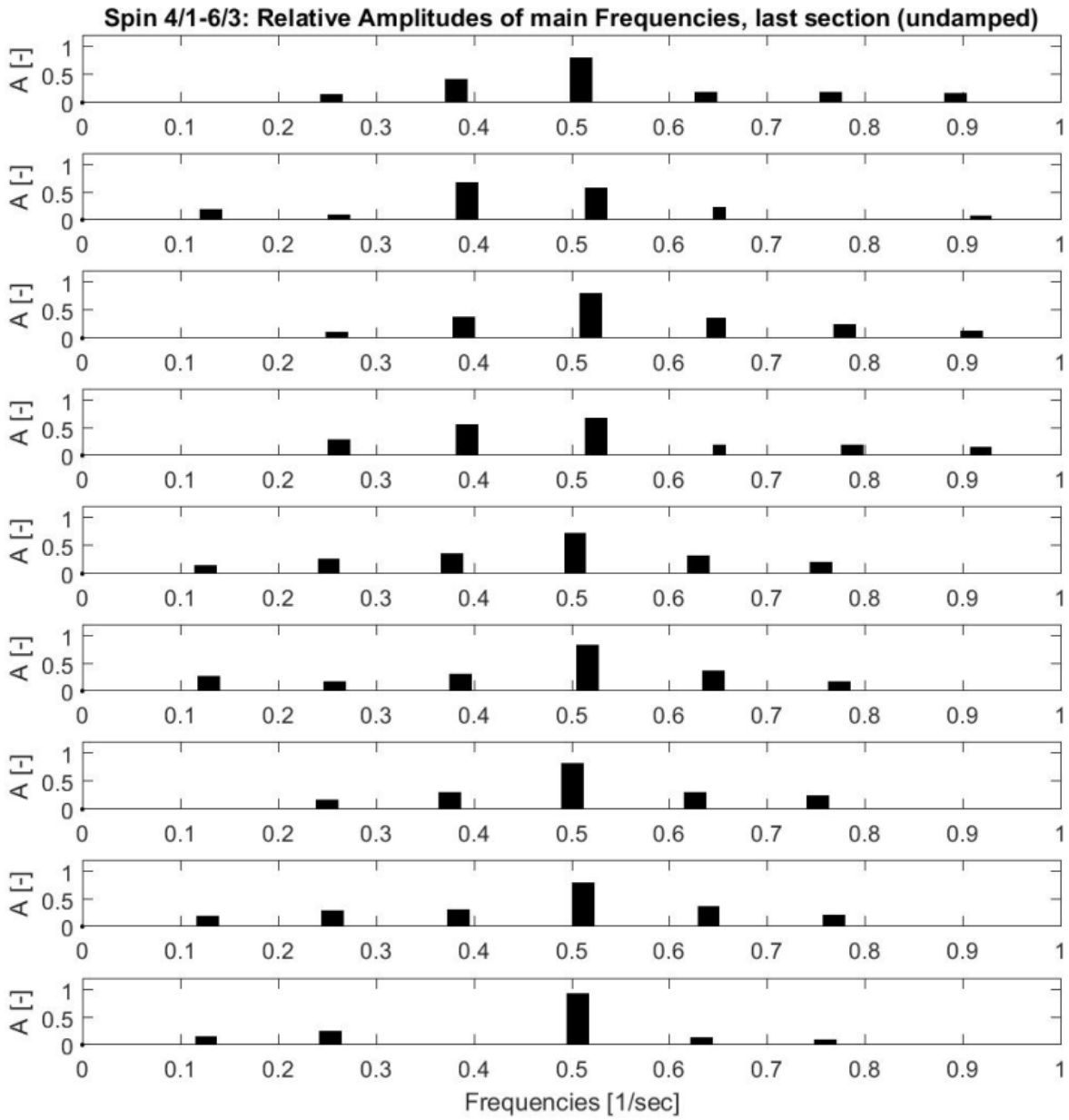

Figure 6.61: Spectrum of spin 4/1 to 6/3 (spin 10 to 18)

The same behaviour can be seen in Figure 6.62. Eight of the nine main frequencies are nearly exactly at 0.5 Hz. The main frequency of spin 8/2 (5th line in the figure below) is around 0.4 Hz. The reason for this is likely to be atmospheric disturbance.

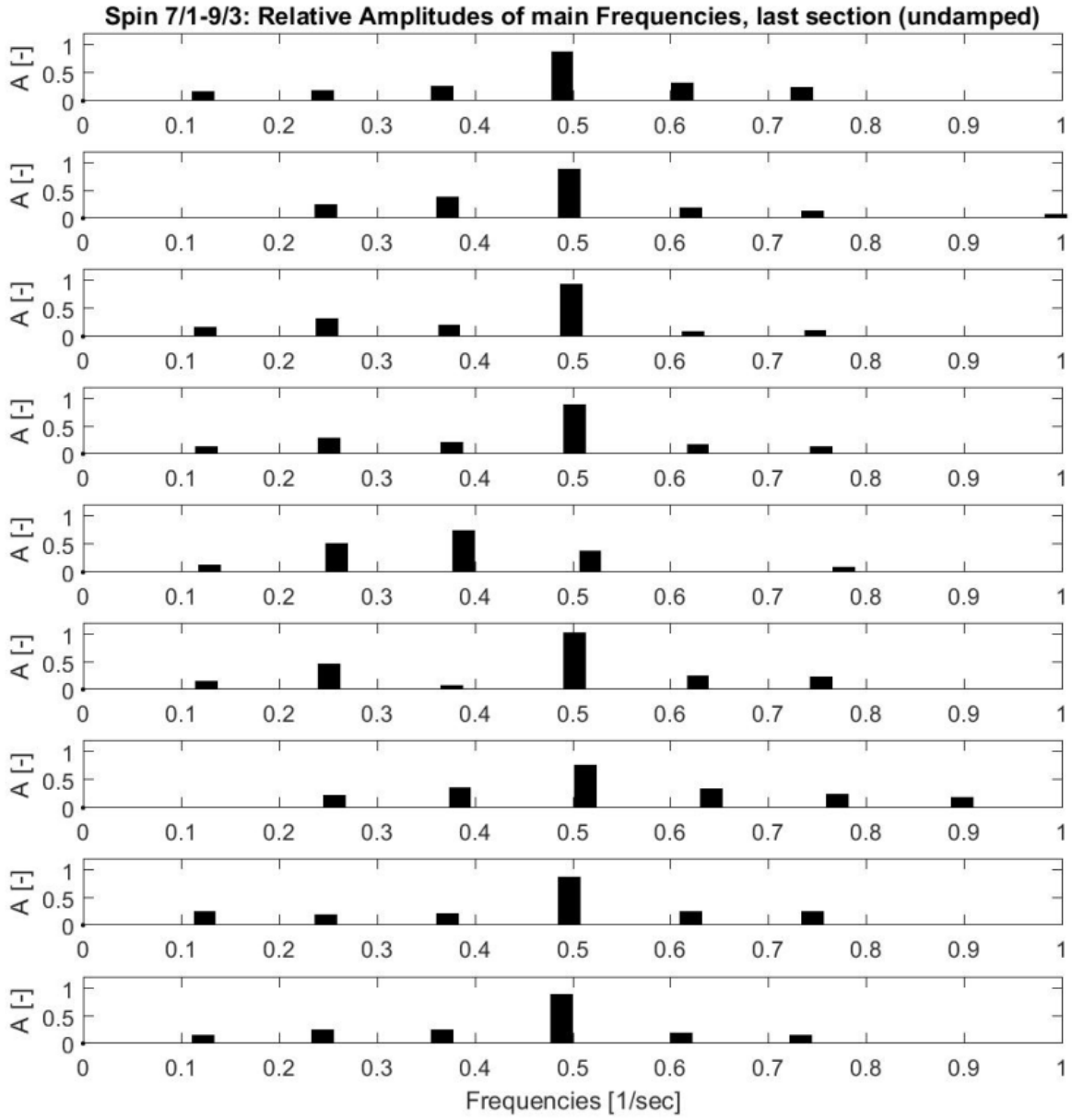

Figure 6.62: Spectrum of spin 7/1 to 9/3 (spin 19 to 27)

In addition to Figure 6.59 an analysis of the spin entry control inputs have been conducted with reference to the phase shift of the CG forward conditions, to the two other CG configurations (Tables 6.4 to 6.6). It was found that in some cases the full rudder deflection (zeta) was initiated slightly after (less than a 1/10 of a second) the full elevator deflection (eta). This was not intentional but occurred because the inputs were made by the pilot rather than an automated system.

Spin number	1st full control deflection	2nd full control deflection	Both control deflections at the same time
1/1	Eta	Zeta	
2/1	Eta	Zeta	
3/1	Eta	Zeta	
1/2	Eta	Zeta	
2/2	Eta	Zeta	
3/2			Both
1/3	Eta	Zeta	
2/3			Both
3/3	Zeta	Eta	

Table 6.4: Spin entry control orders during 1st spin test flight

Spin number	1st full control deflection	2nd full control deflection	Both control deflections at the same time
1/4			Both
2/4	Zeta	Eta	
3/4	Eta	Zeta	
1/5	Zeta	Eta	
2/5	Zeta	Eta	
3/5	Zeta	Eta	
1/6			Both
2/6	Eta	Zeta	
3/6			Both

Table 6.5: Spin entry control orders during 2nd spin test flight

Spin number	1st full control deflection	2nd full control deflection	Both control deflections at the same time
1/7	Eta	Zeta	
2/7	Zeta	Eta	
3/7	Zeta	Eta	
1/8	Zeta	Eta	
2/8	Zeta	Eta	
3/8	Zeta	Eta	
1/9			Both
2/9			Both
3/9			Both

Table 6.6: Spin entry control orders during 2nd spin test flight

These different control input orders influence the spins leading to different amplitudes and frequencies of the θ-functions (see Figure 6.59 above). The second and third test flights produce similar θ-functions because the orders of the control inputs are much the same.

From the data presented in this Chapter many of the parameters have exhibited regularity across the flight envelope. In other words spinning is not a chaotic manoeuvre. As the Fuji is typical in terms of geometrical shape to other aeroplanes in the same category it is not an unreasonable expectation to expect that parametric data from flight tests with these aeroplanes would also exhibit similar regularity.

In the following Chapter 7 a flight test data comparison can be found within which two spin related NASA papers (Sliwa (1979) and Stough (1985)) are discussed. In both cases low-wing, single-engine aeroplanes with similar mass distributions and geometries have been investigated and some flight test data are presented. Thus investigations into observation 9 will be completed in the next Chapter.

6.13 Conclusion of the spin test data analysis

The above discussed results from the conducted flight tests are based on flight test data taken with a proven and calibrated measurement system.

To all 9 discussed observations a detailed data analysis has been conducted and the data development – influenced by the aeroplane's mass and CG – is extrapolated to the aeroplane's flight envelope boundaries. Confidence intervals indicate in the corresponding plots the expected data during the extrapolation with a probability of 95%.

The results of this Chapter bring new insights into the understanding of the Fuji's spin behaviour and its dependencies on certain flight parameters. This study is unique in that it presents flight test results at 27 points in the flight envelope for a number of parameter changes, whereas previous studies by other authors have concentrated on a single point in the flight envelope.

As a very valuable contribution to the Chapter 5 above this Chapter adds for aeroplane designers, flight testers and flying instructor a 'tool box' with which design principles, test and training procedures - which are all flight safety relevant – can be derived.

6.13.1 Conclusions of the observations

#1 (true): It has been shown that the second minimum value of the pitch down function always reaches the highest negative value which indicates the point in time at which spin recovery is most likely to be successful and rudder shielding to be at a minimum.

#2 (true): The results show that the aeroplane always reaches a limiting value of the pitch (Θ_{limit}) which is independent of the actual mass and CG position. This finding is in contradiction to 5 sources in literature.

#3 (true) and #4 (true): The investigations on the respective data show that the CG position and the mass is changing the maximum yaw rate of the aeroplane, as well as changing the yaw rate. Both findings are in contradiction to the literature published on this topic.

#5 (true): The observation that the maximum difference in angle of attack values between left and right wings leads to a maximum in roll rates has been demonstrated to be true across the investigated area of the flight envelope. As this dependency has not been investigated before it contributes to a new section of spin research.

#6 (true): The results indicate that the influence of the mass and CG position is not very high on the roll rate, but over the entire spin run the influence can be such that additional complete turns are experienced.

#7 (true): As the total angular velocity is a key parameter of spinning it is shown that it is strongly influenced by the CG position. The influence of the mass is lower but still an important factor for this parameter.

#8 (true): It was shown that the recovery time becomes shorter when the CG position moves towards the tail of the aeroplane.

#9 (incomplete at this point): This investigation was divided into two parts. In the first part the behaviour of the Fuji has been considered. Since the Fuji shows fairly repeatable behaviour during a spin it is expected that this behaviour is typical of the aircraft in the same category. Thus the second part of the investigation is to study other aircraft in the same category and the results are presented in Chapter 7.

Chapter 7 Flight test data comparison

The aim of this Chapter is to investigate whether the results from, and the observations about, the Fuji FA – 200 -160 are generalizable to the other aircraft in the same category.

7.1 Introduction

In the chapters above it has been presented how the aeroplane was equipped, how the flight tests have been conducted and with which mathematical method the data have been analysed. One question to be answered is whether this aeroplane behaviour is just the behaviour of this specific aeroplane or is it possible to generalize the outcomes at hand to other single-engine, low-wing aeroplanes with a similar geometry, mass and mass distribution?

Stough et al. (1985) undertook a flight investigation using a NASA low-wing, single-engine, T-tail light aeroplane. A summary of the investigation is that:

1. All spin tests were conducted with aft CGs
2. Spin tests were without defined mass changes
3. 6-turn-spins were conducted to the left with power idle, flaps and landing gear up, aileron deflections in the spin direction and in a neutral position
4. Spin tests were performed without the use of a modern, digital computer based measurement system with a high sample rate for data determination, post-processing and digital data storage
5. Spin data and results of similar spins – in comparison to the current project – are presented by only a few time plots
6. No mathematical data analysis was conducted
7. No advice to pilots was given
8. No links to other relevant research projects were given

The parameter values used for the Stough et al. (1985) spins are very close to those used for condition 8 in this thesis (see Table 4.9) which also has one of the most undisturbed data sets (i.e. little atmospheric disturbance).

The NASA aeroplane (Figure 7.1) had a T-tail configuration and the landing gear was always retracted whereas the Fuji (Figure 7.2) has a conventional tail and fixed undercarriage. The opinion of Stough et al. (1985) was that different landing gear positions did not affect the results. For the basic technical data of both aeroplanes see Appendix 4.

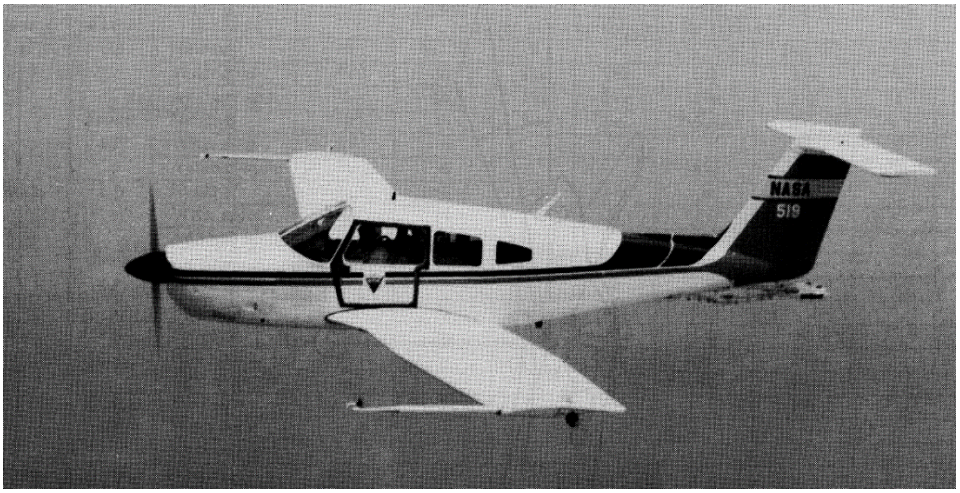

Figure 7.1: Piper PA 28, single-engine, low-wing aeroplane with a T-tail and retracted landing gear. Note: that this aircraft was instrumented for experimental spin tests. (Stough et al., 1985)

Figure 7.2: Fuji FA 200 – 160, single-engine, low-wing aeroplane with a conventional tail and fixed landing gear. Note: that this aircraft was instrumented for experimental spin tests. It is owned by TFF GmbH.

In the following sections the time histories from the two aircraft for the angle of attack, α, sideslip angle, pitch rate, yaw rate and roll rate are compared. These are the only data sets which are available for both aeroplanes measured under very similar CG and mass conditions.

7.2 Comparison of Angle-of-Attack at the Centre of Gravity

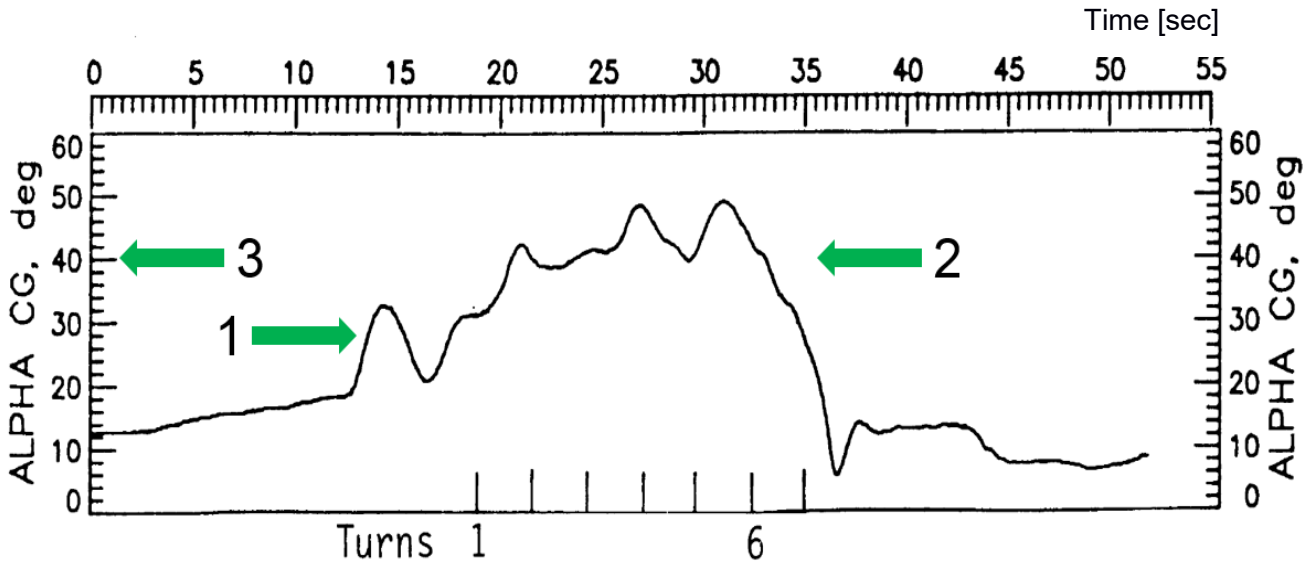

Figure 7.3: Time plot of the angle of attack (ALPHA) of a Piper PA 28 aeroplane during a 6-turn spin to the left with power idle, ailerons neutral, flaps and gear retracted, (Stough et al., 1985)

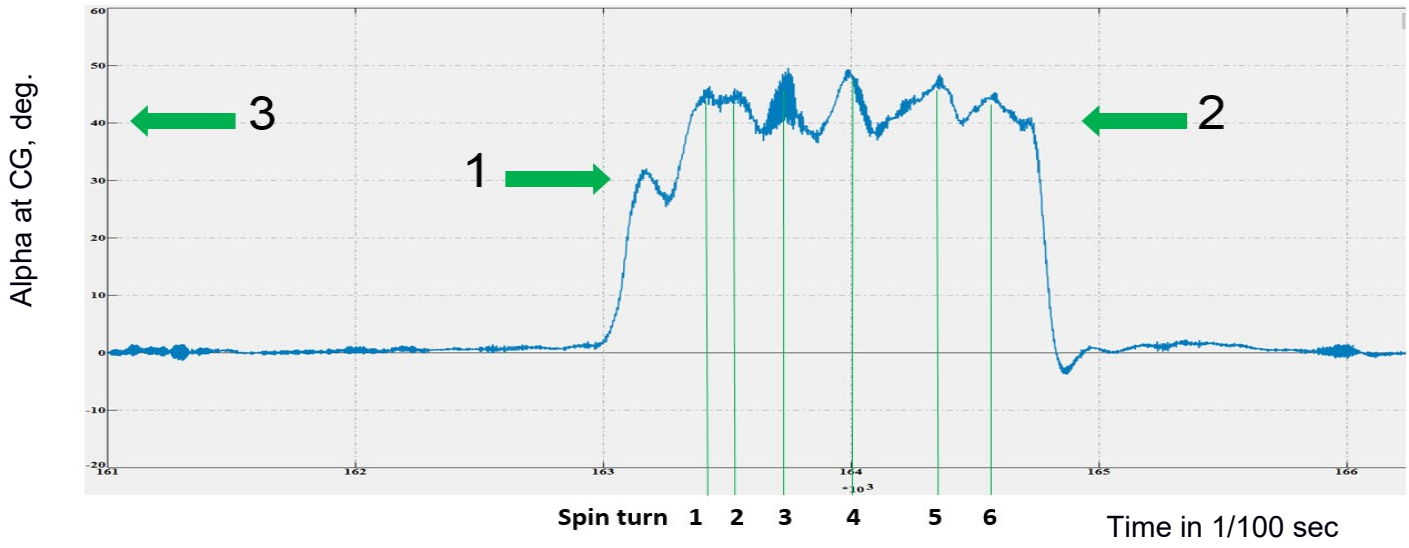

Figure 7.4: Time plot of the angle of attack (Alpha) of a Fuji FA-200 -160 aeroplane during a 6-turn-spin to the left with power idle, ailerons neutral, flaps retracted

The time histories (Figures 7.3 and 7.4) show that in both cases there is an initial rise in the values of the data. The data values then drop at just over 30° angle of attack because of the changing attitude of the aircraft (arrow 1). The data continues to rise and fall in time due to the change in pitch and angle of attack (α) as the spin proceeds per spin turn a separate α peak can be seen. Note that the values rise to a plateau (arrow 2). The α data are oscillating about a mean value that can be found in both cases to be around 40° (arrow 3). This

behaviour is more regular for the Fuji than the Piper. The aeroplane's α behaviour during the recovery phase is similar as well. In the case of the Fuji, the α data drop slightly quicker. As the moment arm and stabilizer area are larger on the Piper there must be other reasons for the Piper being slower: possibilities include pilot's control inputs and atmospheric conditions.

7.3 Comparison of Angle-of-Sideslip at the Centre of Gravity

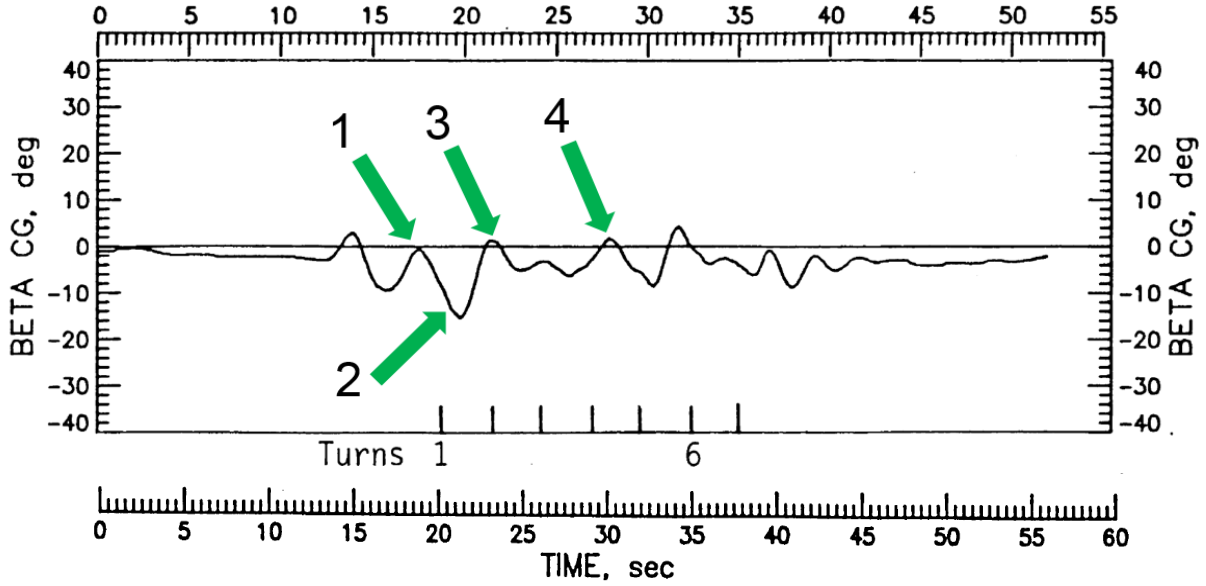

Figure 7.5: Time plot of the sideslip angle (BETA) of the Piper PA 28 aeroplane during a 6-turn spin to the left with power idle, ailerons neutral, flaps and gear retracted, (Stough et al., 1985)

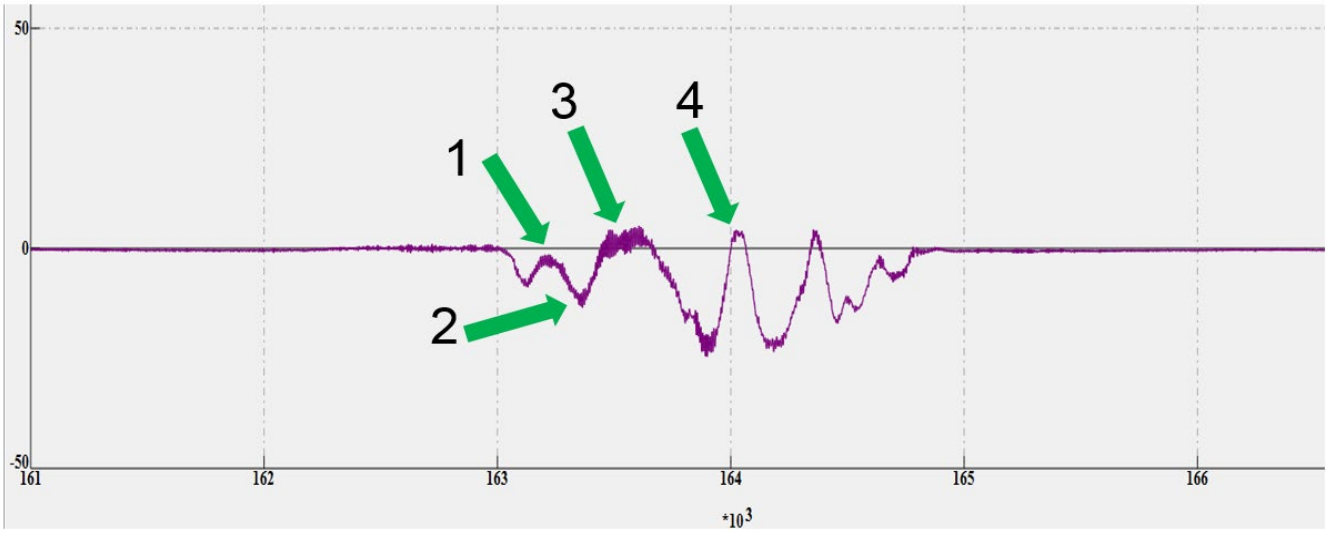

Time in 1/100 sec

Figure 7.6: Time plot of the sideslip angle (Beta) of a Fuji FA-200 aeroplane during a 6-turn spin to the left with power idle, ailerons neutral, flaps retracted

The initial data (Figures 7.5 and 7.6) oscillates in both cases. Consider the Fuji data: the oscillation in the data is shaped like a 'W' with small amplitudes until point 3 and then as a larger 'W' from point 3 to 4. The Piper data follow a similar trend except that initially an additional small control input can be seen. After the first reversal the sideslip values tend to reach 0° (arrow 1). After the second data gradient reversal the sideslip reaches positive values (arrow 3). Thereafter an oscillation starts (arrow 4) which is later influenced by a light damping.

7.4 Comparison of Pitch Rate

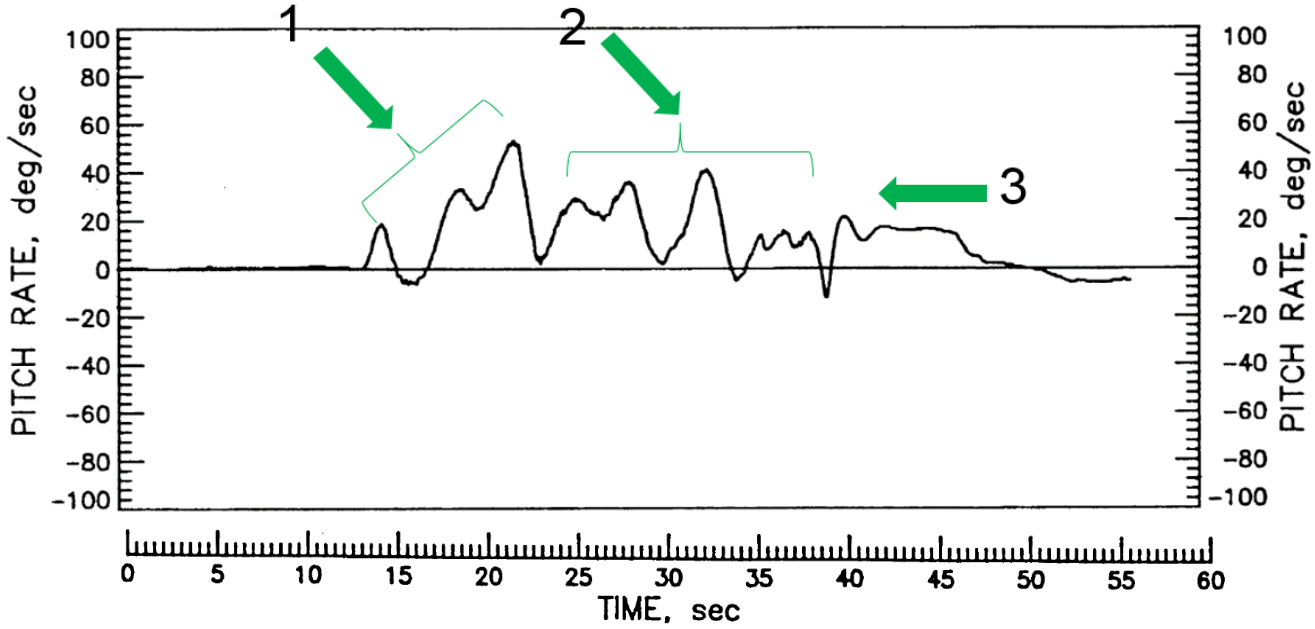

Figure 7.7: Time plot of the pitch rate, q, of a Piper PA 28 aeroplane during a 6 turn spin to the left with power idle, ailerons neutral, flaps & gear retracted, (Stough et al., 1985)

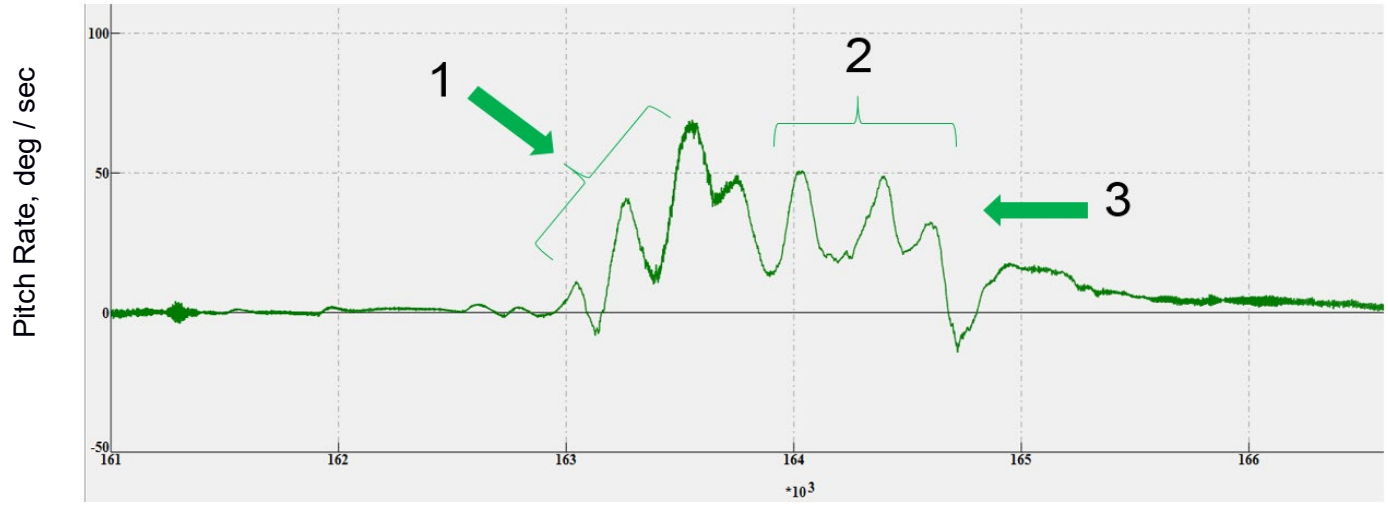

Figure 7.8: Time plot of the pitch rate, q, of a Fuji FA-200-160 aeroplane during a six turn spin to the left with power idle, ailerons neutral & flaps retracted

The pitch rate behaviour of both aeroplanes is very similar (Figures 7.7 and 7.8). Both data intervals (see bracket of arrow 1) show negative values after a first small positive peak. Thereafter the data rise is in both cases interrupted by a data gradient reversal followed by a local minimum (in both cases around +15 to 20 °/second). After that the absolute maximum can be seen, in both cases at approximately +60°/second. This is followed by an oscillation in the positive region of the data (arrow 2). The Fuji's pitch rate is slightly higher than that of the Piper (around 35°/second versus around 25°/second respectively) indicated by arrow 3. Both plots show some unsteadiness in the middle part in the traces but not necessarily in the same places which suggests that external influences are likely to be the cause.

7.5 Comparison of Yaw Rate

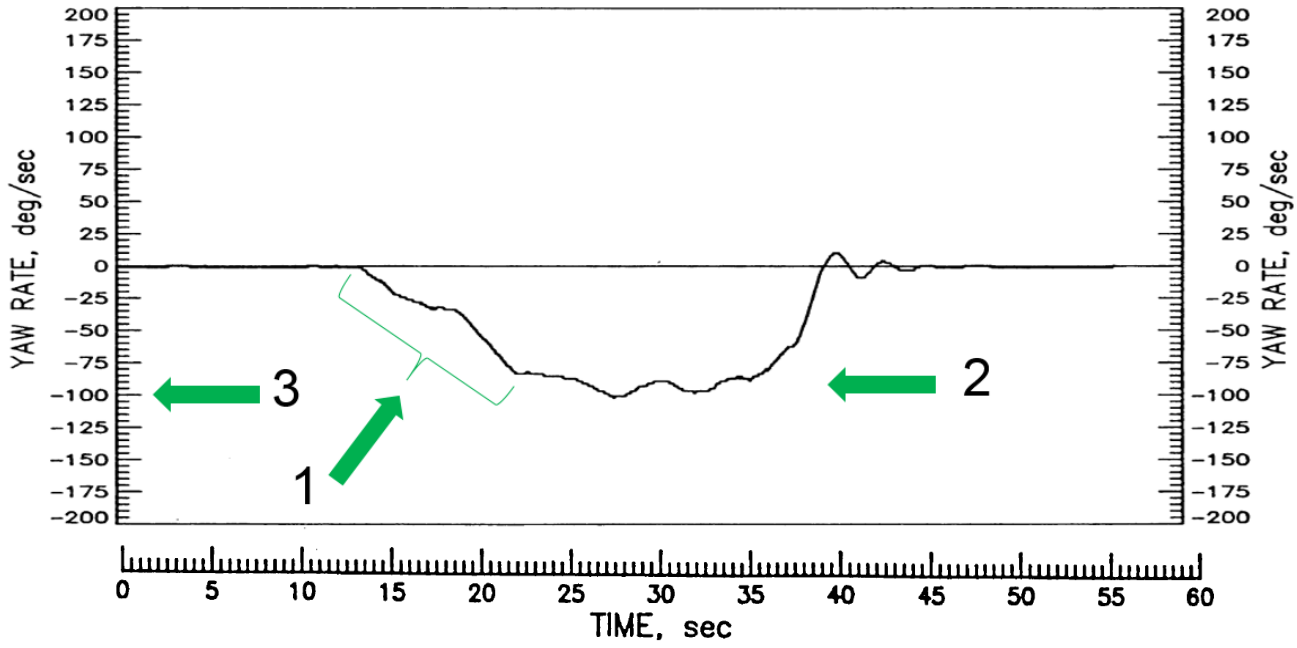

Figure 7.9: Time plot of the yaw rate, r, of a Piper PA 28 aeroplane during a 6 turn spin to the left with power idle, ailerons neutral, flaps & gear retracted, (Stough et al., 1985)

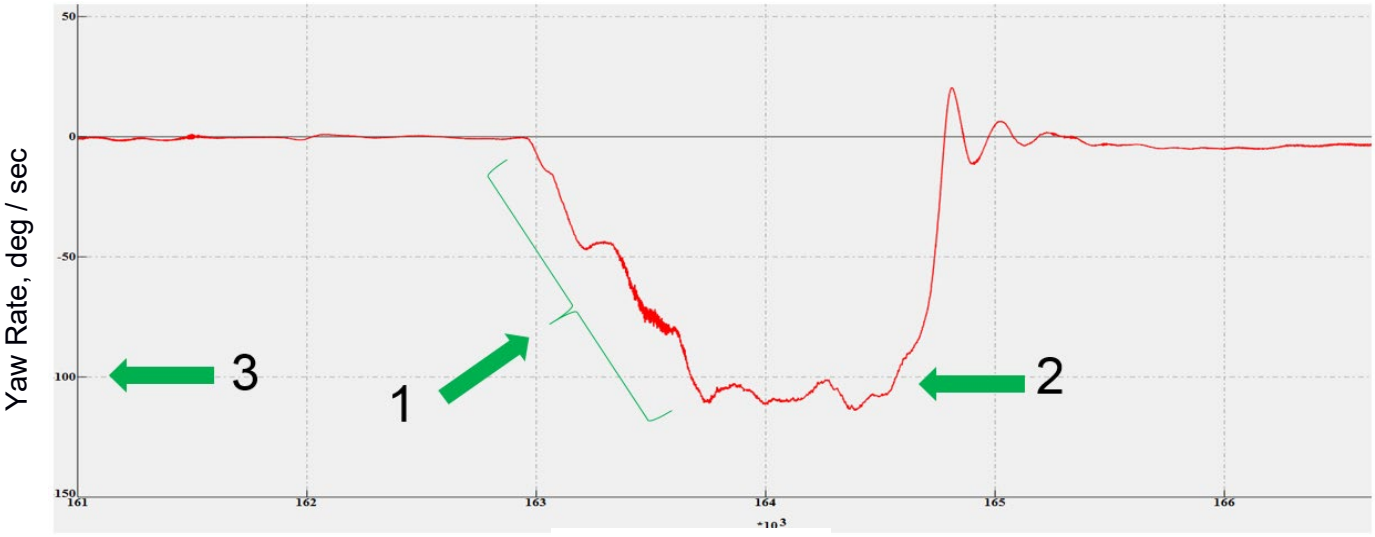

Figure 7.10: Time plot of the yaw rate, r, of a Fuji FA-200-160 aeroplane during a six turn spin to the left with power idle, ailerons neutral, flaps retracted

Both yaw rate behaviours are also very similar (Figures 7.9 and 7.10). During the time interval of bracket 1 the magnitude of yaw rate increases as the values become more negative. This is followed by a plateau of the yaw rate values which is indicated by arrow 2 in the Figures above. Both plateaux can be found at approximately 100 °/second (see arrow 3).

The recovery behaviour of the data is again similar including a highly damped oscillation after the yaw rate values have crossed the time axis.

7.6 Comparison of Roll Rate

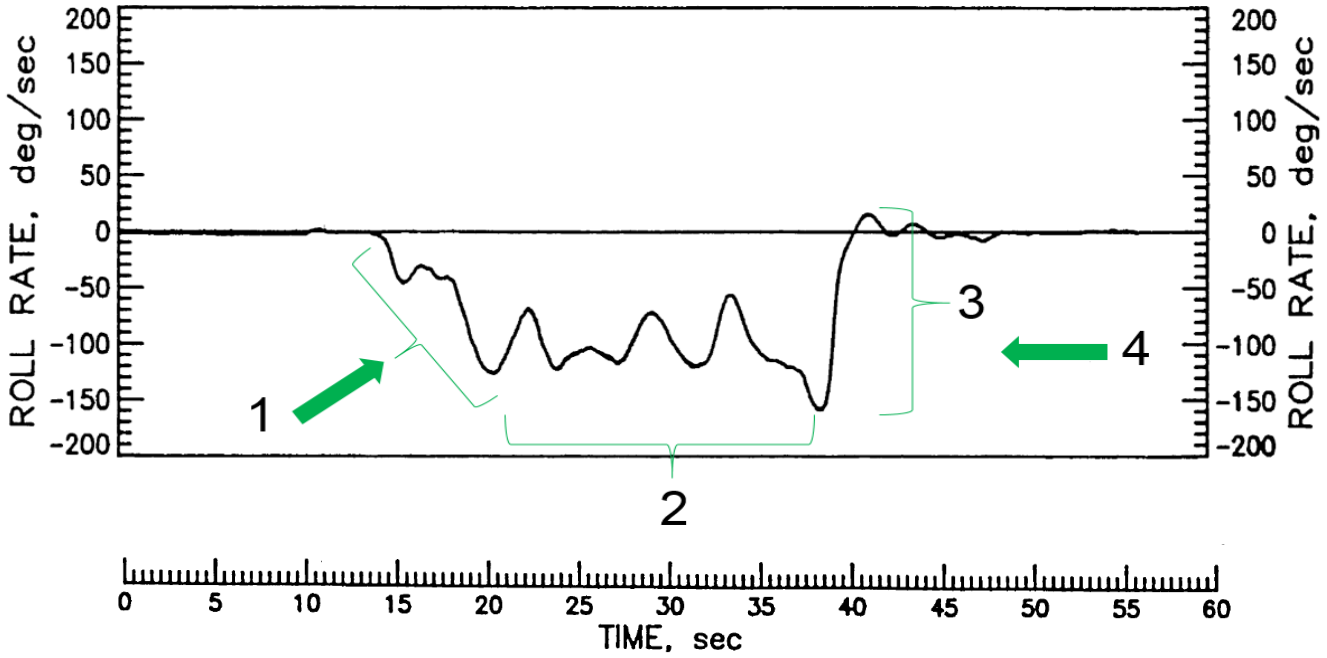

Figure 7.11: Time plot of the roll rate, p, of a Piper PA 28 aeroplane during a 6-turn-spin to the left with power idle, ailerons neutral, flaps & gear retracted, (Stough et al., 1985)

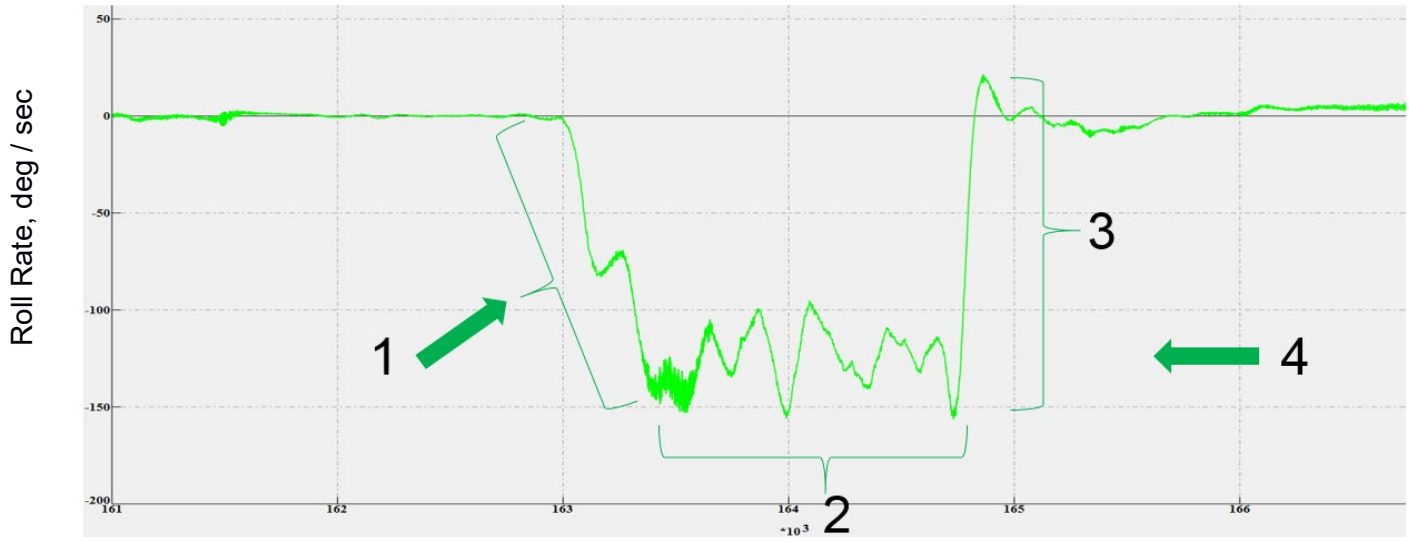

Time in 1/100 sec

Figure 7.12: Time plot of the roll rate, p, of a Fuji FA-200-160 aeroplane during a six turn spin to the left with power idle, ailerons neutral, flaps retracted

The final parameter which can be compared on the basis of measured flight test data is the roll rate of both aeroplanes. It can be identified in Figures 7.11 and 7.12 that the roll rate data show two gradient reversals (see bracket of arrow 1). After the data reach a plateau, an oscillation of the roll rate can be found which is only slightly damped (see bracket 2). After the absolute (negative) maximum of the values is reached, both aeroplanes produce a sharp rise of the roll rate data which ends with a strong damping after the time axis has been crossed (see bracket 3). Arrow 4 indicates that both roll rate data plateaux can be found at approximately 120 °/second. The data in Figures 7.11 and 7.12 indicate that during a spin to the left these aircraft roll to the left (i.e. the roll rate is negative). It is interesting to note that in the case of the Hawker Hunter Jet Fighter (BBC, 1986) as spin to the left would produce a roll rate to the right. This implies that the differences in geometry between a single-engine, low-wing category and other categories can produce fundamental variation in a spin motion.

Sliwa (1979) also used a single-engine, low-wing aeroplane in spin tests with an aft CG. His aeroplane had a conventional tail geometry and a fixed landing gear (Figure 7.13).

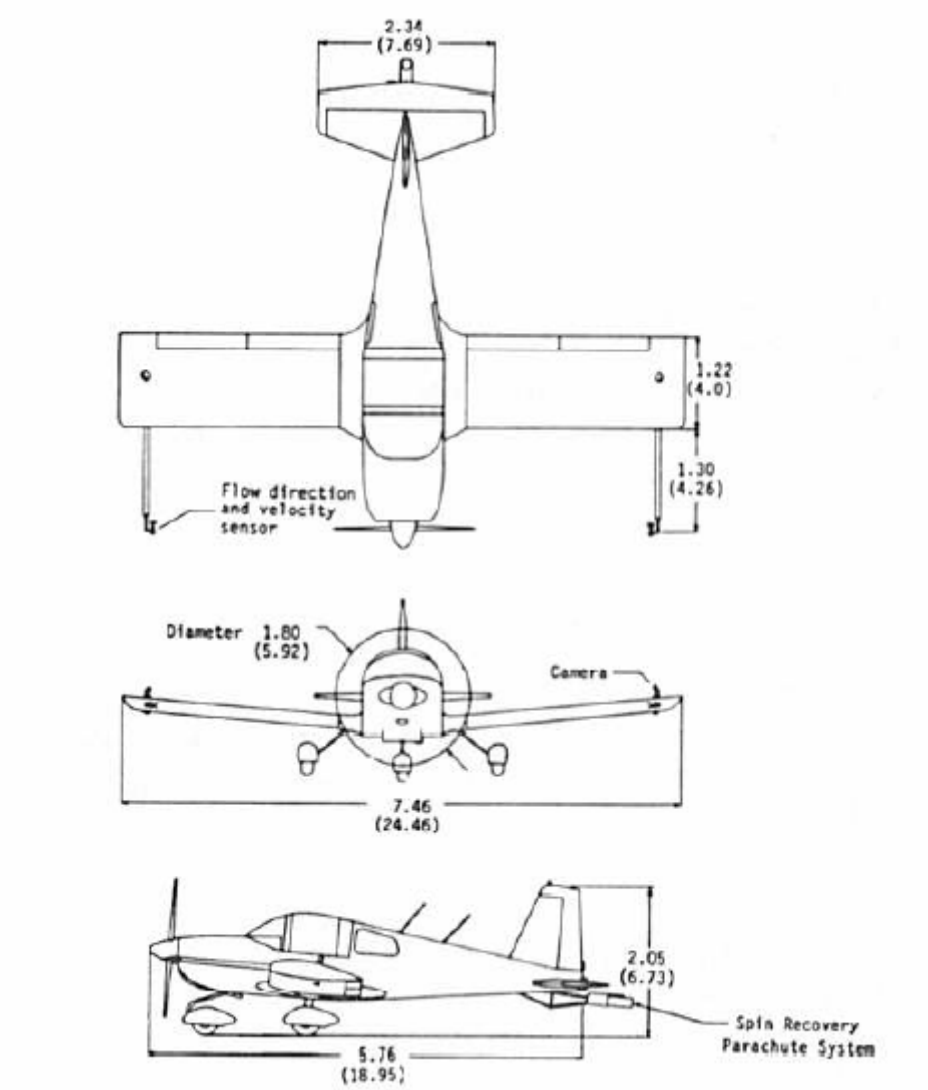

Figure 7.13: Research aeroplane (one of its kind, without name) which has been used for spin research trials by Sliwa (1979)

Within this paper, data for the pitch angle and the angle of attack have been presented. Again the data behaviour is very similar to that of the Fuji.

To show this similarity the pitch angle data have been extracted manually from the corresponding graph in Sliwa (1979) and treated (see Chapter 6) like the pitch data collected during the flight tests with the Fuji (see Figure 7.14). Between the single θ-peak values a linear extrapolation has been conducted and then plotted. It is important to note that the corresponding θ_{limit} value of Sliwa's aeroplane is -47.85° which is very close to the θ_{limit} value of the Fuji which is -47.13°. The analysis produces an improved estimation for θ-limit with a squared error value of $(5°)^2$ (Figure 7.15). A pitch angle limit, θ_{limit}, of -47° corresponds with an angle of attack of 43° (-(-47°) = 90° - 43°), this also corresponds with the average angle of attack by Stough et al. (1985) in spin tests with their T-tail configuration.

As mentioned in section 6.5, the value of θ_{limit} can be used to determine the amount of tail effectiveness (tail shielding) in spin recovery. In the case of Sliwa's aircraft the horizontal tail plane is lower than that of the Fuji. This leads to a less shielded rudder and thus to a better spin recovery behaviour.

The aeroplane used by Sliwa has a lower damping because its length is 5.76 m, whereas for the Fuji the length is 7.96 m, i.e. 2.2 m shorter. In addition, the stabilizer span is only 2.34 m versus 3.46 m for the Fuji.

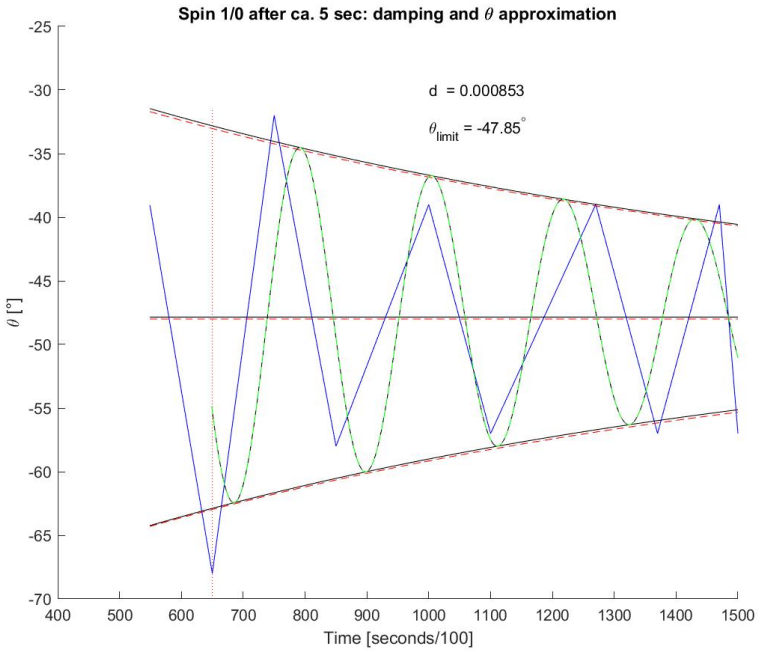

Figure 7.14: Damping coefficient and the resulting θ_{limit} values, blue line peak data taken from Sliwa (1979), green line data post processing by the Author

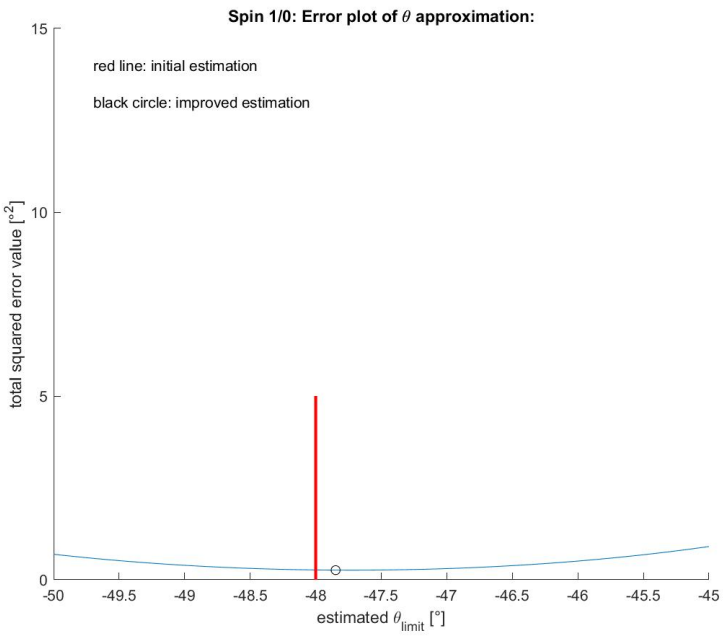

Figure 7.15: Error plot of a θ-approximation for the aircraft of Sliwa (1979). The red line indicates the position of the initial θ-estimation. The open circle indicates the improved estimation for θ-limit (after 50 approximations)

The angle of attack values cannot be extracted manually from Sliwa (1979) due to the size of the plot. But it can be seen that, again, the data behaviour is very similar to that of the Fuji.

7.7 Conclusions

In all cases above, where comparison data exists, the behaviour of the three aircraft is similar for variation of pitch angle, angle of attack, sideslip angle, roll rate, yaw rate and pitch rate. For all three aircraft a pitch angle limit value of minus 47° has been obtained.

If such a similarity in the aircraft behaviour can be observed at these main spin parameters, it supports observation 9 that the Fuji data can be generalized in a qualitative sense, and for theta limit in a quantitative sense, across the category of low-wing, single-engine aeroplanes.

Chapter 8 Conclusion

In the following section the results and findings from Chapters 5 to 7 – based on the aims, principal objectives (Section 1.4), corresponding research questions and subsequent observations (Section 1.5) - are summarized. For an improved readability the original research questions are repeated here. Note that for each research question a list of the observations which contribute to answering the question are given in brackets.

1.) How will changes of the aeroplane's mass and the position of the Centre of Gravity affect the spin behaviour (i.e. phases of a spin) and the output flight parameters (i.e. motion and attitude) of an aeroplane?
(All observations except 1 and 5)

2.) What are the parameters which characterize a spin in motion? What are the relationships between these characteristic parameters?
(Observation 1 and 5)

3.) Where are the differences between real measured spin test data and the traditional spin theories in a spin situation? Are the traditional spin explanations correct?
(Observations 2, 4, 7 and 8)

4.) Which mass and centre of gravity value combinations makes a spin faster and thus confuses the pilot more so that a recovery is more likely to fail?
(Observations 3, 4, 6 and 7)

5.) Is the spin behaviour of a given conventional low-wing, single-engine aeroplane design reproducible or random?
(Observations 2 and 9)

In the section below the main conclusions, contributions and impact of this work is presented. Because there is a general recognition of the need to transfer the results from research directly to potential users in the industry this section is not only written for scientists but also for Flight Testers, Aeroplane Designers and Pilots / Flying Instructors.

8.1 Main conclusions, contributions and impact

Firstly the conclusions of the findings are presented in sequence. All of the observations are deemed to be true from the results of the thesis. Although the supporting evidence is stronger for some of the observations compared to others. Within each observation sub-section the conclusion are divided into those relevant to designers; flight testers; and pilots and flying instructors.

8.1.1 Observation 1: The second minimum value of the pitch down (Θ) function always produces the highest negative value

See section 5.4.2 ‘Acceleration behaviour around all three axes’ and 6.4

This observation is true and the point in time at which second minimum value of the pitch down function is at its most negative, is when spin recovery it is most likely to be successful and rudder shielding to be at a minimum.

Designers:

Observation 1 assists a designer in that the size of the elevator, rudder and fuselage, the tail configuration and rudder position can be designed appropriately.

Flight Testers:

As observation 1 identifies the point in time when the rudder shielding is at a minimum, this affords the flight testers the best opportunity the recover the aircraft. It also gives the flight testers a point of safety because if the minimum rudder shielding is insufficient to recover the aircraft from a spin then no other point in time on the aircraft’s trajectory in future will enable the aircraft to be recovered. Also advice could be included in the pilot’s operating handbook (POH) for this aircraft that a pilot should exit a spin as close as possible to passing the point in time when the second minimum occurs. This would be the first time that such information has been included in a POH.

Pilots and Flying Instructors:

The point in time of the second minimum identifies the best point to recover from a spin. If the recovery from a spin at this point in time is unsuccessful than at no future point will they be able to recover the aircraft (and thus should use their parachutes).

8.1.2 Observation 2: Independent of the aeroplane's mass and CG position, the pitch angle (Θ) approximates to a characteristic value

See sections 5.4.3 and 6.5

This observation is true. Interestingly this finding is in contradiction to 5 sources in literature. Also it should be noted that Chapter 6 presents the first derived mathematical model for the behaviour of the pitch angle Θ.

Designers:

Observation 2 offers an average value for theta that can be used by designers over the whole of the theta envelope. In other words it can be utilized as a value to size the elevator, rudder and fuselage such that the aircraft will be able to recover from a spin no matter at which point in time the aircraft is at within that spin. It also can be taken as a typical value for all aircraft of the same category (low-wing, single-engine) in concept design studies.

Flight Testers:

Observation 2 tells the flight testers that there is a pitch angle value that the aeroplane will tend to in a developed spin condition. The flight testers need to discover during flight tests that the new aeroplane can be recovered from a developed spin. If the aeroplane is recoverable the flight tester could include this limiting pitch angle value in the pilot's operating handbook and advise a pilot that the aeroplane can be recovered even after the second minimum pitch angle value that has been passed. This would be the first time that such information has been included in a POH.

Pilots and Flying Instructors:

Assuming the aircraft is recoverable at this limiting theta value then this finding offers a measure of safety and convenience in that the pilot can wait until the aeroplane reaches this limiting value (for which the aeroplane will stay as this constant attitude) and then the recovery procedure can be applied.

8.1.3 Observation 3: Maximum Yaw rate (ln_r) changes with CG position and mass

See section 6.6

Observation 3 is true.There is a strong dependency between the maximum yaw rate and the CG position. Whereas for the mass case the dependency is moderate. These findings are in contradiction to the literature published on this topic.

Designers:

The higher the yaw rate the higher the stresses on the aircraft and the pilot. Therefore this finding can be used to identify the values of the CG position and mass for which the stresses are deemed too high for the structural factor of safety for the aircraft. Conversely this tells the designer that it may be necessary to redesign parts of the aircraft structure so as to reduce the stresses to a more acceptable level especially during the spin recovery phase. For example a bigger (unshielded) rudder and / or longer aft fuselage is necessary.

Flight Testers:

Observation 3 can improve the flight safety of a test programme. Knowing the effects of mass and CG position of yaw rate enables the flight testers to know which spins are going to be faster or slower and therefore are going to be more disorientating. Also for which parts of the flight envelope, spin recovery is easier or harder to effect.

Another finding in this context is that a faster spin has the potential to take a longer recovery time (see Table 6.3) and thus the corresponding height loss is bigger.

In the case that the aeroplane is under certification flight test and the entire spin behaviour is not known so far than spin test programme should be started with medium values for the aeroplane mass and CG position. This would lead to a medium yaw rate with which the spin behaviour can be studied and documented thoroughly and a potentially un-recoverable flat spin can be avoided. Additionally the maximum negative pitch angle will also reach a medium value. Both effects help flight testers to conduct spin tests without experiencing an overly fast rotating aeroplane.

Pilots and Flying Instructors:

The yaw rate of the Fuji FA-200 -160 increases when the CG position is shifted to the front. This effect follows a strong dependency of 88.6% (see Figure 6.24). One consequence for flight training is that a nose-heavy aeroplane will confuse and disorientates a pilot more easily because of the faster angular velocities than a tail heavy one. Hence, spin accidents will occur sooner with a nose-heavy aeroplane. In addition, lighter loaded Fuji spins fast than a heavier one (see Figure 6.26). As the Fuji is recoverable from the final pitch angle then spin flight training or spin demonstration flights should be conducted with tail heavy aeroplanes.

8.1.4 Observation 4: The yaw rate (ln_r) oscillation changes with CG position or mass

See section 6.7

Observation 4 is true concerning the influence of CG position on the yaw rate but the evidence suggests a moderate (49%) dependency. However, the observation is not true (or extremely weak) for the mass dependency since the coefficient of determination, R^2, is only 17%.

Designers:

Observation 4 offers the Designer an insight into the dynamic nature of the aeroplane's yaw behaviour compared to the previous observation.

The higher the yaw rate change the higher the stresses on the aircraft and the pilot. Therefore this information can be used to identify CG position and mass values for which the stresses are deemed too high for the structural factor of safety for the aircraft. The designer can then choose to redesign parts of the aircraft structure so as to reduce the stresses to a more acceptable level especially during the spin recovery phase. As an example, the mountings of a heavy engine to the nose structure and the structure of the tailplane (the extreme ends of the aeroplane) need to be reinforced when planning to operate an aeroplane in such a flight mode.

Flight Testers:

Observation 4 can be used for spin characteristic evaluations of new aeroplanes. Typically, a test pilot will tend to start a spin evaluation programme with a nose heavy and light aeroplane.

However, it is advised (due to observation 4) that where a spin behaviour is not known, a medium CG position is chosen first so that a test pilot can study the spin better than with a nose-heavy aeroplane which will spin much faster. Not using an aft located CG for a heavy aeroplane avoids, during initial spin experiments, the development of a potentially un-recoverable flat spin mode.

Pilots and Flying Instructors:

Oscillations in the yaw rate (due to the CG position) affect the safety of an aircraft. As Figure 6.29 shows, the maximum value of the yaw rate change occurs when the aeroplane is nose-heavy. Such yaw rate rapid changes are particularly confusing and disorientating for a pilot so that a correct and timely recovery procedure may fail. Following the observation, not only the fastest spins can be observed with forward CG positions but additionally the strongest changes in the yaw rate can be seen here. Both effects should be understood and shown to flying instructors to avoid spin demonstrations or training in such an aeroplane loading situation.

The influence of the mass of this behaviour is much less (see Figure 6.31) although the corresponding values do range from around 5°/sec to 9°/sec.
Cross-coupling of both parameter changes do not influence the dependency significantly.
The above described effect can be observed even more clearly when the corresponding mean values are used.

8.1.5 Observation 5: Maximum difference in AoA values between left and right wings leads to a maximum in roll rates (alpha_le_c – alpha_ri_c; ln_p)

See sections 5.4.3 and 6.8.

This observation looks for whether there is a relationship between two of the characteristic parameters of spin motion, in this case the roll rate and the difference in angle of attack between the left and right wings. This observation is found to be true (see Figure 6.41). As this dependency has not been investigated before it contributes to a new aspect of spin research. The results also indicate that there is little to no dependency of the roll rate on input parameters: mass and CG position.

Designers:
Designers can use the knowledge of this direct relationship to assist the design of similar aeroplane geometries for similar aeroplane behaviour during a spin. The new aeroplane must be flight tested to determine the corresponding values and its behaviour, in relation to other aeroplane geometries.
If known, this understanding will help to size new aeroplanes because an aeroplane will react faster at higher differences of AoA (between the 2 wings), thus imposing larger stresses. Larger stresses will need reinforcements for the aeroplane structure and the corresponding control surfaces in order to recover from this high load flight situation.

Flight Testers:
It was found that the time between the maximum difference of the left and right angle of attack and the maximum value of the aeroplane's roll rate, is a constant for the aircraft (for the Fuji FA-200-160 this is ~1.3 seconds). This observation has not been made in the available literature. The time lag is a useful measure of the agility of the aircraft. Both the time lag and the maximum roll rate can be used for spin characteristic predictions within a spin test programme. With this understanding it can be expected that a specific aeroplane

rolls at its maximum rate to one side, when reaching its maximum AoA-difference after this time constant, and this behaviour is independent of its CG position or its mass.

Pilots and Flying Instructors:

The information about the roll agility during a spin of an aeroplane can be used for flight training especially to avoid disorientation of the pilots. The above explained constant time lag – especially when known for different aeroplane geometries - can be used to categorize aeroplanes and thus the likelihood of a pilot's spatial disorientation.

In addition to this, pilots are always interested in aeroplane behaviour which does not change with mass and CG position; this is of particular importance when conducting aerobatic manoeuvres like spins.

8.1.6 Observation 6: Rate of roll (ln_p) changes with CG Position and aeroplane's mass

See section 6.9

The results indicate that observation 6 is true but the influence of the mass and CG position on the roll rate is moderate. In case the Fuji is nose heavy and / or light additional complete turns are experienced during a spin compared to other values of mass and CG positions.

Designers:

When expecting higher roll rates – due to forward CG positions or light aeroplane masses - higher structural stresses can be expected. These need to be taken into consideration during the design phase of a low-wing, single-engine aircraft which needs to be certified and operated in spin manoeuvres.

Flight Testers:

The findings help for spin prediction and thus the spin test matrix can shrink down to a lower number of potentially high risk trials.

Pilots and Flying Instructors:

As Figure 6.47 in section 6.9 indicates there is only a moderate dependency of 35.3% of the CG shift on the roll rate. Nose-heavy aeroplanes with a similar geometry roll faster than aeroplanes with an aft CG position. This has the potential to confuse and disorientate pilots when entering a spin accidentally. Spin demonstrations should not be conducted with a loading condition which can result in potentially rapid roll rates. By shifting the CG position

from aft to forward positions, flying instructors can use during spin training, a gradual approach for spin training.
A similar dependency (36.5%) can be found for aeroplane mass changes (see Figure 6.49). Heavy aeroplanes of a similar geometry, roll slower than light ones. The effects on pilots or flight training situations are the same as due to CG shifts.

8.1.7 Observation 7: Total Angular Velocity Ω changes with CG position and mass

See section 6.10.

Observation 7 is true. Total angular velocity is one of the main parameters of spinning and it is shown here that it is strongly influenced by the CG position (95%, the highest found during this project). The influence of the mass is lower (52%) but still an important factor for this parameter.

Designers:
As in some observations described above, higher turn rates and thus higher angular accelerations need to be taken into account when designing the structure of an aeroplane such as the Fuji-200-160. For mathematical spin modelling (including flight simulation software), real flight test data provides useful information to develop and validate the models.

Flight Testers:
The safety of the aeroplane is improved as the total angular velocity decreases due to the mass increasing and / or the CG position moving aft, thus reducing the chances of the test pilot becoming disorientated. The addition of a section in Pilot Operating Handbooks with advice and procedures on the total angular velocity behaviour across the flight envelope would be a valuable and new contribution. For example a table of the values for Ω as a function of the values of the mass and CG position, would be of practical use for Test Pilots.

Pilots and Flying Instructors:
The most important contribution from this finding to the flight training and piloting sector is that the measured and proven data taken during this research project are in contrast to the current flight training literature. The reason and history of that contradiction cannot be traced back even after reviewing a major part of the spin relevant literature. The flight training material does not refer to any scientific or flight test sources which have been based on data which have been determined systematically.

As Figure 6.52 shows, the Fuji FA – 200-160 has a higher value for Ω with a forward CG position. The likelihood for a pilot to become disorientated during such a spin is very high, especially if a pilot enters a spin accidentally.
The mass change influences Ω moderately (see Figure 6.54). A lighter weighted Fuji will develop faster spins (around 12% difference of the Ω values) than when heaviest. This can again support a pilot's spatial disorientation. A cross-coupling of both parameters also shows 95% dependency (see Figure 6.56) that shows the dominance of the CG position.
These findings need to be integrated into flight training sorties. Flying instructors should be trained to understand and integrate this into risk analysis measures (e.g. within Safety Management Systems (SMS) of a Flight Training Organisation) and actual flight preparations.

8.1.8 Observation 8: Recovery time becomes shorter with CG moving backwards

See section 6.11

Observation 8 is true.

Designers:
The observation indicates that the aeroplane's mass and CG position can be used to influence the spin recovery and thus the corresponding height loss, which is a major contribution to flight safety. The information from this finding can be used to design an aircraft for precise manoeuvres in spin recovery and this is useful in designing many types of aircraft. E.g. in aerobatic manoeuvres, spin recovery needs to be precise because the aircraft must achieve a specific pre-agreed heading (i.e. away from crowds). If for such a case the numbers of turns (the turn angle) for recovery is known or can be adjusted by an aeroplane mass and CG position combination, a pilot can easily start the spin recovery at a specific heading angle before the target direction is reached.

Flight Testers:
Flight testers are especially interested in the recovery behaviour of a spinning aeroplane which is operated under trial conditions. With the finding related to this observation, a spin test programme should be started with medium values for the CG position and the aeroplane's mass because in this configuration a potential unrecoverable flat spin, as well as extended recovery times due to high turn rates, can be avoided. This understanding is a strong, new contribution to the flight safety during spin trials.
One major requirement of certification specifications is the number of turns an aeroplane needs until the spin has finally stopped and thus recovered. The finding assists the flight tester in that the flight recovery times across the whole envelope can be estimated from only

a few known points in the envelope, hence potentially reducing the number of required spin runs in the spin test programme.

Pilots and Flying Instructors:

The corresponding data analysis using this observation shows that a CG position shift to the back of an aeroplane leads to a shorter recovery time. These findings are contrary to the literature published on this topic.

Spin recovery needs to be most effective and should take as little time as possible. Height losses, potential pilot's disorientation, etc. should be avoided. Taking this into account flying the Fuji with aft – or at least medium - CG positions are a direct contribution to spin flight safety. In some of the observations above it has been discussed that forward CG positions are increasing the turn rates of an aeroplane during a spin. These findings support the longer spin recovery time with forward CG position because the rotational energy of the aeroplane is higher when the turn rate is higher.

8.1.9 Observation 9: The spin behaviour of the Fuji FA 200 – 160 can be generalised for single-engine low-wing aeroplanes

See section 6.12

Observation 9 is true. It was found that two other sources in the literature provided time dependent results of a low-wing, single-engine aircraft similar to the Fuji. These results were compared, wherever possible, for the 3 aircraft. It was found that the qualitative behaviour was similar for variation of pitch angle, angle of attack, sideslip angle, roll rate, yaw rate and pitch rate. For all three aircraft a pitch angle limit value of -47° has been obtained. Since the Fuji shows fairly repeatable behaviour during a spin it is expected that this behaviour is typical of the aircraft in the same category and thus that can be generalised. In addition, those observations above that are true, are also likely to be generalisable for the same category as the Fuji.

8.2 Publications

1.) S.H. Schrader, J. Hoffmann, C.A. Toomer, 2013: ‘Flight physical model of the spin dynamic of single engine aeroplanes’. Lecture at the international scientific conference ’New technologies of the Knowledge intensive Engineering: Priorities of development and training’ at the Kasan National Technical Research University ‘A.N. Tupolev’ (KAI), Nabereschnyje Tschelny, 16 – 17 May 2013. Proceeding, p. 175 – 180. ISBN 987-5-7579-1878-5.

2.) S.H. Schrader, J. Hoffmann, C.A. Toomer, T. Luo, J. Kuenzer, P. Cheng, 2013, Flugphysikalische Modell der Trudeldynamik von einmotorigen Flugzeugen, Doktoranden – Symposium at the Osnabrueck University of Applied Sciences

3.) S.H. Schrader, J. Hoffmann, C.A. Toomer, T. Luo, J. Kuenzer, P. Cheng, 2013, Improvement of spin flight test quality by the evaluation of measured data‘. International scientific conference of quality control. State University for Mechanical Engineering Moscow, 20 – 21 November 2013, Proceeding p. 87 – 93. ISBN 978-5-94099-126-7

4.) S.H. Schrader, J. Hoffmann, C.A. Toomer, T. Luo, J. Kuenzer, P. Cheng, 2014, **‘**Measured data acquisition and evaluation for improvement of spin flight test quality’. Lecture at the international scientific conference ’New technologies of the Knowledge intensive Engineering: Priorities of development and training’ at the Kasan National Technical Research University ‘A.N. Tupolev’ (KAI), Nabereschnyje Tschelny

5.) S.H. Schrader, J. Hoffmann, C.A. Toomer, T. Luo, J. Kuenzer, P. Cheng, 2014, ‘Evaluation of single-engine Aeroplane Spinning by measured data and the use of CFD’. In: RAeS Advanced Aero Concepts, Design and Operations, Bristol, UK, 22 – 24 July 2014. London: Royal Aeronautical Society. Available from: http://eprints.uwe.ac.uk/26799

6.) S.H. Schrader, C.A. Toomer, J. Hoffmann, J. Biermann, 2018, Spin dynamic of single-engine low-wing aeroplanes, Royal Aeronautical Society Applied Aerodynamics Conference, Bristol

q.e.d. (■) and what have been shown

Chapter 9 Recommendations for further work

As this research project is opening up an entire field of flight mechanics research on a modern level with a combination of mathematical (theoretical) and measurement (practical) methods which have not been utilised for spin research, the work at hand finishes with more questions than answers. Due to this, only the main areas for recommendations are mentioned as every below mentioned field includes much more detailed and specific opportunities for research.

To refine the understanding of aeroplane spinning, more aeroplanes with different geometries (e.g. high wing, canard configuration, biplane, twin-engine) need to be taken into a similar research project to gain more flight test data which can be used for analysis to develop more accurate, comprehensive and complete systems of spin modelling and spin characteristic prediction.

Towards this aim, more parameters should be measured and analysed, such as forces of the control surfaces (elevator, aileron, rudder), detailed fuel behaviour (sloshing in non-linear conditions), changing aeroplane geometries like variable control surface deflections or flap position changes during a spin run, gear retractions or extensions, power changes during a spin run, lateral Centre of Gravity changes due to asymmetrical fuel distributions or external loads, high altitude spins with different atmospheric damping, etc. Also the field of inverted spins has not been fully investigated. As well as single parameter effects on spin behaviour, the combinations of spin parameter effects also should be investigated.

As this kind of research and the corresponding flight tests involve a certain higher level of risk it is of paramount importance to reach a full understanding of spinning. To achieve this flight test data are needed to prove the mathematical models against real flight test data. For that it is important to develop methods to reduce the noise in the data sets. Also an even more sophisticated measurement system needs to be developed than that currently available (including measurement of 3-D fuel sloshing).

In addition to these aspects, aeroelastic effects need to be implemented into the field of spin research because so far in spin research, the aeroplane has been treated as a rigid body without any structural deformation due to the airflow.

Research for an advancement of Computational Fluid Dynamics methods for the correct simulation of spin and stall flow conditions needs to be developed.

On the topic of mathematical models, spin warning systems, automated spin prevention or even spin recovery systems can be developed which can take over the aeroplane within a critical flight situation e.g. in clouds or low visibility weather conditions.

With a deeper understanding of spinning, spin training or spin avoidance training needs to be implemented into pilot training so that the actual number of spin accidents during normal aeroplane operation or within certification flight testing can be reduced significantly. This should be done in collaboration with the European and / or U.S. Aviation Authorities to implement the results into the current regulations and pilot training requirements.

Such a spin or spin avoidance training can be supported with the help of spin simulators. Flight simulation is based on mathematical – flight mechanics models, which today do not include spin simulation capabilities. Improvements in the mathematical modelling of spin would thus improve the fidelity of flight simulators.

In addition to that, the current CS 23 regulation can be improved and re-written on the basis of detailed spin knowledge to achieve a more differentiated regulation for different aeroplane types.

A detailed source of spin information – like a free access online library – needs to be implemented with a ‘comment tool’ for other flight testers and researches to gather professional spin data, information, experience and scientific results / papers to distribute those essential information into the flight test community. Further and more detailed recommendations for aeroplane designers, general pilots, flying instructors, test pilots and flight test engineers can be extracted from such a tool to significantly increase flight safety.

With a deeper knowledge other scientific disciplines need to be integrated into this topic, e.g. psychology and aero-medicine. Here e.g. changes of turning rates or accelerations, recovery times, etc. are of particular interest as they are interfering with human performance.

Chapter 10 References and Bibliography

10.1 References

Adams, W.M. Jr., 1972. Analytic Prediction Of Airplane Equilibrium Spin Characteristics, Langley Research Center

Air Ministry, 1995. AP 3456 Royal Air Force Manual of Flying, Training Group Defence Agency

Ambros, G. Seidler, F., 2003. 'Trudeln mit Segelflugzeugen' (not discussed in Literature Review)

Anderson, S.B., Enevoldson, E.K., Nguyen, L.T., 1983. Pilot Human Factors in Stall/Spin Accidents of Supersonic Fighter Aircraft, Langley Research Center

BBC, 1986, Documentary 'Test Pilot', British Broadcasting Company

Belcastro, C., Foster, J.V., 2009. Aircraft Loss-of-Control Accident analysis, NASA, https://ntrs.nasa.gov/archive/nasa/casi.ntrs.nasa.gov/20100030600.pdf (last accessed 03.02.2019)

Berlin Flight Training, 2005. PPL Aerodynamic, Grundbegriffe des Fliegens, Abschnitt 15

Berman, T., 1950. Comparison Of Model And Full-Scale Spin Test Results For 60 Airplane Designs, National Advisory Committee for Aeronautics

BFU, 1985. Sind Stallübungen aus der Mode gekommen? Luftfahrt – Bundesamt

BFU, 1986. Alle Jahre wieder – VFR-Flug bei schlechtem Wetter, Flugunfalluntersuchungsstelle beim Luftfahrt – Bundesamt, https://www.bfu-web.de/DE/Publikationen/Flugunfallinformationen/Berichte/V57%20-%20Flugunfallinfo%20VFR-Flug.pdf?__blob=publicationFile (last accessed, 03.02.2019)

Biermann, J., 2015, Personal Communication.

Bowman, J.S. Jr., 1965. Airplane Spinning, NASA Langley Research Center

Bowman, J.S. Jr., 1971. Summary Of Spin Technology As Related To Light General – Aviation Airplanes, Langley Research Center

Brinkworth, B.J., 2014. On the Early History of Spinning and Spin Research in the UK, Part 1: The period 1909 – 1929

Brinkworth, B.J., 2015. On the Early History of Spinning and Spin Research in the UK, Part 2: The period 1930 – 1940

Brown et al., 2002. Flying Qualities Testing, US Air Force Flight Test Center

Chelette, T.L., Repperger. D.W., Albery, W.B., 1990. A Spatial Disorientation Preditor Device To Enhance Pilot Situational Awareness Regarding Aircraft Attitude', Harry G. Armstrong Aerospace Medical Research Laboratory

Cichocka, E., 2017. Research on light aircraft spinning properties, The Centre of New Technologies, Institute of Aviation, Warsaw, Poland

Cremer, M., 2016a. Datenblatt iVRU-FQ, messWERK GmbH

Cremer, M., 2016b. Datenblatt messRechner mR11, messWERK GmbH

Cremer, M., 2016c. Datenblatt messWERK Messkopf mit Windfahne und Thermometer, messWERK GmbH

Cremer, M., 2016d. Datenblatt Seilzugpotentiometer: Micro-Epsilon WPS 30 MK, messWERK GmbH

Cremer, M., 2016e. Datenblatt Differenzdrucksensor Setra 239, messWERK GmbH

Cremer, M., 2016f. Datenblatt Absolutdrucksensor Setra 270, messWERK GmbH

Cremer, M., 2016g. Einbaubeschreibung Dok.-Nr. mW-TFF-2014-01, Messwerk GmbH

EASA, 2011a. Verordnung (EU) Nr. 1178/2011 der Kommission, FCL.820: Testflugberechtigung

EASA, 2011b. Commission Regulation (EU) No 1178 /2011 (Part FCL), Official Journal of the European Union

EASA, 2012. Certification Specification for Normal, Utility, Aerobatic, and Commuter Category Aeroplanes (CS-23), Amendment 3, European Aviation Safety Agency

FAA, 2004. Airplane Flying Handbook, Chapter 4 Slow Flight, Stalls, and Spins, U.S. Department of Transportation, Federal Aviation Administration

FAA, 2008. Pilot´s Handbook of Aeronautical Knowledge, Chapter 4 Aerodynamics of Flight, U.S. Department of Transportation, Federal Aviation Administration

FAA, 2011. Flight Test Guide For Certification Of Part 23 Airplanes, U.S. Department of Transportation, Federal Aviation Administration

FAA, 2017. FAR Federal Aviation Regulations, Part 23 Airworthiness Standards: Normal, Utility, Acrobatic and Commuter Category Airplanes, U.S. Department of Transportation, Federal Aviation Administration

Forsythe, J.R., Squires, K., Wurtzler, K.E., & Spalart, P.R. et al, 2002. Detached-eddy simulation of fighter aircraft at high alpha, 40th AIAA Aerospace Sciences Meeting & Exhibit, Reno, USA

Fuji Heavy Industries, 1971. Service Manual, Fuji FA 200 – 160

Fuji Heavy Industries, 2011. Airplane Flight Manual, Fuji FA 200 – 160

Gates, S.B. & Bryant, L.W., 1926. The Spinning of Aeroplanes. ACA R&M 1001

Gobeltz, J., 1959. Development Of Spin Testing Technique As A Function Of Spin Of Modern Aircraft, Institut de Mécanique des Fluides de Lille (France)

Goraj, Z., Baron, A., Kacprzyk, J., 2002. "Dynamics of a light aircraft in spin", Aircraft Engineering and Aerospace Technology, Vol. 74 Issue: 3, pp.237-251, https://doi.org/10.1108/00022660210427422

Hoff, R.I., Gratton, G.B., 2012. Camera Tracking And Qualitative Airflow Assessment Of A Two-Turn Erect Spin, RAeS

Jansson, J., Krishnasamy, E., Leoni, M., Jansson, N., & Hoffman, J., 2018. Time-resolved Adaptive, Direct FEM, Simulation of High-Lift Aircraft, Numerical Simulation of the Aerodynamics of High-Lift Configurations, pp 67-92, Springer

Johnson, A.E., 1971. A Literature Survey Of The Problem Of Aircraft Spins, Naval Postgraduate School

Kimberlin, R.D., 2003. Flight Testing of Fixed-Wing Aircraft, AIAA Education Series

Kredel, H., 1998. Aerodynamik Version 2.0, Civil Aviation Training GmbH

Kwatny, H.G., Dongmo, J.-E. and Chang, B.C., 2009. 'Aircraft Accident Prevention: Loss-of-Control Analysis', NASA LRC (not discussed in Literature Review)

Lawless, A. et al, 1999. Spins, National Test Pilot School

Lindemann, F.A., Glauert, H. and Harris, R.G., 1918. The Experimental and Mathematical Investigation of Spinning, ACA R&M 411

Martin, C., 1988. The Spinning Of Aircraft – A Discussion Of Spin Prediction Techniques Including A Chronological Bibliography, Defence Science and Technology Organisation Aeronautical Research Laboratory, Melbourne

Moens, F., Perraud, J., Knumbein, A., Toulorge, T., Lannelli, P., Eliasson, P., & Hanifi, A., 2007. Transition Prediction & impact on 3D high-lift wing configuration, 25th AIAA Applied Aerodynamics Conference, AIAA 2007-4302

Neihouse, A.I., Klinar, W.J., Scher, S.H., 1957. Status Of Spin Research For Recent Airplane Designs, Langley Research Center

Neumann, H., 2002. Personal Conversation

Neumann, H., 2003. Flugerprobung, Kapitel 16, NN

Pamadi, B.N., 2004. Performance, Stability, Dynamics and Control of Airplanes, AIAA Education Series

Pätzold, F., Rausch, T., 2013. Sicherheitsaspekte des “Spin Resistant”-Konzeptes für einmotorigen Leichtflugzeuge, Technische Universität Braunschweig

Rahman, H., Khushnood, S., Raza, A. & Ahmad, K., 2013. Experimental & computational investigation of delta wing aerodynamics. Proceedings of the 10th International Bhurban Conference in Applied Sciences and Technology

Ranaudo, R.J., 1977. Exploratory Investigation Of The Incipient Spinning Characteristics Of A Typical Light General Aviation Airplane, Lewis Research Center

Ray, S.G. & Ballmann, J., 2018. An efficient and reliable numerical model to simulate flow over a high lift configuration, Fluid Mechanics Research International Journal, Vol.2, No.5.

Riley, D.R., 1985. Simulator Study of the Stall Departure Characteristics of a Light General Aviation Airplane With and Without a Wing-Leading-Edge Modification, Langley Research Center

Schrader, S.H., Hoffmann, J., Toomer, C.A. , Luo, T., Kuenzer, J. , Cheng, P., 2013. Improvement of spin flight test quality by evaluation of measured data, Control over Quality Conference, Moscow State University of Mechanical Engineering (not discussed in Literature Review)

Schrader, S.H., Hoffmann, J., Toomer, C.A. , Luo, T., Kuenzer, J. , Cheng, P., 2014. Evaluation of Single Engine Aerospace Spinning by Measured data and the Use of CFD, Royal Aeronautical Society Applied Aerodynamics Conference, Bristol (not discussed in Literature Review)

Seidman O., Donlan C.J.,1939. An Approximate Spin Design Criterion for Monoplanes, Technical Notes, National Advisory Committee for Aeronautics No. 711

Sliwa, S.M., 1979. Some Flight Data Extraction Techniques Used on a General Aviation Spin Research Aircraft, Langley Research Center

Soulé, H. A., Sudder, N. F., 1931. A Method Of Flight Measurement Of Spin, National Advisory Committee for Aeronautics

Stewart, E.C. et al., 1982. Spin Tests of a Single-Engine, High-Wing Light Airplane, Langley Research Center

Stough, H.P. III, DiCarlo, D.J., Patton, J.M. Jr., 1985. Flight Investigation of Stall, Spin, and Recovery Characteristics of a Low-Wing, Single-Engine, T-Tail Light Airplane, Langley Research Center

Stough, H.P. III, DiCarlo, D.J., Patton, J.M. Jr., 1987a. Flight Investigation of the Effects of an Outboard Wing-leading-Edge Modification on Stall/Spin Characteristics of a Low-Wing, Single-Engine, T-Tail Light Airplane, Langley Research Center

Stough, H.P. III, Patton, J.M. Jr., Sliwa, S.M., 1987b. Flight Investigation of the Effect of Tail Configuration on Stall, Spin, and Recovery Characteristics of a Low-Wing General Aviation Research Airplane, Langley Research Center

Woodcock, R.J. & Weissman, R., 1976. Stall/Spin Problems of Military Aircraft, AGARD AD A029 071 U.S. Department of Commerce, National Technical Information Service

10.2 Bibliography

Cook, M.V., 2007. Flight Dynamics Principles, Elsevier

Crawford, unknown. Flight Ground School, Chapter 10 Spins, Flight Emergency & Advanced Maneuvers

Cremer, M.C., Hanks, R. et al, 2007. Investigation of the technical feasibility and safety Benefit of a light aeroplane Flight Data Monitoring (FDM) system (Research Project EASA.2007/2), Messwerk and Technische Universität Braunschweig

Cremer, M.C., Hanks, R. et al, 2008. Safety Aspects of Light Aircraft Spin Resistance Concept Research Project EASA 2008/03), Messwerk and Technische Universität Braunschweig

Denham, C, & Owens, D.B., 2016. Rotary Balance Wind Tunnel Testing for the FASER Flight Research Aircraft

EASA, 2003. Certification Specifications for Normal, Utility, Aerobatic, and Commuter Category Aeroplanes CS-23 (issued 14.11.2003)

EASA, 2010. Certification Specifications for Normal, Utility, Aerobatic, and Commuter Category Aeroplanes CS-23 Amendment 2, § CS 23.221 Spinning

EASA, 2015. Verordnung (EU) 2015/1039 der Kommission, Appendix XII: Testflugkategorien und zugehörige Qualifikationen von Testflugbesatzungen, Abs. C. Testflugkategorien (issued 30.06.2015)

Experimental, 2016. Stalling Effects, Spinning, www.experimentalaircraft.info/flight-planning/aircraft-stall-effect-1.php, last accessed 08.10.2016

FAA, 2004. Airplane Flying Handbook, U.S. Department of Transportation, Federal Aviation Administration, Airman Testing Standards Branch, FAA-H8083-3A. Oklahoma City (USA), pp. 4-1 to 4-16

Hoff, R. I., 2014. The Aeroplane Spin Motion and an Investigation into Factors Affecting The Aeroplane Spin, Brunel University London, College of Engineering, Design and Physical Sciences. Dissertation

Lawford, J.A., Nippress, K.R., 1984. Calibration of Air-Data Systems and Flow Direction Sensors, North Atlantic Treaty Organization, AGARD (Advisory Group for Aerospace Research and Development, AGARD AG-300 – Vol.1

Lawless, A., Stanko, D., 2007. Angle of Attack and Sideslip Vane Calibration, Society of Flight Test Engineers

NASA, 2016. Wind Tunnels at NASA Langley Research Center from NASA http://www.nasa.gov/centers/langley/news/factsheets/windtunnels.html , (02.11.2016)

NASA, 2016. NASA Loves Sending Spacecraft Into Wild Tumbles in This Spin Tunnel, gizmodo http://gizmodo.com/nasa-loves-sending-spacecraft-into-wild-tumbles-in-this-1730647894 , (05.11.2016)

NASA, 2016. Experiments Result in Safer, Spin-Resistant Aircraft https://spinoff.nasa.gov/Spinoff2013/t_1.html , (05.11.2016)

NTPS, 1991. Flying Qualities Flight Testing Phase, Vol.2, Chapter 10, High Angle of Attack, Mojave, National Test Pilot School

Scudder, N. F., 1934. A Flight Investigation of the Spinning of the NY-1 Airplane with varied Mass Distribution and other Modifications, and an Analysis based on Wind-Tunnel Tests, Langley Memorial Aeronautical Laboratory Hampton (USA), pp. 37 – 42

Seidman, Oscar; and Neihouse, A. I.: Free-Spinning Wind-Tunnel Tests of a Low-Wing Monoplane With Systematic Changes in Wings and Tails. IV. Effect of Center-of-Gravity Location. NACA Rep. 672, 1939

Sohi, N.P. Modeling of spin modes of supersonic aircraft in horizontal wind tunnel, ICAS, 2004. http://icas.org/icas_archive/icas2004/papers/025.pdf

Stephen J. Gill, Mark H. Lowenberg, Simon A. Neild, Luis G. Crespo, Bernd Krauskopf, and Guilhem Puyou. "Nonlinear Dynamics of Aircraft Controller Characteristics Outside the Standard Flight Envelope", Journal of Guidance, Control, and Dynamics, Vol. 38, No. 12 (2015). pp. 2301-2308. https://doi.org/10.2514/1.G000966

Stowell, R., 1996. Emergency Maneuver Training – Controlling Your Airplane During A Crisis, Chapter 7: Spins. Venture (USA)

USAF, 1997. Performance Phase Textbook, Vol. 1. Edwards Air Force Base, USAF Test Pilot School

USAF, 1997. Performance Phase Textbook, Vol. 2. Edwards Air Force Base, USAF Test Pilot School

USAF, 1997. Performance Phase Textbook, Vol. 3. Edwards Air Force Base, USAF Test Pilot School

USAF, 1998. Test Management Phase Planning Guide. Edwards Air Force Base, USAF Test Pilot School

USAF, 1999. Modeling and Simulation. Edwards Air Force Base, USAF Test Pilot School

USAF, 2000. Flying Qualities Testing, Part I, Chapter 1: Introduction, Edwards Air Force Base, USAF Test Pilot School

USAF, 2000. Flying Qualities Testing, Part I, Chapter 2: Vectors, Matrices, and Linear Systems, Edwards Air Force Base, USAF Test Pilot School:

USAF, 2000. Flying Qualities Testing, Part I, Chapter 3: Differential Equations and Transfer Functions. Edwards Air Force Base, USAF Test Pilot School

USAF, 2000. Flying Qualities Testing, Part II, Chapter 4: Building the Equation of Motion. Edwards Air Force Base, USAF Test Pilot School

USAF, 2000. Flying Qualities Testing, Part II, Chapter 5: Solving the Equation of Motion. Edwards Air Force Base, USAF Test Pilot School

USAF, 2000. Flying Qualities Testing, Part II, Appendix 5A: A Longitudinal and Lateral-Directional Simulator. Edwards Air Force Base, USAF Test Pilot School

USAF, 2000. Flying Qualities Testing, Part II, Chapter 6: Introducing the Flying Qualities Military. Edwards Air Force Base, USAF Test Pilot School

USAF, 2000. Flying Qualities Testing, Part II, Chapter 7: Stability Derivatives. Edwards Air Force Base, USAF Test Pilot School

USAF, 2000. Flying Qualities Testing, Part II, Chapter 8: Unaugmented Trim and Stability. Edwards Air Force Base, USAF Test Pilot School

USAF, 2000. Flying Qualities Testing, Part III, Chapter 9: Fundamentals of Flight Control Systems. Edwards Air Force Base, USAF Test Pilot School

USAF, 2000. Flying Qualities Testing, Part III, Chapter 10: The Root Locus Method. Edwards Air Force Base, USAF Test Pilot School

USAF, 2000. Flying Qualities Testing, Part III, Chapter 11: Frequency Response. Edwards Air Force Base, USAF Test Pilot School

USAF, 2000. Flying Qualities Testing, Part III, Chapter 12: Frequency Content, Filters, and Aliasing. Edwards Air Force Base, USAF Test Pilot School

USAF, 2000. Flying Qualities Testing, Part III, Chapter 13: Structural Coupling and Rigid Body Limit Cycle. Edwards Air Force Base, USAF Test Pilot School

USAF, 2000. Flying Qualities Testing, Part III, Chapter 14: Fundamental Features of Flight Control Systems. Edwards Air Force Base, USAF Test Pilot School

USAF, 2000. Flying Qualities Testing, Part III, Chapter 15: Digital Flight Control Systems. Edwards Air Force Base, USAF Test Pilot School

USAF, 2000. Flying Qualities Testing, Part III, Chapter 16: Handling Qualities Design Guidance. Edwards Air Force Base, USAF Test Pilot School

USAF, 2000. Flying Qualities Testing, Part III, Chapter 17: Introducing the Military Specification for Flight Control Systems. Edwards Air Force Base, USAF Test Pilot School

USAF, 2000. Flying Qualities Testing, Part IV, Chapter 18: The Flight Control System Design Problem. Edwards Air Force Base, USAF Test Pilot School

USAF, 2000. Flying Qualities Testing, Part IVa, Chapter 19: Configuration for Flying Qualities Model Validation Testing. Edwards Air Force Base, USAF Test Pilot School

USAF, 2000. Flying Qualities Testing, Part IVa, Chapter 20: Flying Qualities Flight Test Simulators. Edwards Air Force Base, USAF Test Pilot School

USAF, 2000. Flying Qualities Testing, Part IVa, Chapter 21: Handling Qualities. Edwards Air Force Base, USAF Test Pilot School

USAF, 2000. Flying Qualities Testing, Part IVa, Chapter 22: Pilot Evaluation of Handling Qualities. Edwards Air Force Base, USAF Test Pilot School

USAF, 2000. Flying Qualities Testing, Part IVa, Chapter 22 A: Cooper-Harper Report. Edwards Air Force Base, USAF Test Pilot School

USAF, 2000. Flying Qualities Testing, Part IVa, Chapter 22 B: Analog Scales for Evaluating Handling Qualities. Edwards Air Force Base, USAF Test Pilot School

USAF, 2000. Flying Qualities Testing, Part IVa, Chapter 23: Handling Qualities Stress Testing. Edwards Air Force Base, USAF Test Pilot School

USAF, 2000. Flying Qualities Testing, Part IVa, Chapter 24: Aerodynamic Model Validation Testing. Edwards Air Force Base, USAF Test Pilot School

USAF, 2000. Flying Qualities Testing, Part IVa, Chapter 25: Frequency Response Estimation. Edwards Air Force Base, USAF Test Pilot School

USAF, 2000. Flying Qualities Ground Testing, Part IVb, Chapter 26: Flight Control System Verification and Validation Ground Testing. Edwards Air Force Base, USAF Test Pilot School

USAF, 2000. Flying Qualities Ground Testing, Part IVb, Chapter 27: Taxi Testing. Edwards Air Force Base, USAF Test Pilot School

USAF, 2000. Flying Qualities Flight Testing, Part IVc, Chapter 28: First Flight Flying Qualities Testing. Edwards Air Force Base, USAF Test Pilot School

USAF, 2000. Flying Qualities Flight Testing, Part IVc, Chapter 29: Flying Qualities Envelope Expansion Testing. Edwards Air Force Base, USAF Test Pilot School

USAF, 2000. Flying Qualities Flight Testing, Part IVc, Chapter 30: Handling Qualities Flight Test. Edwards Air Force Base, USAF Test Pilot School

USAF, 2000, Flying Qualities Flight Testing, Part IVc, Chapter 31: Stall, Departure, and Spin Test, Edwards Air Force Base, USAF Test Pilot School

USAF, 2000. Flying Qualities Flight Testing, Part IVc, Chapter 32: Failure State Testing. Edwards Air Force Base, USAF Test Pilot School

USAF, 2000. Flying Qualities Flight Testing, Part IVc, Chapter 33: One-Flight Flying Qualities Evaluation. Edwards Air Force Base, USAF Test Pilot School

USAF, 2000. Aerodynamics. Edwards Air Force Base, USAF Test Pilot School

USAF, 2000. Aircraft Performance. Edwards Air Force Base, USAF Test Pilot School

USAF, 2001. Performance Phase Planning Guide. Edwards Air Force Base, USAF Test Pilot School

USAF, 2002. TPS Data Reduction Handbook. Edwards Air Force Base, USAF Test Pilot School

USAF, 2002. Flying Qualities Phase Planning Guide. Edwards Air Force Base, USAF Test Pilot School

US-NAVY, 1997. Flight Test Manual, Chapter 3 Spins. Patuxent River, U.S. Naval Test Pilot School

Valentine, B.L., 1997. Safety Recommendation (PA 38 spin accident report), National Transportation Safety Board

Zimmerman, C.H.,1936, Effect of Changes in Tail Arrangement Upon the Spinning of a Low-Wing Monoplane Model, NACA TN 570.

Appendices

Appendix 1a General understanding of spinning

Spinning is a complex motion which is a complicated subject to make generalizations which are valid for all aeroplanes. A specific type of aeroplane may behave in a certain way whereas another type behaves entirely different under the same conditions. This section describes the general understanding for intended, erect spins of aeroplanes with a conventional design, i.e. no Canard or three wing configurations.

The open literature on flight training purposes contains little information on spinning. The British Royal Airforce's flight training manual (Air Ministry, 1995) contains by far the most detailed explanation of spinning apart from literature written for test pilots or flight test engineers training - which is not meant for standard flight training situations. This source has been used for the definitions presented below.

A1.1 Phases of a Spin

A spin can be divided into three phases:

a. Incipient spin
b. Developed spin
c. Recovery

For the initiation of a spin the aerodynamic phenomenon of autorotation is imperative. This will lead to an unsteady manoeuvre which is a combination of a ballistic path of the aeroplane and an increasing angular velocity which is generated by an auto-rotative rolling moment and a drag-induced yawing moment. This phase will last for approximately 2-6 turns before the aeroplane settles into a stable spin. During a stable or steady spin a sideslip and a rotation about all three axes is present. Without suggesting that all aeroplanes can achieve a steady spin, a stable spin is defined by a steady rate of rotation and a steady rate of descent. Spin recovery is initiated by a pilot using control inputs which aim at first opposing the autorotation and then reducing the angle of attack (α) to un-stall the aerofoils. The aeroplane will be in an almost vertical dive from which recovery is possible by applying elevator deflection.

A1.2 The Steady Erect Spin

While rotating to one direction the aeroplane describes a ballistic trajectory which depends on the entry manoeuvre. For the pilot this is an unsteady, oscillatory motion until the aeroplane reaches a stable spin about the spin axis. The stable spin will occur when aerodynamic and inertia forces and moments achieve a state of equilibrium. The aeroplane's attitude at this phase depends on the geometry of the aeroplane, the position of the flight control and the distribution of the mass within the aeroplane.

A1.3 Motion of the aeroplane

The motion of the aeroplane and thus of its centre of gravity (CG) in a spin has two components:

a. A vertical linear velocity (rate of descent = V [feet per second])

b. An angular velocity, Ω (radians/sec) about a vertical axis (spin axis). The distance between the CG and the spin axis is the radius of the spin (R) and is normally small (about a wing semi-span)

The combination of these motions result in a vertical spiral or helix. The helix angle is small, usually less the 10°. Figure A1.1 shows the motion of an aeroplane in a spin. As the aeroplane presents always the same face to the spin axis, it follows that it must be rotating about a vertical axis passing through the centre of gravity (CG) at the same rate as the CG about the spin axis. This angular velocity may be resolved into components of roll, pitch and yaw with respect to the aeroplane's body axes. In the spin illustrated in Figure A1.1b the aeroplane is rolling to the right, pitching up and yawing to the right. For convenience the direction of the spin is defined by the direction of the yaw.

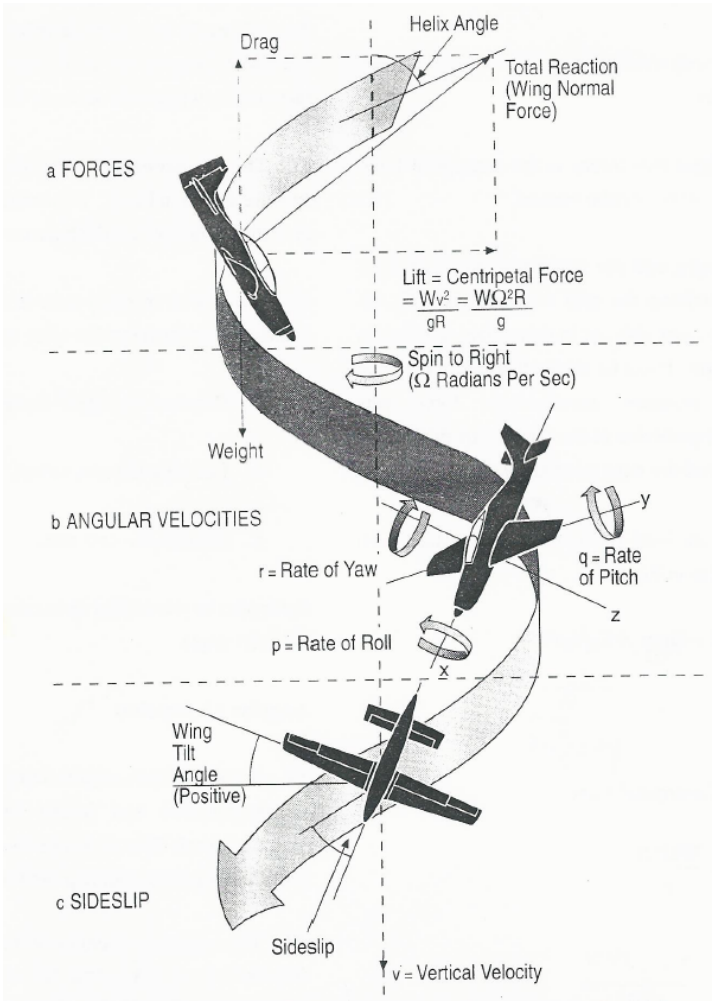

Figure A1.1: Motion of an aeroplane in an erect spin to the right (Air Ministry, 1995)

AXIS (Symbol)	LONGITUDINAL(x)	LATERAL (y)	NORMAL (z)
Positive Direction	Forwards	To right	Downwards
ANGULAR VELOCITY			
Designation	Roll	Pitch	Yaw
Symbol	p	q	r
Positive Direction	to right	nose-up	to right
MOMENTS OF INERTIA	A	B	C
MOMENTS			
Designation	rolling moment	pitching moment	yawing moment
Symbol	L	M	N
Positive Direction	to right	nose-up	to right

Table A1.1: Sign conventions used in the thesis, (Air Ministry, 1995)

In order to understand the relationship between the angular velocities and the aeroplane's attitude (note the sign conventions given in Table A1.1), it is useful to consider three limiting cases:

a. Longitudinal Axis Vertical: when the longitudinal axis is vertical the angular motion will be all roll
b. Lateral Axis Vertical: For the aeroplane to present the same face (pilot´s head) to the spin axis, the aeroplane must rotate about the lateral axis. The angular motion is all pitch
c. Normal Axis Vertical: For the aeroplane to present the same face (inner wing tip) to the axis of rotation, the aeroplane must rotate about the normal axis at the same rate as the aeroplane rotates about this axis of rotation. Thus the angular motion is all yaw.

Although these are hypothetical examples which may not be possible in practice, they illustrate the relationship between aeroplane attitude and angular velocities. Between the extremes quoted above the motion will be a combination of roll, pitch and yaw, and depends on:

a. The rate of rotation of the aeroplane about the spin axis
b. The attitude of the aeroplane, which is usually defined in terms of the pitch angle and the wing tilt angle. Wing tilt angle, often confused with bank angle, involves displacement about the normal and the longitudinal axes

The aeroplane´s attitude in the spin has an important effect on the sideslip (Figure A1.1c). If the wings are level, there will be outward sideslip; i.e. the relative airflow will be from the direction of the outside wing (to the right (port) in the diagram). If the attitude of the aeroplane is changed such that the outer wing is raised relative to the horizon, the sideslip is reduced. This attitude change can only be due to a rotation of the aeroplane about the

normal axis. The angle through which the aeroplane is rotated, in the plane containing the lateral and longitudinal axes, is known as the wing tilt angle and is positive with the outer wing up. If the wing tilt can be increased sufficiently to reduce the sideslip significantly, the pro-spin aerodynamic rolling moment will be reduced.

A1.4 Balance of Forces in the Spin

Only two forces are acting on the CG while it moves along its helical path (Figure A1.1a)

a. Weight (W)

b. The aerodynamic force (N) coming mainly from the wings

The resultant of these two forces is the centripetal force necessary to produce the angular motion. Since the weight and the centripetal forces act in a vertical plane containing the spin axis and the CG, the aerodynamic force must also act in this plane, i.e. it passes through the spin axis. It can be shown that, when the wing is stalled, the resultant aerodynamic force acts approximately perpendicular to the wing. For this reason it is sometimes called the wing normal force. If the wings are level (lateral axis horizontal), from the balance of forces in Figure A1.1a:

$$\text{W = Weight = Drag = } = C_D \tfrac{1}{2}\rho V^2 S$$

Rearranging gives:

$$V = \sqrt{\frac{W}{C_D \frac{1}{2}\rho S}}$$

Whereas L = Lift = Centripetal force

$$L = C_L \frac{1}{2}\rho V^2 S = \frac{W\Omega^2 R}{g}$$

Rearranging gives:

$$R = \frac{g C_L \frac{1}{2}\rho V^2 S}{W\Omega^2}$$

Where: g is gravity, R is spin radius; S is wing surface area; V is rate of descent; W is weight, Ω is angular velocity.

If the wings are not level, it has been seen that the departure from the level condition can be regarded as a rotation of the aeroplane about the longitudinal and normal axes. Usually this angle, the wing tilt angle, is small and does not affect the following reasoning.

A1.5 Effect of Attitude on Spin Radius

If for some reason the angle of attack is increased by a nose-up change in the aeroplanes attitude, the vertical rate of descent (V) will decrease because of the higher C_D. The increased angle of attack on the other hand, will decrease C_L which, together with the

lower rate of descent, results in a decrease in spin radius. It can also be shown that an increase in pitch increases the rate of spin, which will decrease R still further.

The two extremes of aeroplane attitude possible in the spin are shown in Figure A1.2.

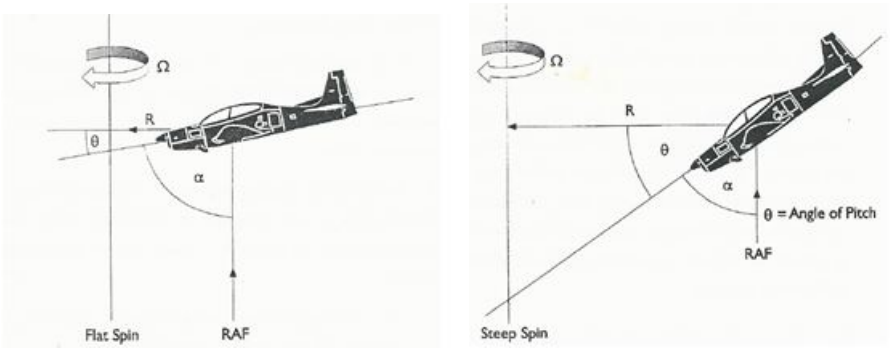

Figure A1.2: Flat and steep spin, from (Air Ministry, 1995)

The effects of pitch attitude are summarised below: an increase in pitch (e.g. flat spin) will:

a. Decrease the rate of descent

b. Decrease the spin radius

c. Increase the spin rate

It can also be shown that an increase in pitch will decrease the helix angle.

A1.6 Angular Momentum

In a steady spin, equilibrium is achieved by a balance of aerodynamic and inertia moments. The inertia moments result from a change in angular momentum due to the inertia cross coupling between the three axes. The angular momentum about an axis depends on the distribution of mass and the rate of rotation.

A1.7 Moment of Inertia (I)

The moment of inertia not only represents the amount of mass but also its distribution about the axis of rotation. The product of moment of inertia (mass distribution) and angular velocity measures the angular momentum of a rotating body (Figure A1.3).

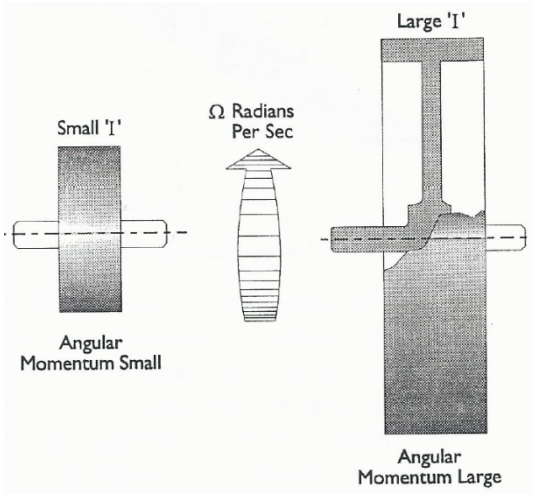

Figure A1.3: Two Rotors of the same weight and angular velocity (Air Ministry, 1995)

The concept of moment of inertia may be applied to an aeroplane by measuring the distribution of mass about each of the body axes:

a. Longitudinal Axis: The longitudinal axis mass distribution determines the moment of inertia in the rolling plane, denoted by A (Table A1.1). An aeroplane with fuel stored in the wings and external tanks will have a large moment of inertia value, particularly if the tanks are close to the wing tips. Modern training aeroplanes tend to have thinner wings. This has necessitated the stowage of fuel elsewhere and this, in combination with lower aspect ratios, has resulted in a reduction in their moment of inertia value.

b. Lateral Axis: The distribution of mass about the lateral axis determines the moment of inertia in pitching plane, denoted by B (Table A1.1). The increasing complexity of modern aeroplanes has resulted in an increase in the density of the fuselage with the mass being distributed along the whole length of the fuselage and a consequent increase in the value of B.

c. Normal Axis: The distribution of mass about the normal axis determines the moment of inertia in the yawing plane, denoted by C (Table A1.1). This quantity will be approximately equal to the sum of the moments of inertia in the rolling and pitching planes. Therefore C will always be larger than A or B.

A1.8 Inertia Moments in a Spin

The inertia moments generated in a spin are described below. Another explanation using a gyroscopic analogy, is given in Appendix 1b.

a. Roll: It is difficult to represent the rolling moments using concentrated masses, as is done for the other axes. For an aeroplane in the spinning attitude under consideration (inner wing down pitching nose up), the inertia moment is anti-spin i.e. tending to roll the aeroplane out of the spin. The equation for the inertia rolling moment is:

$$L = -(C - B)\,rq$$

b. Pitch: The imaginary concentrated masses of the fuselage (Figure A1.4), tend to flatten the spin. The equation for the moment is:

$$M = (C - A)\,rp$$

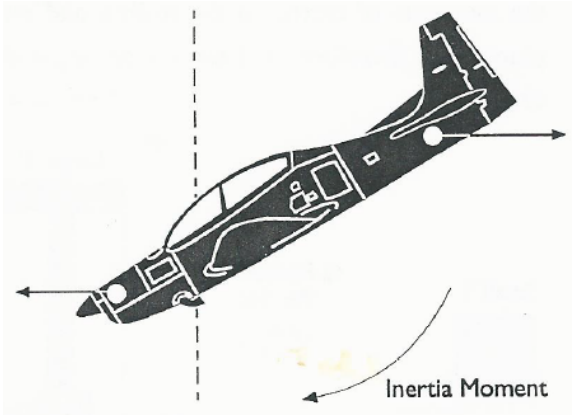

Figure A1.4: Inertia Pitching Moment, (Air Ministry, 1995)

c. Yaw: The inertia couple is complicated by the fact that it comprises two opposing couples caused by the wings and the fuselage, see Figure A1.5. Depending on the dominant component, the couple can be of either sign and of varying magnitude. The inertia yawing moment can be expressed as:

$$N = (A - B)\, p$$

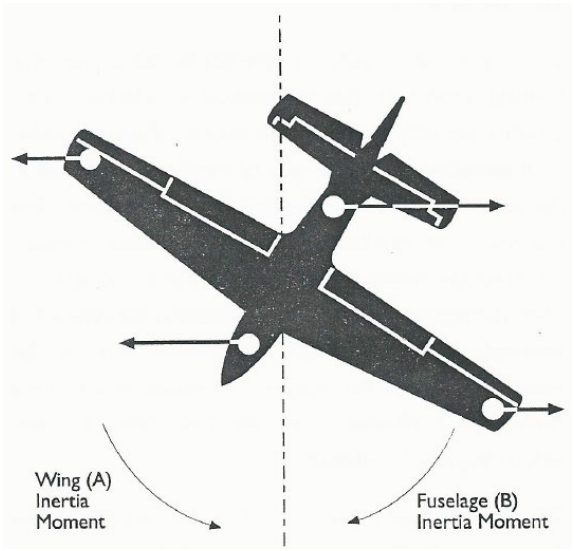

Figure A1.5: Inertia Yawing Moment, (Air Ministry, 1995)

This moment value is negative and thus anti-spin when B > A, and positive and pro-spin when A > B. The B/A ratio has a profound effect on the aeroplane spinning characteristics.

A1.9 Factor Contributions of Aerodynamic Moments

Aerodynamic factors affect the balance of moments in roll, pitch and yaw.

Aerodynamic Rolling Moments: The aerodynamic contributions to the balance of moments about the longitudinal axis to produce a steady rate of roll are as follows:

a. Rolling Moment due to Sideslip: The design features of the aeroplane which contribute towards positive lateral stability produce an aerodynamic rolling moment as a result of sideslip. It can be shown that, even at angles of attack above the

stall, this still remains true and the dihedral effect induces a rolling moment in the opposite sense to the sideslip. In the spin the relative airflow is from the direction of the outer wing (outward sideslip) and the result is a rolling moment in the direction in which the aeroplane is spinning; this contribution is therefore pro-spin.

b. Autorotative Rolling Moment: The normal damping in roll effect is reversed at angles of attack above the stall. This contribution is therefore pro-spin.

c. Rolling Moment due to Yaw: The yawing velocity in the spin includes a rolling moment for two reasons:

   1. Difference in Speed of the Wings: Lift of the outside wing is increased and that of the inner wing decreased inducing a pro-spin rolling moment.

   2. Difference in Angle of Attack of the Wings: In a spin the direction of the free airstream is practically vertical whereas the direction of the wing motion due to yaw is parallel to the longitudinal axis. The yawing velocity not only changes the speed but also the angle of attack of the wings. Figure A1.6 illustrates the vector addition of the yawing velocity to the vertical velocity of the outer wing. The effect is to reduce the angle of attack of the outer wing and increase that of the inner wing. Because the wings are stalled (slope of C_L curve is negative), the C_L of the outer wing is increased and the C_L of the inner wing decreased thus producing another pro-spin rolling moment.

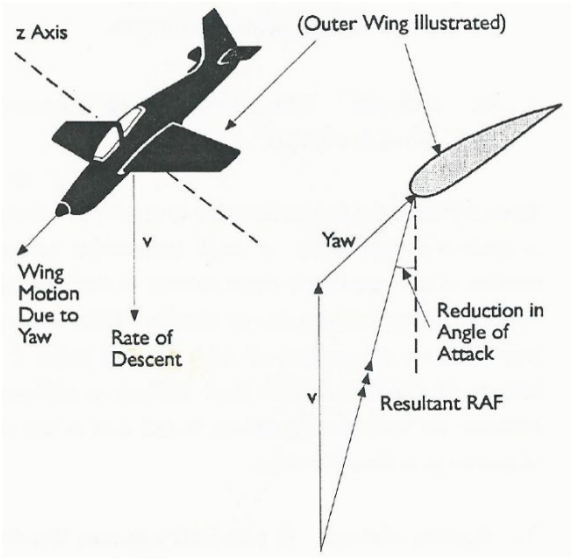

Figure A1.6: Change in Angle of Attack due to Yaw (outer wing), (Air Ministry, 1995)

d. Aileron Response: Ailerons produce a rolling moment in the conventional sense even though the wing is stalled.

Aerodynamic Pitching Moments: The aerodynamic contribution to the balance of moments about the lateral axis to produce a steady rate of pitch are as follows:

a. Positive Longitudinal Static Stability: In a spin the aeroplane is at a high angle of attack and therefore distributed in a nose-up sense from the trimmed condition. The positive longitudinal stability responds to this disturbance to produce a nose-down aerodynamic moment. This effect may be considerably reduced if the tailplane lies in the wing wake.

b. Damping in Pitch Effect: When the aeroplane is pitching nose-up the tailplane is moving down and its angle of attack is increased (the principle is the same as the damping in roll effect). The pitching velocity therefore produces a pitching moment in a nose-down sense. The rate of pitch in a spin is usually very low and consequently the damping in pitch contribution is small.

c. Elevator Response: The elevator act in the conventional sense. Down-elevator increases the nose-down aerodynamic moment whereas up-elevator produces a nose-up aerodynamic moment. It should be noted, that down-elevator usually increases the shielded area of the fin and rudder.

Aerodynamic Yawing Moments: The overall aerodynamic yawing moment is made up of a large number of separate parts, some arising out of the yawing motion of the aeroplane and some arising out of the side-slipping motion. The main contribution to the balance of moments about the normal axis to produce a steady rate of yaw are as follows:

a. Positive Directional Static Stability: When sideslip is present keel surfaces aft of the CG produce an aerodynamic yawing moment tending to turn the aeroplane into line with the sideslip vector (e.g. positive directional static stability or ‘weathercock effect’). This is an anti-spin effect, the greatest contribution to which is from the vertical fin. Vertical surfaces forward of the CG will tend to yaw the aeroplane further into the spin, i.e. they have a pro-spin effect. In a spin outward sideslip is present which, usually produces a net yawing moment towards the outer wing; i.e. in an anti-spin sense. Because of possible shielding effects from the tailplane and elevator and because the fin may be stalled, the directional stability is considerably reduced and this anti-spin contribution is usually small.

b. Damping in Yaw Effect: Applying the principle of the damping in roll effect to the yawing velocity, the keel surfaces produce an aerodynamic yawing moment to oppose the yaw. The greatest contribution to this damping moment is from the rear fuselage and fin. In this respect the cross-sectional shape of the fuselage is critical and has a profound effect on the damping moment. The following figures give some indication of the importance of cross-section:

Cross-Section	Damping Effect (anti-spin)
Circular	1

Rectangular	2.5
Elliptical	3.5
Round top / flat bottom	1.8
Round bottom / flat top	4.2
Round bottom / flat top with strakes	5.8

Damping effect = Damping from body cross-section / Damping from circular cylinder

Fuselage strakes are useful devices for improving the spinning characteristics of a prototype aeroplane. The anti-spin damping moment is very depending on the design of the tailplane / fin combination. Shielding of the fin by the tailplane can considerably reduce the effectiveness of the fin. In extreme cases a low-set tailplane may even change the anti-spin effect into a pro-spin effect.

c. Rudder Response: The rudder acts in the conventional sense, i.e. the in-spin rudder produces a pro-spin yawing moment and out-spin rudder produces an anti-spin yawing moment. Because of the shielding effect of the elevator, it is usual during recovery to pause after applying out-spin rudder so that the anti-spin yawing moment may take effect before down-elevator is applied.

A1.10 Balance of Moments

The balance of forces in the spin has a strong influence on the rate of descent. It does not determine the rate of rotation, wing tilt or angle of attack at which the spin occurs: The actual attitude, rate of descent, sideslip, rate of rotation and radius of a spinning aeroplane can only be determined by applying specific numerical values of the aeroplane´s aerodynamic and inertia data to the general relationships discussed below.

Rolling Moments: The balance of rolling moments in an erect spin is:

a. Pro-spin: the following aerodynamic rolling moments in an erect spin are:
   1. Autorotative rolling moment
   2. Rolling moment due to sideslip
   3. Rolling moment due to yaw

b. Anti-spin: The inertia rolling moment – (C – B) * rq, is anti-spin

These factors show that autorotation is usually necessary to achieve a stable spin. A small autorotative rolling moment would necessitate large sideslip to increase the effect of rolling moment due to sideslip. This in turn would reduce the amount of wing tilt and make the balance of moments in yaw more difficult to achieve, however the balance of moments in this axis is not as important as in the other two.

Pitching Moments: As discussed above the inertia pitching moment (C – A) * rp of the aeroplane is always nose-up in an erect spin. This is balanced by the nose-down

aerodynamic pitching moment. The balance between these two moments is the main factor relating angle of attack to rate of rotation in any given case and equilibrium can usually be achieved over a wide range. It can be shown that an increase in pitch will cause an increase in the rate of rotation (spin rate). This, in turn, will decrease the spin radius.

Yawing Moments: The balance of yawing moments in an erect spin is:

a. Pro-spin:
    1. Yawing moment due to applied rudder
    2. A small contribution from the wing, due to yaw, is possible at large angles of attack
    3. Yawing moment due to sideslip (vertical surfaces forward of CG)
    4. Inertia yawing moment (A – B) * pq, if A > B

b. Anti-spin:
    1. Inertia yawing moment (A – B) pq, if B > A
    2. Yawing moment due to sideslip (vertical surfaces aft of the CG)
    3. Damping in yaw effect

It can be seen that in-spin rudder is usually necessary to achieve balance of the yawing moments and hold the aeroplane in a spin.

Normal Axis: For conventional aeroplanes (A and B are nearly equal), it is relatively easy to achieve balance about the normal axis and the spin tends to be limited to a single set of conditions (angle of attack, spin rate, attitude). For aeroplanes in which B is much larger than A, the inertia yawing moment can be large and, thus difficult to balance. This is probably the cause of the oscillatory spin exhibited by these types of aeroplanes.

Yaw and Roll Axis: The requirements of balance about the yaw and roll axes greatly limit the range of angles of attack in which spinning can occur and determine the amount of sideslip and wing tilt involved. The final balance of the yawing moments is achieved by the aeroplanes taking up the appropriate angle of attack at which the inertia moments just balance the aerodynamic moments. This particular angle of attack also has to be associated with the appropriate rate of spin required to balance the pitching moments and the appropriate angle of sideslip required to balance the rolling moments.

A1.11 Effects of Controls in Recovery from a Spin

The relative effectiveness of the three controls in recovering from a spin will now be considered. Recovery is aimed at stopping the rotation by reducing the pro-spin rolling moment and / or increasing the anti-spin yawing moment. The yawing moment is the more important but because of the strong cross-coupling between motions about the three axes through the inertia moments, the rudder is not the only means by which yawing may be induced by the pilot.

Modern aeroplanes do not necessarily have the same spin characteristics and recovery must be conducted in accordance with the most effective control inputs. The control movements generally most favourable to the recovery from the spin have been in use for a long time, i.e. apply full rudder in the opposite direction of the spin and then move the elevator control forward until the spin stops, maintaining the ailerons neutral. The rudder is normally the primary control but, because the inertia moments are generally large in modern aeroplanes aileron deflection may be also important. Where the response of the aeroplane to rudder is reduced in the spin the aileron may even be the primary control although in the final analysis it is its effect on the yawing moment which makes it work.

The initial effect of applying a control deflection will be to change the aerodynamic moment about one or more axes. This will cause a change in aeroplane´s attitude and a change in the rates of rotation about all corresponding axes. These changes will, in turn, change the inertia moments.

A1.12 Effect of Ailerons

Even at the high angle of attack in the spin the ailerons act in the normal sense. Application of aileron in the same direction as the aeroplane is rolling will therefore increase the aerodynamic rolling moment. This will increase the roll rate p and affect the inertia yawing moment (A – B) * pq. The effect of an increase in p on the inertia yawing moment depends on the mass distribution or B/A ratio:

a. B/A > 1: In an aeroplane where B/A > 1, the inertia yawing moment is anti-spin (negative) and an increasing in p will decrease it still further e.g. make it more anti-spin. The increase in anti-spin inertia yawing moment will tend to raise the outer wing (increase wing tilt) which will decrease the outward sideslip. This will restore the balance of rolling moments by decreasing the pro-spin aerodynamic moment due to lateral stability. The increase in wing tilt will also cause the rate of pitch q to increase which in turn:

    1. Cause a small increase in the anti-spin inertia rolling moment –(C - B) * rq, (C > B) and thus helps to restore balance about the roll axis
    2. Further increases the anti-spin inertia yawing moment

b. B/A < 1: A low B/A ratio will reverse the effects described above. The inertia yawing moment will be pro-spin (positive) and will increase with an increase in p.

Due to secondary effects associated with directional stability, the reversal point actually occurs at a B/A ratio of 1.3 thus:

a. B/A > 1.3: Aileron with roll (in-spin) has an anti-spin effect

b. B/A < 1.3: Aileron with roll (in-spin) has a pro-spin effect

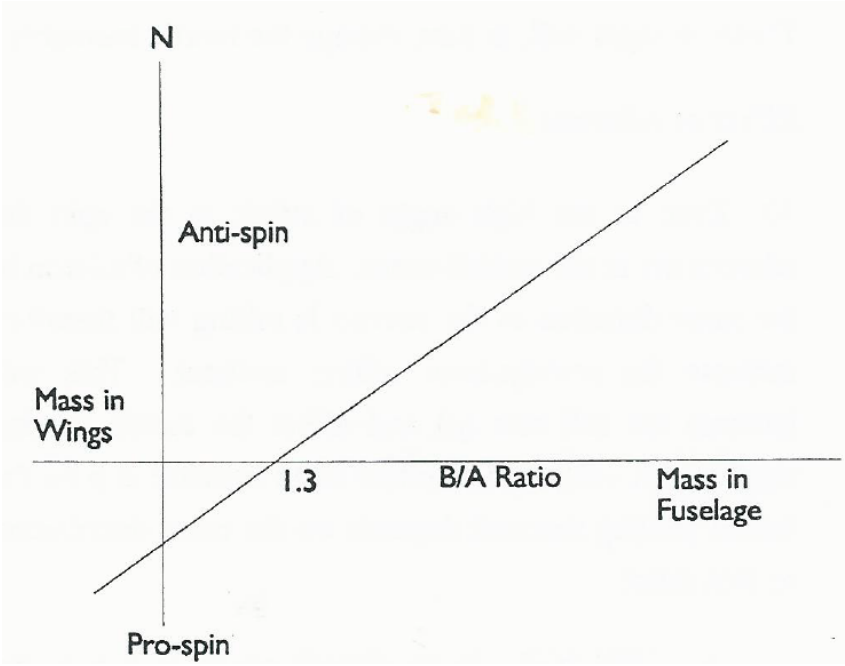

Figure A1.7: Yawing Moment (N) per Degree of Aileron (Air Ministry, 1995)

Some aircraft change their B/A ratio in flight as stores and fuel are consumed. The pilot has no accurate indication of the value of B/A ratio and, where this value may vary either side of 1.3, it is desirable to maintain the ailerons neutral to avoid an unfavourable response which may delay or even prohibit recovery.

An additional effect of aileron applied with roll is to increase the anti-spin yawing moments due to aileron drag.

A1.13 Effect of Elevator

In the explanations above, it was seen that down-elevator produces a nose-down aerodynamic pitching moment. This will initially reduce the nose-up pitching velocity q. Although this will tend to reduce the angle of attack, the effect on the inertia yawing and rolling moments is as follows:

a. Inertia Yawing Moment (A – B) *pq: If B > A, the inertia yawing moment is anti-spin. A reduction in q will make the inertia moment less anti-spin, i.e. a pro-spin change. When A > B down-elevator will cause a change in inertia yawing moment in the anti-spin sense.

b. Inertia Rolling Moment – (C – B) * rq: The inertia rolling moment is always anti-spin because C > B. A reduction in q will therefore make it less anti-spin which is again a change in the pro-spin sense.

The result of these pro-spin changes in the inertia yawing and rolling moments is to decrease the wing tilt thus increasing the sideslip angle (see Figure A1.8) and rate of roll. It can also be shown that the rate of rotation about the spin axis will increase.

Although the change in the inertia yawing moment is unfavourable, the increased sideslip may produce an anti-spin aerodynamic yawing moment if the directional stability is positive. This contribution will be reduced if the down elevator seriously increases the shielding of the fin and rudder.

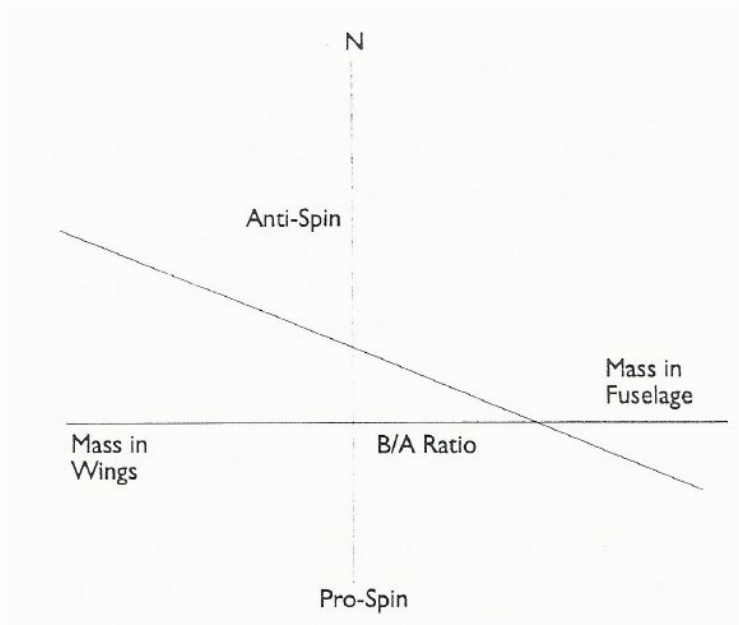

Figure A1.8: Yawing Moment (N) per Degree of Down Elevator (Air Ministry, 1995)

The overall effect of down-elevator on the yawing moments therefore depends on:

a. The pro-spin inertia moment when B > A

b. The anti-spin moment due to directional stability

c. the loss of rudder effectiveness due to shielding

In general, the net result of moving the elevators down is beneficial when A > B and rather less so when B > A, assuming that the elevator movement does not significantly increase the shielding of the fin and rudder.

A1.14 Effect of Rudder

The rudder is nearly always effective in producing an anti-spin aerodynamic yawing moment though the effectiveness may be greatly reduced when the rudder lies in the wake of the wing or tailplane. The resulting increase in the wing tilt angle will increase the anti-spin inertia yawing moment (when B > A) through an increase in pitching velocity.

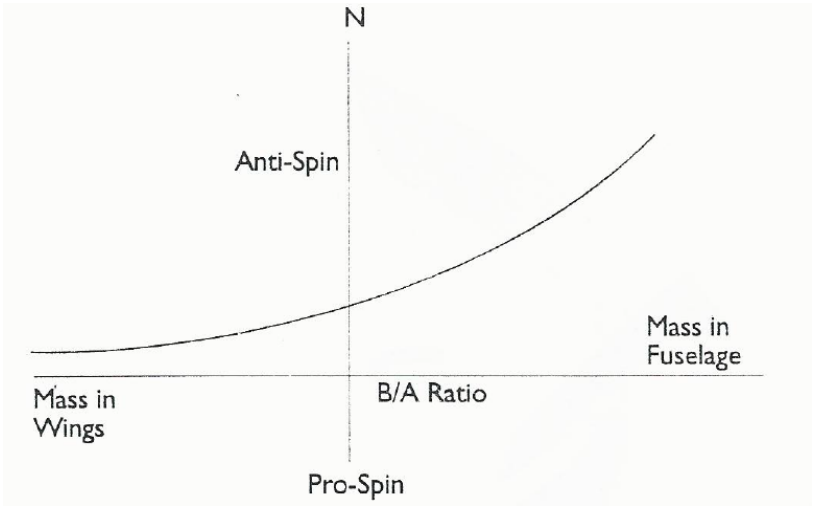

Figure A1.9: Yawing Moment (N) per Degree of Anti-spin Rudder, (Air Ministry, 1995)

The overall effect of applying anti-spin rudder is always beneficial and is enhanced when the B/A ratio is increased.

1.15 Inverted Spin

Figure A1.10 shows an aeroplane in an inverted spin but following the same flight path as in Figure A1.1. Relative to the pilot the motion is now compound of a pitching velocity in the nose-down sense, a rolling velocity to the right and a yawing velocity to the left. Thus roll and yaw are in opposite directions, a fact which affects the recovery action, particularly if the aeroplane has a high B/A ratio.

The inverted spin is fundamentally similar to the erect spin and the principles of moment balance discussed in previous sections are equally valid for the inverted spin. The values of the aerodynamic moments are unlikely to be the same since, in the inverted attitude, the shielding effect of the wing and tail may change markedly.

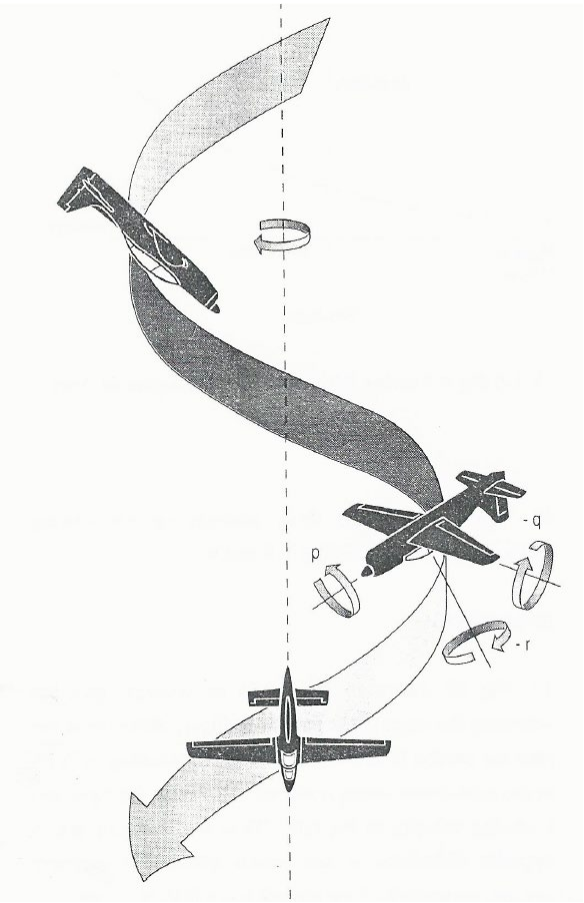

Figure A1.10: The Inverted Spin; (Air Ministry, 1995)

The main difference will be caused by the change in relative positions of the fin and rudder and the tailplane. An aeroplane with a low-mounted tailplane will tend to have a flatter erect spin and recovery will be made more difficult due to shielding of the rudder. The same aeroplane inverted will respond much better to recovery rudder since it is unshielded and the effectiveness of the rudder increased by the position of the tailplane. The converse is true for an aeroplane with a high tailplane.

The control deflections required for recovery are dictated by the direction of roll, pitch and yaw and the aeroplanes B/A ratio. These are:

a. Rudder to oppose yaw as indicated by the spin direction (turn needle deflection)

b. Aileron in the same direction as the observed roll, if the B/A ratio is high

c. Elevator up is generally the case for conventional aeroplanes but, if the aeroplane has a high B/A ratio and suffers from the shielding problems previously discussed, this control input may be less favourable and may even become pro-spin.

A1.16 Oscillatory Spin

A combination of high wing loading and high B/A ratio makes it difficult for spinning aeroplanes to achieve equilibrium about the yaw axis. This is thought to be the most

probable reason for the oscillatory spin. In this type of spin the rate of roll and pitch are changing during each oscillation. In a mild form it appears to the pilot as a continuously changing angle of wing tilt, from outer wing well above the horizon back to the horizontal once each turn; the aeroplane seems to wallow in the spin.

In a fully-developed oscillatory spin the oscillations in the rates of roll and pitch can be quite violent. The rate of roll during each turn can vary from zero to about 200°/ sec. At the maximum rate of roll the rising wing is unstalled which probably accounts for the violence of this type of spin. Large changes in attitude usually take place from fully nose-down at the peak rate of roll, to nose-up at the minimum rate of roll.

The use of the controls to effect a change in attitude can change the characteristics of an oscillatory spin quite markedly. In particular:

a. Anything which increases the wing tilt will increase the violence of the oscillations, e.g. in-spin aileron or anti-spin rudder

b. A decrease in the wing tilt angle will reduce the violence of the oscillations, e.g. out-spin aileron or down-elevator

The recovery from this type of spin has been found to be relatively easy, although the shortest recovery times are obtained if recovery is initiated when the nose of the aeroplane is falling relative to the horizon.

A1.17 Conclusion (of Appendix A1a)

The foregoing sections make it clear that the characteristics of the spin and the effect of controls in recovery are specific to type. In general the aerodynamic factors are determined by the geometry of the aeroplane and the inertial factors by the distribution of mass. In Appendix 1b the gyroscopic cross-coupling between axes are explained.

Appendix 1b Gyroscopic cross-coupling between axes

1. Introduction

In Appendix 1a, the effects of the inertia moments have been explained by considering the masses of fuselage and wings acting either side of a centreline. The effect of these concentrated masses when rotating, can be visualised as acting in the manner of the bob-weights of a governor. Another, and more versatile, explanation of the cross-coupling effects can be made using a gyroscopic analogy; regarding the aeroplane as a rotor.

2. Inertia Moments in a Spin

The inertia moments generated in a spin are the same as the torque exerted by a precessing gyroscope. Figures A1b.1, A1b.2 and A1b.3 illustrate the inertia or gyroscopic moments about the body axes. These effects are described as follows:

a. Inertia Rolling Moments (Figure A1b.1): The angular momentum in the yawing plane is C*r, and by imposing on it a pitching velocity of q, an inertia rolling moment is generated equal to –C*r*q, i.e. in the opposite sense to the direction of roll in an erect spin. The inertia rolling moment due to imposing the yawing velocity on the angular momentum in the pitching plane is in a pro-spin sense equal to +B*r*q. The total inertia rolling moment is therefore equal to (B – C) r*q, or since C > B: - (C – B) r*q.

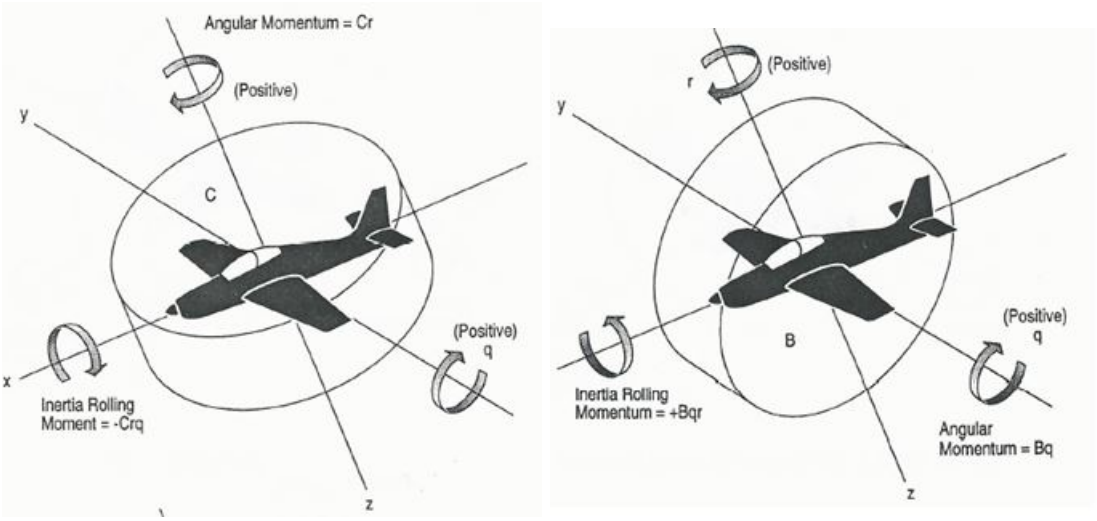

Figure A1b.1: Total Inertia Rolling Moment (Air Ministry, 1995)

b. Inertia Pitching Moments (see Figure A1b.2): The angular momentum in the rolling plane is A*p and imposing a yawing velocity of r on the rolling plane rotor causes it to precess in pitch in a nose-down sense due to inertia pitching moment (-A*p*r). Similarly, the angular momentum in the yawing plane is C*r, and imposing a roll velocity of p on the yawing plane rotor generates an inertia pitching moment (+C*r*p) in the nose-up sense. The total inertia moment is therefore (C – A)*r*p. In

an erect spin, roll and yaw are always in the same direction and C is always greater than A. The inertia pitching moment is therefore positive (nose-up) in an erect spin.

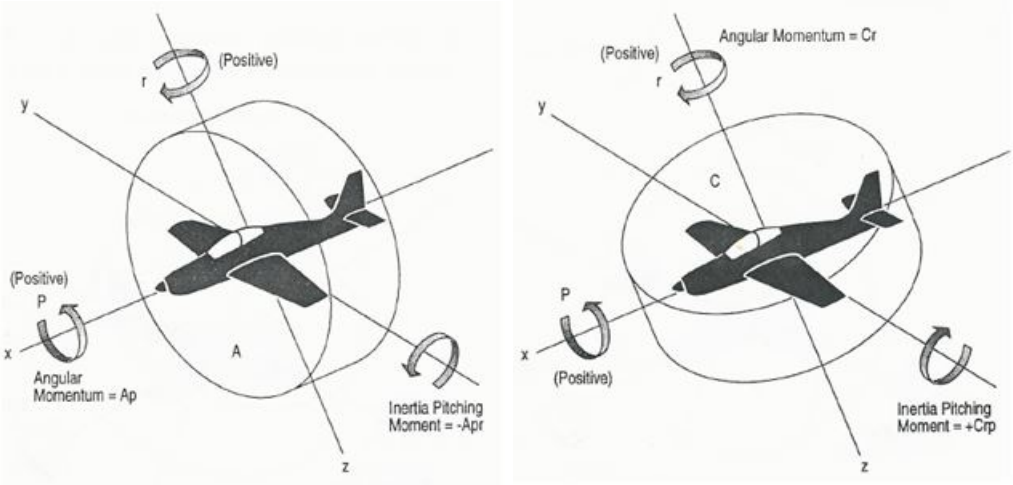

Figure A1b.2: Total Inertia Pitching Moment (Air Ministry, 1995)

c. Inertia Yawing Moments (see Figure A1b.3): Replacing the aeroplane by a rotor having the same moment of inertia in the rolling plane, its angular momentum is the product of the moment of inertia and angular velocity (A*p). Imposing a pitching velocity q on the rotor will generate a torque tending to precess the rotor about the normal axis in the same direction as the spin. It can be shown that this inertia yawing moment is equal in value to +A*p*q where the positive sign indicates a pro-sign torque. Similarly, the angular momentum in the pitching plane is equal to B*q. Imposing a roll velocity of p on the pitching plane rotor will generate an inertia yawing moment in an anti-spin sense equal to –B*p*q. the total inertia yawing moment is therefore equal to (A – B)*p*q, or if B > A: - (B – A)*p*q.

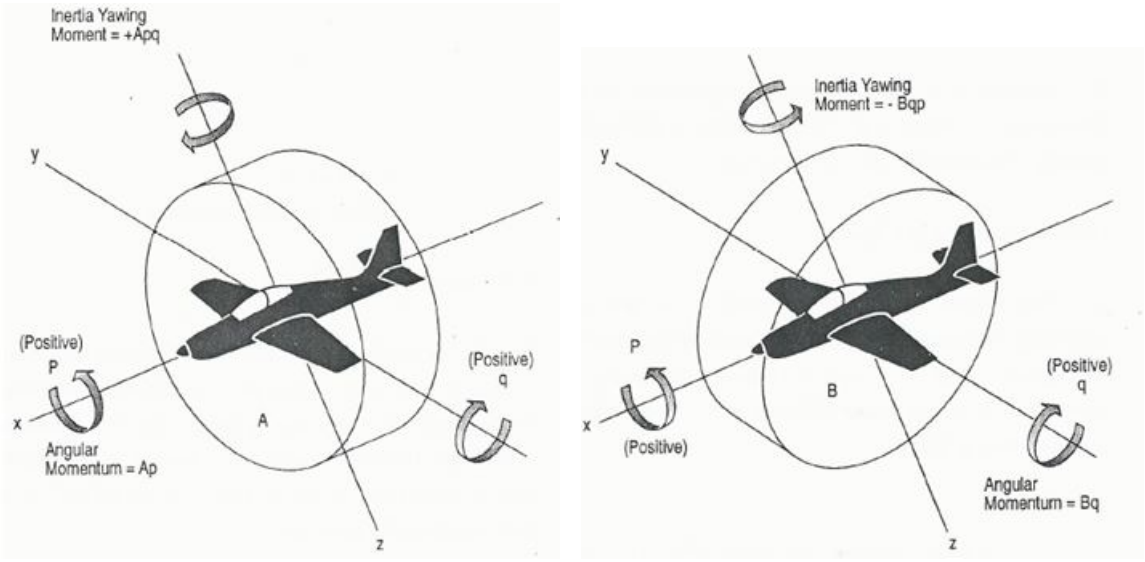

Figure A1b.3: Total Inertia Yawing Moment (Air Ministry, 1995)

Appendix 2 Example of a certification spin test planning

Table of contents

A2 I Introduction

The below document – written by the author in 2003 in preparation of an actual spin test programme - guides a test pilot through the main topics of certification spin tests. This example of a certification spin test planning begins with the current regulations of the CS 23 - the corresponding European Certification Specification - which are published by the European Aviation Safety Agency. Thereafter it provides a brief statement on the purpose of the tests, the test descriptions and the aeroplanes configuration which need to be investigated.

The minimum instrumentation to comply with the requirements of the CS 23 is listed followed by safety requirements, the processing of a spin matrix and the flight envelope.

A flight envelope is a ‘field’ of aeroplanes masses versus centre of gravity positions (expressed in percent of the length of the mean aerodynamic chord line (MAC) of the wing) within which the corresponding Design Organisation plans to test the new type of aeroplane. To conduct the required tests the following flight test matrix is defined. Those test points need to be investigated per every condition defined below. The document is ending with the ‘Procedures and Acceptance Criteria’ which the aeroplane needs to comply with.

From this practical approach to spin tests it can be seen that a very high number of spin runs are necessary. Most of these spin runs are uncritical – which means easy recoverable - but an unknown part of this flight envelope contains parameter combinations which may lead to spins which are not recoverable and thus dangerous for even highly experienced Test Pilots.

A2 1. References

CS 23 §	AC 23–8 B § (taken from FAR 23)
21	
141	
143 (b) (c)	
171	
201	86
203	87
207 (a) (b) (c) (e)	89
221 (a)	100

A2 2. Purpose and test description

The fundamental objective of spin testing is to demonstrate that the airplane will not become uncontrollable within one turn (or 3 seconds, whichever takes longer) for normal category aeroplanes or 6 turns for utility or aerobatic category aeroplanes if a spin should be encountered inadvertently or deliberately and that recovery is conducted without exceeding the airplane design limitations.
The effect of gear, flaps, power, accelerated entry and control abuse is evaluated.
Obtained data will also lead to a system statement concerning Governor Overspeed during spin recovery low idle conditions in case a variable pitch propeller is installed.

A2 3. Configuration

Recovery parachute is mandatory.

A2 4. Conformity

The following conformity requests must be satisfactorily completed in accordance with Design Organisation Handbook procedures before certification testing:

Conformity #	Description

Table A2a.1: Example list of conformity requests

A2 5. Instrumentation and data

The following parameters are required to demonstrate compliance with the CS-23. They represent the minimum instrumentation and data supply needed for certification. A cockpit camera is desirable but not part of the minimum instrumentation. All items on the list require a pre-flight verification.
When data from a measuring system are not required to be recorded, handwritten data are acceptable.

Aircraft gross weight (GRWT) and CG	Boom airspeed and boom altitude (KCAS, CALT)
Gear position (LGPS)	Pilot event or co-pilot event (PILOT or COPLT)
Flap positions (FLPPS)	Pilot column force (ELFOR)
(Torque / Engine (TRQU,N_2)) (if applicable)	Fuel quantities (1FULQ, 2FULQ)
Data on event (DATAON)	Crew comments (REMARKS)
Outside air temperature (OATC)	Type of entry
Number of recovery turns	Recovery speed
Max g-load (N_Z)	Prop condition: feather (low, high idle)
Loss of height (entry and exit altitude)	

Table A2a.2: Minimum additional aeroplane instrumentation for spin tests

A2 6. Safety

Crew member must review the Threat and Hazard Assessment (THA) documents before conducting this test.

Risk Assessment:	High	Personal Parachute / Helmet:	Yes
Chase aeroplane:	No	Aircraft Spin recovery parachute:	Yes / Low Speed
Minimum Crew:	1 pilot	Escape Hatch:	Armed

Table A2a.3: Minimum standards concerning the required ‘Threat and Hazard Assessment’

A2 7. Processing of a spin test matrix

The aggregated requirements concerning spinning are defined in EASA CS 23, Subpart B (Flight), Spinning, § 221 (refer to Appendix 3). In order to develop an entire load and configuration matrix the following information are taken from CS 23.221 (Appendix H) as well as the corresponding Advisory Circular AC 23 – 8 C material (Federal Aviation Administration, 2011) which is provided by the U.S. Federal Aviation Administration (FAA). The compliance with both systems of regulations – the European and the U.S. - is demonstrated during a spin test programme at the same time.

The demand on certification spin testing is to demonstrate acceptable spin characteristics for any kind of configuration covering the entire flight envelope which results in a large number of test points.
To support the corresponding Design Organisations and thus the certification spin tests the Advisory Circular (23 – 8 B §100 (d) (4)) recommends a spin matrix (Figure A1a.1) that considers the effects of flaps, gear, cowl flaps, power, CG position, spin direction, normal and accelerated entries as well as normal and abnormal control use.

SPIN EVALUATION CONFIGURATION

Flight Condition Spins from Wing Level Attitude	Spin Number	Flaps Up	Flaps Approach (As Approp.)	Flaps Landing	Gear Up	Gear Down	Cowl Flaps Closed	Cowl Flaps As Required	Power Off	Power On	Forward C.G.	Aft C.G.	Lateral C.G.	Slow Elevator Releases
Test with Normal Spin Controls	1	X			X		X		X		X	X	X	
Left Spin 1 thru 6	2		X			X	X		X		X	X	X	
	3			X		X	X		X		X	X	X	
	4	X			X			X		X	X	X	X	
	5		X			X		X		X	X	X	X	
	6			X		X		X		X	X	X	X	
Repeat 1 Through 6 from a right spin. Repeat 1 through 6 from left and right turning flight.														
Tests with Abnormal Spin Controls	7	X			X		X		X		X	X	X	X
	8		X			X	X		X		X	X	X	X
Left Spin Aileron Against 7 Thru 12	9			X		X	X		X		X	X	X	X
	10	X			X			X		X	X	X	X	X
	11		X			X		X		X	X	X	X	X
	12			X		X		X		X	X	X	X	X
Repeat 7 Through 12 From a Right Spin														
Left Spin Aileron with 13 Thru 18	13	X			X		X		X		X	X	X	X
	14		X			X	X		X		X	X	X	X
	15			X		X	X		X		X	X	X	X
	16	X			X			X		X	X	X	X	X
	17		X			X		X		X	X	X	X	X
	18			X		X		X		X	X	X	X	X
Repeat 13 Through 18 From a Right Spin Repeat 7 Through 18 From Left & Right Turning Flight														

Figure A2a.1: Spin Evaluation Configuration Matrix (Federal Aviation Administration, 2011)

The following systematics are used in processing the spin test matrix

Flaps and Gear Setting:

Flap position 0 is combined with gear UP position which represents cruise configuration. All other flap settings (1-3) are performed with gear down.

Power:

Tests are conducted with power on (MCP: Maximum continuous power) and power off (flight idle).

Procedure:

The entry procedure has to result in a spin. Spins are excited by the same procedure as stalls according to §23.201 (Wings level) and §23.203 (Turning Flight and Accelerated Turning Flight).

As the aeroplane stalls (with ailerons neutral and full-up elevator) full rudder is applied in the direction of spin desired. The rudder input direction is defined as 'Spin Dir.' in the matrix below and is LH (left hand spin direction) or RH (right hand spin direction).

In order to perform turning flights the initial turn direction has to be defined (see 'Turning Flight' column). Control inputs or turns in relation to the spin direction are defined as 'pro' or 'contra'. In case of wings level entries no turning flight direction is applicable thus 'neutral' is stated.

Spin or stall entries are performed 'normal' or 'accelerated'. This is stated in the 'Entry' column.

The 'Procedure' column shall provide an overview and gives better understanding what procedure has to be performed.

Control:

All types of control usage that might be used during the operation of the aeroplane have to be induced, whether they are supporting a recovery or not. Ailerons with and against the spin should be applied at entry and during spins. This is stated by 'neutral', 'pro' and 'contra' in the 'Aileron' column.

With the above systematics the matrix covers the flap and gear setting in combination with any procedure and control input required.

A2 8. Envelope Range

The aeroplane has to proof acceptable spinning characteristics for any kind of mass and centre of gravity positions combinations normally expected in service. Thus the entire flight envelope has to be evaluated.

The following sketch is attached to the given FAA spin test matrix. It provides an overview about the envelope range that has to be covered by the tests. Each loading condition required for aircraft configuration is also defined.

Condition1:	low fuel	min. payload	CG forward
Condition 2:	max fuel	max payload	CG forward
Condition 3:	max fuel	max payload	CG central
Condition 4:	max fuel	max payload	CG aft
Condition 5:	low fuel	max payload	CG aft
Condition 6:	low fuel	min. payload	CG aft
Condition 7:	low fuel	min. payload	CG central
Condition 8:	low fuel	min. payload	CG forward

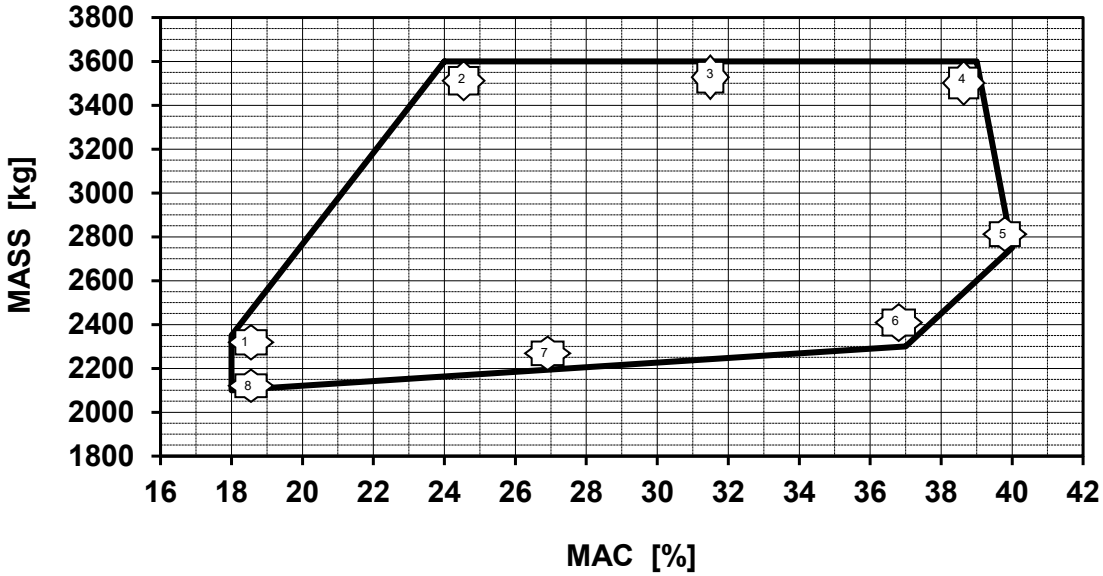

Figure A2a.2: Example of a flight envelope for processing a spin test matrix (by the Author)

Notes: Condition 1 and 8 in the example-envelope above show similar mass and CG configurations. This is to double check the first spin test results after the entire

programme approaches the end. This is because during the programme the Test Pilot gains a higher level of spin experience which may influence the test results.

Maximum mass configurations of condition 2, 3 and 4 are expected to cover the main part of the critical spin evaluation configurations. Those spin tests do have the highest priority during an actual spin certification and need special safety attention. Conditions 5, 6 and 7 normally represent uncritical spin characteristics.

Thus the corresponding spin test matrix covers 240 test points for 8 mass and CG combinations so that a total number of 1920 test points need to be investigated

Such a high number of spin tests are not feasible because of time and economical limits so that a – still high number – of spot checks need to be agreed with the competent Aviation Authority.

A2 9. Spin test matrix

The following matrices of spin conditions and influencing factors show the typical extent of a spin certification programme of an aeroplane.

Test Point	Flaps	Gear	Power	Turning Flight	Spin Dir.	Aileron	Entry	Procedure
1	0	Up	OFF	neutral	LH	neutral	normal	Wings level, normal entry
2	1	Down	OFF	neutral	LH	neutral	normal	"
3	2	Down	OFF	neutral	LH	neutral	normal	"
4	3	Down	OFF	neutral	LH	neutral	normal	"
5	0	Up	ON	neutral	LH	neutral	normal	"
6	1	Down	ON	neutral	LH	neutral	normal	"
7	2	Down	ON	neutral	LH	neutral	normal	"
8	3	Down	ON	neutral	LH	neutral	normal	"
9	0	Up	OFF	neutral	LH	pro	normal	"
10	1	Down	OFF	neutral	LH	pro	normal	"
11	2	Down	OFF	neutral	LH	pro	normal	"
12	3	Down	OFF	neutral	LH	pro	normal	"
13	0	Up	ON	neutral	LH	pro	normal	"
14	1	Down	ON	neutral	LH	pro	normal	"
15	2	Down	ON	neutral	LH	pro	normal	"
16	3	Down	ON	neutral	LH	pro	normal	"
17	0	Up	OFF	neutral	LH	contra	normal	"
18	1	Down	OFF	neutral	LH	contra	normal	"
19	2	Down	OFF	neutral	LH	contra	normal	"
20	3	Down	OFF	neutral	LH	contra	normal	"
21	0	Up	ON	neutral	LH	contra	normal	"
22	1	Down	ON	neutral	LH	contra	normal	"
23	2	Down	ON	neutral	LH	contra	normal	"
24	3	Down	ON	neutral	LH	contra	normal	"
25	0	Up	OFF	neutral	RH	neutral	normal	"
26	1	Down	OFF	neutral	RH	neutral	normal	"
27	2	Down	OFF	neutral	RH	neutral	normal	"
28	3	Down	OFF	neutral	RH	neutral	normal	"

Test Point	Flaps	Gear	Power	Turning Flight	Spin Dir.	Aileron	Entry	Procedure
29	0	Up	ON	neutral	RH	neutral	normal	"
30	1	Down	ON	neutral	RH	neutral	normal	"
31	2	Down	ON	neutral	RH	neutral	normal	"
32	3	Down	ON	neutral	RH	neutral	normal	"
33	0	Up	OFF	neutral	RH	pro	normal	"
34	1	Down	OFF	neutral	RH	pro	normal	"
35	2	Down	OFF	neutral	RH	pro	normal	"
36	3	Down	OFF	neutral	RH	pro	normal	"
37	0	Up	ON	neutral	RH	pro	normal	"
38	1	Down	ON	neutral	RH	pro	normal	"
39	2	Down	ON	neutral	RH	pro	normal	"
40	3	Down	ON	neutral	RH	pro	normal	"
41	0	Up	OFF	neutral	RH	contra	normal	"
42	1	Down	OFF	neutral	RH	contra	normal	"
43	2	Down	OFF	neutral	RH	contra	normal	"
44	3	Down	OFF	neutral	RH	contra	normal	"
45	0	Up	ON	neutral	RH	contra	normal	"
46	1	Down	ON	neutral	RH	contra	normal	"
47	2	Down	ON	neutral	RH	contra	normal	"
48	3	Down	ON	neutral	RH	contra	normal	"

Table A2a.4: Spin sub-matix for wings level, normal entry

Test Point	Flaps	Gear	Power	Turning Flight	Spin Dir.	Aileron	Entry	Procedure
49	0	Up	OFF	pro	LH	neutral	normal	Pro Turn, normal entry
50	1	Down	OFF	pro	LH	neutral	normal	"
51	2	Down	OFF	pro	LH	neutral	normal	"
52	3	Down	OFF	pro	LH	neutral	normal	"
53	0	Up	ON	pro	LH	neutral	normal	"
54	1	Down	ON	pro	LH	neutral	normal	"
55	2	Down	ON	pro	LH	neutral	normal	"

Test Point	Flaps	Gear	Power	Turning Flight	Spin Dir.	Aileron	Entry	Procedure
56	3	Down	ON	pro	LH	neutral	normal	"
57	0	Up	OFF	pro	LH	pro	normal	"
58	1	Down	OFF	pro	LH	pro	normal	"
59	2	Down	OFF	pro	LH	pro	normal	"
60	3	Down	OFF	pro	LH	pro	normal	"
61	0	Up	ON	pro	LH	pro	normal	"
62	1	Down	ON	pro	LH	pro	normal	"
63	2	Down	ON	pro	LH	pro	normal	"
64	3	Down	ON	pro	LH	pro	normal	"
65	0	Up	OFF	pro	LH	contra	normal	"
66	1	Down	OFF	pro	LH	contra	normal	"
67	2	Down	OFF	pro	LH	contra	normal	"
68	3	Down	OFF	pro	LH	contra	normal	"
69	0	Up	ON	pro	LH	contra	normal	"
70	1	Down	ON	pro	LH	contra	normal	"
71	2	Down	ON	pro	LH	contra	normal	"
72	3	Down	ON	pro	LH	contra	normal	"
73	0	Up	OFF	pro	RH	neutral	normal	"
74	1	Down	OFF	pro	RH	neutral	normal	"
75	2	Down	OFF	pro	RH	neutral	normal	"
76	3	Down	OFF	pro	RH	neutral	normal	"
77	0	Up	ON	pro	RH	neutral	normal	"
78	1	Down	ON	pro	RH	neutral	normal	"
79	2	Down	ON	pro	RH	neutral	normal	"
80	3	Down	ON	pro	RH	neutral	normal	"
81	0	Up	OFF	pro	RH	pro	normal	"
82	1	Down	OFF	pro	RH	pro	normal	"
83	2	Down	OFF	pro	RH	pro	normal	"
84	3	Down	OFF	pro	RH	pro	normal	"
85	0	Up	ON	pro	RH	pro	normal	"
86	1	Down	ON	pro	RH	pro	normal	"
87	2	Down	ON	pro	RH	pro	normal	"
88	3	Down	ON	pro	RH	pro	normal	"

Test Point	Flaps	Gear	Power	Turning Flight	Spin Dir.	Aileron	Entry	Procedure
89	0	Up	OFF	pro	RH	contra	normal	"
90	1	Down	OFF	pro	RH	contra	normal	"
91	2	Down	OFF	pro	RH	contra	normal	"
92	3	Down	OFF	pro	RH	contra	normal	"
93	0	Up	ON	pro	RH	contra	normal	"
94	1	Down	ON	pro	RH	contra	normal	"
95	2	Down	ON	pro	RH	contra	normal	"
96	3	Down	ON	pro	RH	contra	normal	"

Table A2a.5: Spin sub-matrix for pro turn, normal entry

Test Point	Flaps	Gear	Power	Turning Flight	Spin Dir.	Aileron	Entry	Procedure
97	0	Up	OFF	contra	LH	neutral	normal	Contra turn, normal entry
98	1	Down	OFF	contra	LH	neutral	normal	"
99	2	Down	OFF	contra	LH	neutral	normal	"
100	3	Down	OFF	contra	LH	neutral	normal	"
101	0	Up	ON	contra	LH	neutral	normal	"
102	1	Down	ON	contra	LH	neutral	normal	"
103	2	Down	ON	contra	LH	neutral	normal	"
104	3	Down	ON	contra	LH	neutral	normal	"
105	0	Up	OFF	contra	LH	pro	normal	"
106	1	Down	OFF	contra	LH	pro	normal	"
107	2	Down	OFF	contra	LH	pro	normal	"
108	3	Down	OFF	contra	LH	pro	normal	"
109	0	Up	ON	contra	LH	pro	normal	"
110	1	Down	ON	contra	LH	pro	normal	"
111	2	Down	ON	contra	LH	pro	normal	"
112	3	Down	ON	contra	LH	pro	normal	"
113	0	Up	OFF	contra	LH	contra	normal	"
114	1	Down	OFF	contra	LH	contra	normal	"

Test Point	Flaps	Gear	Power	Turning Flight	Spin Dir.	Aileron	Entry	Procedure
115	2	Down	OFF	contra	LH	contra	normal	"
116	3	Down	OFF	contra	LH	contra	normal	"
117	0	Up	ON	contra	LH	contra	normal	"
118	1	Down	ON	contra	LH	contra	normal	"
119	2	Down	ON	contra	LH	contra	normal	"
120	3	Down	ON	contra	LH	contra	normal	"
121	0	Up	OFF	contra	RH	neutral	normal	"
122	1	Down	OFF	contra	RH	neutral	normal	"
123	2	Down	OFF	contra	RH	neutral	normal	"
124	3	Down	OFF	contra	RH	neutral	normal	"
125	0	Up	ON	contra	RH	neutral	normal	"
126	1	Down	ON	contra	RH	neutral	normal	"
127	2	Down	ON	contra	RH	neutral	normal	"
128	3	Down	ON	contra	RH	neutral	normal	"
129	0	Up	OFF	contra	RH	pro	normal	"
130	1	Down	OFF	contra	RH	pro	normal	"
131	2	Down	OFF	contra	RH	pro	normal	"
132	3	Down	OFF	contra	RH	pro	normal	"
133	0	Up	ON	contra	RH	pro	normal	"
134	1	Down	ON	contra	RH	pro	normal	"
135	2	Down	ON	contra	RH	pro	normal	"
136	3	Down	ON	contra	RH	pro	normal	"
137	0	Up	OFF	contra	RH	contra	normal	"
138	1	Down	OFF	contra	RH	contra	normal	"
139	2	Down	OFF	contra	RH	contra	normal	"
140	3	Down	OFF	contra	RH	contra	normal	"
141	0	Up	ON	contra	RH	contra	normal	"
142	1	Down	ON	contra	RH	contra	normal	"
143	2	Down	ON	contra	RH	contra	normal	"
144	3	Down	ON	contra	RH	contra	normal	"

Table A2a.6: Spin sub-matix for contra turn, normal entry

Test Point	Flaps	Gear	Power	Turning Flight	Spin Dir.	Aileron	Entry	Procedure
145	0	Up	OFF	pro	LH	neutral	accelerated	Pro Turn, accel. entry
146	1	Down	OFF	pro	LH	neutral	accelerated	"
147	2	Down	OFF	pro	LH	neutral	accelerated	"
148	3	Down	OFF	pro	LH	neutral	accelerated	"
149	0	Up	ON	pro	LH	neutral	accelerated	"
150	1	Down	ON	pro	LH	neutral	accelerated	"
151	2	Down	ON	pro	LH	neutral	accelerated	"
152	3	Down	ON	pro	LH	neutral	accelerated	"
153	0	Up	OFF	pro	LH	pro	accelerated	"
154	1	Down	OFF	pro	LH	pro	accelerated	"
155	2	Down	OFF	pro	LH	pro	accelerated	"
156	3	Down	OFF	pro	LH	pro	accelerated	"
157	0	Up	ON	pro	LH	pro	accelerated	"
158	1	Down	ON	pro	LH	pro	accelerated	"
159	2	Down	ON	pro	LH	pro	accelerated	"
160	3	Down	ON	pro	LH	pro	accelerated	"
161	0	Up	OFF	pro	LH	contra	accelerated	"
162	1	Down	OFF	pro	LH	contra	accelerated	"
163	2	Down	OFF	pro	LH	contra	accelerated	"
164	3	Down	OFF	pro	LH	contra	accelerated	"
165	0	Up	ON	pro	LH	contra	accelerated	"
166	1	Down	ON	pro	LH	contra	accelerated	"
167	2	Down	ON	pro	LH	contra	accelerated	"
168	3	Down	ON	pro	LH	contra	accelerated	"
169	0	Up	OFF	pro	RH	neutral	accelerated	"
170	1	Down	OFF	pro	RH	neutral	accelerated	"
171	2	Down	OFF	pro	RH	neutral	accelerated	"
172	3	Down	OFF	pro	RH	neutral	accelerated	"
173	0	Up	ON	pro	RH	neutral	accelerated	"
174	1	Down	ON	pro	RH	neutral	accelerated	"
175	2	Down	ON	pro	RH	neutral	accelerated	"
176	3	Down	ON	pro	RH	neutral	accelerated	"
177	0	Up	OFF	pro	RH	pro	accelerated	"

Test Point	Flaps	Gear	Power	Turning Flight	Spin Dir.	Aileron	Entry	Procedure
178	1	Down	OFF	pro	RH	pro	accelerated	"
179	2	Down	OFF	pro	RH	pro	accelerated	"
180	3	Down	OFF	pro	RH	pro	accelerated	"
181	0	Up	ON	pro	RH	pro	accelerated	"
182	1	Down	ON	pro	RH	pro	accelerated	"
183	2	Down	ON	pro	RH	pro	accelerated	"
184	3	Down	ON	pro	RH	pro	accelerated	"
185	0	Up	OFF	pro	RH	contra	accelerated	"
186	1	Down	OFF	pro	RH	contra	accelerated	"
187	2	Down	OFF	pro	RH	contra	accelerated	"
188	3	Down	OFF	pro	RH	contra	accelerated	"
189	0	Up	ON	pro	RH	contra	accelerated	"
190	1	Down	ON	pro	RH	contra	accelerated	"
191	2	Down	ON	pro	RH	contra	accelerated	"
192	3	Down	ON	pro	RH	contra	accelerated	"

Table A2a.7: Spin sub-matrix for pro turn, accelerated entry

Test Point	Flaps	Gear	Power	Turning Flight	Spin Dir.	Aileron	Entry	Procedure
193	0	Up	OFF	contra	LH	neutral	accelerated	Contra turn, accel.entry
194	1	Down	OFF	contra	LH	neutral	accelerated	"
195	2	Down	OFF	contra	LH	neutral	accelerated	"
196	3	Down	OFF	contra	LH	neutral	accelerated	"
197	0	Up	ON	contra	LH	neutral	accelerated	"
198	1	Down	ON	contra	LH	neutral	accelerated	"
199	2	Down	ON	contra	LH	neutral	accelerated	"
200	3	Down	ON	contra	LH	neutral	accelerated	"
201	0	Up	OFF	contra	LH	pro	accelerated	"
202	1	Down	OFF	contra	LH	pro	accelerated	"
203	2	Down	OFF	contra	LH	pro	accelerated	"

Test Point	Flaps	Gear	Power	Turning Flight	Spin Dir.	Aileron	Entry	Procedure
204	3	Down	OFF	contra	LH	pro	accelerated	"
205	0	Up	ON	contra	LH	pro	accelerated	"
206	1	Down	ON	contra	LH	pro	accelerated	"
207	2	Down	ON	contra	LH	pro	accelerated	"
208	3	Down	ON	contra	LH	pro	accelerated	"
209	0	Up	OFF	contra	LH	contra	accelerated	"
210	1	Down	OFF	contra	LH	contra	accelerated	"
211	2	Down	OFF	contra	LH	contra	accelerated	"
212	3	Down	OFF	contra	LH	contra	accelerated	"
213	0	Up	ON	contra	LH	contra	accelerated	"
214	1	Down	ON	contra	LH	contra	accelerated	"
215	2	Down	ON	contra	LH	contra	accelerated	"
216	3	Down	ON	contra	LH	contra	accelerated	"
217	0	Up	OFF	contra	RH	neutral	accelerated	"
218	1	Down	OFF	contra	RH	neutral	accelerated	"
219	2	Down	OFF	contra	RH	neutral	accelerated	"
220	3	Down	OFF	contra	RH	neutral	accelerated	"
221	0	Up	ON	contra	RH	neutral	accelerated	"
222	1	Down	ON	contra	RH	neutral	accelerated	"
223	2	Down	ON	contra	RH	neutral	accelerated	"
224	3	Down	ON	contra	RH	neutral	accelerated	"
225	0	Up	OFF	contra	RH	pro	accelerated	"
226	1	Down	OFF	contra	RH	pro	accelerated	"
227	2	Down	OFF	contra	RH	pro	accelerated	"
228	3	Down	OFF	contra	RH	pro	accelerated	"
229	0	Up	ON	contra	RH	pro	accelerated	"
230	1	Down	ON	contra	RH	pro	accelerated	"
231	2	Down	ON	contra	RH	pro	accelerated	"
232	3	Down	ON	contra	RH	pro	accelerated	"
233	0	Up	OFF	contra	RH	contra	accelerated	"
234	1	Down	OFF	contra	RH	contra	accelerated	"
235	2	Down	OFF	contra	RH	contra	accelerated	"
236	3	Down	OFF	contra	RH	contra	accelerated	"

Test Point	Flaps	Gear	Power	Turning Flight	Spin Dir.	Aileron	Entry	Procedure
237	0	Up	ON	contra	RH	contra	accelerated	"
238	1	Down	ON	contra	RH	contra	accelerated	"
239	2	Down	ON	contra	RH	contra	accelerated	"
240	3	Down	ON	contra	RH	contra	accelerated	"

Table A2a.8: Spin sub-matix for contra turn, accelerated entry

Note: If a spin cannot be excited by Wings Level Normal Spin Entry procedure it is appropriate to perform a Wings Level Accelerated Spin Entry

A2 10. Procedures and Acceptance criteria

Test Points 1 - 48 (Wings Level / Normal Entry / Normal and Abnormal Control Usage)
§ 23.141, 23.143 (b) (c), 23.171, 23.201, 23.207 (a) (b) (c), 23.221 (a)

Procedure (CS 23.201)

- Establish and verify maximum allowable fuel imbalance
- Select flaps, gear and power per the requirements in conditions above
- Trim aircraft for 1.5 V_{s1}
- Starting at least 10 kts above the stall speed, apply longitudinal control to decelerate the aircraft
    - Normal Entry: decelerate the aircraft at about one knot per second (range of 0.5 - 1.5 kts / sec)
- Maintain a constant deceleration until full stall occurs indicated by the following:
    - An uncontrollable downward pitching motion, or
    - The elevator control reaches the stop
- At the stall point apply full-up elevator and full rudder in the direction of the desired spin with ailerons neutral
- Recover from spin with control usage
- Repeat the above procedure in the opposite direction

Test Points 49 - 144 (Turning Flight / Neutral Entry / Normal and Abnormal Control Usage)

- Procedure as defined below

Test Points 145 - 240 (Turning Flight / Accelerated Entry / Normal and Abnormal Control Usage)

- Procedure as defined below

§23.141, 23.143 (b) (c), 23.171, 23.201, 23.203, 23.207 (a) (b) (c) (e), 23.221 (a)

Procedure (CS 23.203)

- Establish and verify maximum allowable fuel imbalance
- Select flaps, gear and power per the requirements in conditions above
- Trim the aircraft for 1.5 V_{s1}
- Establish and maintain a coordinated 30 degrees of bank turn
- Starting at least 10 kts above the stall speed reduce speed steadily and progressively by tightening the turn by elevator control until aircraft stalls
    - Normal Entry: decelerate the aircraft at about one knot per second (range of 0.5 - 1.5 kts / sec)
    - Accelerated Entry: speed reduction of 3 to 5 knots per second
- Maintain a constant deceleration until full stall occurs indicated by the following:

- An uncontrollable downward pitching motion, or
- The elevator control reaches the stop

➢ At the stall point apply full-up elevator and full rudder in the direction of the desired spin with ailerons neutral

➢ Recover from spin with control usage

➢ Repeat the above procedure in the opposite direction

Acceptance criteria

✓ It must be possible to enter and recover from each stall without the use of exceptional pilot skill, alertness, or strength (23.141)

✓ It must be possible to make a smooth transition from one flight condition to another without danger of exceeding the limit load factor under any probable operating condition (23.143(b))

✓ If marginal conditions exist with regard to pilot strength, the control forces required must be determined by quantitative tests (23.143(c))

✓ Stick force has to remain positive up to the stall (23.171)

✓ There must be a clear and distinctive stall warning in straight flight, with the flaps and landing gear in any normal position, in straight flight (23.207(a))

✓ The stall warning has to give clearly distinguishable indications that a stall condition is approached either through the inherent aerodynamic qualities of the aeroplane or by another device excluding visual stall warning (23.207 (b))

✓ The stall warning must begin at least 5 kts above the stall speed and continue until the stall occurs (23.207(c))

✓ During the stall tests required by CS 23.203 (a) (2), the stall warning must begin sufficiently in advance of the stall for the stall to be averted by pilot action taken after the stall warning first occurs (23.207(e))

✓ A Single engined, normal category aeroplane must be able to recover from a one-turn spin or a three-second spin, whichever takes longer, in not more than one additional turn, after initiation of the first control action for recovery (23.221(a)). In addition -

- For both the flaps-retracted and flaps-extended conditions, the applicable airspeed limit and positive limit manoeuvring load factor must not be exceeded (1);
- No control forces or characteristic encountered during the spin or recovery may adversely affect prompt recovery (2);
- It must be impossible to obtain unrecoverable spins with any use of the flight or engine power controls either at the entry into or during the spin (3); and

For the flaps extended condition, the flaps may be retracted during the recovery but not before rotation has ceased (4)

Appendix 3 Excerpt from the current Certification Specification EASA CS 23 on Spinning

CS 23.221 Spinning

(**a)** ***Normal Category aeroplanes***. A Single engine, normal category aeroplane must be able to recover from a one-turn spin or a three-second spin, whichever takes longer, in not more than one additional turn, after initiation of the first control action for recovery. In addition

(1) For both the flaps-retracted and flaps-extended conditions, the applicable airspeed limit and positive limit manoeuvring load factor must not be exceeded;
(2) No control forces or characteristic encountered during the spin or recovery may adversely affect prompt recovery;
(3) It must be impossible to obtain unrecoverable spins with any use of the flight or engine power controls either at the entry into or during the spin; and
(4) For the flaps extended condition, the flaps may be retracted during the recovery but not before rotation has ceased.

(b) ***Utility category aeroplanes*.** A utility category aeroplane must meet the requirements of sub-paragraph (a) of this paragraph. In addition, the requirements of sub-paragraph (c) of this paragraph and CS 23.807 (b) (7) must be met if approval for spinning is requested.

(c) ***Aerobatic category aeroplanes***. An aerobatic category aeroplane must meet the requirements of sub-paragraph (a) of this paragraph and CS 23.807 (b) (6). In addition, the following requirements must be met in each configuration for which approval for spinning is requested -
(1) The aeroplane must recover from any point in a spin up to and including six turns, or any greater number of turns for which certification is requested, in not more than one and one-half additional turns after initiation of the first control action for recovery. However, beyond three turns, the spin may be discontinued if spiral characteristics appear;
(2) The applicable airspeed limits and limit manoeuvring load factors must not be exceeded. For flaps-extended configurations for which approval is requested, the flaps must not be retracted during the recovery;
(3) It must be impossible to obtain unrecoverable spins with any use of the flight or engine power controls either at the entry into or during the spin; and
(4) There must be no characteristics during the spin (such as excessive rates of rotation or extreme oscillatory motion) which might prevent a successful recovery due to disorientation or incapacitation of the pilot.

Appendix 4 Technical data of the research aeroplanes

A4 1. **NASA** research aeroplane, Piper PA 28 RT-201T Turbo Arrow IV

TABLE 1. AIRPLANE PHYSICAL CHARACTERISTICS

Overall dimensions:	
Span, ft	35.43
Length, ft	27.80
Height, ft	8.26
Powerplant:	
Type	Reciprocating, four cylinder, horizontally opposed
Rated power at sea level, hp	200
Rated continuous speed, rpm	2700
Propeller:	
Type	Two blades, constant speed
Diameter, in.	76
Pitch (variable), deg	14 to 31
Wing:	
Area, ft^2	173.7
Root chord, in.	74.0
Chord of constant section, in.	63.0
Tip chord, in.	42.2
Mean aerodynamic chord, in.	62.16
Aspect ratio	7.24
Dihedral, deg	7.0
Incidence at root, deg	2.0
Incidence at tip, deg	−1.0
Airfoil section	NACA 65_2-415 modified
Flap:	
Chord, in.	12.26
Span, in.	85.50
Area (each), ft^2	7.3
Hinge line, percent flap chord	20.0
Deflection, deg	40 down
Aileron:	
Mean chord, in.	10.01
Span, in.	100.05
Area (each), ft^2	6.95
Deflection, deg	30 up, 16 down
Stabilator:	
Area (including tab), ft^2	25.0
Chord (constant), in.	30.0
Aspect ratio	4.0
Dihedral, deg	0
Hinge line, percent stabilator chord	26.97
Deflection, deg	10 up, 10 down
Airfoil section	NACA 0012
Tab:	
Chord (constant), in.	6.0
Span, in.	106.2
Area, ft^2	4.4
Tab hinge line to stabilator hinge line, in.	15.91

Vertical tail:	
Area (including rudder), ft^2	17.6
Root chord, in.	54.52
Tip chord, in.	28.62
Mean aerodynamic chord, in.	42.91
Span, in.	60.84
Aspect ratio	1.47
Leading edge sweep back, deg	33.91
Rudder:	
Area, ft^2	5.8
Average chord aft of hinge line, in.	11.85
Span (parallel to hinge line), in.	61.6
Deflection, deg	28 left, 28 right
Test weight at altitude, lb	2420
Relative density, μ, at 9000 ft altitude	6.7
Representative center-of-gravity position:	
FS, in.	95.85 (27.82 percent $\bar{c}$)
BL, in.	−0.56
WL, in.	38.15
Moments of inertia about body axes (based on above center-of-gravity position):	
I_x, slug-ft^2	1789
I_y, slug-ft^2	2486
I_z, slug-ft^2	3796
Inertia yawing-moment parameter, $\frac{I_x - I_y}{mb^2}$	-74×10^{-4}

Table A4.1: Technical data of the **NASA** research aeroplane, (Stough et al., 1985)

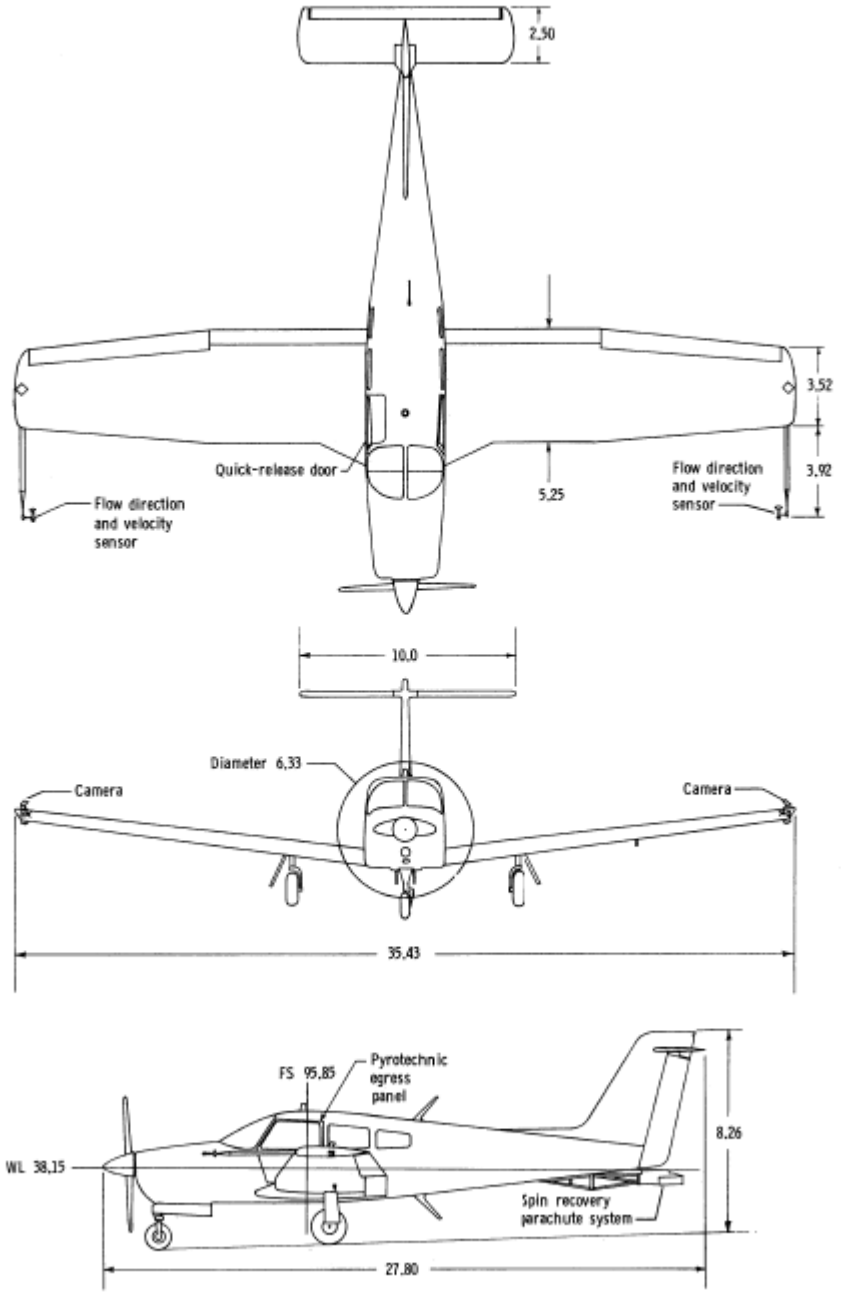

Figure 3. Three-view drawing of test airplane. Dimensions are in feet.

Figure A4.1: Dimensions of the **NASA** research aeroplane, (Stough et al, 1985)

A4 2 Research aeroplane of the collaborating ATO, **Fuji FA – 200 – 160**

I-2 BASIC DIMENSIONS AND DESIGN DATA OF AIRFRAME

	FA-200-160	FA-200-180
Engine	Lycoming 0-320-D2A (160 HP, 2700 rpm)	Lycoming IO-360BIB (180 HP, 2700 rpm)
Propeller	McCauley IC172MGM7656 or 7662 Fixed pitch propeller	McCauley B2D34C53/74E-0 Constant-speed propeller
Maximum Diameter of Propeller	76 in	74 in
Minimum Diameter of Propeller	74 in	72.5 in
Overall Width	30 ft 10.87 in	30 ft 10.87 in
Overall Lenght	26 ft 1.39 in	26 ft 1.39 in
Overall Height	8 ft 5.97 in	8 ft 5.97 in
Wing Area	150.69 ft² = 14,00 m²	150.69 ft²
Length of Chord of Wing	5 ft = 1,524 m	5 ft
Taper Ratio of Wing	1.0 λ = Chord tip / Chord root	1.0
Sweep Back of Wing	0°	0°
Twist of Wing	0°	0°
Incidence Angle of wing	2.5° = Einstellwinkel	2.5°
Dihedral Angle of Wing	7.0°	7.0°
H. Stabilizer Area	35.73 ft²	35.73 ft²

TABLE I-1 BASIC DIMENSIONS AND DESIGN DATA OF AIRFRAME(1/3)

Table A4.2: Technical data of the research aeroplane of the collaborating ATO, from Fuji Service Manual (Fuji, 1971)

	FA-200-160	FA-200-180
H. Stabilizer Span	$11^{ft}\ 4.42^{in}$	$11^{ft}\ 4.42^{in}$
Dihedral Angle of H.T.	0°	0°
Incidence Angle of H.T.	0°	0°
V. Stabilizer Area	16.11^{ft^2}	16.11^{ft^2}
Incidence Angle of V.T.	0° from center line of airframe	0° from center line of airframe
Flap Area	20.16^{ft^2}	20.16^{ft^2}
Flap Span	$13^{ft}\ 2.82^{in}$	$13^{ft}\ 2.82^{in}$
Aileron Area	12.10^{ft^2}	12.10^{ft^2}
Aileron Span	$12^{ft}\ 5.61^{in}$	$12^{ft}\ 5.61^{in}$
Elevator Area	15.45^{ft^2}	15.45^{ft^2}
Rudder Area	9.58^{ft^2}	9.58^{ft^2}
Empty Weight (STD)	1,367 lbs	1,433 lbs
Max. Weight N	2,335 lbs (for 7656 propeller) 2,270 lbs (for 7662 propeller)	2,535 lbs
U	2,137 lbs	2,425 lbs
A	1,940 lbs	2,072 lbs
Fuel Capacity	54 US.GAL	54 US.GAL
Fuel Grade	Grade 91/96 (100/130)	Grade 91/96 (100/130)
Oil Capacity	8QT.	8QT.
Oil Grade	SAE50: above 60° F SAE40: 30°F - 90°F SAE30: 0°F - 70°F SAE20: below 10°F	SAE50: above 60°F SAE40: 30°F - 90°F SAE30: 0°F - 70°F SAE20: below 10°F
Main Wheel Track	$8^{ft}\ 7.39^{in}$	$8^{ft}\ 7.39^{in}$
Nose and Main Wheel Distance	$5^{ft}\ 8.90^{in}$	$5^{ft}\ 8.90^{in}$
Main Landing Gear Tire (STD)	6.00-6 4ply 28psi±2	6.00-6 4ply 28psi±2
Main landing Gear Tire (OPT)	15×6.00-6 4ply $40psi^{+2}_{-4}$	15×6.00-6 4ply $40psi^{+2}_{-4}$

TABLE I-1 BASIC DIMENSIONS AND DESIGN DATA OF AIRFRAME(3/3)

Table A4.2 (cont.): Technical data of the research aeroplane of the collaborating ATO, from Fuji Service Manual (Fuji, 1971)

	FA-200-160	FA-200-180
Main Landing Gear Oleo Pressure (For Serial NOS.12 Thru 55)	90psi±5	90psi±5
Nose Landing Gear Tire (STD)	5.00-5 4ply (T.T.) 30psi $^{+2}_{-4}$	5.00-5 4ply (T.T.) 30 $^{+2}_{-4}$
Nose Landing Gear Tire (OPT)	5.00-5 4ply (T.L) 30psi $^{+2}_{-4}$	5.00-5 4ply (T.L) 30psi $^{+2}_{-4}$
Nose Landing Gear Oleo Pressure (For Serial NOS. 12 Thru 55)	65psi $\pm$5	85psi $\pm$5
Nose Landing Gear Oleo Pressure (For Serial NOS.56 & ON)	100psi±10	100psi±10
Flap Travel: Down	$35^{+2°}_{-1°}$	$35^{+2°}_{-1°}$
Aileron Travel: Down	15±1°	15±1°
: Up	20±1°	20±1°
Rudder Travel: Left	25±1°	25±1°
: Right	25±1°	25±1°
Elevator Travel: Down	15±1°	15±1°
: Up	25±1° (S/Ns 12 THRU 126)	25±1° (S/Ns 12 THRU 126)
: Up	30±1° (S/N 127 & ON)	30±1° (S/N 127 & ON)
Elevator Trim Tab Travel : Down	20±1°	20±1°
: Up	15±1°	15±1°
Flap Cable Tension	20±10 lbs	20±10 lbs
Aileron Cable Tension		
(control column-bellcrank)	45±5 lbs	45±5 lbs
(R. bellcrank-L. bellcrank)	35±5 lbs	35±5 lbs
Rudder Cable Tension (with Steering)	30 ~ 50 lbs	30 ~ 50 lbs
Elevator Cable Tension	Upper cable: 43±5 lbs	Upper cable: 43±5 lbs
	Lower cable: 37±5 lbs	Lower cable: 37±5 lbs
Elevator Trim Tab Cable Tension	15±5 lbs	15±5 lbs

Table A4.2 (cont.): Technical data of the research aeroplane of the collaborating ATO, from Fuji Service Manual (Fuji, 1971)

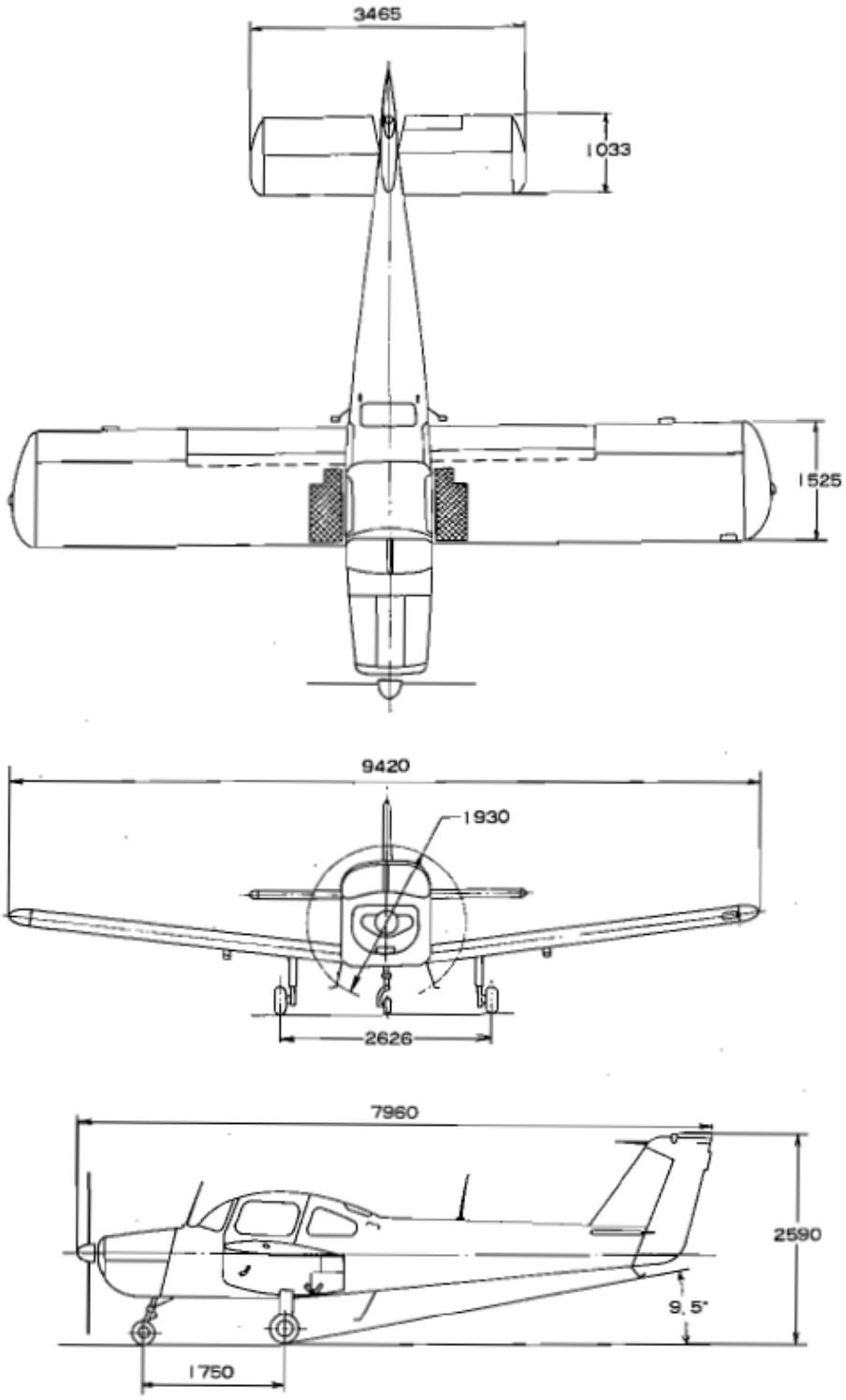

FIG 1-1 THREE VIEW DRAWING FA-200-160 (SCALE m/m)

Figure A4.2: Dimensions (in metres) of the research aeroplane of the collaborating ATO, from Fuji Service Manual (Fuji, 1971)

Appendix 5 Aeroplane Categories

CS 23.3 Aeroplane categories

(a) The normal category is limited to non-aerobatic operations. Non-aerobatic operations include –

(1) Any manoeuvre incident to normal flying;

(2) Stalls (except whip stalls); and

(3) Lazy eights, chandelles and steep turns or similar manoeuvres, in which the angle of bank is not more than 60°.

(b) The utility category is limited to any of the operations covered under sub-paragraph (a); plus –

(1) Spins (if approved for the particular type of aeroplane); and

(2) Lazy eights, chandelles, and steep turns, or similar manoeuvres in which the angle of bank is more than 60° but not more than 90°.

(c) The aerobatic category is without restrictions, other than those shown to be necessary as a result of required flight tests.

(d) Commuter category operation is limited to any manoeuvre incident to normal flying, stalls (except whip stalls) and steep turns in which the angle of bank is not more than 60°.

(e) Except for commuter category, aeroplanes may be certificated in more than one category if the requirements of each requested category are met.

Figure A5.1: Excerpt from EASA CS 23

Appendix 6 Calibration protocols

Table of contents of calibration protocols

In all of the following cases, the calibration of the sensor has been conducted by comparing the data set of the used sensor with a (officially) calibrated sensor (of the same type).The calibration protocol using in that process is also presented.

All error values from these used sensors meet the necessary precision

Three graphs are shown for each sensor. The second graph always shows that the measured reference values against a straight line which is in all cases a close fit.

Next to the calibrated sensor systems the core system of the measurement system is the data acquisition computer which is explained in section ‘3.4 Data acquisition’ in Chapter 3.

CP 1 Total pressure sensor calibration

	name	unit		
			date	29.09.2014
in acro	Pstau_r	V	aircraft type	Fuji
out acro	Pstau_r	hPa		

sensor		reference sensor	
type	D239	type	DPM7885
sensor no.	DD-11	sensor no.	Weston2, Weston1

description of calibration:

zero refe-rence:	n/a
positive:	n/a
remark:	
data file:	Fuji-cal_20140929_1.mat
events:	4 5

coefficients to compute Pstau_r:
[7.549341,-37.722]

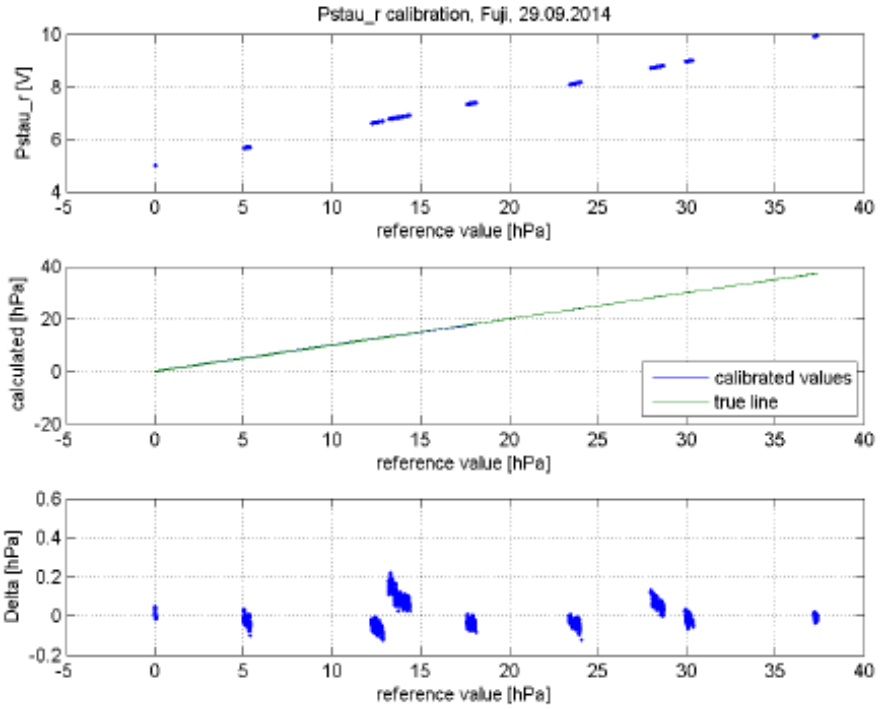

Figure A6.1: Total pressure sensor calibration

In Figure A6.1 the first graph shows the output voltage Pstau_r [V] versus the reference total pressure within a range of -5 to + 37 hPa measured several times at 9 different values. The third graph shows the variation about the measured pressure values [Delta [hPa] versus reference value [hPa]. This graph shows that the reference pressure values have a variation of approximately +/- 0.2 hPa.

CP 2 Total temperature sensor calibration:

	name	unit		
			date	29.09.2014
in acro	Ttotal_r	V	aircraft type	Fuji
out acro	Ttotal_r	degC		

sensor		reference sensor	
type	PT100	type	PT100-Box
sensor no.	mK-01	sensor no.	n/a

description of calibration:

zero refe-rence:	n/a
positive:	n/a
remark:	
data file:	Fuji-cal_20140929_1.mat
events:	6 7 8 9 10

coefficients to compute Ttotal_r:
[7.549341,-37.722]

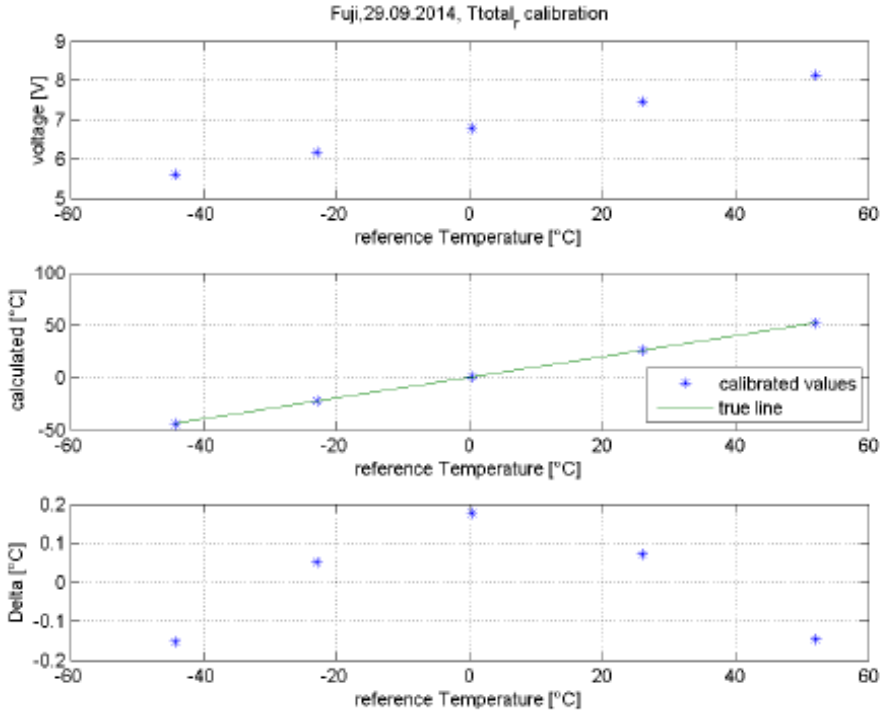

Figure A6.2: Total temperature sensor calibration

In Figure A6.2 the first graph shows the output voltage [V] versus the reference temperature [°C] within a range of +/- 50°C measured several times at 5 different temperature values. The third graph shows the variation about the measured temperature values (Delta [°C] versus reference Temperature [°C]). The temperature values have a variation of approximately +/- 0.2 °C.

CP 3 Left-hand Angle-of-Attack sensor calibration

	name	unit		
			date	29.09.2014
in acro	alpha_le_r	V	aircraft type	Fuji
out acro	alpha_le_m	deg		

sensor		reference sensor	
type	CP-2UTX mK-05	type	angle sensor
sensor no.	cover	sensor no.	ssi

description of calibration:

zero refe-rence:	vane aligned to boom
positive:	airflow from bottom
remark:	
data file:	Fuji-cal_20140929_1.mat
events:	12 13

coefficients to compute alpha_le_m from alpha_le_r:
[1.477762,-21.753744,140.968760,-351.537]

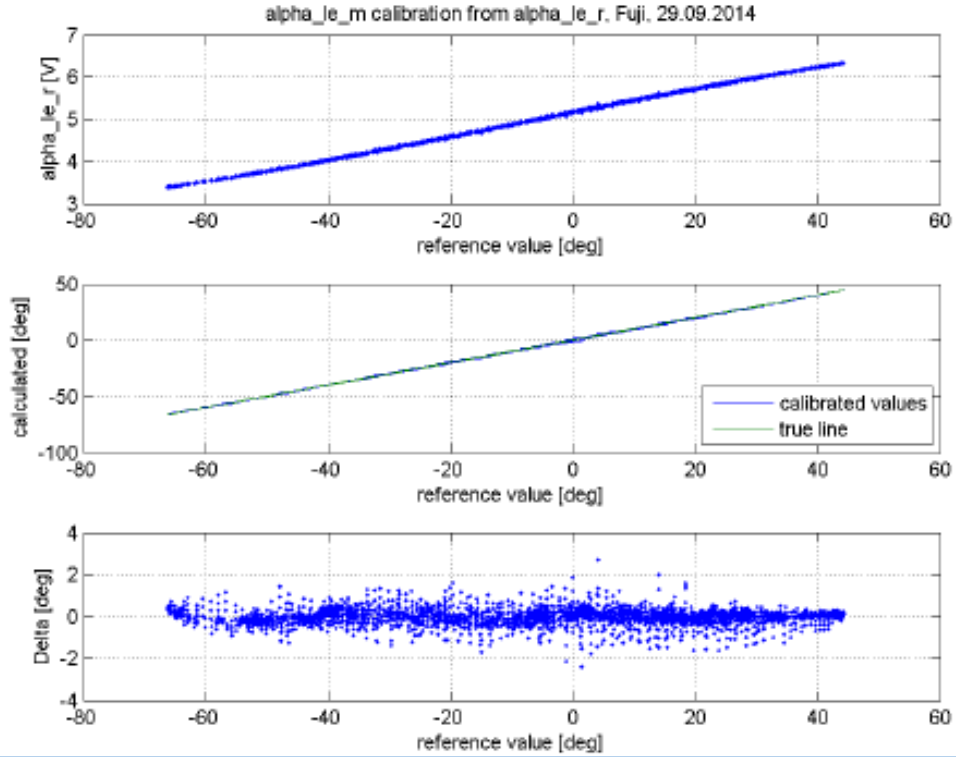

Figure A6.3: Left Angle-of Attack sensor calibration

In Figure A6.3 the first graph shows the output voltage alpha_le_r [V] versus the reference values [°] of the left wing angle of attack sensor within a range of – 70° to + 45° measured several times through the sensor range. The third graph shows the variation about the measured angles of approximately +/- 1.5°.

CP 4 Left-hand Sideslip Angle sensor calibration

	name	unit		
			date	29.09.2014
in acro	beta_le_r	V	aircraft type	Fuji
out acro	beta_le_m	deg		

sensor		reference sensor	
type	CP-2UTX mK-05	type	angle sensor
sensor no.	cover	sensor no.	ssi

description of calibration:

zero reference:	vane aligned to boom
positive:	Airflow from right side
remark:	
data file:	Fuji-cal_20140929_1.mat
events:	15 16

coefficients to compute beta_le_m from beta_le_r:
[-0.499270,7.326799,-65.164082,211.977]

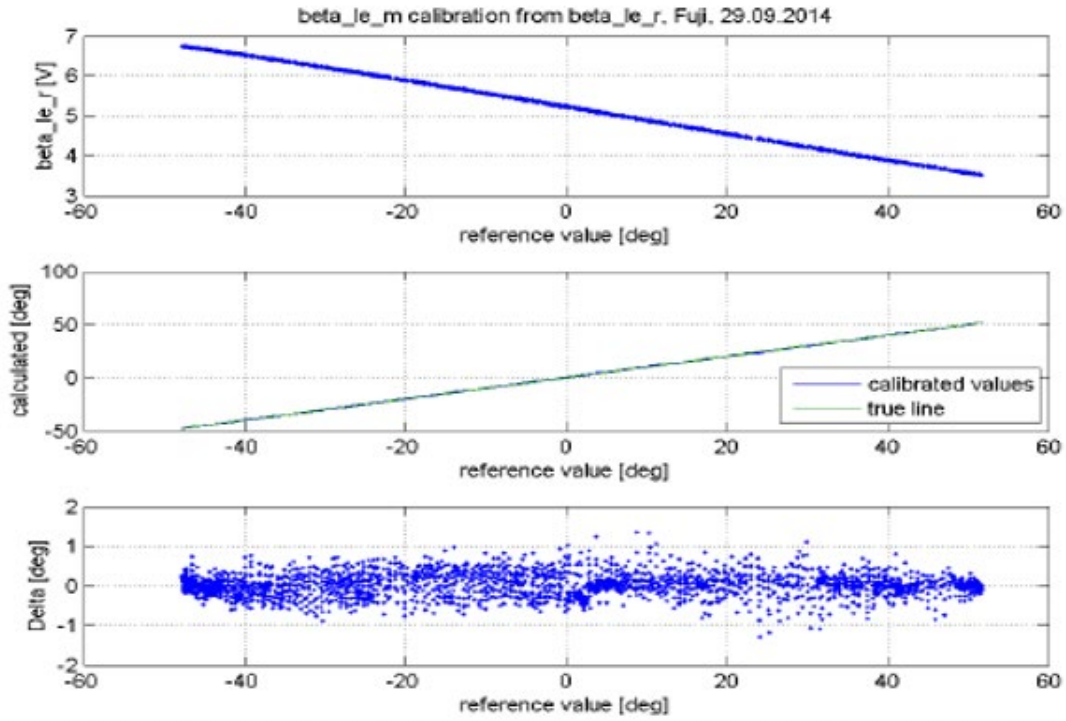

Figure A6.4: Left Sideslip Angle sensor calibration

In Figure A6.4 the first graph shows the output voltage beta_le_r [V] versus the reference values [°] of the left wing sideslip angle sensor within a range of – 50° to + 50° measured several times through the sensor range. The third graph shows the variation about the measured angles of approximately +/- 1°.

CP 5 Right-hand Angle-of-Attack sensor calibration

Calibration protocoll

	name	unit		
			date	29.09.2014
in acro	alpha_ri_r	V	aircraft type	Fuji
out acro	alpha_ri_m	deg		

sensor		reference sensor	
type	CP-2UTX	type	angle sensor
sensor no.	mK-06	sensor no.	ssi

description of calibration:

zero refe-	
rence:	vane aligned to boom
positive:	airflow from bottom
remark:	
	Fuji-
data file:	cal_20140929_1.mat
events:	22 23

coefficients to compute alpha_ri_m from alpha_ri_r:
[-0.158662,1.996391,33.341935,-199.764]

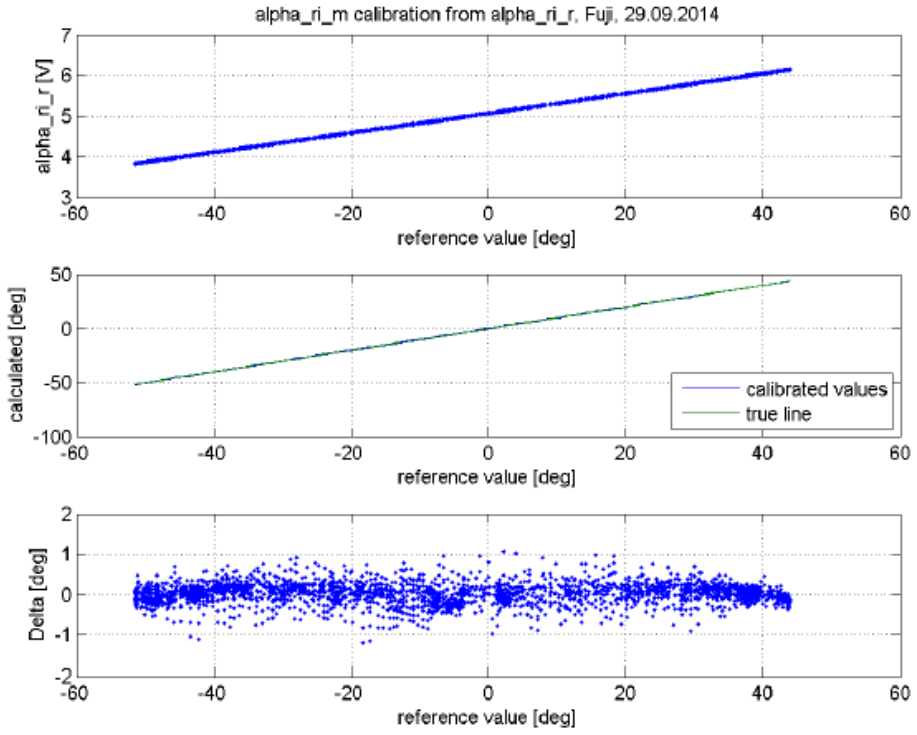

Figure A6.5: Right Angle-of-Attack sensor calibration

In Figure A6.5 the first graph shows the output voltage alpha_ri_r [V] versus the reference values [°] of the right wing angle of attack sensor within a range of – 50° to + 50° measured several times through the sensor range. The third graph shows the variation about the measured angles of approximately +/- 1°.

	name	unit		
			date	29.09.2014
in acro	beta_ri_r	V	aircraft type	Fuji
out acro	beta_ri_m	deg		

sensor		reference sensor	
type	CP-2UTX	type	angle sensor
sensor no.	mK-06	sensor no.	ssi

description of calibration:

zero refe-rence:	vane aligned to boom
positive:	Airflow from right side
remark:	
data file:	Fuji-cal_20140929_1.mat
events:	18 19

coefficients to compute beta_ri_m from beta_ri_r:
[0.455879,-6.162142,63.904378,-223.312]

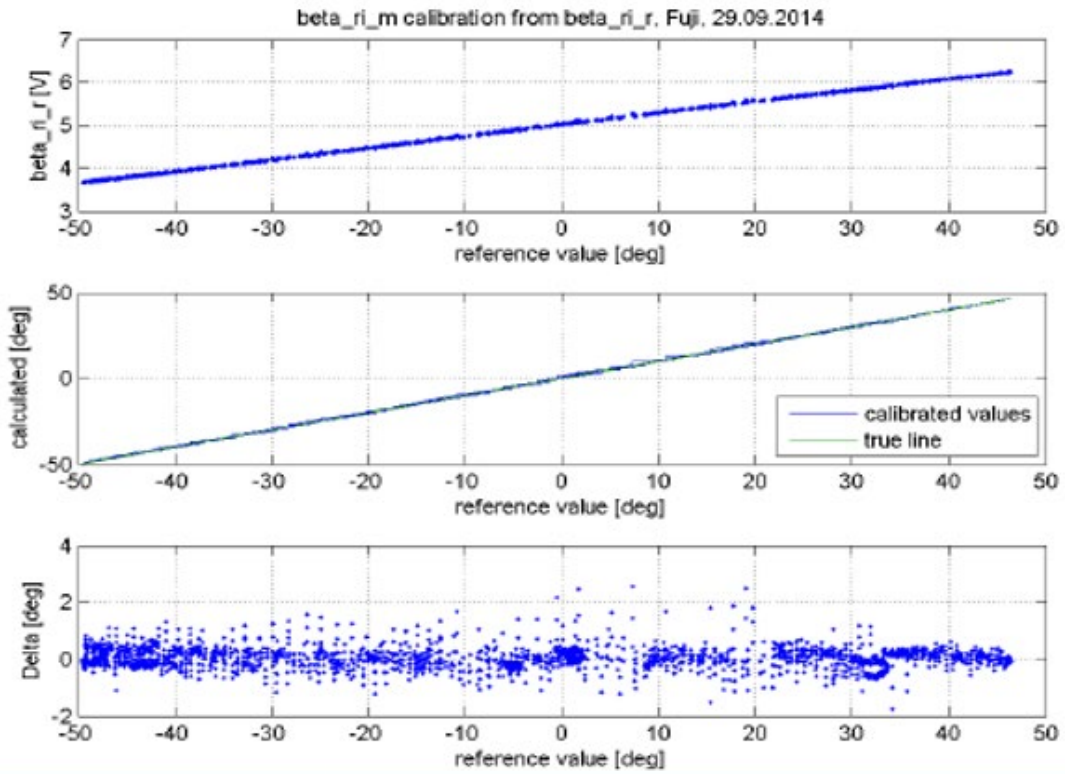

Figure A6.6: Right Sideslip Angle sensor calibration

In Figure A6.6 the first graph shows the output voltage beta_ri_r [V] versus the reference values [°] of the right wing sideslip angle sensor within a range of – 50° to + 50° measured several times through the sensor range. The third graph shows the variation about the measured angles of approximately +/- 1.5°.

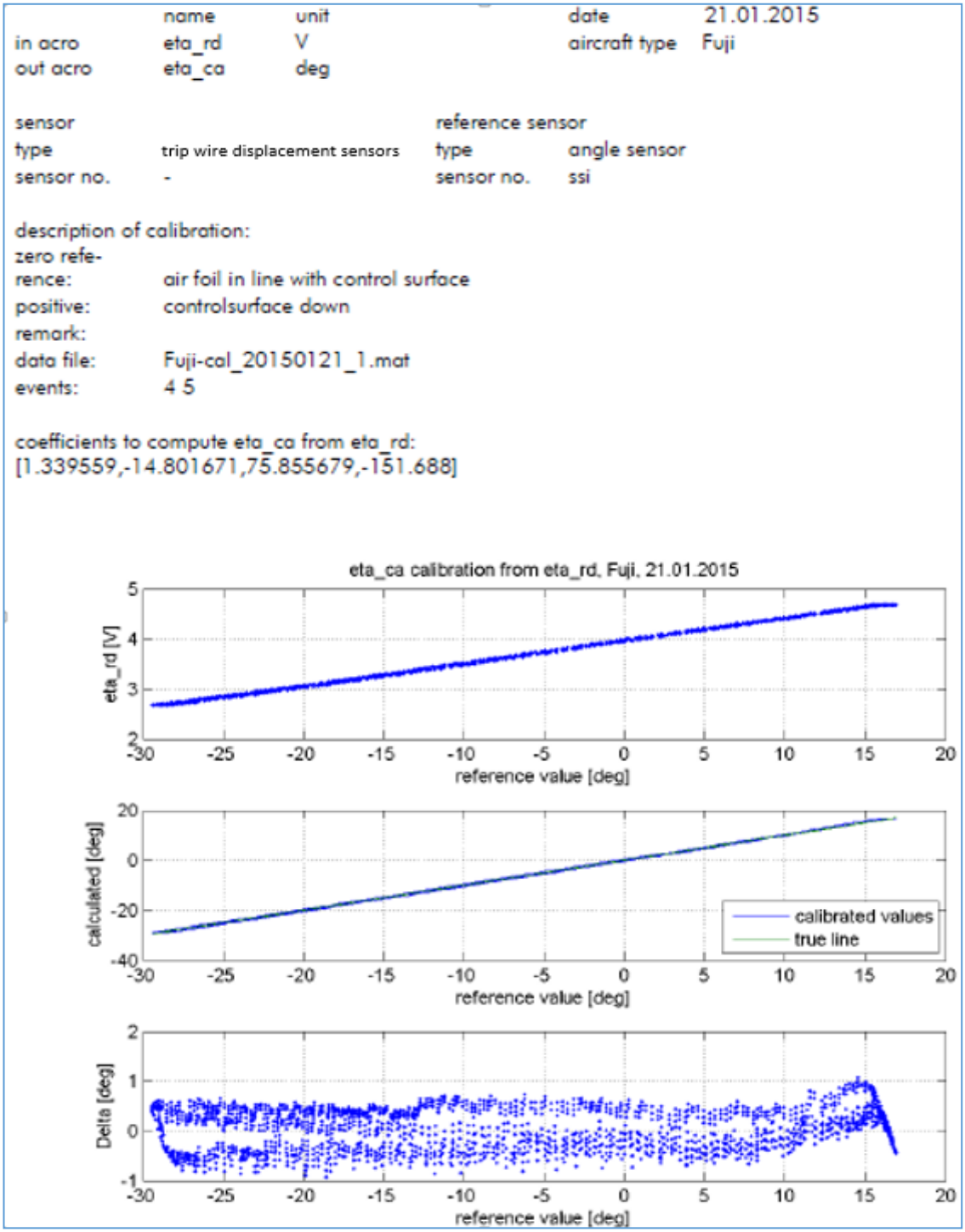

Figure A6.7: Elevator deflection sensor calibration

In Figure A6.7 the first graph shows the output voltage eta_rd [V] versus the reference value [°] of the elevator deflection in a range of – 30° to + 20° measured several times through the entire sensor range. The third graph shows the variation about the measured deflection values of approximately +/- 1°. These error values meet the necessary precision of +/- 2°.

	name	unit		
			date	21.01.2015
in acro	eta_rd	V	aircraft type	Fuji
out acro	eta_horn	mm		

sensor		reference sensor	
type	trip wire displacement sensors	type	Seilzug
sensor no.	-	sensor no.	mW-SZ07

description of calibration:

zero refe-rence:	air foil in line with control surface
positive:	controlsurface down
remark:	
data file:	Fuji-cal_20150121_1.mat
events:	4 5

coefficients to compute eta_horn from eta_rd:
[-2.152636,19.746810,47.621494,-365.649]

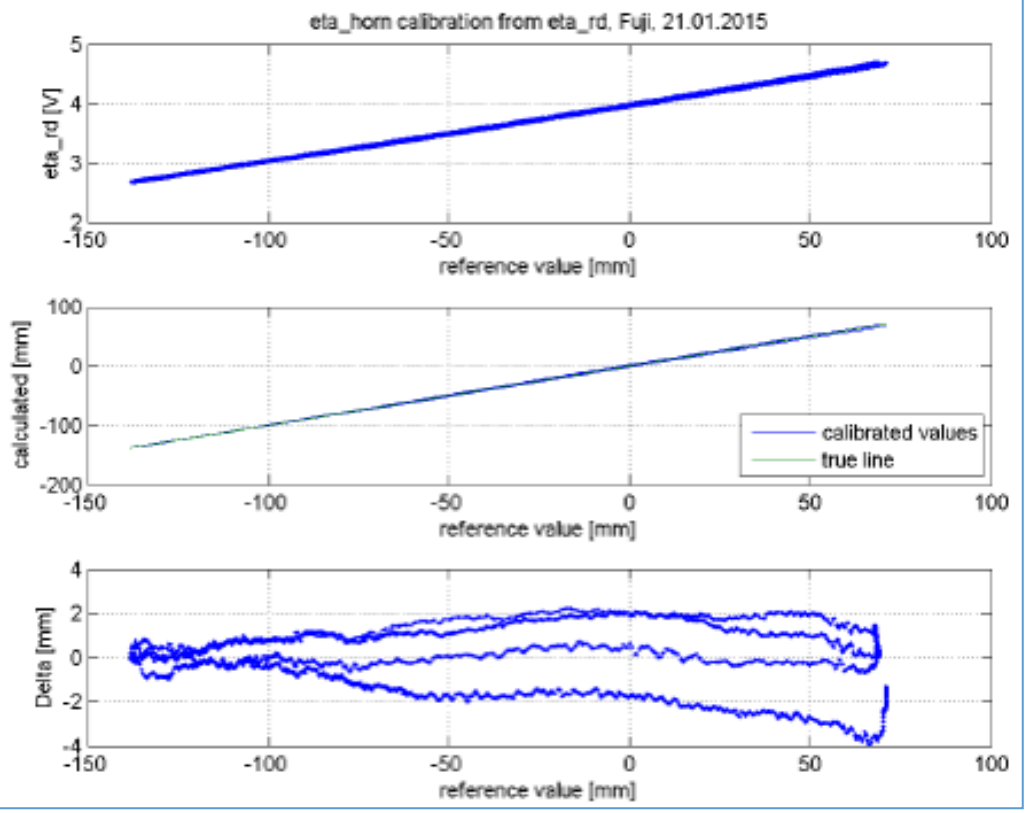

Figure A6.8: Elevator control deflection sensor calibration

In Figure A6.8 the first graph shows the output voltage eta_rd [V] versus the reference value [mm] of the elevator control deflection in a range of – 130 mm to + 70 mm measured several times through the entire sensor range. The third graph shows the variation about the measured control deflection values of approximately +2° and -4°.

	name	unit		
			date	21.01.2015
in acro	zeta_rd	V	aircraft type	Fuji
out acro	zeta_ca	deg		

sensor		reference sensor	
type	trip wire displacement sensors	type	angle sensor
sensor no.	-	sensor no.	ssi

description of calibration:

zero refe-rence:	air foil in line with control surface
positive:	controlsurface left
remark:	
data file:	Fuji-cal_20150121_1.mat
events:	14 15

coefficients to compute zeta_ca from zeta_rd:
[0.401875,-3.733146,30.724795,-77.071]

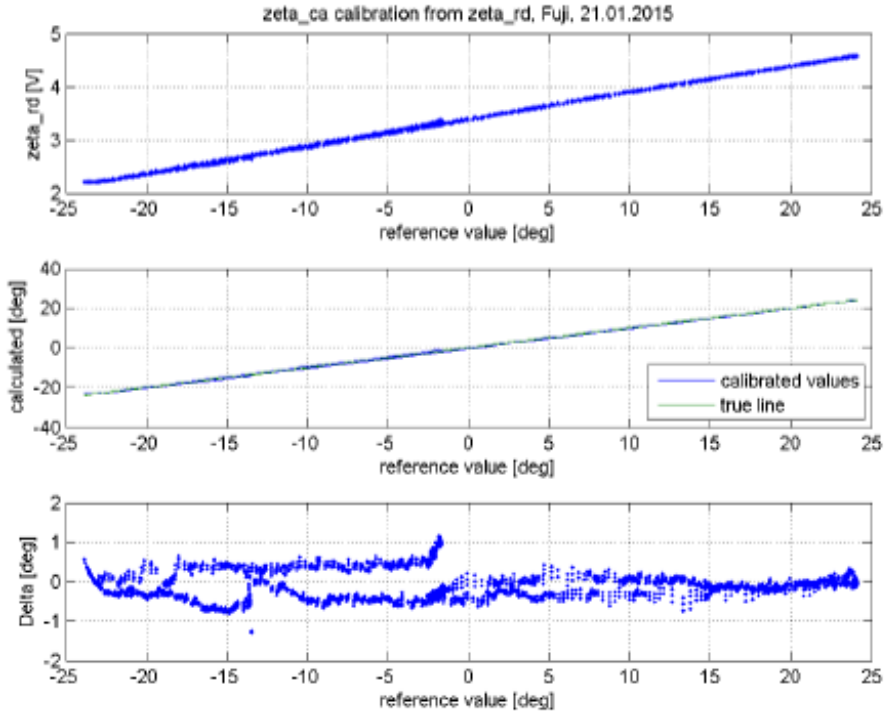

Figure A6.9: Rudder deflection sensor calibration

In Figure A6.9 the first graph shows the output voltage zeta_rd [V] versus the reference value [°] of the rudder deflection in a range of – 24° to + 24° measured several times through the entire sensor range. The third graph shows the variation about the measured rudder deflection values of approximately +/- 1°. These error values meet the necessary precision of +/- 2°.

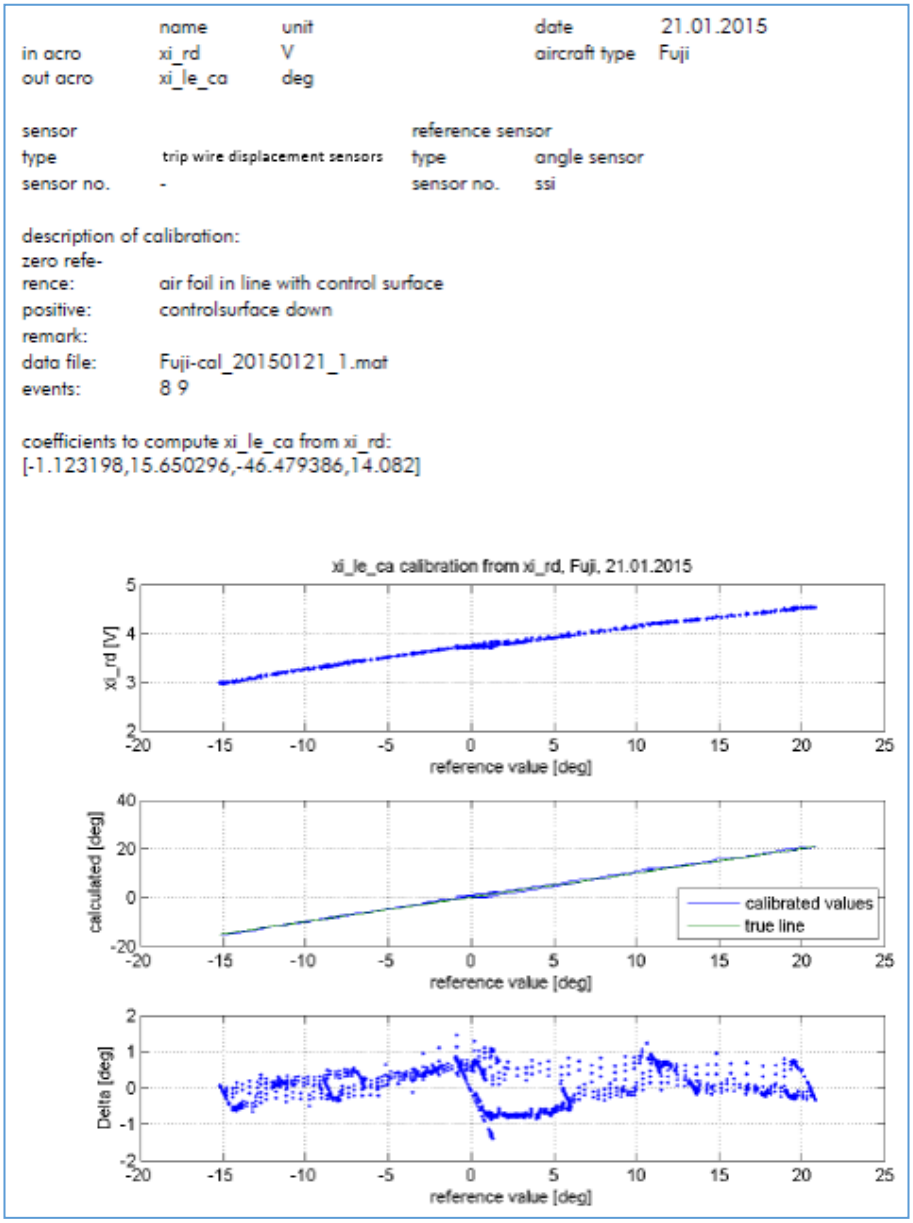

Figure A6.10: Left aileron deflection sensor calibration

In Figure A6.10 the first graph shows the output voltage xi_rd [V] versus the reference value [°] of the left aileron deflection in a range of – 15° to + 21° measured several times through the entire sensor range. The third graph shows the variation about the measured left aileron deflection values of approximately +/- 1°. These error values meet the necessary precision of +/- 2°.

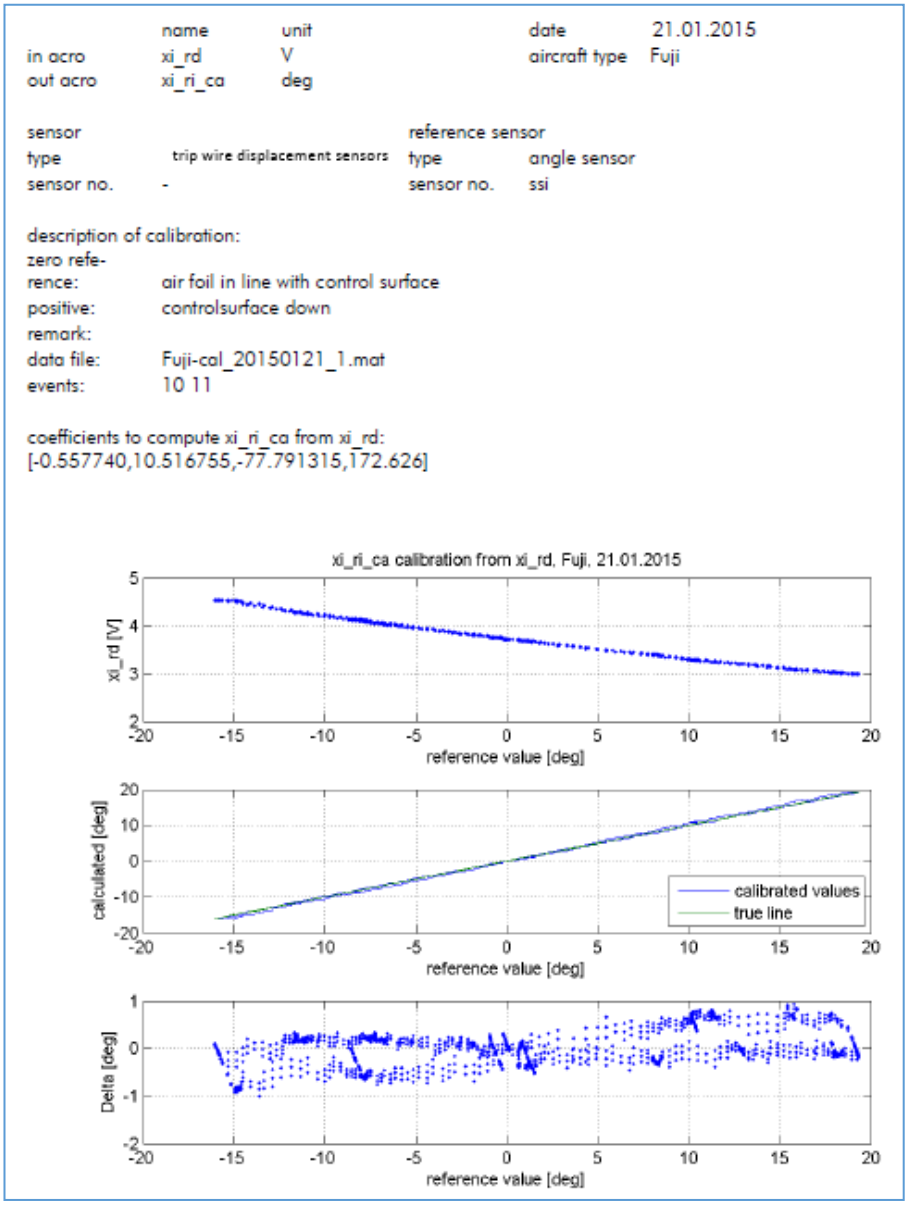

Figure A6.11: Right aileron deflection sensor calibration

In Figure A6.11 the first graph shows the output voltage xi_rd [V] versus the reference value [°] of the right aileron deflection in a range of – 16° to + 20° measured several times through the entire sensor range. The third graph shows the variation about the measured left aileron deflection values of approximately +/- 1°. These error values meet the necessary precision of +/- 2°.

	name	unit		
			date	21.01.2015
in acro	xi_rd	V	aircraft type	Fuji
out acro	xi_horn	deg		

sensor		reference sensor	
type	trip wire displacement sensors	type	inclinometer
sensor no.	-	sensor no.	Oak

description of calibration:

zero refe-rence:	air foil in line with control surface control to
positive:	left
remark:	
data file:	Fuji-cal_20150121_1.mat
events:	8 9

coefficients to compute xi_horn from xi_rd:
[-4.161891,49.599547,-258.813797,490.951]

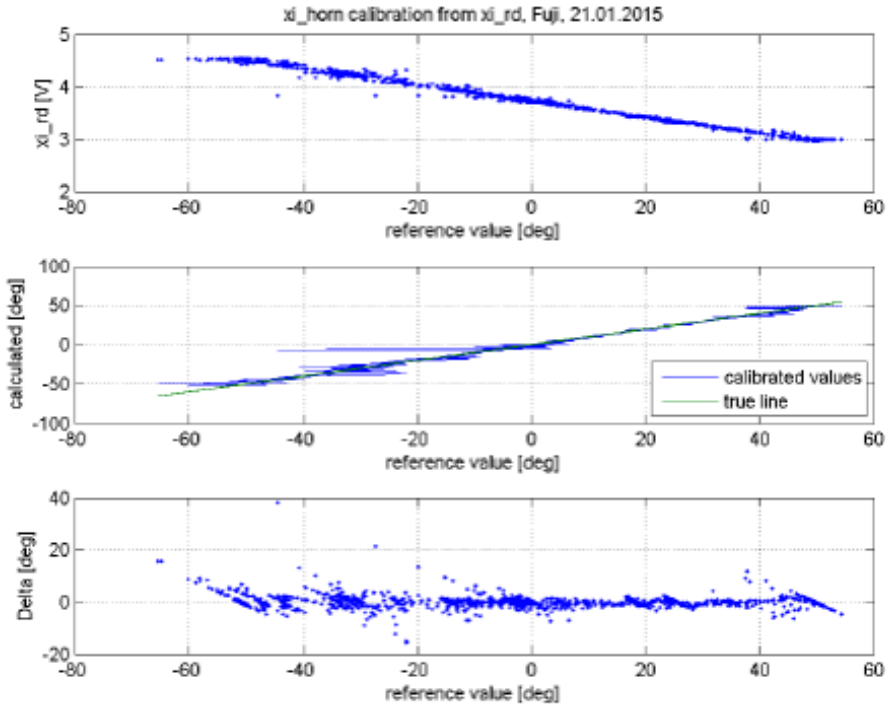

Figure A6.12: Aileron control deflection sensor calibration

In Figure A6.12, the first graph shows the output voltage xi_rd [V] versus the reference value [°] of the aileron control deflection in a range of – 65° to + 60° measured several times through the entire sensor range. The third graph shows the variation about the measured rudder deflection values of approximately +/- 10°.

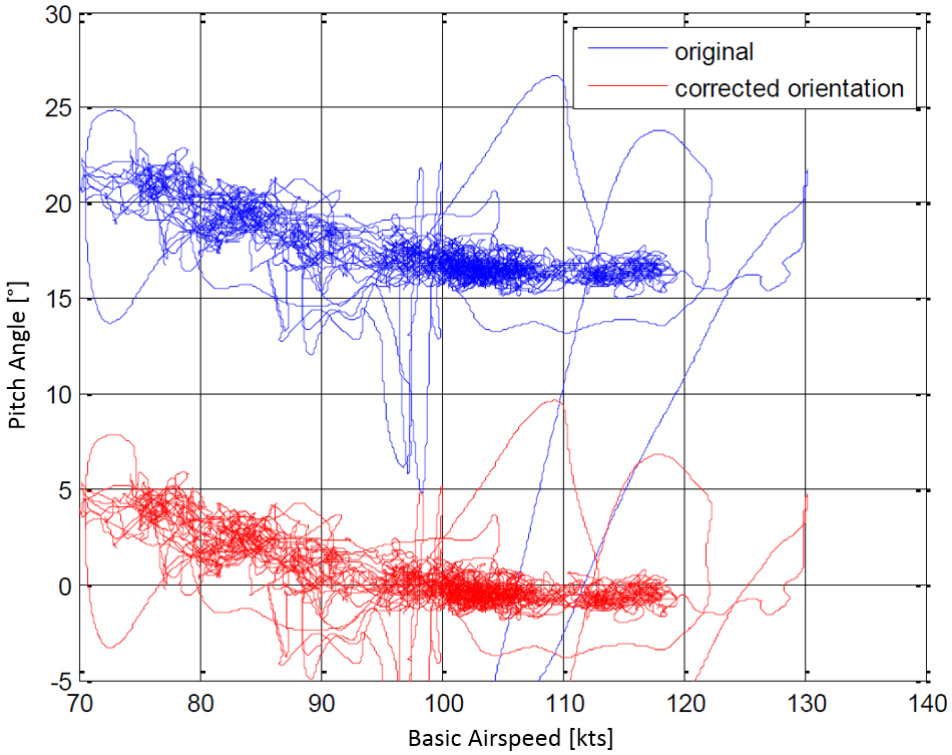

Figure A6.13: IMU data calibration

Calibration of the IMU data after a shift of – 17° (red line)

CP 14 Wind vane sensor calibration (Angle-of-Attack)

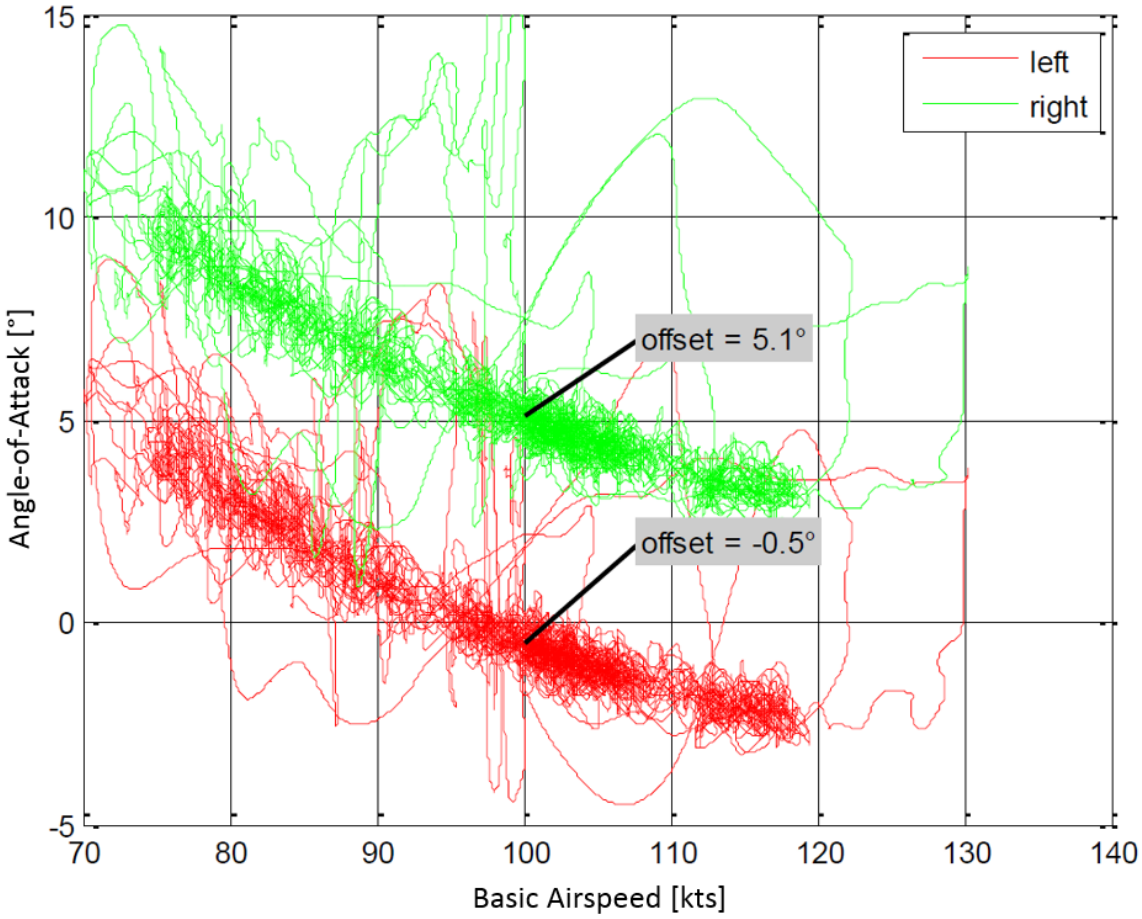

Figure A6.14: Angle-of-Attack data shift for calibration

Calibration of the Angle-of-Attack sensor data after a shift of + 0.5° (red line) and -5.1° (green line).

CP 15 Wind vane sensor calibration (Angle-of-Sideslip)

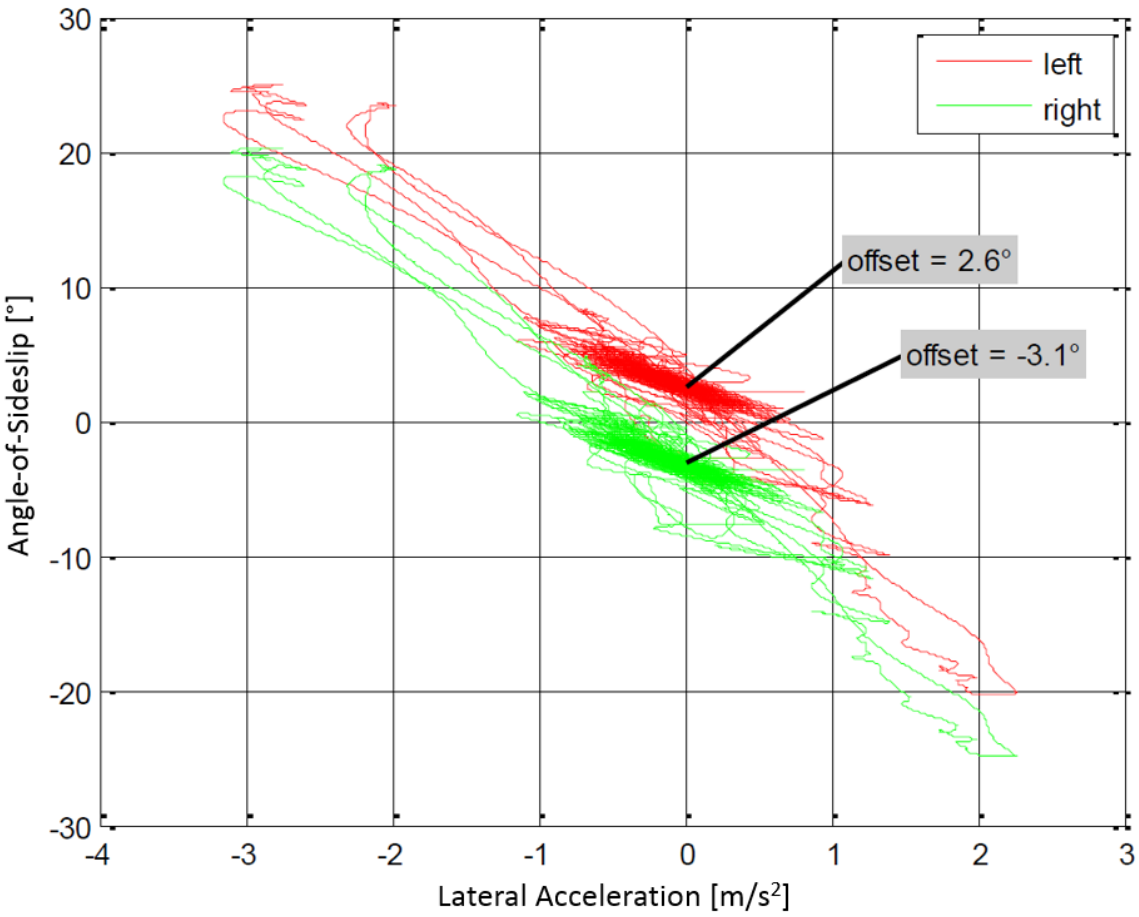

Figure A6.15: Angle-of-Sideslip data shift for calibration

Calibration of the Angle-of-Sideslip sensor data with a shift of 2.6° (red line) and -3.1° (green line).

Appendix 7 Mathematical methods

Introduction

In the following the mathematical methods used for the analysis of the measured flight data and the corresponding results are explained. It is divided into the sections ‘General methods’ und ‘Statistical methods’.

7.1 General methods

7.1.1 Gradient descent

The gradient of a differentiable function of several variables $f(\vec{x}) = f(x_1, \ldots, x_p)$ is the vector consisting of the partial derivatives

$$\nabla f(x_1, \ldots, x_p) = \left(\frac{\partial}{\partial_{x1}} f(\vec{x}) \ldots, \frac{\partial}{\partial_{xp}} f(\vec{x}) \right)^t \quad \text{(A1)}$$

In the case of $\nabla f(\vec{x}) \neq 0$ it is possible to diminish the function value by going a small step into the inverse direction of the gradient:

$$f(\vec{x}) > f(\vec{x} - \sigma \cdot \nabla f(\vec{x})) \quad \text{(A1a)}$$

with a sufficiently small step size σ > 0. If the procedure is started with a value of $\vec{x}$ which is close to a local minimum of the function by taking a larger number of steps of this kind one will approach that local minimum even better.

7.1.2 Smoothing, detection of relative maximum / minimum of a time series (y_i)

Smoothing is done by calculating *moving averages*:

$$\widetilde{y_i} = \frac{1}{2k+1} \sum_{l=i-k}^{i+k} y_l \quad \text{(A2)}$$

Here it is used with $k = 10$. Detection of local maxima and minima is done after smoothing. The value at an index is considered as maximal or minimal when it is the maximal or minimal value of a subsequence surrounding $\widetilde{y_l}$:

$$\widetilde{y_i} = \max(\widetilde{y_{i-k}}, \ldots, \widetilde{y_i}, \ldots, \widetilde{y_{i+k}})$$

or

$$\widetilde{y_i} = \min(\widetilde{y_{i-k}}, \ldots, \widetilde{y_i}, \ldots, \widetilde{y_{i+k}}) \quad \text{(A3)}$$

Here it is used with k = 20.

7.1.3 Numerical Derivation

For the calculation of the numerical derivative of a time series (x_i) the smoothed data values $\widetilde{x_i}$ are used; the numerical derivative is obtained by calculating the symmetric difference quotient at time value number i

$$\dot{y}_i \approx \frac{\widetilde{y_{i+1}} - \widetilde{y_{i-1}}}{2 \cdot \Delta t} \quad \text{(A4)}$$

where Δt is a constant time step.

7.1.4 Periodic linear regression Model

$$y_t = \bar{y} + A \cdot \sin(2\pi \cdot f \cdot t + \varphi) + e_t \qquad \text{with } t = 0, \ldots, n-1 \quad \text{(A5)}$$

with small noise values

$$e_0, e_1, \ldots, e_{n-1} \quad \text{(A6)}$$

$\bar{y}$ is the mean of the *y*-values:

$$\bar{y} = \frac{1}{n} \sum_{i=0}^{n-1} y_i$$

This is equivalent to

$$y_t = \bar{y} + a \cdot \cos(2\pi \cdot f \cdot t) + \mathrm{b} \cdot \sin(2\pi \cdot f \cdot t) + e_t \quad \text{(A7)}$$

with coefficients a and b.

Calculation of the coefficients a and b by finding the minimum values of (least square method):

$$\sum_{t=0}^{n-1}(y_t - \bar{y} - (a \cdot \cos(2\pi \cdot f \cdot t) + \mathrm{b} \cdot \sin(2\pi \cdot f \cdot t)))^2 \quad \text{(A8)}$$

Finding the minimum value by setting

$$\vec{y} = \begin{pmatrix} y_0 - \bar{y} \\ \vdots \\ y_{n-1} - \bar{y} \end{pmatrix} \in \mathbb{R}^n \qquad \vec{a} = \begin{pmatrix} \mathrm{a} \\ \mathrm{b} \end{pmatrix} \in \mathbb{R}^2 \quad \text{(A9)}$$

and

$$\mathrm{R} = \begin{pmatrix} \cos(2\pi \cdot f \cdot 0) & \sin(2\pi \cdot f \cdot 0) \\ \vdots & \vdots \\ \cos(2\pi \cdot f \cdot (n-1) & \sin(2\pi \cdot f \cdot (n-1) \end{pmatrix} \in M^{n,2} \quad \text{(A10)}$$

and solving the normal equation

$R^t \circ \vec{x} = (R^t \circ R) \circ \vec{a}$

7.1.5 Discrete Fourier Transformation (DFT)

The frequency value *f* in equation (A7) can also be found by calculation of the DFT (by using the FFT algorithm)

$$F_j = \sum_{i=0}^{n-1} e^{\frac{-j \cdot i}{\mathrm{n}}} \cdot y_i \qquad (\mathrm{j} = 0, \ldots, \mathrm{n} - 1) \quad \text{(A11)}$$

and taking the value of the DFT with the largest absolute value.

7.1.6 Linear homogenous ordinary differential equation of second order

$$0 = \mathrm{y}''(\mathrm{t}) - \mathrm{by}'(\mathrm{t}) - \mathrm{ay}(\mathrm{t})$$

a and b are constant coefficients. Here always $b^2 + 4a < 0$ is assumed. In this case a solution with initial values $s_0 = y(0)$, $s_1 = y'(0)$ is given by

$$y(t) = (u \cos(\omega\, t) + v \sin(\omega\, t))e^{-d\, t}$$

where $\mathrm{d} = {}^{-b}/_{2}$, $\omega = {}^{1}/_{2}\sqrt{-b^2 - 4a}$, $u = s_1$, and $v = {}^{1}/_{\omega}\,(s_1 + d\, s_0)$.

The solution is transferred into the form

$$y(t) = A\, sin(\omega t + \varphi) e^{-d\, t}$$

with $A = \sqrt{u^2 + v^2}$ and $\varphi = \arctan(u/v)$ for $v > 0$ and $\varphi = \arctan(u/v) + \pi$ for $v < 0$

The general solution is obtained by

$$c_1 y_1(t) + c_2 y_2(t)$$

with real coefficients c_1, c_2, the solution $y_1(t)$ with the initial values $s_0 = 1$, $s_1 = 0$ and the solution $y_2(t)$ with the initial values $s_0 = 0$, $s_1 = 1$.

Additional inhomogeneous equation of the shape

$$0 = y''(t) - by'(t) - ay(t) + f(t)$$

with a function $f(t)$ are considered. As only sample values $f(t_i)$ of this function are known, a numerical procedure for solving it is applied. Here Heun's method (improved Euler method) is used: Setting as abbreviation $F(t, y, \tilde{y}) = b\tilde{y} + ay - f(t)$ and beginning with the initial values $y_0 = s_0$, $\tilde{y}_0 = s_1$, and $t_0 = 0$ one performs steps (with step size $\Delta t = t_i - t_{i-1}$)

$$y_i = y_{i-1} + \Delta t\, \tilde{y}_{i-1} + (\Delta t)^2/2\; F(t_{i-1}, y_{i-1}, \tilde{y}_{i-1})$$

$$\tilde{y}_i = \tilde{y}_{i-1} + \Delta t/2\, (F(t_{i-1}, y_{i-1}, \tilde{y}_{i-1}) + F(t_i, y_{i-1} + \Delta t\, \tilde{y}_{i-1}, \tilde{y}_{i-1} + \Delta t\, F(t_{i-1}, y_{i-1}, \tilde{y}_{i-1})))\ ,$$

in order to get approximations

$$y(t_i) \approx y_i$$
$$y'(t_i) \approx \tilde{y}_i$$

of the solution of the equation with initial values $s_0 = y(0)$, $s_1 = y'(0)$.

7.2 Statistical Methods

7.2.1 Multi-linear regression, coefficient of determination (multiple regression coefficient)

Given data consisting of $p+1$ time (or other kinds of) series of equal length, each of them being one column of the matrix

$$S = \begin{pmatrix} s_{11} & s_{12} & \cdots & s_{1p} & y_1 \\ \vdots & & \ddots & \vdots & \\ s_{n1} & s_{n2} & \cdots & s_{np} & y_n \end{pmatrix} \in M^{n,p+1}(\mathbb{R}) \qquad \text{(A12)}$$

It is assumed, that the last time series (y_i) can be calculated approximately by a linear function of the first p time series (explanatory variables).

Thus a linear Model (analogous to equation (A7))

$$y_i = a_0 + a_1 s_{i1} + a_2 s_{i2} + \ldots + a_p s_{ip} + e_i \qquad \text{for } i = 1, \ldots, n \qquad \text{(A13)}$$

with small noise values

$$e_1, e_2, \ldots, e_n \qquad \text{(A14)}$$

is to be calculated.

The determination of the coefficients $a_0, \ldots, a_p$ is done by least square estimation: this sum should take its least value:

$$\sum_{i=1}^{n} \left(y_i - \left(a_0 + a_1 s_{i1} + a_2 s_{i2} + \cdots + a_p s_{ip}\right)\right)^2 \qquad \text{(A15)}$$

By setting $\vec{a}^t = (a_0, a_1, \ldots, a_p)$ and

$$R = \begin{pmatrix} 1 & s_{11} & \cdots & s_{1p} \\ \vdots & & \ddots & \vdots \\ 1 & s_{n1} & \cdots & s_{np} \end{pmatrix} \in M^{n,p+1}(\mathbb{R}) \qquad \text{(A16)}$$

the equation (A15) is rewritten in the form:

$$\|\vec{y} - R \circ \vec{a}\|^2 \qquad \text{(A15a)}$$

Finding the coefficients $\vec{a}^t = (a_0, a_1, \ldots, a_p)$ belonging to the minimum of equation (A15), equation (A15a) is done by solving the normal equation

$R^t \circ \vec{y} = (R^t \circ R) \circ \vec{x}$ (A15c)

Solving this yields the vector $\vec{a}^t = (a_0, a_1, \ldots, a_p)$ consisting of the desired coefficients. The obtained minimum values of equation (A4) is

The values delivered by the model and by these coefficients are the components of the vector

$R \circ \vec{a}$ (A16a)

Here this is only used for one or two input variables (p = 1 or p = 2).

7.2.2 Coefficient of Determination

The coefficient of determination is a measure of the quality of the fit of the linear model (2). Let be $\bar{t}$ the mean value of the sample values $t_1, \ldots, t_n$

$$\bar{t} = \frac{1}{n} \sum_{i=1}^{n} t_i$$

and $\vec{e} = (1,1, \ldots 1)^t$ the vector of dimension *n* containing only 1s. The coefficient of determination is defined by

$$R^2 = \frac{\|R \circ \vec{a} - \bar{t}\,\vec{e}\|^2}{\|\vec{t} - \bar{t}\,\vec{e}\|^2} \quad \text{(A16b)}$$

The denominator of equation (A9)

$\|\vec{t} - \bar{t}\,\vec{e}\|^2 = \sum_{i=1}^{n} (t_i - \bar{t})^2$ (A16c)

is the deviance of the samples $t_1, \ldots, t_n$ from their mean values. Multiplying it with the factor $\frac{1}{(n-1)}$ one gets the variance of the $t_1, \ldots, t_n$. In order to explain the nominator of equation (A9) one calculates

$\|\vec{t} - \bar{t}\,\vec{e}\|^2 = \|(\vec{t} - R \circ \vec{a}) + (R \circ \vec{a} - \bar{t}\,\vec{e})\|^2$

$= \|\vec{t} - R \circ \vec{a}\|^2 + \|R \circ \vec{a} - \bar{t}\,\vec{e}\|^2$ (A16d)

The last equation (A16d) is true because $\vec{a}$ is the solution of equation (A15c), therefore $R^t \circ \left(\vec{t} - R \circ \vec{a}\right) = 0$ and $R \circ \vec{a}$ and $\vec{e}$ (being the first column of R) are orthogonal to $\left(\vec{t} - R \circ \vec{a}\right)$. This yields

$$\|R \circ \vec{a} - \bar{t}\,\vec{e}\|^2 = \left\|\vec{t} - \bar{t}\,\vec{e}\right\|^2 - \left\|\vec{t} - R \circ \vec{a}\right\|^2 \qquad \text{(A16e)}$$

Using this in the nominator of equation (A16b) one gets

$$R^2 = \frac{\|\vec{t} - \bar{t}\,\vec{e}\|^2 - \|\vec{t} - R \circ \vec{a}\|^2}{\|\vec{t} - \bar{t}\,\vec{e}\|^2} \qquad \text{(A16f)}$$

$$= 1 - \frac{\|\vec{t} - R \circ \vec{a}\|^2}{\|\vec{t} - \bar{t}\,\vec{e}\|^2} \qquad \text{(A16g)}$$

Note:
The right side of equation (A16g) is never negative:

With $\vec{b} = (\bar{t}, 0, \ldots, 0)^2$ it is $\bar{t}\,\vec{e} = R \circ \vec{b}$ and

$\left\|\vec{t} - R \circ \vec{a}\right\|^2 \leq \left\|\vec{t} - R \circ \vec{b}\right\|^2$ for $\vec{a}$ minimizes equation (A15a).

The nominator of the second term in equation (A16g) is the sum of the squared errors (noise values) e_i of the linear model in equation (A13). It is considered as the deviance of the sample values t_i from the values $R \circ \vec{a}$ delivered by the linear model. The denominator is the complete deviance of the sample values from their mean value (which is considered as the simplest model to describe t_i). So the second term in equation (A16g) is considered as the portion of the deviation remaining, when the approximation by the linear model is done, within the complete deviation of the sample values.
It follows that R^2, being one minus this portion, is the portion of the deviation which is removed by the linear model.
If this value is 1 no more deviation exists and the model completely explains the value t_i. Otherwise if $R^2 = 0$ the linear model does not reduce the deviation and hence does not fit at all.

7.2.3 Analysis of variance (ANOVA)

a) Comparing several means: A group of continues random variables

$(X_{1,1}, X_{1,2}, \ldots, X_{1,n1}, X_{2,1}, \ldots, X_{2,n2}, \ldots, X_{m,1}, X_{1,2}, \ldots, X_{m,nm})$ (A17)

is divided into *m* subgroups

$(X_{j,1}, X_{j,2}, \ldots, X_{j,nj})$ $j = 1, \ldots, m$ (A18)

given by the values of one or several factors. The mean of the j^{th} group is

$E(X_{j,i}) = \mu_j$ (A19)

The analysis of variance is used to test the null hypothesis that all means are equal against the alternative hypothesis that the means differ and are depending of the factor values.

b) Comparing linear models:

Let

$y_i = a_0 + a_1 s_{i1} + a_2 s_{i2} + \ldots + a_p s_{ip} + e_i$ *for i = 1, … , n* (A20)

a linear model and

$y_i = a_0 + a_1 s_{i1} + a_2 s_{i2} + \ldots + a_q s_{iq} + \tilde{e}_i$ *for i = 1, … , n* (A21)

a reduced linear model with q < p. Assuming that the first model fits the data well one tests the null hypotheses that the reduced model already fits the data sufficiently against the alternative hypothesis that the larger model has to be used.

A prerequisite for applying the variance analysis is that all residual values e_i and $\tilde{e}_i$ are normal distributed with the expectation zero and equal variances.

7.2.4 Wilcoxon – Test

The Wilcoxon – Test is a nonparametric test. The occurring probability distribution must be continuous, however no assumptions about the shape of the occurring probability distributions are required.

Here an one-sided Wilcoxon – Test is applied:

Given are two continuous random variables X and Y, one tests the null hypothesis. That one can expect the values of X to be smaller than those of Y. In terms of distribution function the null hypothesis says $F_X(t) \geq F_Y(t)$.

For performing the test one gets values $x_1, \ldots, x_m$ of random variables $X_1, \ldots, X_m$ which are all distributed like X, and one gets values $y_1, \ldots, y_n$ of random variables $Y_1, \ldots, Y_n$ being distributed like Y.

All variables $X_1, \ldots, X_m, Y_1, \ldots, Y_n$ must be independent from each other.
In order to get a test statistic one counts, how often an $x_i - \text{value}$ is bigger than an y_j – value:

$$\text{U}\,(X_1, \ldots, X_m, Y_1, \ldots, Y_n = \sum_{i=1}^{m} \sum_{j=1}^{n} \left(I\,(X_i > Y_j) + \frac{1}{2}\, I\,(X_i = Y_j)\right) \qquad \text{(A22)}$$

with the indicator function

$$I\,(condition) = \begin{cases} 1 & the\ condition\ is\ true \\ 0 & otherwise \end{cases}$$

One calculates for the sample value $x_1, \ldots, x_m, y_1, \ldots, y_n$ the value of the test statistic in equation (A22). If this value becomes sufficient large, one rejects the null hypothesis.

If the numbers *m* and *n* are small *(n,m ≤ 50)* and if ties *(x_i = y_j for any $i \in 1, \ldots, m$ and $j \in 1, \ldots, n$)* do not occur, the required values of the probability distribution of the test statistic are taken from tables containing pre-calculated values. Otherwise one uses approximations of equation (A22) by normal distributions.

7.2.5 Confidence interval for values predicted by linear regression

Using a model of the shape (2) a prediction is to be obtained by taking instead of the values
$s_{i1}, \ldots, s_{ip}$ on the right hand side of (2) new values $x_{01}, \ldots, x_{0p}$. However the resulting value Y_0 is only an estimation of the true value y_0 resulted from the $x_{01}, \ldots, x_{0p}$, for the calculation depends of the randomly measured values $t_1, \ldots, t_n$ (see the last column of (1)). Therefore it is preferred to calculate a confidence interval, which will contain the unknown value with a probability of 95%.
The basis of the following calculation is the linear regression again. One starts with the linear model

$$\vec{Y} \quad = R \circ \vec{\alpha} + \vec{E} \qquad (32)$$

$\vec{Y}$ = ($Y_1, \ldots, Y_n$) is a vector of *n* random variables. It stands for the values to be measured. R is the n *x* r-Matrix in (5) (with r = p + 1). $\vec{E}$ is a vector if independent identical normal

distributed random variables with expectation E (E_i) = 0 and variance Var (E_i) = σ^2 . $\vec{\alpha}$ = (α_0, α_1, …, α_{r-1}) is a vector of unknown coefficients.
In order to get the desired estimation for the value y_0 belonging to the given values x_1, …, x_p one performs

1. a least square estimation $\vec{a}$ of $\vec{\alpha}$ (see (6)):

$$\vec{a} \;=\; (R^t \circ R)^{-1} \circ R^t \circ \vec{Y} \tag{33}$$

This is a random vector. It is an unbiased estimator of $\vec{\alpha}$ (that is E ($\vec{a}$) = $\vec{\alpha}$)
with covariance matrix $\mathrm{Cov}(\vec{a})) = \sigma^2 (R^t \circ R)^{-1}$.

2. the estimation of the desired value y_0

$$Y_0 \;=\; \vec{a}^{\,t} \circ \vec{x}_0 \;=\; \vec{x}_0^{\,t} \circ \vec{a} \qquad \text{with} \quad \vec{x}_0 \;=\; \begin{pmatrix} 1 \\ x_{0,1} \\ \vdots \\ x_{0,p} \end{pmatrix} \tag{34}$$

This is again an unbiased estimator with a variance obtained from Cov ($\vec{a}$)):

$$\begin{aligned} \mathrm{E}(Y_0) \;&=\; \mathrm{E}(\vec{x}^{\,t} \circ \vec{a}) \;=\; \vec{x}^{\,t} \circ \vec{\alpha} \;=\; y_0 \\ \mathrm{Var}(Y_0) \;&=\; \mathrm{Var}(\vec{x}^{\,t} \circ \vec{a}) \;=\; \sigma^2\, \vec{x}_0^{\,t} \circ (R^t \circ R)^{-1} \circ \vec{x}_0 \end{aligned} \tag{35}$$

Due to (35) the random variable

$$W \;=\; \frac{\vec{\alpha}^{\,t} \circ \vec{x}_0 - \vec{a}^{\,t} \circ \vec{x}_0}{\sqrt{\sigma^2\, \vec{x}_0^{\,t} \circ (R^t \circ R)^{-1} \circ \vec{x}_0}} \tag{36}$$

is standard normal distributed (N(0, 1)). It is shown that

$$V \;=\; \frac{1}{\sigma^2}\, ||\vec{Y} - R \circ \vec{a}||^2 \tag{37}$$

is X_{n-r} - distributed and that V and W are independent. This gives the t_{n-r} - distributed random variable

$$\frac{W}{\sqrt{V/(n-r)}} = \frac{\vec{\alpha}^{\,t} \circ \vec{x}_0 - \vec{a}^{\,t} \circ \vec{x}_0}{\sqrt{D}\,\sqrt{\vec{x}_0^{\,t} \circ (R^{\,t} \circ R)^{-1} \circ \vec{x}_0}} \tag{38}$$

$$\text{with } D = \frac{\sigma^2}{n-r} V = \frac{1}{n-r} ||\vec{Y} - R \circ \vec{a}||^2$$

D is an unbiased estimator of σ^2 = Var (E_i).

Taking $t_{0.975,\,n\text{-}r}$ - the 0.975-quantile of the $t_{n\text{-}r}$ - distribution - one gets

$$\mathrm{P}\left(-t_{0.975,n-r} \le \frac{\vec{\alpha}^{\,t} \circ \vec{x}_0 - \vec{a}^{\,t} \circ \vec{x}_0}{\sqrt{D}\,\sqrt{\vec{x}_0^{\,t} \circ (R^{\,t} \circ R)^{-1} \circ \vec{x}_0}} \le t_{0.975,n-r}\right) = 0.95$$

or equivalently

$$\begin{aligned} \mathrm{P}\Big(&\vec{a}^{\,t} \circ \vec{x}_0 - t_{0.975,n-r}\,\sqrt{D}\,\sqrt{\vec{x}_0^{\,t} \circ (R^{\,t} \circ R)^{-1} \circ \vec{x}_0} \\ &\le \vec{\alpha}^{\,t} \circ \vec{x}_0 \le \\ &\vec{a}^{\,t} \circ \vec{x}_0 + t_{0.975,n-r}\,\sqrt{D}\,\sqrt{\vec{x}_0^{\,t} \circ (R^{\,t} \circ R)^{-1} \circ \vec{x}_0}\Big) = 0.95 \end{aligned} \tag{39}$$

This yields the desired 95% confidence interval for $y_0 = \vec{\alpha}^{\,t} \circ \vec{x}_0$ with the lower and upper boundary

$$\begin{aligned} \text{lwr} &= \vec{a}^{\,t} \circ \vec{x}_0 - t_{0.975,n-r}\,\sqrt{D}\,\sqrt{\vec{x}_0^{\,t} \circ (R^{\,t} \circ R)^{-1} \circ \vec{x}_0} \\ \text{upr} &= \vec{a}^{\,t} \circ \vec{x}_0 + t_{0.975,n-r}\,\sqrt{D}\,\sqrt{\vec{x}_0^{\,t} \circ (R^{\,t} \circ R)^{-1} \circ \vec{x}_0} \end{aligned} \tag{40}$$